

https://dspace.org/

Exploration of an Electro-Magneto-Responsive Polymeric drug delivery system for enhanced nose-to-brain delivery

Akilo, Olufemi David

2016

https://hdl.handle.net/10539/34134

Akilo, O. U. Exploration of an Electro-Magneto-Responsive Polymeric drug delivery system for enhanced nose-to-brain delivery. University of the Witwatersrand; Johannesburg: 2016

Downloaded from a DSpace repository. https://dspace.org/

EXPLORATION OF AN ELECTRO-MAGNETO-RESPONSIVE POLYMERIC DRUG DELIVERY SYSTEM FOR ENHANCED NOSE-TO-BRAIN DELIVERY

OLUFEMI DAVID AKILO



A thesis submitted to the Faculty of Health Sciences, University of the Witwatersrand in fulfilment of the requirements for the degree of Doctor of Philosophy

Supervisor:

Professor Viness Pillay

University of the Witwatersrand, Department of Pharmacy and Pharmacology, Johannesburg, South Africa

Co-Supervisors:

Professor Yahya Essop Choonara

University of the Witwatersrand, Department of Pharmacy and Pharmacology, Johannesburg, South Africa

and

Professor Girish Modi

University of the Witwatersrand, Division of Neurosciences, Department of Neurology, Johannesburg, South Africa

Johannesburg

2016

DECLARATION

I, Olufemi David Akilo, declare that this thesis is my own work. It has been submitted for the degree of Doctor of Philosophy in the Faculty of Health Sciences in the University of the Witwatersrand, Johannesburg. It has not been submitted before for any degree or examination at this or any other University.

.....

This 27th day of May, 2016

PUBLICATIONS

1. Nose-to-Brain Neurotherapeutic Interventions: Olufemi D Akilo, Yahya E Choonara, Pradeep Kumar, Lisa C du Toit and Viness Pillay, Chapter 6 of Advances in Neurotherapeutic Delivery Technologies, OMICS Group eBooks, 80-107, 2015.

2. An *in vitro* evaluation of a carmustine-loaded Nano-co-Plex for potential magnetic-targeted intranasal delivery to the brain: Olufemi D. Akilo, Yahya E. Choonara, André M. Strydom, Lisa C. du Toit, Pradeep Kumar, Girish Modi and Viness Pillay, International Journal of Pharmaceutics, 500, 196-209, 2016.

3. A Lactoferrin-Galantamine Proteo-Alkaloid Conjugate for the Management of Alzheimer's disease: Olufemi D Akilo, Yahya E Choonara, Pradeep Kumar, Lisa C du Toit and Viness Pillay. Submitted to Medical Hypotheses, January, 2016.

4. Preparation, Physicochemical and Physicomechanical Characterization of an Optimized Nanogel Drug Composite for Potential Intranasal Drug delivery: Olufemi D Akilo, Yahya E Choonara, Pradeep Kumar, Lisa C du Toit and Viness Pillay. Submitted to Biomaterials, February, 2016.

5. *In Vitro, Ex Vivo* and *In Vivo* Evaluation of an Electro-Magneto-Responsive Nanogel Composite for Nose-to-brain Delivery. Olufemi D Akilo, Yahya E Choonara, Pradeep Kumar, Lisa C du Toit and Viness Pillay. Submitted to Journal of Pharmaceutical Sciences, March, 2016.

RESEARCH OUTPUTS AT CONFERENCE PROCEEDINGS

1. Olufemi David Akilo, Yahya Essop Choonara, Girish Modi and Viness Pillay. Preparation and Characterization of a Dual Responsive Polymeric Gel for Intranasal Drug Delivery. ***(Poster Presentation).*** *School of Therapeutic Sciences Research Day*, University of the Witwatersrand, Johannesburg, South Africa, September 10th, 2013.

2. Olufemi David Akilo, Yahya Essop Choonara, Lisa Claire Du Toit, Pradeep Kumar, Girish Modi and Viness Pillay. Synthesis of Carmustine-Loaded Ferrous-Based Nanoconstructs for Targeted Intranasal Delivery to the Brain. ***(Poster Presentation).*** *6th Cross-Faculty Graduate Symposium,* University of the Witwatersrand, Johannesburg, South Africa, October 27th-31st, 2014.

3. Olufemi David Akilo, Yahya Essop Choonara, Lisa Claire Du Toit, Pradeep Kumar, Girish Modi and Viness Pillay. Preparation and Characterization of a Mucoadhesive-Dual Responsive Polymeric Gel for Intranasal Drug Delivery. ***(Poster Presentation).*** International Society of Biomedical Polymers and Polymeric Biomaterials, Orlando, Florida USA, 8th-10th July, 2015.

4. Olufemi David Akilo, Yahya Essop Choonara, Lisa Claire Du Toit, Pradeep Kumar, Girish Modi and Viness Pillay. Synthesis of a carmustine-loaded Polyplex coated iron oxide nanoparticles for targeted intranasal delivery to the brain ***(Podium Presentation).*** International Society of Biomedical Polymers and Polymeric Biomaterials, Orlando, Florida USA, 8th-10th July, 2015.

5. Olufemi David Akilo, Yahya Essop Choonara, Lisa Claire Du Toit, Pradeep Kumar, Girish Modi and Viness Pillay. Preparation of a Gadolinium based Nanoparticles Coated with Polyethyleneimine-Galantamine-Lactoferrin Complex for Intranasal Drug Delivery in Treating Alzheimer's Disease ***(Podium Presentation)***. Faculty of Health Sciences Research Day, University of the Witwatersrand, Johannesburg, South Africa, September 8-9, 2015.

6. Olufemi David Akilo, Yahya Essop Choonara, Lisa Claire Du Toit, Pradeep Kumar, Girish Modi and Viness Pillay. An *In Vitro* Evaluation of Carmustine-Loaded Nano-co-Plex for Potential Magnetically Targeted Intranasal Delivery to the Brain. ***(Podium Presentation)***. Academy of Pharmaceutical Sciences of South Africa, Johannesburg, South Africa, September 17-19, 2015.

7. Olufemi David Akilo, Yahya Essop Choonara, Lisa Claire Du Toit, Pradeep Kumar, Girish Modi and Viness Pillay. Synthesis of gadolinium oxide coated with Galantamine-loaded PEG for the management of Alzheimer's disease. ***(Podium Presentation)***. Academy of Pharmaceutical Sciences of South Africa, Johannesburg, South Africa, March 2-3, 2016.

PATENT FILED

A novel drug-loaded Nano-co-Plex incorporated into a mucoadhesive-electro responsive polymeric gel for controlled and magnetically targeted nose-to-brain drug delivery. O. D. Akilo, V. Pillay, Y.E. Choonara L.C. du Toit, P. Kumar.
SA 2015/06543.

ABSTRACT

Delivering drugs to the brain for the treatment of brain diseases has been fraught with low bioavailability of drugs due to the Blood-Brain Barrier (BBB). The intranasal (IN) route of delivery has purportedly been given recognition as an alternative route of delivering drugs to the brain with improved bioavailability if the nose-to-brain option is considered. However, drugs administered through the nasal mucosa suffer some challenges such as mucocilliary clearance, enzymatic degradation, inability of a controllable drug release to give a precise dose, resulting in frequent dosing and absorption into the systemic circulation through the blood rich vessels in the mucosa, thus facing the BBB challenge. The aim of this study was to develop a novel Nano-co-Plex (NCP), a magnetic nano-carrier loaded with a therapeutic agent which is further incorporated into a nasal thermosensitive electro-responsive mucogel (TERM) for *in situ* gelling, for electro-actuated release of the incorporated drug-loaded NCP in a controllable "on-off" pulsatile manner, which is achieved with the aid of an external electric stimulation (ES). The released drug-loaded NCP was then targeted to the brain via a direct nose-to-brain drug delivery pathway with the aid of an external magnetic field (MF) for rapid transportation. The ES was brought about by applying a 5V potential difference (PD) using electrodes on the nose and the external MF would then be applied by placing a magnetic headband on the head of the patient. In this research, the drug-loaded NCP was prepared by firstly synthesizing iron oxide nanoparticles (Magnetite) which were then coated with Polyplex; a polymeric complex fabricated employing polyvinyl alcohol (PVA), polyethyleneimine (PEI) and fluorecein isothiocyanate (FITC). The coated magnetite was thereafter loaded with Carmustine (BCNU), an effective drug commonly used in brain tumor treatment, to formulate the BCNU-NCP. The TERM was prepared by blending a thermosensitive polymer, Pluronic F127 (F127) with mucoadhesive polymers, chitosan (CS) and hydroxypropyl methylcellulose (HPMC). Polyaniline (PANI) was included in the blend as the electo-active moiety of the formulation. Finally, the BCNU-NCP was incorporated into the gel to form a Nanogel-Composite. A Box–Behnken design model was employed for the optimization of the Nanogel Composite. TERM, BCNU-NCP and Nanogel Composite were characterized employing Thermogravimetric analysis (TGA), Superconducting Quantum Interference Device (SQUID) magnetometry, Fourier Transform Infrared Spectroscopy (FTIR), Nuclear Magnetic Resonance (NMR), X-ray Diffractometry (XRD), Scanning Electron Microscopy (SEM), Cyclic Voltammetry (CV), Transmission Electron Microscopy (TEM), Rheological, Porositometry, Textural and Zetasize analyses. *In vitro* drug release*, ex vivo* permeation and *in vivo* studies were performed. The BCNU-NCP was found to be paramagnetic with a magnetization value of 61emu/g, possessing a mixture of spherical and hexagonal shaped core-shell nanoparticles of size 30-50nm with zeta potential of +32 ±2mV. The NCP displayed a high degree of crystallinity with 32% Polyplex coating. The loading capacity of NCP was 176.86µg BCNU/mg of the carrier and maximum release of 75.8% of the loaded BCNU was achieved after 24 hours. FTIR and NMR confirmed the conjugation of PVA and PEI of the Polyplex at a ratio of 1:4. Cytotoxicity of the BCNU-loaded Nano-co-Plex displayed superiority over the conventional BCNU towards human glioblastoma (HG) A170 cells. Cell studies revealed enhanced uptake and internalization of BCNU-NCP in HG A170 cells in the presence of an external MF. BCNU-NCP was found to be non-toxic to healthy brain cells. A thermally stable gel with desirable rheological and mucoadhesive properties was developed. The results revealed gelation temperature of 27.5±0.5°C with a porous morphology. Nanogel Composite possesses electroactive properties and shows response to ES and releases incorporated BCNU-NCP in an "on-off" pulsatile drug release profile upon application of a 5V PD. The *in vitro* release studies showed an average release of BCNU-NCP per release cycle to be 10.28%. *Ex vivo* permeation studies were performed using a freshly excised nasal tissue of the New Zealand white rabbit; the results showed that BCNU-NCP was able to permeate through the nasal tissue at a 6 times greater amount in the presence of a MF than in the absence of MF. BCNU concentration was found to be high in the brain and CSF of rabbit when the Nanogel Composite is intranasally administered compared to the IV injection of the conventional BCNU. Furthermore, application of the MF was found to increase the concentration of BCNU in the brain and CSF of the rabbit. The result of Field Emission Electron Probe Micro Analyzer (FE EPMA) was further used to confirm the presence of NCP in the rabbit brain tissue. Histopathological results indicated mild lesions in the nasal mucosa of the rabbit after IN administration of Nanogel Composite. The results of the *in vitro*, *ex vivo* and the *in vivo* proved that the Nanogel Composite is superior in delivering BCNU into the brain than the conventional drug delivery system for the treatment of brain tumor as it was able to release the therapeutic agent in a controllable manner. The MF applied aided drug to be targeted and rapidly transported to the brain via a direct nose-to-brain pathway thereby circumventing the BBB and increasing bioavailability of drug in the brain. This vehicle may also be used to deliver other similar therapeutic agents into the brain for the treatment of various brain diseases.

ACKNOWLEDGEMENTS

I am grateful to God, The Almighty. I thank my wife and children for their love and cooperation.

I sincerely acknowledge and appreciate the invaluable role of my supervisor, Professor Viness Pillay whose mentorship and guidance have been most inspiring and motivating. I am highly impressed by his prompt and swift responses to situations which is second to none. I am so ever grateful for giving me the opportunity to be part of WADDP. I will also like to acknowledge my co-supervisors, Professor Yahya Essop Choonara and Professor Girish Modi who were always willing to provide the necessary assistance and direction at all times. I will like to thank Prof. Paul Danckwerts for his assistance whenever needed.

My profound gratitude goes to Professor Lisa du Toit and Pradeep Kumar. The time and effort you invested has only made the completion of this thesis so much easier. Your valuable feedback and suggestions helped me improve both my lab experiments and my thesis in many ways. I wish you all success in your future endeavours. My gratitude also goes to Prof. Andre Strydom, Prof. and Dr. Mrs. Amadi Ihunwo and Dr. Ndidi Ngwuluka, for their assistance in various dispensations. To my friends, colleagues and fellow researchers, Kenny Debayo-Sanusi, Dr. Patrick Adebola Dr., Joseph Eguale, Maluta Mufamadi, Olatunbosun Olaleye, Samson Adeyemi, Martina Manyikana, Kealeboga Mokolobate, Jonathan Pantshwa, Prof. Kennedy Erlwanger Dr. Pierre Kondiah, Dr. Thashree Marimuthu, Dr. Ravindra Badhe, Dr. Dharmesh Chejara, Dr. Mostafa Mabrouk, Dr. Mershen Govender, Sunaina Indermun, Greta Mbitsi-ibouily, Fatema Mia, Mukaza Eliphaz, Khuphukile Madida, Karmani Muruga, Margaret Siyawamwaya, Poornima Ramburrun, Bibi Choonara, Mduduzi Sithole, Zikhona Hayiyana, Pride Mothobi, Pariksha Kondiah. I thank you all for your supports. I thank the technical staff of the Department of Pharmacy and Pharmacology, Mr. Sello Ramarumo, Ms. Nompumelelo Damane, Mr. Kleinbooi (Mkhaya) Mohlabi, Mr. Bafana Themba and Phumzile Madodo. I also thank the staff of the CAS at Wits, Sr. Mary-Ann Costello, Patrick Selahle, Sr. Ammelia Rammekwa, Kershneee Chetty, Lorrraine Setimo and Nico Douths.

DEDICATION

This work is dedicated to my late father, Simon Babatunde Akilo.

ANIMAL ETHICS DECLARATION

I, Olufemi David Akilo confirm that the study entitled "*In vivo* animal studies to assess the performance of an intranasal drug delivery device in a rabbit model" received the approval from the Animal Ethics Committee of the University of the Witwatersrand with ethics clearance number 2015/05/C (see Appendix D)

TABLE OF CONTENTS

DECLARATION.....i

PUBLICATIONS.....ii

RESEARCH OUTPUTS AT CONFERENCE PROCEEDINGS.....iii

PATENT FILED.....v

ABSTRACT.....vi

ACKNOWLEDGEMENTS.....vii

DEDICATION.....viii

ANIMAL ETHICS DECLARATION….....ix

TABLE OF CONTENTS……..……x

LIST OF FIGURES.....xxviii

LIST OF TABLES.....xxxv

LIST OF EQUATIONS……..……...xxxviii

LIST OF ABBREVIATIONS……..xxxix

CHAPTER 1
INTRODUCTION

1. CHAPTER 1 1

1.1. BACKGROUND TO THIS STUDY 1

1.2. RATIONALE AND MOTIVATION FOR THIS STUDY 4

1.3. AIM AND OBJECTIVES 7

1.4. NOVELTY OF THIS WORK 8

1.5. OVERVIEW OF THIS THESIS 9

1.6. CONCLUDING REMARKS 11

1.7. REFERENCES 11

CHAPTER 2

A REVIEW OF NOSE-TO-BRAIN NEUROTHERAPEUTIC INTERVENTIONS

2. CHAPTER 2 14

2.1. INTRODUCTION 14

2.2. BIOLOGICAL BARRIERS AS AN IMPEDIMENT TO CNS DRUG DELIVERY.. 15

2.2.1. Blood-Brain Barrier 15

2.2.2. Blood-Cerebrospinal Fluid Barrier 16

2.2.3. Blood-Tumor Barrier 16

2.3. NASAL ANATOMY AS AN AID TO CNS DRUG DELIVERY 17

2.3.1. The Olfactory Pathway as an Opportunity for CNS Drug Delivery 22

2.3.2. Proposed Pathways of Therapeutic Agents Introduced into the Nasal Cavity…… 23

2.3.3. Mechanism of Direct Nasal Mucosa to Brain Delivery via the Olfactory Pathway 24

2.4. EVIDENCE OF NOSE-TO-BRAIN DRUG DELIVERY 26

2.4.1. Delivery of RNA, Enzymes, Insulin and Protein 26

2.4.2. Delivery of Drug-Loaded Nanoparticles 28

2.4.3. Microemulsion Formulations 31

2.4.4. Liposomes as Delivery Vehicles 33

2.4.5. Direct Drug Application into the Nasal Cavity 35

2.5. CONVENTIONAL NASAL DRUG DELIVERY DOSAGE FORMS 37

2.5.1. Nasal Drops 37

2.5.2. Nasal Sprays 37

2.5.3. Nasal Gels 38

2.5.4. Nasal Powders 40

2.6. THE USE OF SPECIALIZED INTRANASAL DRUG DELIVERY SYSTEMS..... 40

2.6.1. Liposomes 41

2.6.2. Microspheres 41

2.6.3. Nanoparticles 42

2.6.4. Microemulsions 43

2.6.5. Nanoemulsions 45

2.6.6. Iontophoretic Delivery 46

2.7. CHALLENGES AND FUTURE TRENDS OF DIRECT NOSE-TO-BRAIN DELIVERY 46

2.8. CONCLUDING REMARKS 49

2.9. REFERENCES 50

CHAPTER 3

AN *IN VITRO* EVALUATION OF A CARMUSTINE-LOADED NANO-CO-PLEX FOR POTENTIAL MAGNETIC-TARGETED INTRANASAL DELIVERY TO THE BRAIN

3. CHAPTER 3 67

3.1. INTRODUCTION 67

3.2. MATERIALS AND METHODS 69

3.2.1. Materials 69

3.2.2. Preparation of the Iron Oxide Nanoparticles 70

3.2.3. Preparation of the Nano-co-Plex 70

3.2.4. Determination of Structural Integrity of the BCNU-loaded Nano-co-Plex…….. 72

3.2.4.1. Fourier Transform Infrared spectroscopy analysis of the BCNU-loaded Nano-co-Plex 72

3.2.4.2. Nuclear Magnetic Resonance analysis of the Nano-co-Plex 72

3.2.5. Thermal Stability and Quantitative Analysis of the Nano-co-Plex 72

3.2.6. Size and Stability Analysis of the BCNU-Loaded Nano-co-Plex 72

3.2.7. Determination of Size and Morphology of BCNU-Loaded Nano-co-Plex…… 73

3.2.8. Determination of Magnetization Properties of the BCNU-Loaded Nano-co-Plex…….. 73

3.2.9. Analysis of the Crystalline Structural Properties of BCNU-Loaded Nano-co-Plex…….. 73

3.2.10. Establishment and Confirmation of the Interaction Profile Employing Computational Simulations 73

3.2.11. Determination of the Loading Capacity and Efficiency of BCNU within the Nano-Co-Plex 74

3.2.12. Determination of the *In Vitro* Drug Release Profile of BCNU released from the BCNU-Loaded Nano-co-Plex..... 75

3.2.13. Cytotoxicity Analysis, Cellular Uptake and Internalization of the BCNU-Loaded Nano-co-Plex 75

3.2.13.1. Cytotoxicity studies via 3-(4,5-dimethylthiazole-2-yl)-2,5-diphenyl tetrazolium bromide assay on the conventional BCNU and BCNU-loaded Nano-co-Plex..... 75

3.2.13.2. Cellular uptake and internalization studies of the BCNU-loaded Nano-co-Plex..... 77

3.3. RESULTS AND DISCUSSION..... 78

3.3.1. Synthesis of the BCNU-Loaded Nano-co-Plex 78

3.3.2. Assessment of the Structural Modifications of the BCNU-Loaded Nano-co-Plex…… 80

3.3.2.1. Structural modification assessment via Fourier Transform Infrared spectroscopy 80

3.3.2.2. Structural modification assessment via Nuclear Magnetic Resonance analysis 82

3.3.3. Morphology and Particle Size of the BCNU-Loaded Nano-co-Plex 83

3.3.4. Size Distribution and Zeta Potential Analysis of the BCNU-Loaded Nano-co-Plex 85

3.3.5. Assessment of the Crystalline Structural Properties of the BCNU-Loaded Nano-co-Plex 87

3.3.6. Assessment of the Thermal Stability and Quantitative Analysis of the Nano-co-Plex 88

3.3.7. Assessment of Attraction Sensitivity of the BCNU-Loaded Nano-co-Plex to an External Magnetic Field 90

3.3.8. BCNU Loading into the Nano-co-Plex 92

3.3.9. Assessment of the *In Vitro* Drug Release Profile of BCNU from the Nano-co-Plex 93

3.3.10. Establishment and Confirmation of the Interaction Profile Employing Computational Simulations 95

3.3.11. Assessment of the Cytotoxicity and Cellular Uptake of the BCNU-Loaded Nano-co-Plex 96

3.3.11.1. Cytotoxicity studies of the BCNU-loaded Nano-co-Plex 96

3.3.11.2. Cellular uptake and internalization of the BCNU-loaded Nano-co-Plex…… 98

3.4. CONCLUDING REMARKS 99

3.5. REFERENCES 100

CHAPTER 4

PREPARATION, PHYSICOCHEMICAL AND PHYSICOMECHANICAL CHARACTERIZATION OF AN OPTIMIZED NANOGEL COMPOSITE

4. CHAPTER 4 106

4.1. INTRODUCTION 106

4.2. MATERIALS AND METHODS 108

4.2.1. Materials 108

4.2.2. Preparation of the Thermosensitive Electro-Responsive Mucogel 108

4.2.3. Preparation of Carmustine-Loaded Nano-co-Plex 108

4.2.4. Incorporation of the Carmustine-Loaded Nano-co-Plex into the Thermosensitive Electro-Responsive Mucogel 109

4.2.5. Optimization Studies Employing a Box-Behnken Experimental Design for the Nanogel Composite 109

4.2.6. Determination of Structural Modification and Chemical Interaction of the Nanogel Composite 110

4.2.7. Determination of the Mucoadhesive Behavior of the Nanogel Composite…… 111

4.2.8. Determination of Gelation Temperature of the Nanogel Composite ... 111

4.2.9. Determination of the Electrical Conductivity of the 15 Nanogel Composite Formulations 112

4.2.10. *In vitro* Determination of the Release Profiles of the 15 Nanogel Composite Formulations upon Application of an Electrical Stimulation 112

4.2.10.1. Quantitative analysis of the BCNU-loaded Nano-co-Plex released from the Nanogel Composite 113

4.2.11. *Ex Vivo* Evaluation of Mucoadhesive Strength of the Nanogel Composite 114

4.2.12. Evaluation of the Thermal Behavior of the Optimized Nanogel Composite 115

4.2.13. Determination of Surface Morphology and Porosity of the Optimized Nanogel Composite 115

4.2.13.1. Scanning Electron Microscopy 115

4.2.13.2. Determination of the porosity profile of the Nanogel Composite . 116

4.2.14. Rheological Analysis of the Optimized Nanogel Composite 117

4.2.15. Evaluation of the Electro-activity of the Optimized Nanogel Composite……..... 118

4.2.16. *In Vitro* Drug Release Analysis from the Optimized Nanogel Composite on the Application of an Electrical Stimulation 119

4.2.16.1. Quantitative determination of the BCNU-loaded Nano-co-Plex released from the optimized Nanogel Composite 119

4.3. RESULTS AND DISCUSSION 119

4.3.1. Preparation of the Thermosensitive Electro-Responsive Mucogel and the Nanogel Composite 119

4.3.2. Evaluation of Box–Behnken experimental design optimization..... 120

4.3.3. Assessment of the Mucoadhesive Behavior of the Nanogel Composite…….. 124

4.3.4. Assessment of the Gelation Temperature 126

4.3.5. Electro-Responsiveness of the Nanogel Composite via Electric Conductivity Assessment..... 127

4.3.6. *In Vitro* Assessment of Release Behavior of the 15 Nanogel Composite Formulations on Application of Electrical Stimulation 128

4.3.7. *Ex vivo* Mucoadhesion Analysis 131

4.3.8. Assessment of the Structural Modification of the Optimized Nanogel Composite 133

4.3.8.1. Assessment of the structural modification employing Fourier Transmission Infrared spectroscopy..... 133

4.3.8.2. Assessment of structural integrity by XRD spectroscopy 136

4.3.9. Evaluation of the Thermal Stability of the Optimized Nanogel Composite…..... 137

4.3.10. Assessment of the Surface Morphology and Porosity of the Nanogel Composite 139

4.3.11. Assessment of Gelation Temperature of the Optimized Nanogel Composite 145

4.3.12. Assessment of Rheological Properties of the Nanogel Composite.. 145

4.3.12.1. Shear viscosity 145

4.3.12.2. Yield stress..... 146

4.3.12.3. Oscillation stress sweep..... 147

4.3.12.4. Frequency sweep..... 148

4.3.12.5. Creep recovery test..... 150

4.3.12.6. Temperature ramp analysis..... 151

4.3.13. Assessment of the Electro-active Properties of the Nanogel Composite Employing Cyclic Voltammetric Analysis 153

4.3.14. Assessment of the *In Vitro* Drug Release Analysis of the Optimized Nanogel Composite on Application of Electrical Stimulation..... 154

4.4. CONCLUDING REMARKS 157

4.5. REFERENCES..... 157

CHAPTER 5

EX VIVO EVALUATION OF AN *IN SITU* NANOGEL COMPOSITE

5. CHAPTER 5 161

5.1. INTRODUCTION 161

5.2. MATERIALS AND METHODS 162

5.2.1. Materials 162

5.2.2. Preparation of the Nanogel Composite 162

5.2.3. *Ex Vivo* Evaluation of the Nanogel Composite 162

5.2.3.1. Preparation of the rabbit nasal tissue for permeation studies 162

5.2.4. *Ex Vivo* Evaluation of Mucoadhesive Strength of the Nanogel Composite.. 163

5.2.5. Determination of the Permeation Capability of the BCNU-Loaded Nano-co-Plex across Rabbit Nasal Tissue 163

5.2.5.1. Quantitative analysis of the BCNU-loaded Nano-co-Plex permeated through the rabbit nasal epithelial tissue from the Nanogel Composite 165

5.2.5.2. Evaluation of BCNU-loaded Nano-co-Plex permeability 165

5.2.5.3. Evaluation of the effect of magnetic field on cytotoxicity of the BCNU-loaded Nano-co-Plex on human glioblastoma A170 cells 166

5.3. RESULTS AND DISCUSSION 167

5.3.1. *Ex Vivo* Evaluation of Mucoadhesive Strength of the Optimized Nanogel Composite 167

5.3.2. Calibration Curve of Iron 168

5.3.3. Assessment of the Permeation of the BCNU-Loaded Nano-co-Plex across the Rabbit Nasal Tissue 169

5.3.4. Assessment of the Magnetic Field Influence on the Cytotoxicity of BCNU-Loaded Nano-co-Plex on Human Glioblastoma A170 Cells 172

5.4. CONCLUDING REMARKS 173

5.5. REFERENCES..... 174

CHAPTER 6

IN VIVO EVALUATION OF THE OPTIMIZED NANOGEL COMPOSITE

6. CHAPTER 6 176

6.1. INTRODUCTION 176

6.2. MATERIALS AND METHODS 177

6.2.1. Materials 177

6.2.2. Animal Ethics Clearance 178

6.2.3. Preparation and Sterilization of Nanogel Composite 178

6.2.4. *In Vivo* Experimental Studies 178

6.2.4.1. Pilot studies for determining the workability and suitability of the application of electric stimulation and magnetic field. 178

6.2.4.2. In vivo experimental design and procedure for the studies 181

6.2.5. Quantitative Chromatographic Determination of BCNU in Plasma, CSF and the Brain Tissue of Rabbit 187

6.2.5.1. Development of a method for sample analysis employing Ultra Performance Liquid Chromatography 188

6.2.5.2. Extraction of BCNU from rabbit plasma and CSF for UPLC analysis……..... 188

6.2.5.3. Validation of liquid-liquid extraction procedure 189

6.2.5.4. Preparation of calibration curve 190

6.2.5.5. Determination of BCNU-NCP in the brain tissue employing Field Emission Electron Probe Micro Analyzer (FE EPMA) 191

6.2.5.6. Histopathological Evaluation of the Nasal Mucosa of the Rabbits 191

6.3. RESULTS AND DISCUSSION 191

6.3.1. Pilot Study to Assess the Effect of Electric Stimulation, Magnetic Headband and Fluid Sampling on the Rabbits 191

6.3.2. Drug Extraction, UPLC Method Validation and Assay Procedure..... 193

6.3.3. Concentration of BCNU in the blood, CSF and brain tissue of the rabbit model……..... 196

6.3.4. Assessment of BCNU-NCP in the Brain Tissue Employing Field Emission Electron Probe Micro Analyzer (FE EPMA)..... 205

6.3.5. Histopathological Evaluation of the Nasal Epithelia of the Rabbit..... 206

6.4. CONCLUDING REMARKS 208

CHAPTER 7
RECOMMENDATIONS AND FUTURE OUTLOOK

7. CHAPTER 7 211

7.1. RECOMMENDATIONS 211

7.2. FUTURE OUTLOOK 213

7.2.1. Hypothesis: Lactoferrin-Galantamine Proteo-Alkaloid Conjugate for The Management of Alzheimer's Disease 214

7.2.1.1. Introduction 214

7.2.1.2. The hypothesis 216

7.2.1.3. Evaluation of the hypothesis 216

7.2.1.4. Galantamine and Alzheimer's intervention 217

7.2.1.5. Lactoferrin and metal chelation 218

7.2.1.6. Lactoferrin-Galantamine Proteo-Alkaloid conjugate 219

7.2.2. Concluding Remarks 222

7.3. REFERENCES 222

APPENDICES

8. APPENDICES 228

8.1. APPENDIX A 228

8.1.1. Research Publications 228

8.1.1.1. Book chapter 228

8.1.1.2. Research paper 229

8.2. APPENDIX B 230

8.2.1. Abstracts of Research Outputs at Conference Proceedings 230

8.2.1.1. School of Therapeutic Sciences Research Day, University of the Witwatersrand, Johannesburg, South Africa, September 10, 2013, Poster presentation). 230

8.2.1.2. 6th Cross-Faculty Graduate Symposium, University of the Witwatersrand, Johannesburg, South Africa, September 17, 2014, (Poster presentation). 231

8.2.1.3. International Society of Biomedical Polymers and Polymeric Biomaterials, Orlando, Florida USA, 8th-10th July, 2015, (Poster presentation). 232

8.2.1.4. International Society of Biomedical Polymers and Polymeric Biomaterials, Orlando, Florida USA, 8th-10th July, 2015, (Podium presentatation). 233

8.2.1.5. Faculty of Health Sciences Research Day, University of the Witwatersrand, Johannesburg, South Africa, September 8-9, 2015. (Podium Presentation). 234

8.2.1.6. Academy of Pharmaceutical Sciences of South Africa, Johannesburg, South Africa, September 17-19, 2015, (Podium Presentation). 235

8.2.1.7. 7th Cross-Faculty Graduate Symposium, University of the Witwatersrand, Johannesburg, South Africa, March 2-3, 2016, (Podium presentation). 236

LIST OF FIGURES

Figure 1.1: Schematic conceptualization of design criteria for release of drugs using an external electric stimulation and a magnetic field 6

Figure 2.1: Lateral wall of the nasal cavity, and cross-sections through the internal ostium, the middle of the nasal cavity, and the choanae. Hatched area in the upper figure, olfactory region. NV, nasal vestibule, IT, inferior turbinate and orifice of the nasolacrimal duct; MT, middle turbinate and orifices of frontal sinus, anterior ethmoidal sinuses and maxillary sinus; ST, superior turbinate and orifices of posterior ethmoidal sinuses. Source (Mygind and Dahl, 1998). 19

Figure 2.2: Illustrations of the various types of cells in the olfactory region. Reproduced from (Mistry et al., 2009). 23

Figure 2.3: Possible transport pathways of a compound introduced into the nasal cavity. Adapted from (Graff and Pollack, 2005; Illum, 2004, 2003, 2000). 24

Figure 2.4: Showing fluorescently labeled siRNA distribution in the olfactory bulb of rat. Scale= 30µm: ONB=olfactory nerve bundle, OM=olfactory mucosa, CP=cribiform plate, ONL=olfactory nerve layer, GL=glomerular layer. Adapted from (Renner et al., 2012b). 28

Figure 2.5: Distribution and retention of Cy5.5-Lf in the brain following intranasal administration. Adapted from (Liu et al., 2013). 29

Figure 2.6: SEM image showing surface morphology of optimized bromocriptine loaded Chitosan nanoparticles. Adapted from (Shadab et al., 2012). 30

Figure 2.7: Dynamics of MPEG–PCL–Tat complex in brain tissue following intranasal and intravenous administration (Kanazawa et al., 2013). 31

Figure 2.8: Environmental scanning electron microscopy (ESEM) micrographs of unloaded (A) and UDCA–AZT loaded (B) SLMs based on tristearin (Dalpiaz et al., 2014). 33

Figure 2.9: TEM image of GH loaded flexible liposomes adapted from (W. Li et al., 2012) 35

Figure 3.1: Schematic of the synthesis of BCNU-loaded Nano-co-Plex. 80

Figure 3.2: FTIR spectra of a) synthesized magnetite, b) native PVA, c) native PEI, d) native FITC, e) BCNU, f) NCP-3 and g) BCNU-NCP-3. 82

Figure 3.3: ^{1}H NMR spectra of (a) PVA, (b) PEI and (c) Polyplex. The red circle and arrow indicating the new NH-CH_2 bond formed by the conjugation of PEI and PVA at peak 3.14 ppm. 83

Figure 3.4: TEM image of a) Uncoated magnetite, b), c) and d) BCNU-loaded Nano-co-Plex (BCNU-NCP-1, BCNU- NCP-2 and BCNU- NCP-3 respectively). The blue box in a) indicates uncoated particle while the red boxes in b), c) and d) indicate coated particles. 85

Figure 3.5: Zeta potential of a) synthesized magnetite b) Nano-co-Plex (NCP-3) and c) BCNU-loaded Nano-co-Plex (BCNU-NCP-3). 87

Figure 3.6: XRD spectra of uncoated Magnetite and Nano-co-Plex (NCP-1, NCP-2 and NCP-3). 88

Figure 3.7: TGA thermograms of a) uncoated magnetite and Nano-co-Plex b) NCP-1, c) NCP-2 and d) NCP-3. 89

Figure 3.8: Magnetization curve of the synthesized magnetite and that of the Nano-co-Plex (NCP-1, NCP-2 and NCP-3) measured at 25°C showing the hysteresis loop. 91

Figure 3.9: BCNU loading profile of Nano-co-Plex (NCP-1, NCP-2 and NCP-3)..... 93

Figure 3.10: *In vitro* release profile of BCNU-loaded Nano-co-Plex (NCP-1, NCP-2 and NCP-3). 94

Figure 3.11: Computational simulations of interaction profile of a) PVA and PEI, b) FITC and PEI and c) BCNU and PEI. The color codes for various elements are as

follows: Carbon=cyan, Nitrogen=blue, Oxygen=red, Sulphur=yellow and Hydrogen=white. 96

Figure 3.12: Cell viability of human glioblastoma A172 cell line treated with BCNU-NCP-1, BCNU-NCP-2, BCNU-NCP-3 and BCNU incubated at 37°C for 72 hours… 98

Figure 3.13: Fluorescent microscopy analysis of human glioblastoma A172 cell line treated with BCNU-NCP-1, BCNU-NCP-2 and BCNU-NCP-3 incubated at 37°C for 2 hours without and with application of magnet. 99

Figure 4.1: A schematic diagram depicting the electro-stimulation *in vitro* release experimental setup. 113

Figure 4.2: Residual plots of (a) average release per cycle, (b) conductivity and (c) mucoadhesion. 122

Figure 4.3: Response surface plots showing the effects of F127, CS and PANI on (a) electro-responsive drug release, (b) conductivity and (c) mucoadhesion. 123

Figure 4.4: Response Optimization output plot by desirability function with the values of independent variables and predicted values of the responses of Nanogel Composite. 124

Figure 4.5: Percentage of mucin adsorbed by the 15 formulations. 125

Figure 4.6: Electrical conductivity of the 15 formulations of the Nanogel Composite 128

Figure 4.7: BCNU-NCP release profiles in simulated nasal fluid (pH 6.0) for Formulations 1-15. 130

Figure 4.8: Tensile detachment measurement displaying Maximum force of adhesion of the Nanogel Composite formulations from rabbit nasal mucosal tissue wetted with simulated nasal buffer at pH 6.0 (SD≤ 0.015; N=5). 132

Figure 4.9: The total work of adhesion for removing Nanogel Composite from rabbit nasal mucosal tissue wetted with simulated nasal buffer at pH 6.0 (SD≤ 0.00997; N=5). 132

Figure 4.10: FTIR spectra of a) HPMC, b) PANI, c) CS and d) F127. 133

Figure 4.11: FTIR spectra of a) F127, b) TERM and c) Nanogel Composite..... 136

Figure 4.12: XRD spectra of the Nanogel Composite (black), F127 (red), CS (green), PANI (blue) and HPMC (purple). 137

Figure 4.13: TGA thermograms of a) Nanogel Composite, b) F127, c) CS, d) HPMC and f) PANI..... 138

Figure 4.14: DSC thermogram of Nanogel Composite (black), F127 (red), CS (green), PANI (blue) and HPMC (purple). 139

Figure 4.15: SEM images of native a) F127, b) CS, c) HPMC and d) PANI. Magnification=740x. 141

Figure 4.16: SEM images of a) TERM b) cross section view of TERM, c) Nanogel Composite before application of electrical stimulation and d) Nanogel Composite after application of electrical stimulation and 5 released cycle. Magnification=740x. 142

Figure 4.17: Isotherm linear plots of a) TERM, b) Nanogel Composite before application of electrical stimulation and c) Nanogel Composite after application of electrical stimulation. (N_2 adsorption in red and desorption in burgundy color). 143

Figure 4.18: Test tube inverted method for the determination of gelation temperature, a) before gelation at room temperature and b) immediately after gelation at 29±1°C. 145

Figure 4.19: Rheogram of viscosity as a function of shear rate of Nanogel Composite and F127. 146

Figure 4.20: Rheogram of Yield stress of Nanogel Composite and F127..... 147

Figure 4.21: Rheogram of oscillation stress sweep of Nanogel Composite and F127. 148

Figure 4.22: Frequency sweep rheogram of Nanogel Composite and F127. 149

Figure 4.23: Rheogram of creep recovery test for the Nanogel Composite and F127. 150

Figure 4.24: Rheogram of temperature ramp of Nanogel Composite and F127..... 151

Figure 4.25: Rheogram showing G'G" plot against temperature for a) F127 and b) Nanogel Composite..... 152

Figure 4.26: Voltammogram of a) PANI and b) Nanogel Composite..... 154

Figure 4.27: The three forms of PANI showing their transition and reversible states 154

Figure 4.28: BCNU-NCP release profile in simulated nasal fluid (pH 6.0)..... 156

Figure 4.29: *In vitro* BCNU release profile from the BCNU-NCP for a period of 6 hours..... 156

Figure 5.1: Schematic diagram of side-by-side diffusion cell..... 165

Figure 5.2: Calibration curve of iron 169

Figure 5.3: Permeation curve showing the cumulative amount of BCNU-NCP Permeated across the nasal epithelial tissue of rabbit at 34±1°C in a diffusion cell. Data are expressed as mean ± SD (N=3). 170

Figure 5.4: effect on toxicity of human glioblastoma A172 cell line showing the control treatment, treated with NCP, BCNU, BCNU-NCP and BCNU-NCP (with magnetic field) incubated at 37°C for 72 hours. 173

Figure 6.1: Digital images of a) application of electric stimulus on the nose and b) Magnetic Headband fitted on the head of the rabbit..... 180

Figure 6.2: A digital image depicting the conditions under which the rabbits were housed in a vivarium according to ARVO Resolution guidelines..... 181

Figure 6.3: Schematic diagrams showing the outline summary of the in vivo animal studies..... 183

Figure 6.4: Digital images of the procedure for withdrawing CSF from the rabbit showing a) shaving of the back of the neck of rabbit, b) shaved area, c) insertion of needle directed towards the nose of the rabbit and d) the withdrawal of CSF with the aid of 1mL syringe). 184

Figure 6.5: Photographic evidence of (a) Housing of the rabbits (b) preparation for surgery with anesthetization (c) intravenous dosing (d) intranasal dosing e) application of ES (f) blood withdrawal (g) CSF withdrawal (h) administration of oxygen after dosing and sampling (i) rabbit recovering from sedation. 187

Figure 6.6: Typical chromatogram displaying a) the spiking plasma separation of the Gal, b) BCNU and c) the separation of both Gal and BCNU after plasma extraction. 193

Figure 6.7: Typical chromatogram depicting a) the spiking CSF separation of the Gal, b) BCNU and c) the separation of both Gal and BCNU after CSF extraction. 195

Figure 6.8: Calibration curve of BCNU at 230nm. 196

Figure 6.9: Mean BCNU concentration-time profile in plasma after IV injection of the conventional BCNU, IN administration of Nanogel Composite without application of ES/MFand IN administration of Nanogel Composite with the application of ES/MF (SD≤ 0.053; N=5 at each time point). 197

Figure 6.10: Mean BCNU concentration–time profile in CSF after IV injection of conventional BCNU, IN administration of Nanogel Composite without application of ES and IN administration of Nanogel Composite with the application of ES and MF at 1mg/kg dose in rabbits. (SD≤ 0.051; N=5 at each time point). 199

Figure 6.11: Percentage of BCNU released in CSF following IN administration. (SD≤ 0.051; N=5 at each time point). 200

Figure 6.12: Mean BCNU concentration–time profile in Brain after IV injection of the conventional BCNU, IN administration of Nanogel Composite without application of ES and IN administration Nanogel Composite with the application of ES and MF at 1mg/kg dose in rabbits. (SD≤ 0.05; N=5 at each time point). 201

Figure 6.13: BCNU concentration in the Plasma, CSF and Brain tissue after IV injection of conventional BCNU. 203

Figure 6.14: BCNU concentration in the Plasma, CSF and Brain tissue after IN administration of Nanogel Composite with application of ES and MF. 204

Figure 6.15: BCNU concentration in the plasma, CSF and brain tissue after IN administration of Nanogel Composite without application of ES and MF. 204

Figure 6.16: Comparison of the concentration of BCNU in CSF and brain following IV of conventional BCNU and IN administration of Nanogel Composite with application of ES and MF. 205

Figure 6.17: FE EPMA spectra of brain tissue of rabbit after IN administration of Nanogel Composite for Fe detection. 206

Figure 6.18: Histological evaluation of nasal epithelia tissue samples from rabbits showing light digital microscopic images of the H&E stained slides of a) normal nasal epithelia tissue, b) placebo sample, c) control group sample and d) experimental group sample. Magnification is x10. 208

Figure 7.1: Molecular structure of Galantamine 213

Figure 7.2: Schematic diagram of the mechanism of release of Galantamine and absorption of iron by Lf-Gal conjugate..... 221

Figure 7.3: Schematic diagram demonstrating the potential neuroprotective-neurotherapeutic interventional mechanism of the lactoferrin-galantamine conjugate. 221

LIST OF TABLES

Table 2.1: Advantages and Limitation of Intranasal Drug Administration. 21

Table 2.2: Review of recent development in nasal sprays for delivery of therapeutic agents. 38

Table 2.3: Review of recent development in nasal gel for delivery of therapeutic agents 39

Table 2.4: Review of recent development in nasal powder for delivery of therapeutic agents. 40

Table 2.5: Review of recent development in nasal liposomes for delivery of therapeutic agents. 41

Table 2.6: Review of recent development in microspheres for nasal delivery of therapeutic agents. 42

Table 2.7: Summary of recent development in nanoparticles for intranasal delivery of therapeutic agents. 44

Table 2.8: Summary of recent development in microemulsion for intranasal delivery of therapeutic agents. 45

Table 2.9: Review of recent development in nanoemulsion for nasal delivery of therapeutic agents. 46

Table 3.1: Formulation percentage ratio of conjugated polymers used 71

Table 3.2: DPBS, NCP, BCNU-NCP and BCNU contents distribution in each plate 76

Table 3.3: Percentage weight loss of the synthesized magnetite and the various formulations. 89

Table 4.1: Lower and upper limits of the variables employed for the Box- Behnken design 109

Table 4.2: Series of formulations statistically generated by the Box–Behnken design. 110

Table 4.3: X-ray diffraction parameters 111

Table 4.4: The parameter settings for the mucoadhesion analysis of the Nanogel Composite. 115

Table 4.5: Porositometry parameters employed in the measurement of TERM/Nanogel Composite 116

Table 4.6: The parameter settings for the rheological analysis of Nanogel Composite and F127. 118

Table 4.7: Formulations and their corresponding responses 121

Table 4.8: Gelation temperature of the 15 formulations 126

Table 4.9: FTIR spectra of HPMC, PANI, CS and F127 showing their major characteristic native bands. 134

Table 4.10: Results of the porosity analysis of the TERM and the Nanogel Composite 144

Table 5.1: Assessment procedures used in the permeation studies 165

Table 5.2: Distribution of DPBS, NCP, BCNU-NCP and BCNU contents in individual plate. 167

Table 5.3: Flux, Permeability coefficient and Enhancement ratio for permeation of BCNU-NCP through the nasal tissue of New Zealand white rabbit. 172

Table 6.1: Details of drugs, anesthetics, analgesics and other medicinal or experimental substances used, including the doses and routes of administration . 178

Table 6.2: Weight of the three rabbits on day of arrival and a day prior to procedure. 179

Table 6.3: UPLC parameters employed for the determination of BCNU concentration 188

LIST OF EQUATIONS

Equation 3.1 77

Equation 4.1 116

Equation 4.2 117

Equation 4.3 117

Equation 5.1 166

Equation 5.2 166

Equation 5.3 166

Equation 6.1 190

LIST OF ABBREVIATIONS

AESC	Animal Ethics Screening Committee
BBB	Blood-Brain Barrier
BET	Brunauer-Emmett-Teller
BHN	Brinell Hardness Number
BCNU	Carmustine
BCNU-NCP	Carmustine-loaded Nano-co-Plex
CAS	Central Animal Service
CSF	Cerebrospinal Fluid
CV	Cyclic Voltammetry
ES	Electric Stimulation
F127	Pluronic F127
FE EPMA	Field Emission Electron Probe Micro Analyzer
FTIR	Fourier Transform Infrared Spectroscopy
FITC	FIuorecein isothiocyanate
Gal	Galantamine
HG	Human Glioblastoma
HPLC	High Performance Liquid Chromatographic
HPMC	hydroxypropyl methylcellulose
IN	Intranasal
IS	Internal Standard
MF	Magnetic Field
NCP	Nano-co-Plex
NMR	Nuclear Magnetic Resonance

PANI	Polyaniline
PD	Potential Difference
PEI	Polyethyleneimine
PVA	Polyvinyl alcohol
SEM	Scanning Electron Microscopy
SQUID	Superconducting Quantum Interference Device
TEM	Transmission Electron Microscopy
TERM	Thermosensitive Electro-Responsive Mucogel
TGA	Thermogravimetric analysis
UPLC	Ultra Performance Liquid Chromatographic
UV	Ultraviolet-visible
WITS	Witwatersrand University
XRD	X-ray Diffractometry

CHAPTER 1

INTRODUCTION

1.1. BACKGROUND TO THIS STUDY

Delivery of drugs to the brain has been fraught with issues of low bioavailability. This is due to the impervious nature of the Blood-Brain-Barrier (BBB). The BBB consists of an endothelial membrane separating the systemic circulation and central interstitial fluid (Pardridge, 1999). The vasculature serving the Central Nervous System (CNS) has capillaries with tight junctions preventing permeation of drugs. The BBB also comprises a double layered structure called the arachnoid membrane, which acts as a barrier between the blood and Cerebrospinal Fluid (CSF) (Vyas et al., 2005a). These characteristics of the BBB restrict the movement of molecules from the general circulation to the brain and spinal cord (Lerner et al., 2004). The BBB usually restricts the passage of hydrophilic substances from the blood to the brain but allows certain lipophilic substances to pass through to the brain (Sharma et al., 2015). The development of therapies to treat brain diseases has long been frustrated by the failure of systemically administered drugs to permeate the brain. The delivery mechanism through the BBB and the physicochemical properties of the molecule of the drug are factors that must be considered when designing drug delivery systems for brain targeting.

The systemic delivery of drugs through the oral, intravenous and the transdermal routes requires drug to pass through the blood circulation in order to reach the brain, and it is fraught with the challenge of passing through the BBB. The delivery of drugs using intranasal delivery has been explored by a number of investigators as it is purportedly a more reliable method for drug delivery to the brain than the systemic administration (Serralheiro et al., 2015; Mistry et al., 2015; Nasr, 2015; Serralheiro et al., 2014). This is due to its ability to bypass the BBB and directly propel the drugs through the olfactory lobe to the brain which enhances their bioavailability. Many therapeutic agents such as peptides and proteins which are poorly absorbed orally and extensively metabolized in the gastrointestinal tract

(GIT) and the liver have been found to be ideally delivered through the nasal route. Advantages of intranasal delivery over other routes of delivery include; 1) non-invasiveness, 2) affords direct delivery of drug to brain by circumventing theBBB, 3) targeted delivery to the brain is possible, 4) rapid delivery, low toxicity and side effects, 5) by-passes first-pass metabolism, and 6) provides a larger surface area for drug delivery.

Comparative studies of the nasal route and other routes of administration such as intravenous, oral and transdermal have been explored (Lalatsa et al., 2014; Kumar et al., 2008a; Westin et al., 2005). It was observed that the nasal route was more efficient in delivering a wide range of therapeutic compounds including peptides and proteins in the presence of permeation enhancers resulting in higher bioavailability (Costantino et al., 2007; Türker et al., 2004). The drug uptake into the brain from the nasal mucosa mainly occurs via two different pathways. One is the systemic pathway by which some of the drugs administered into the nasal cavity are absorbed into the systemic circulation via the blood-rich vessels and capillaries of the nasal mucosa. The other is the olfactory pathway by which the drug travels from the nasal cavity directly to CSF and brain tissue (Mistry et al., 2009; Seju et al., 2011; Shah et al., 2015; Vyas et al., 2005b).

Almost all research in intranasal drug delivery have employed the mechanism of passive diffusion that relies mainly on a combination of proper drug instillation deep in the nasal cavity, gravity, and the properties of the neuro-epithelium to gain access to the CNS. However, a substantial quantity of drugs goes through the systemic pathway thereby reducing the quantity via the olfactory pathway (Kumar et al., 2008a). Such phenomenon is a limitation in the intranasal delivery of drugs directly to the brain as this reduces the bioavailability of the drugs delivered to the brain. Furthermore, there has been no controlled way in which the therapeutics get delivered to the brain when they are introduced into the nasal cavity. Furthermore, drugs meant for direct nose-to-brain delivery should have a protective embodiment that can entrap/encapsulate the therapeutic substances whilst in the nasal cavity. There is therefore a need for the drugs to be protected whilst in the nasal cavity and be delivered into the brain in a controlled manner in conjuction with a ‘driving

force' that can propel the drugs directly to the brain after being released in the nasal mucosa.

The use of electroactive polymers as a protective embodiment as well as in release of therapeutics when external electric stimulus is applied may be very useful. The use of magnetic nanoparticles in fabricating the drug delivery systems, which on application of magnetic field may act as a 'driving force', has the potential of guiding and propelling the drugs to the brain via the olfactory pathway and therefore bypassing the systemic pathway. This will improve the bioavailability of drugs in the CNS. It is envisaged that the application of an external electric and magnetic fields may cause controlled release and uptake of drugs through the olfactory pathway thereby circumventing the BBB thus enhancing the delivery and subsequent distribution of drug within the brain.

Learner and coworkers (2004) investigated a method to increase intranasal delivery and drug distribution within the brain using iontophoresis, to actively drive drug movement across an electric field to the brain. In their method, electrodes containing a drug reservoir were applied to the nasal neuro-epithelium of the rabbit with a return electrode placed at the back of the rabbit's head. Upon the application of a relatively small sustained current, charged drug molecules were driven from the nasal cavity into the brain. This method actually allows the passage of more drugs to the brain compared to other methods. However, the method is cumbersome and invasive since electrodes have to be inserted deep into the nasal cavity and patience non-compliance is envisaged. Therefore, a drug delivery device administered via the intranasal route which applies electric and magnetic fields, and is not cumbersome and invasive, for targeted brain delivery is paramount for the management of CNS diseases in order to enhance the bioavailability of drug in the brain. Hence this study was undertaken to explore the use of electro-active polymers to formulate an electro-responsive gel and containing drug-loaded magnetic nanoparticles which in the presence of an external electric stimulus, control the release of drug and the presence of external magnetic field enhances rapid transportation of the drug-loaded nanoparticles to the brain and CNS via the olfactory pathway.

1.2. RATIONALE AND MOTIVATION FOR THIS STUDY

This study proposed to develop an electro-magneto-responsive polymeric drug delivery system by exploring the use electro-active polymers which are polymers that respond to external electric stimulations. These polymers include polyaniline (PANI), polypyrrole (PPy), ethylene vinyl acetate (EVA), polyethylene, polylactic acid (PLA), polyglycolic acid (PGA), polylactic-co-glycolic acid (PLGA), and polythiophene which could be employed in preparing a drug delivery system for direct delivery of therapeutics to the brain through the nasal mucosa. A number of these polymers were explored in designing the intranasal drug delivery system described herein. The applications of these polymers are mostly in the production of artificial muscles. On application of an electric field these polymers are able to swell and/or contract. Such physicochemical changes are converted into mechanical work in a muscle actuator. This concept was employed in designing a drug delivery system that can deliver therapeutic drugs directly to the brain through the nasal cavity.

Magnetic nanoparticles were fabricated by employing substances and compounds which possess the capacity to respond to a magnetic field. Such substances include iron and gadolinium compounds. These compounds were employed to develop the magnetic nanoparticles using techniques such as co-precipitation in an alkaline medium. The magnetic nanoparticles were coated with biodegradable and biocompatible polymers such as polyvinyl alcohol (PVA), poly ethylene glycol (PEG), polyethyleneimine (PEI) and loaded with the therapeutic agents. Due to the magnetic property of the nanoparticles, it is anticipated that the nanoparticles would move in the direction of the magnetic field which would be positioned on the patient's head in the form of a headband for a nose-to-brain delivery. The target size of the nanoparticles was less than 200nm. The driving force which is the magnetic field would create a 'pulling' effect on the nanoparticles attracting them towards the brain. By so doing it was envisaged that the nanoparticles would bypass the systemic pathway for uptake of drugs into the brain through the olfactory pathway thereby circumventing the BBB since most of the nanoparticles would migrate rapidly to the brain through the olfactory pathway. When the

nanoparticles reach the brain, the drug would be released by dissolution and diffusion into the cells thereby evading the BBB.

The magnetic nanoparticles would be subsequently incorporated into a gel. The gel was fabricated employing thermosensitive and mucoadhesive polymers in addition to the electroactive polymers, this was to enable the gel to be liquid at room temperature and then gel at physiological temperature for ease of administration. This gel would possess mucoadhesive capabilities in order to provide a long residence time in the nasal mucosa. In developing the electro-responsive gel, the electroactive polymer would be incorporated or blended homogenously with the other polymers such as chitosan and hydroxypropyl methylcellulose using techniques such as polymer blending, copolymerization or crosslinking to generate an inter-penetrating network that would erode degrade or dissociate in the presence of an electric field. When the gel erodes, degrades or dissociates, the drug-loaded nanoparticles embedded within the gel would be released and in the presence of external magnetic field, the drug-loaded nanoparticles would migrate rapidly to the brain through the olfactory pathway with the aid of external magnetic field.

The gel was employed to control the release of the drug-loaded nanoparticles for 24 hours as well as confine the drug-loaded nanoparticles in the nasal region to prevent premature clearance into the tracheal region as the patient breathes. The gel should be thermosensitive, and thermoreversible, possessed mucoadhesion capability and responded to an applied external electric field. The use of self-adhesive patch electrodes and a magnetic headband were employed to create an electric and magnetic field respectively. The electric field was required to dissociate or degrade the gel and transport the drug-loaded nanoparticles through the olfactory pathway to the brain. The self-adhesive patched electrode would be placed on the nose of the patient to generate an electric field creating an electric stimulus that dissociated or degraded the polymeric gel to release the drug-loaded nanoparticles. The magnetic headband would be able to generate magnetic fields thereby attracting the nanoparticles towards the brain for a nose-to-brain drug delivery. On reaching the brain, the nanoparticles were anticipated to circumvent

the BBB and then release the drugs in the brain cells. Figure 1.1 shows a schematic of the design. The nanoparticles were labelled with fluorescent markers such as fluorescein isothiocyanate (FITC) to aid imaging of the transport and bio-distribution of the nanoparticles.

This drug delivery system may find applications in CNS diseases such as Alzheimer's and Parkinson's disease, schizophrenia, stroke, epilepsy, AIDS dementia Complex and brain tumor wherein drugs such as Galantamine, Levodopa, Clozapine, Alteplase, Clopidogrel, Zidovudine and Carmustine may be suitably incorporated into the nanoparticles. It is envisaged that the proposed drug delivery system, by circumventing BBB, will improve the bioavailability of CNS drugs thereby enhancing the pharmacological management of CNS diseases using an intranasal drug delivery system.

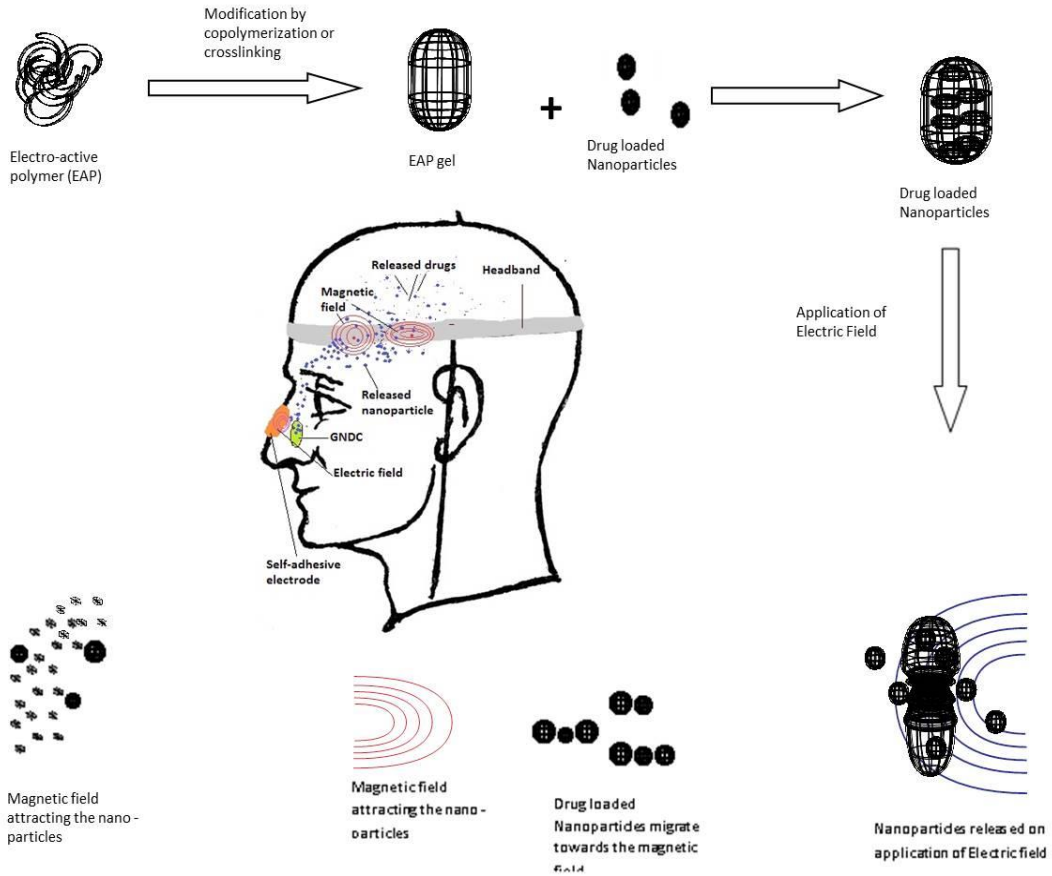

Figure 1.1: Schematic conceptualization of design criteria for release of drugs using an external electric stimulation and a magnetic field

1.3. AIM AND OBJECTIVES

The aim of this study was to design an intranasal drug delivery system that encompasses drug loaded magnetic nanoparticles which are incorporated into a thermosensitive electro-responsive mucoadhesive gel for controlled and targeted “nose-to-brain” delivery of therapeutic agents via the olfactory pathway with the aid of an external electric and magnetic fields for enhanced delivery. Figure 1 provides a schematic conceptualization of the design criteria for drug release using an electric and magnetic fields as examples of applied stimuli. In order to achieve this aim, the following objectives were fulfilled:

1. To undertake preliminary studies on the electro-active, mucoadhesive and thermosensitive polymers including modification of these polymers using techniques such as blending, copolymerization and crosslinking to assess their suitability for the development of a responsive gel.

2. To characterize the selected polymers employed in the formulation of the gel, using various techniques such as, Fourier Transform Infrared Spectroscopy (FTIR), Differential Scanning Calorimetry (DSC), Thermogravimetric Analysis (TGA) and Scanning Electron Microscopy (SEM).

3. To fabricate stimuli-responsive polymeric nanostructures such as magnetic responsive nanoparticles via precipitation, chemical crosslinking, solvent evaporation/emulsification. The nanostructures were labelled using fluorescent markers such as fluorescein isothiocyanate (FITC), to aid imaging and detection of the bio-distribution of the nanostructures.

4. To incorporate a drug model such as carmustine, galantamine, levodopa, clozapine, alteplase, clopidogrel or zidovudine in the nanostructures for the treatment of brain tumors, Alzheimer’s diseases (AD), Parkinson’s, Schizophrenia, Stroke, epilepsy or AIDS dementia Complex, respectively.

5. To evaluate the physicochemical and electro-active properties of the nanogel using rheological and textural profiling analyses, as well as cyclic voltammetry in order to further characterize the nanogel.

6. To evaluate the physicochemical properties of the nanostructures using zetasize and zeta potential analyses, surface morphological characterization, drug loading/entrapment efficiency and conductivity analysis.

7. To assess *in vitro* drug release from the nanogel in the presence of various stimuli such as electric field and determine the optimum parameter required for the release and transport of nanostructures from the gel into the brain with the aid of an external magnetic field.

8. To undertake *in vivo* studies using New Zealand White rabbits to assess the performance of the novel intranasal drug delivery system, and evaluate the influence of an electric and magnetic stimuli.

1.4. NOVELTY OF THIS WORK

The following points highlight the novelty of this research.

1. Design and formulation of novel nanoparticles employing polyvinyl alcohol (PVA), polyethyleneimine (PEI) and fluorescein isothiocyanate (FITC) referred to as Polyplex.

2. Coating of iron oxide nanoparticles with the Polyplex to form a Nano-co-Plex with the capability of significant drug loading and release. The drug-loaded Nano-co-Plex possesses the ability to respond to magnetic field.

3. Formulation of a thermosensitive electro-responsive mucogel (TERM) as an *in situ* intranasal drug delivery system that is liquid at room temperature and can form a gel at physiological temperature. The gel has the ability to control the release of therapeutic agents incorporated in it upon the application of external

electrical stimulus. The released therapeutic agents have the potential to be attracted to the brain via the olfactory pathway with the aid of an external magnetic stimulus. The electrical stimulus is in form of a self-adhesive electrode and the magnetic stimulus is in form of a magnetic headband.

4. The use of electrical stimulation on the nose in form of patched electrode to actuate controlled release of drug from the nasal mucosa.

5. The use of a magnet in form of a magnetic headband to enhance rapid migration of the drug-loaded nanoparticles to the brain after being released in the nasal cavity via the olfactory pathway.

1.5. OVERVIEW OF THIS THESIS

Chapter 1 provides an introduction and background of the study, delineating the challenges experienced with delivering drug to the brain due to BBB. The use of intranasal drug delivery as alternative to systemic delivery was enumerated. The rationale and motivation for this research as well as the aim and objectives are outlined in this chapter.

Chapter 2 provides a literature review, focusing on intranasal delivery of drugs for nose-to-brain delivery employing the olfactory route for the management of brain diseases. Techniques employed to fabricate and evaluate the intranasal drug delivery was enumerated.

Chapter 3 provides a description of the synthesis of Nano-co-Plex by exploring the use of magnetic iron oxide nanoparticles and coated with Polyplex which was sythesized from PVA, PEI and FITC conjugate, loaded with carmustine (BCNU), an effective brain tumor chemotherapeutic agent. Detailed characterization of the Nano-co-Plex was carried out. *In vitro* drug release and cell studies were undertaken to determine the cytotoxicity and cellular uptake, as well as internalization of the drug-loaded Nano-co-Plex, in the absence and presence of a magnetic field.

Chapter 4 provides a description of formulating a thermosensitive electro-responsive mucogel (TERM) as a potential controlled intranasal drug delivery system, possessing mucoadhesive properties, which responds to an external electric field in releasing therapeutic agents. The carmustine-loaded Nano-co-Plex was incorporated into the gel to formulate the Nanogel Composite. A Design of Experiment (DoE) was extensively evaluated using a Box-Behnken Experimental Design (BBED). The BBED desirability function was employed to generate an optimized Nanogel Composite. Furthermore, this chapter deals with the physicochemical and physicomechanical characterization of the optimized Nanogel Composite. Chemical structure evaluation was undertaken using FTIR, XRD and NMR analyses. DSC and TGA were used to evaluate the thermal behaviour of the Nanogel Composite. SEM and porositometry analyses were undertaken to assess the surface morphology. Rheological evaluation was used to assess the viscoelastic properties and the gelation temperature of the Nanogel Composite. Cyclic voltammetry and conductivity analyses were employed to observe the electro-activity of the formulation. Texture profiling was undertaken to evaluate the mucoadhesive strength of the Nanogel Composite. *In vitro* studies were undertaken on the Nanogel Composite using an electrical stimulation to assess the release characteristics of the formulation.

Chapter 5 provides the *ex vivo* evaluation of Nanogel Composite using an excised nasal epithelial tissue of New Zealand White rabbit. The *ex vivo* permeation studies were conducted to ensure the viability of the application of an electric stimulation on Nanogel Composite to release BCNU-loaded Nano-co-Plex. Furthermore, the effect of a magnetic field on the transportation of the BCNU-loaded Nano-co-Plex across the nasal epithelial tissue of rabbit was evaluated. This study represents a prototype investigation prior to *in vivo* studies.

Chapter 6 details the *in vivo* performance of the optimized Nanogel Composite in comparison to the conventional drug available on the market. *In vivo* studies were carried out using New Zealand White rabbits. The effect of electric stimulation on the release behaviour of the nanoparticles and the effect of magnetic field on the

transport of the nanoparticles to the brain via the olfactory pathway were evaluated.

Chapter 7 provides recommendations and future outlook of the study. A hypothesis based on “Proteo-Alkaloid” conjugation of Lactoferrin (Lf) and Galantamine (Gal) via the self-assembly functionality of Lf was postulated. The hypothesis explored the combination of these two compounds as one dosage form, taking into consideration their iron and free radical scavenging abilities. A dual neuroprotection and neurotherapeutic interventional approach was postulated.

1.6. CONCLUDING REMARKS

The novel thermosensitive electro-responsive mucogel containing drug-loaded magnetic nanoparticles can be considered as an alternative therapy for circumventing the BBB. The novel development has the potential to increase bioavailability of drugs to the brain via a direct nose-to-brain delivery. It is therefore envisaged that this system is a promising technology for non-invasive treatment of brain diseases and disorders.

1.7. REFERENCES

Costantino, H.R., Illum, L., Brandt, G., Johnson, P.H., Quay, S.C., 2007. Intranasal delivery: physicochemical and therapeutic aspects. Int. J. Pharm. 337, 1–24.

Kumar, M., Misra, A., Babbar, A., Mishra, A., Mishra, P., Pathak, K., 2008. Intranasal nanoemulsion based brain targeting drug delivery system of risperidone. Int. J. Pharm. 358, 285–291.

Lalatsa, A., Schatzlein, A.G., Uchegbu, I.F., 2014. Strategies to Deliver Peptide Drugs to the Brain. Mol. Pharm. 11, 1081–1093. doi:10.1021/mp400680d

Lerner, E.N., van Zanten, E.H., Stewart, G.R., 2004. Enhanced delivery of octreotide to the brain via transnasal iontophoretic administration. J. Drug Target. 12, 273–280.

Mistry, A., Stolnik, S., Illum, L., 2015. Nose-to-Brain Delivery: Investigation of the Transport of Nanoparticles with Different Surface Characteristics and Sizes in Excised Porcine Olfactory Epithelium. Mol. Pharm. 12, 2755–2766.

Mistry, A., Stolnik, S., Illum, L., 2009. Nanoparticles for direct nose-to-brain delivery of drugs. Int. J. Pharm. 379, 146–157.

Nasr, M., 2015. Development of an optimized hyaluronic acid-based lipidic nanoemulsion co-encapsulating two polyphenols for nose to brain delivery. Drug Deliv. 0, 1–9.

Pardridge, W.M., 1999. Non-invasive drug delivery to the human brain using endogenous blood–brain barrier transport systems. Pharm. Sci. Technol. Today 2, 49–59.

Seju, U., Kumar, A., Sawant, K.K., 2011. Development and evaluation of olanzapine-loaded PLGA nanoparticles for nose-to-brain delivery: *In vitro* and in vivo studies. Acta Biomater. 7, 4169–4176.

Serralheiro, A., Alves, G., Fortuna, A., Falcão, A., 2015. Direct nose-to-brain delivery of lamotrigine following intranasal administration to mice. Int. J. Pharm. 490, 39–46.

Serralheiro, A., Alves, G., Fortuna, A., Falcão, A., 2014. Intranasal administration of carbamazepine to mice: A direct delivery pathway for brain targeting. Eur. J. Pharm. Sci. 60, 32–39.

Shah, B.M., Misra, M., Shishoo, C.J., Padh, H., 2015. Nose to brain microemulsion-based drug delivery system of rivastigmine: formulation and ex-vivo characterization. Drug Deliv. 22, 918–930.

Sharma, U., Badyal, P.N., Gupta, S., 2015. Polymeric Nanoparticles Drug Delivery to Brain: A Review 2, 60–69.

Türker, S., Onur, E., Ózer, Y., 2004. Nasal route and drug delivery systems. Pharm. World Sci. 26, 137–142.

Vyas, T.K., Shahiwala, A., Marathe, S., Misra, A., 2005a. Intranasal Drug Delivery for Brain Targeting. Curr. Drug Deliv. 2, 165–175.

Vyas, T.K., Shahiwala, A., Marathe, S., Misra, A., 2005b. Intranasal Drug Delivery for Brain Targeting. Curr. Drug Deliv. 2, 165–175.

Westin, U., Piras, E., Jansson, B., Bergström, U., Dahlin, M., Brittebo, E., Björk, E., 2005. Transfer of morphine along the olfactory pathway to the central nervous system after nasal administration to rodents. Eur. J. Pharm. Sci. 24, 565–573.

CHAPTER 2

A REVIEW OF NOSE-TO-BRAIN NEUROTHERAPEUTIC INTERVENTIONS

2.1. INTRODUCTION

Delivery of drugs to the brain has been fraught with issues of low bioavailability (Krol, 2012). The central nervous system (CNS) which is made up of the brain and the spinal cord do not have adequate access to the blood compartment due to the Blood-Brain Barrier (BBB) and other barriers. CNS disorders have been recorded as the number one source of disability and account for more extended care and hospitalizations than the combination of most other diseases (Misra et al., 2003). For instance, over 36 million people in the world today have CNS related diseases and disorders, the numbers will continue to rise to about 66 million by 2030, and projected to be around 115 million by 2050 (Liu et al., 2013). Treating CNS disorders and ailments in general which include Alzheimer's disease, Parkinson's, Schizophrenia, Stroke, epilepsy, AIDS dementia Complex, brain tumor and Huntington disease is extremely challenging due to the presence of various obstacles that restrict passage of drug across the BBB for onward delivery to the brain (Radhika et al., 2011).

The BBB which is both physiologically and anatomically a biological natural occurrence with no single scientific theory to explain all the events happening therein (Roth and Barlow, 1961) according to Roth and Barlow five decades ago, the challenges are still on even as of today. Researchers are therefore searching for the best methods to develop drug delivery systems and techniques to transfer pharmaceutical substances to the brain and CNS for the management of neurodegenerative disorders and delivery of drugs to the brain and the CNS in general having in mind the BBB obstacle. Lipophilic substances with molecular weight less than 600 Da are known to permeate the BBB, which implies that the more lipophilic the drug molecules the better the permeability of the drug, the use of prodrug will be an excellent approach in increasing the permeability, the prodrug on getting to the brain will be converted to the parent drug (Illum, 2000). Several

attempts and strategies such as disturbing the BBB (Alves, 2014), carrier mediated drug delivery osmotic BBB disruptions (Aryal et al., 2014), biochemical BBB disruption (Griep et al., 2013), drug manipulations including prodrugs, receptor-mediated drug delivery, chemical drug delivery, vector-mediated drug delivery (Lu et al., 2014), alternative routes such as intraventricular and intrathecal route, olfactory pathway, other techniques include injections, catheters, and pumps technique, implant of device directly to the brain, biodegradable polymer wafers, microspheres and nanoparticles techniques, have been explored (Misra et al., 2003). The use of intranasal route has been explored by various researchers and has been established to be a promising route of transferring therapeutic substances directly to the brain by employing the olfactory pathway through the nasal mucosa in order to bypass the BBB and its associated problems.

2.2. BIOLOGICAL BARRIERS AS AN IMPEDIMENT TO CNS DRUG DELIVERY

There are biological barriers limiting the delivery of drugs to the CNS thereby contributing to the difficulties in treating CNS diseases and disorder. Due to these biological barriers, transcranial drug delivery has been used to overcome these barriers. This approach entails three types of delivery systems which are; intra-cerebroventricular injection, convection enhanced diffusion and intracerebral implantation. These methods however require an invasive approach through into the brain. Implantation of transcranial catheters has been confirmed to be connected to numerous complications and is known to be temporary (Bleier et al., 2013). These barriers are enumerated below.

2.2.1. Blood-Brain Barrier

Knowledge about the BBB might assist researchers in designing better drugs or approaches in fabricating systems for delivering therapeutic agents to the brain. The BBB is a special membranous barrier that distinguishes the CNS from the systemic circulation (Begley, 1996; Misra et al., 2003; Schlosshauer and Steuer, 2002). The BBB is naturally designed to protect the brain from foreign organisms and deleterious chemicals in the blood, but allows the supply of necessary

nutrients to the brain for the well-being of the brain to maintain and regulate the microenvironment for accurate neuronal signaling (Abbott et al., 2010) and other functions. The protection of the Brain and the CNS is sorted by the barrier function of the brain capillary endothelial and the choroid epithelial cells. The blood capillaries of the brain are anatomically different from that of other tissues and organs. The blood capillaries consist of special cells known as endothelial cells; these cells are sealed with tight junctions with their membrane separating the systemic circulation and the central extracellular fluid of the brain. The vasculature serving the CNS also has capillaries with tight junctions. The arachnoid membrane which is a doubled layered structure covers the brain and constitutes a barrier between the blood and the CSF (Shawahna et al., 2013; Kuhnline Sloan et al., 2012; Nag et al., 2011; Kaur et al., 2008; Vyas et al., 2005a). Therefore, BBB is primarily a prominent obstruction in drug delivery to the brain.

2.2.2. Blood-Cerebrospinal Fluid Barrier

The Blood Cerebrospinal Fluid Barrier (BCSFB) (Lam et al., 2012) is another barrier that exists, it inhibits the passage of drugs to the CNS during systemic administration (Chalbot et al., 2010; Yasuda et al., 2013). BCSFB is resides in the epithelium of the choroids plexus (Johanson et al., 2011), the arrangement of which limits the passage of therapeutic molecules into the CSF. The choroid plexus and the arachnoid membranes play a major role at the barriers between the blood and CSF (Chalbot et al., 2010; Misra et al., 2003). It is clear that the endothelium of the cerebral blood vessels and the epithelium of the choroid plexus prevent the penetration of large solutes directly into the brain and CSF.

2.2.3. Blood-Tumor Barrier

Blood Tumor Barrier (BTB) is a barrier formation at the local site of the tumor cells that do not permit drugs from reaching brain tumors in therapeutic quantity to exterminate the tumor cells. A range of barriers that are physiologically oriented are found in solid tumors and they prevent drug delivery via the cardiovascular system. Solid tumor consists of neoplastic cells, drug delivery to these cells is hindered because uneven distribution of microvasculature throughout the tumor

interstitial resulting into drug delivery inconsistency (Misra et al., 2003). Apart from dealing with the BBB, there is also the problem of BTB. Many innovative methods have been used to improve drug delivery to the tumor cells, of which has been reviewed by Groothuis (2000).

2.3. NASAL ANATOMY AS AN AID TO CNS DRUG DELIVERY

It is pertinent to understand the anatomy of the nasal cavity when discussing the intranasal administration, absorption and transporting of drugs to the brain and CNS. Figure 2.1 shows the Lateral wall of the nasal cavity. The nasal cavity is located within the skull; it spans from the base of the skull to the roof of the mouth. It is a midline structure that is divided into two equal haves by the nasal septum. Each half which consists of the roof and the floor as well as medial and lateral walls (formed by the bone and cartilage skeleton of the skull) begins from the nostril at the anterior part and ends up at the nasopharynx at the posterior part where the two airways confluence (Hinchcliffe and Illum, 1999). The nasal cavity roof consists of frontal and nasal bones anteriorly, in the middle is the cribriform plate of ethmoid bone, ala of the vomer and the sphenoidal process of the palatine bone posteriorly (James Zinreich et al., 1990). The floor is composed of the bones of the hard palate which are the palatine process of maxilla anteriorly and horizontal plate of palatine bone posteriorly. The middle wall is made up of the nasal septum which passes from the roof to the floor of the nasal cavity (Peter, 2003).

The nasal cavity consists of paranasal sinuses which are frontal sinuses, ethmoid sinuses, maxilla sinuses and sphenoid sinuses, they are air-filled spaces surrounding the nasal cavity and are lined with mucosa membrane with small openings into the nasal cavity (Napier, 2013). The nomenclatures and locations of these sinuses are derived from the bones in which they lie, which are the frontal, ethmoid, maxilla and sphenoid respectively. Both the frontal and maxilla sinuses open into the nasal cavity through the semilunar hiatus (El-Gendy and Alsafy, 2010; Langille et al., 2012; Thiagarajan, 2013), sphenoid sinuses open into the speno ethmoid recess (Weiglein et al., 1992) and ethmoid sinuses which consist of

the anterior, middle and posterior parts open into the nasal cavity by the infundiblum, ethmoidal bulla and the superior meatus respectively (Napier, 2013; Shanmugam et al., 2011). The nasal cavity communicates through the lateral nasal wall with the maxillary and frontal sinuses and more posteriorly with the sphenoid sinuses. The septum provides support for the nasal structures and regulates nasal passage while the middle concha warms up and humidifies the inspired air (Aktas et al., 2003).

The nasal cavity which has a total volume and surface area of approximately 20ml and 150 cm^2 respectively (Chaturvedi et al., 2011) is splited into three areas which are (1) the vestibular section which is the most anterior part of the nasal cavity and surrounded by the nose cartilages with epithelium lining same as that of the skin. The anterior area is between 10–20 cm^2. (2) The respiratory section with area of approximately 130 cm^2, is the main area of the nasal cavity, this is the part where the absorption of therapeutic compounds into the systemic circulation takes place. The respiratory section is made up of the respiratory epithelium which consists of ciliated and non-ciliated columnar cells, mucous secreting goblet cells and the basal cells. Many of the epithelial cells are covered on their apical surface with microvilli. The ciliated cells protrude out of the surface with few micrometers and can make synchronized movement that can push the mucus layer on the surface of the respiratory epithelium towards the nasopharynx, this is a useful action that is responsible for the mucociliary clearance mechanisms which eliminate foreign and undesired substances from the nasal mucosa into the GIT via the nasopharynx. (3) The olfactory section which occupies 10–20 cm^2 in the roof of the nasal cavity (Hinchcliffe and Illum, 1999). Figure 2.1 shows the anatomy of the nose.

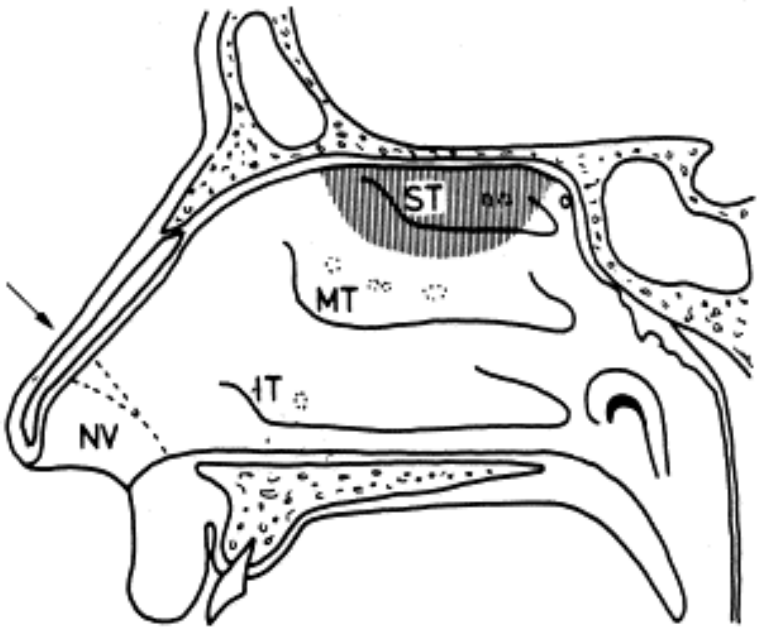

Figure 2.1: Lateral wall of the nasal cavity, and cross-sections through the internal ostium, the middle of the nasal cavity, and the choanae. Hatched area in the upper figure, olfactory region. NV, nasal vestibule, IT, inferior turbinate and orifice of the nasolacrimal duct; MT, middle turbinate and orifices of frontal sinus, anterior ethmoidal sinuses and maxillary sinus; ST, superior turbinate and orifices of posterior ethmoidal sinuses. Source (Mygind and Dahl, 1998).

Intranasal drug delivery has fascinated the interest of researchers based on the fact that the nasal mucosa has been established as a substitute route for the delivery of high molecular weight therapeutic substances including protein and peptides that are liable to either acidic or enzymatic degradation as well as first pass hepatic metabolism when administered orally. It has also been explored as a promising route for the administration of vaccines (Singh et al., 2012), and a viable route for the delivery of biopharmaceuticals (Tong-un et al., 2010). The initial use of nasal delivery was largely confined to topical applications, example of such applications include nasal steroids for treatment of nasal allergies, also phenylephrine and oxymetazoline for the treatment of nasal decongestion. These drugs operate locally at the site of administration and does not require passing through the systemic pathway (Maggio and Pillion, 2013). Intranasal route provides a non-invasive and alternative method of delivering therapeutic compounds with ease of administration of those drugs that are restricted by the BBB to the brain and CNS than the systemic administration which is associated

with various side effects (Hanson and Frey, 2008). The nose-to-brain drug delivery is possible because of the position of the trigeminal as well as the olfactory nerves which connect the brain to the nasal cavity. Drugs can be transported directly from the nasal mucosa to the brain through the olfactory region which is strategically located in between the nasal cavity and the CNS region allowing drugs to bypass the BBB and BCSFB. The penetration of drugs to the brain however depends on several factors such as properties of nasal formulations, types of nasal device, dosing, drug amount and deposition, mechanism of transport, mucocilliary clearance and other local site barriers.

There are several advantages of intranasal drug delivery over the systemic delivery of drugs some of which are listed in Table 2.1. The advantages and the limitation of intranasal drug administration are shown in Table 2.1. It is obvious that the advantages overweigh the limitations thereby making intranasal administration of drugs a better method of drug administration especially to the brain and CNS than the oral, intravenous, transdermal administration and of course implantations. The delivery systems and devices are considerable factors in intranasal drug delivery because of the physiology and structure of the nose.

Table 2.1: Advantages and Limitation of Intranasal Drug Administration.

	Advantages	Limitations
1	The surface area of the nasal mucosa is large for dose administration (Misra et al., 2003)	Amount of administered drugs is limited to 25-200 µl. (Afifi et al., 2005)
2	Rapid absorption of drug is possible due to rich blood capillaries and vessels in the nasal mucosa (Andrews et al., 2009; Soane et al., 1999)	Adversely affected by pathological conditions (Alam et al., 2010; Misra et al., 2003)
3	Possibility of Rapid onset action of delivery (Li et al., 2002; Vyas et al., 2005a)	Drug permeability may be affected due to the ciliary movement (Andrews et al., 2009)
4	Ease of administration, noninvasive (Andrews et al., 2009; Mistri et al., 2012)	Drug permeability is limited due to enzymatic inhibition (Ozsoy et al., 2009)
5	Bypasses BBB (Singh et al., 2012)	Drug with nasal irritation may not be acceptable through this route (Alam et al., 2010)
6	Evade the gastrointestinal tract and first pass metabolism (Soane et al., 1999; Vyas et al., 2005)	
7	Improved bioavailability (Dhuria et al., 2009; Vyas et al., 2005a)	
8	Possibility of direct absorption into systemic circulation and CNS (Ozsoy et al., 2009)	
9	Lower dose amount to reduction of side effects (Alam et al., 2010; Vyas et al., 2005)	
10	Improved convenience and compliance	
11	Self-administration of drugs (Alam et al., 2010)	
12	It avoids the use of sterile procedure (Alam et al., 2010)	

2.3.1. The Olfactory Pathway as an Opportunity for CNS Drug Delivery

The Olfactory region is located at the roof of the nasal cavity just below the cribiform plate of the ethmoid bone and crosses a bit down the septum and lateral wall. Its position is strategic as one end interacts with the nasal cavity and the other end with the CSF. It is therefore the only area of the CNS that has external link to the outside surroundings. Olfactory neurons directly penetrate through the cribiform plate into the olfactory epithelium of the nasal cavity (Padowski and Pollack, 2010). The olfactory epithelium is formed by the olfactory receptor neurons which are arranged at intervals among the other sustaining cells and the basal cells. The olfactory system is responsible for perceiving smell. Variety and numerous odorant molecules can be perceived by mammals and humans through their sense of smell which is mediated by the olfactory system.

The olfactory system has the ability to detect different kinds of odors by applying information theory measurements to olfactory bulb activity images (Fonollosa et al., 2012). Humans can sense approximately between 10 000 to 100 000 substances as having a distinct odor (Buck, 2005). The olfactory bulb is a structure found at the bottom of the brains of human and it is being protected and cradled by the cribiform plate which also separates it from the nasal cavity. It is the site that processes information about odors, which is the principal purpose of the olfactory (Buck and Axel, 1991). Figure 2.2 shows the schematic illustrations of the various types of cell in the olfactory region. Receptor cells which are the neurones are situated among columnar sustentacular cells. The axons of the receptor cells emerge from the epithelium in bundles enclosed by ensheathing glial cells. Spherical globose basal cells and flattened horizontal basal cells lie on the basal lamina. The Bowman’s gland opens on to the surface via their intraepithelial ducts. At the surface are cilia of the receptor cells and microvilli of the supporting cells.

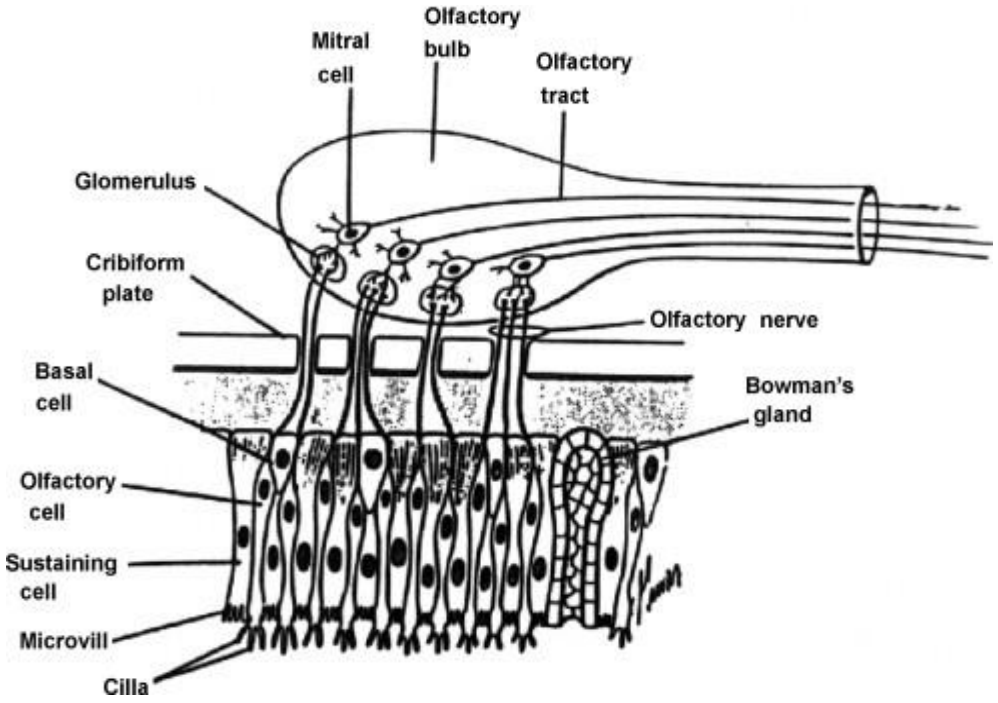

Figure 2.2: Illustrations of the various types of cells in the olfactory region. Reproduced from (Mistry et al., 2009).

2.3.2. Proposed Pathways of Therapeutic Agents Introduced into the Nasal Cavity

When therapeutic compound is intranasally administered, it is liable to follow different routes as depicted in Figure 2.3. The drug may find its way into the systemic pathway via the blood vessels and capillaries in the nasal mucosal. The probability of the drug going into the blood is very high considering the fact that the nasal cavity is very rich in blood supply. This is one of the reasons intranasal administrations of drugs is preferred for the drugs that have a high risk of being significantly degraded in the gastrointestinal tract or those that are highly metabolized through the first pass effect of the liver. An example of this is highlighted in the oral administration of Olanzapine (Kumar et al., 2008) where 40 percent of the drug was metabolized in GIT and liver prior to reaching the systemic circulation. The drug may also find its way into the olfactory system and ultimately reach the CNS. The trigeminal nerve which controls the facial sensation has been established to transport drugs to CNS and brain in particular. In the nasal cavity, the drugs that could not make it to the blood, olfactory and the trigeminal pathway may be degraded through the action of the enzymes in the nasal cavity or be

eliminated via mucocilliary clearance (Preetha et al., 2013). Drugs that find their way into the systemic circulation may be delivered to the body tissues and organs or be eliminated from the blood by normal clearance mechanism. Drugs may also be distributed from the CNS to brain or migrate from the brain to the CNS. Drugs in the CNS and brain may also be eliminated by clearance into the blood.

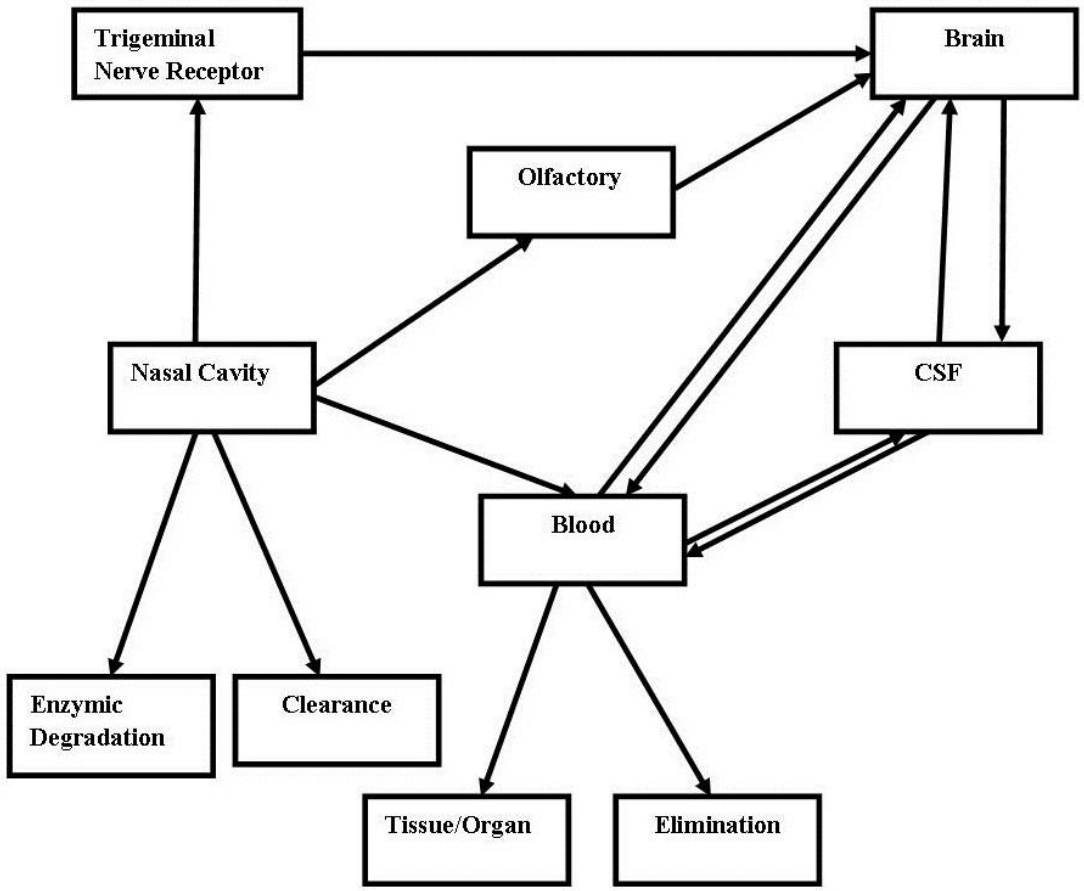

Figure 2.3: Possible transport pathways of a compound introduced into the nasal cavity. Adapted from (Graff and Pollack, 2005; Illum, 2004, 2003, 2000).

2.3.3. Mechanism of Direct Nasal Mucosa to Brain Delivery via the Olfactory Pathway

The mechanism of direct nasal mucosa to brain drug delivery has not been firmly established but it has been evidenced by the work of various researchers that intranasal delivery of therapeutic agents is delivered to the brain along the olfactory and trigeminal pathway. For example, Renner et al. (2012) intranasally

administered fluorescently labeled insulin into mice; the insulin migrated deep into the anterior area of the olfactory region moving across from the nasal mucosa epithelium to the cribriform plate to gain access to the olfactory bulb. Higher quantities of insulin were found in the in the olfactory nerve layer up to the glomerular layer. Similarly, insulin labeled with nanogold was delivered intranasally to mice, insulin was also found in the olfactory nerve layer of the mice and intracellular nanogold was detected in the nucleus of the cells of the olfactory bulb (Renner et al., 2012). Various researches have been conducted to demonstrate that molecules can be transported from the nasal mucosa by widely dispersing these molecules throughout the olfactory region, carrying them across to the olfactory bulb and subsequently reaching the brain.

Dhuria et al. (2010) described the mechanism involved in the transporting drug molecules to the brain and CNS. They reported that drugs interact with the nasal mucosa comprising nasal epithelium and the drug molecules are distributed by both olfactory and trigeminal nerves where the nerve endings send chemosensory information to the brain. Drugs may be transported to the brain through perivascular spaces which is located in the lamina propria or through intracellular and extracellular pathways. On reaching the lamina propria, drugs may pass into the openings formed by unsheathing cells neighboring the olfactory nerves, and then penetrate the olfactory bulb including the CSF. From the CSF, drugs can diffuse and blend with interstitial fluid of the brain via bulk flow mechanisms. Drugs that pass through the perivascular channels may also exit through the same channels; this is an important process by which substances get eliminated from the CNS to the external environment. The mechanism may also involve the passage of the drug into the primary neurons found in the olfactory epithelium and then penetrate to the olfactory bulb via intracellular axonal transport. Axonal transport occurs when the drugs penetrate the neurons by endocytosis for onward movement to the CNS with subsequent possible circulation of the drug into inner brain tissues (Illum, 2004).

2.4. EVIDENCE OF NOSE-TO-BRAIN DRUG DELIVERY

Nose-to-brain delivery of drugs and neurologic substances such as insulin and other growth factors along the olfactory neural pathway to treat neurological disorders was first proposed and patented in 1989 by W. H Frey II (2010). Recent developments in intranasal drug delivery have shown intranasal administration of drugs as a harmless and suitable route for delivering drugs to the brain and CNS generally for the treatment of neurodegenerative ailments, for the special reason of the existence of the BBB which does not allow the passage of most therapeutic agents to the brain and CNS. Lipophilic compounds penetrate quickly and effectively across the nasal membranes into the systemic circulation through the transcellular pathway which shows the same plasma profile to that of intravenous injection in terms of absorption with bioavalaibility of drugs up to a 100%. Because of this quick action, lipophilic compounds seldom pass through the olfactory pathway in the nasal cavity. However hydrophilic compounds and larger compounds have serious difficulty in passing across the nasal membrane into the blood circulation for systemic delivery, even if they do cross, they are still faced with the issue of BBB for brain delivery. It has been established that the bioavailability of less lipophilic molecules and large molecules is about 1-10% (Illum, 2004). The olfactory pathway is therefore an inevitable route for the delivery of these compounds to the brain and CNS via the nasal cavity. Several therapeutic agents have been successfully delivered to the CNS using the intranasal route of administration.

2.4.1. Delivery of RNA, Enzymes, Insulin and Protein

Enzymes, proteins and insulin have been successfully delivered to the brain through the nasal mucosa. Trigeminal nerve has been known to also contribute to the movement of drugs to the brain. Renner et al. (2012a) examined delivery of fluorescently labeled Small interfering Ribonucleic acid (siRNA) from the nasal mucosa to the olfactory bulbs via the olfactory pathway. Their result showed that after thirty minutes of intranasal administration, fluorescently labeled siRNA was detected in the olfactory epithelia, lamina propria as well as the olfactory bulbs

along the olfactory pathway and was dispersed throughout the olfactory region as depicted in Figure 2.4.

Recently, α-l-iduronidase (IDUA) action was detected widely in the brains of IDUA-deficient mice after concentrated laronidase administration via the nasal mucosa and it was also detected after intranasal treatment with an adeno-associated virus (AAV) vector expressing human IDUA. This was demonstrated by Wolf et al. in the course of providing the first evidence of lysosomal enzyme passing the BBB when administered via the nasal route (Wolf et al., 2012). Brain-derived neurotrophic factor, ciliary neurotrophic factor, and neurotrophin-4/5 can promote neuronal survival in event of injury to the CNS. Delivery of these substances is difficult because of their large molecular weights which prevent them from crossing the BBB. These proteins have been successfully delivered intranasally and high concentrations of the proteins were detected in the brain 25 minutes after nasal administration (Alcalá-Barraza et al., 2010). Delivery of insulin employing the olfactory nerve pathway was carried out by Renner et al., the aim of their study was to deliver insulin directly to the olfactory bulbs through the olfactory nerve pathway employing the intranasal route of administration (Renner et al., 2012a).

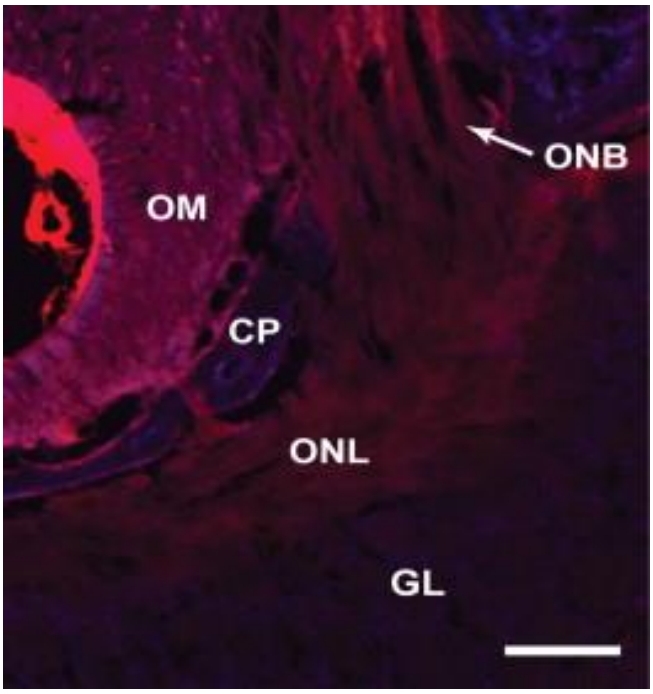

Figure 2.4: Showing fluorescently labeled siRNA distribution in the olfactory bulb of rat. Scale= 30µm: ONB=olfactory nerve bundle, OM=olfactory mucosa, CP=cribiform plate, ONL=olfactory nerve layer, GL=glomerular layer. Adapted from (Renner et al., 2012b).

2.4.2. Delivery of Drug-Loaded Nanoparticles

Liu et al. (2013) modified poly(ethyleneglycol)-poly (ε-caprolactone) nanoparticles by conjugating the nanoparticles with Lactoferrin to obtain Lactoferrin-conjugated PEG-PCL nanoparticle (Lf-NP) using a maleimide-thiol reaction for delivering of neuroprotective drugs to treat Alzheimer's Disease (AD) employing intranasal route for direct nasal mucosa to CNS delivery. In their experiment, the Lf-NP was labeled with Cy5.5 a fluorecein probe for real time imaging and biodistribution in mice. Three hours after intranasal administration, they observed a very strong fluorescent signal of Cy5.5-labeled Lf-NP in the brain of the mice as shown in Figure 2.5. They used NAP (NAPVSIPQ), an 8-amino acid neuropeptide fragment as model drug. The outcome when their system was evaluated in AD mice intranasally showed an enhancement delivery of the neuroprotective drug in the brain.

Chitosan nanoparticles have demonstrated the potential for enhancing the brain uptake of venlafaxine hydrochloride a drug for the management of depression via

nasal route. Venlafaxine side effects such as increased blood pressure, tiredness, pain, tachyarrhythmia, dizziness, sexual dysfunction observed when administered via oral or intravenous make its intranasal delivery to brain and CNS a promising and preferred method (Haque et al., 2012).

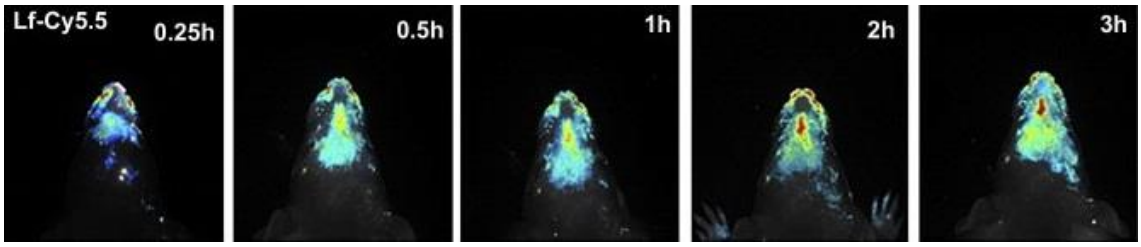

Figure 2.5: Distribution and retention of Cy5.5-Lf in the brain following intranasal administration. Adapted from (Liu et al., 2013).

Rivastigmine (Fazil et al., 2012) and thymoquinone (S. Alam et al., 2012) loaded Chitosan nanoparticles have been produced by ionic gelation method to increase the uptake of drug to the brain and to enhance the bioavailability of the drug in CNS following administration through the nasal route. Shadab et al. (2012) investigated the potential use of Chitosan nanoparticles for the purpose of delivering therapeutic agents to the brain intranasally. This was achieved by preparing bromocriptine (BRC) loaded Chitosan nanoparticles using ionic gelation of Chitosan with tripolyphosphate anions with mean size of 161nm. Figure 2.6 shows the SEM image of the nanoparticle revealing the morphology of the optimized BRC loaded nanoparticles. Optimized technetium labeled BRC was employed in investigating the biodistribution of the BRC in the brain and blood of the mice after intranasal and intravenous administration. At 30 minutes following administration, the brain/blood ratio of BRC loaded chitosan nanoparticles administered intranasally was found to be higher than that of intravenous administration. These results indicate a direct nasal mucosa to brain transport bypassing the BBB. Al-Ghananeem et al. (2010) have used Chitosan nanoparticles to delivered Didanosine an HIV reverse transcriptase inhibitor to the brain via the nasal mucosa. The didanosine-loaded Chitosan nanoparticles were made by ionotropic gelation of Chitosan with tripolyphosphonate anions. They compared the intranasal delivery to intravenous delivery. Their findings highlighted that the concentration of therapeutics in the olfactory bulb, CSF and brain were

considerably higher after intranasal administration than those after intravenous administration of didanosine aqueous solution.

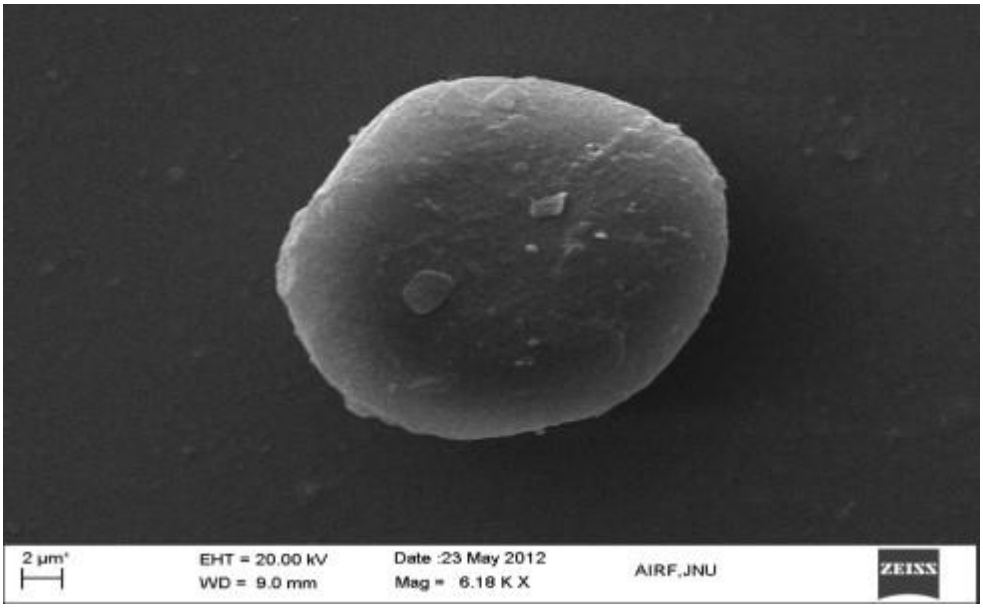

Figure 2.6: SEM image showing surface morphology of optimized bromocriptine loaded Chitosan nanoparticles. Adapted from (Shadab et al., 2012).

Thermo-sensitive gels with lorazepam microspheres using Chitosan and pluronics were prepared and characterized for nasal delivery to the brain by Jose et al (2013). *In vitro* drug release and permeation studies of their investigation showed that the gel formulation is capable of sustaining a 24-hour drug release. This may provide controlled release advantage and improved bioavailability for nasal drug delivery.

Nose-to-brain delivery system in combination with cell-penetrating peptide (CPP) modified nano-micelles comprising polyethylene glycol–polycaprolactone (PEG–PCL) copolymers conjugated with the CPP, Tat (MPEG–PCL–Tat) (Kanazawa et al., 2013) has been synthesized to deliver siNRA to the brain following intranasal administration. Alexa-dextran (Anionic dextran labeled with Alexa Fluor 568) as a model siRNA was complexed with Tat to obtain MPEG–PCL–Tat/Alexa-dextran nano complex. Sprague–Dawley male rats were employed for *in vivo* study, 100µL was administered intravenously and 80µL intranasally to the rats, the result of intranasal administration was compared with intravenous administration as

depicted in Figure 2.7 revealed the presence of Alexa-dextran in those rats that were dosed intranasally and none in those that were dosed intravenously. The results confirm intervention of nose-to-brain of therapeutic agents to the brain for managing neurogenerative diseases.

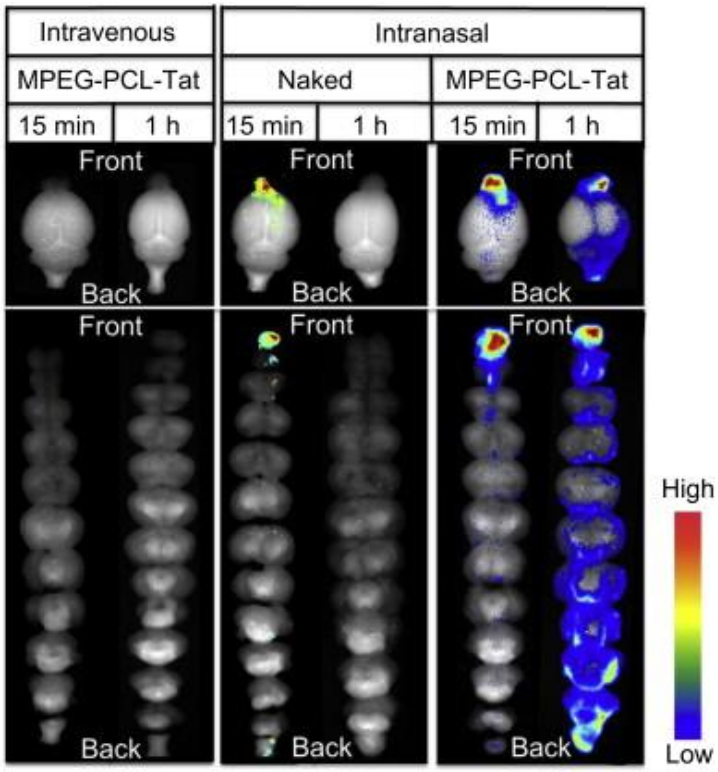

Figure 2.7: Dynamics of MPEG–PCL–Tat complex in brain tissue following intranasal and intravenous administration (Kanazawa et al., 2013).

2.4.3. Microemulsion Formulations

Thakkar et al. (2013) prepared and characterized mirtazapine microemulsion for intranasal delivery, to determine its brain drug delivery using pharmacokinetic studies, and assess its performance pharmacodynamically for the antidepressant activity. Their investigation demonstrated a rapid movement and higher concentration of mirtazapine into the brain with intranasal administration compare to oral administration, which may be helpful for the treatment of depression. Acharya et al. (2013) prepared and evaluated intranasal oil in water microemulsion of carbamazepine to improve its solubility and enhance the brain uptake. Intranasal microemulsion of carbamazepine was prepared by water titration method using oleic acid as oil, Tween 80 as surfactant and Transcutol® as co-

surfactant. Their experiment resulted in higher brain/plasma ratio with nasal microemulsion in comparison to ratio obtained after intraperitoneal injection of carbamazepine solution. Porecha et al. (2009) prepared and characterized microemulsions/mucoadhesive microemulsions of Diazepam, Lorazepam and Alprazolam, evaluated their pharmacodynamic behavior by carrying out comparative sleep induction studies in male albino rats to appraise their role in effectual management of insomnia patients, intranasal administration of these drugs was compared with oral administration, They observed faster onset sleep after intranasal administration compare to oral. The result of their investigation also showed that the mucoadhesive microemulsions of the formulation following intranasal administration indicated rapid and higher drug transport to the rat brain and thereby induced quick sleep and prolonged sleep.

Kumar et al. (2008a) have prepared nanoemulsions which contain risperidone to achieve brain uptake of drug through the nasal mucosa; they compared a risperidone nanoemulsion and risperidone mucoadhesive nanoemulsion via intranasal and intravenous administration. Their results showed that intranasally administered mucoadhesive nanoemulsion was a more efficient and exhibit better brain targeting of risperidone, which is an indication of how important mucoadhesion is in nasal drug delivery. They also prepared nanoemulsions and olanzapine mucoadhesive nanoemulsions employing water titration method, these formulations were intranasally and intravenously administered to rats. It was observed that the biodistribution of olanzapine in the brain and blood of rats (brain/blood uptake ratios) after intranasal and intravenous administrations of olanzapine formulations at 30 minutes were 0.88 and 0.04 respectively (Kumar et al., 2008b). This result proved that intranasal administration enhances bioavailability of drugs compare to intravenous administration. Zhang et al. (2004) while investigating ways of enhancing the solubility of nimodipine and its brain absorption in microemulsion, their result showed absorption of nimopidine in the olfactory bulb to be enhanced three-fold after intranasal administration, compared with intravenous injection.

Dalpiaz et al. (2014) have used solid lipid microparticles (SLMs) as a carrier system for the nasal administration of antiretroviral drug zidovudine (AZT) with ursodeoxycholic acid (UDCA) (UDCA−AZT) prodrug for direct nose to brain targeting, Figure 2.8 shows the micrographs of unloaded (A) and UDCA–AZT loaded (B) SLMs based on tristearin. They employed hot emulsion technique using tristearin and stearic acid as lipidic carrier. Their study showed that in the presence of chitosan, there is six-fold bioavailability of prodrug in the CSF, and up to 1.5 μg/mL of prodrug within 150 min after nasal administration, which is an evidence of direct nose- to-brain delivery pathway.

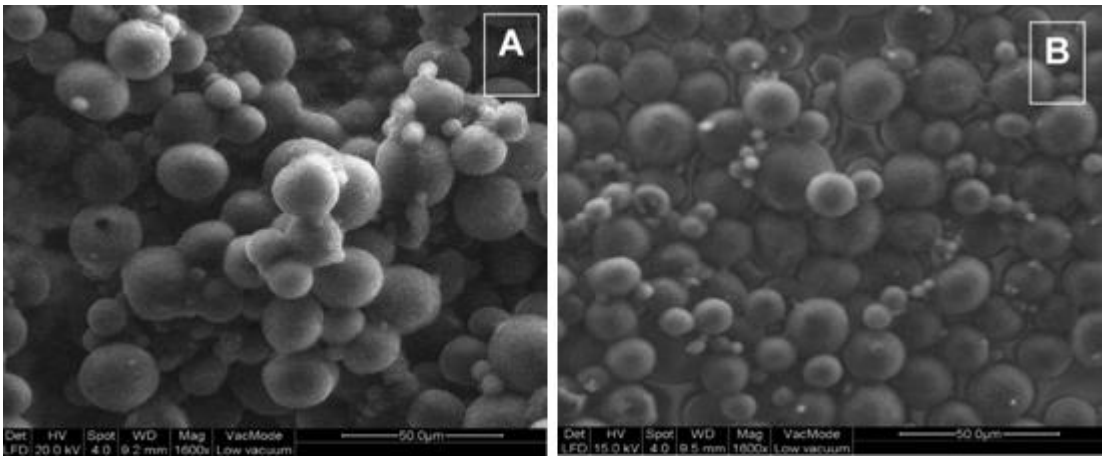

Figure 2.8: Environmental scanning electron microscopy (ESEM) micrographs of unloaded (A) and UDCA–AZT loaded (B) SLMs based on tristearin (Dalpiaz et al., 2014).

2.4.4. Liposomes as Delivery Vehicles

Galanthamine hydrobromide (GH) which is an effective therapeutic agent that is widely used in Alzheimer's disease management has been delivered into the rat brain successfully through the intranasal route of administration employing flexible liposomes as the delivery vehicle (W. Li et al., 2012). Salama et al. (2012) prepared phospolipid based colloidal nanocubic vesicles by integrating non-ionic copolymers, poloxamer 188 or 407, in the lipid bilayer. Their aim was to encapsulate olanzapine in the matrix. Their investigation resulted in development of nanocubic vesicles and enhancement of the delivery of olanzapine to the brain with bioavailability up to 37.9% and brain targeting efficiency of100% after intranasal administration. Liposomes have been employed in delivering

rivastigmine to the brain tissue through intranasal administration. Liposomes as delivery vehicle significantly improved the exposure and resulted in higher concentration of the therapeutic agent in the brain (Mutlu et al., 2011; Arumugam et al., 2008).

Alam et al (2014) prepared nanostructured lipid carrier (NLC) to confirm and assess the improvement of duloxetine (DLX) loaded NLC in the brain folowing intranasal administration, they employed Gamma imaging technique to study the localization of DLX, their result revealed about 8 fold of DLX concentration in the brain in comparison to being administered intravenously. Li Weize et al. (2012) delivered GH successfully into the rat brain through the olfactory pathway while investigating the intranasal administration effects of GH loaded flexible liposomes on the effectiveness of acetylcholinesterase inhibition. Figure 2.9 shows the TEM image of the GH loaded liposomes. They discovered a quick action of movement of GH into the brain with the flexible liposomes following intranasal administration. Their investigation therefore indicates that the intranasal administration of GH loaded liposomes may be a promising technology to be explored in future for the treatment of AD.

Eskandari et al. (2011) have developed nasal nanostructured lipid carriers of valproic acid for direct nasal mucosa to brain delivery. Their aim was to lower the dosage, provide prolonged action of the drug and evaluate its efficacy against generalized tonic-clonic seizures in rats, their study established that administration of vaproic acid nanostructure via the nasal route is an appropriate method in maintaining vaproic acid effect with a higher brain uptake using much lower dose compare to systemic adminstration. Migliore et al. (2010) evaluated the efficiency of cationic liposomes for the delivery of proteins to the brain by employing the nasal route of administration. They loaded the liposomes with ovalbumin and a 50μg was intranasally administered to rat, it was observed that after 6 hours, ovalbumin was widely distributed throughout the brain of the rat. Solid lipid nanoparticles (SLNs) have been developed and optimized as intranasal drug delivery system for ondansetron (Joshi et al., 2012) and risperidone (Patel et al., 2011). The method employed for preparing the SLNs was solvent diffusion-solvent

evaporation method. Significant quantities of therapeutic agents were rapidly delivered to the CNS and brain after intranasal administration of the drug-loaded solid lipid nanoparticles that were formulated.

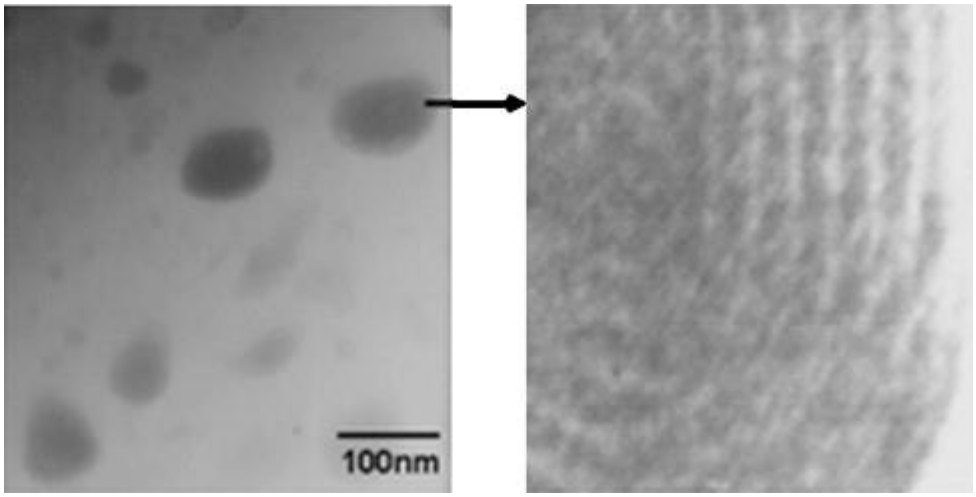

Figure 2.9: TEM image of GH loaded flexible liposomes adapted from (W. Li et al., 2012)

Polymeric micelles have been developed for intranasal drug delivery. Chiappetta et al. (2013) prepared poly(ethylene oxide)–poly(propylene oxide) polymeric micelles for intranasal administration which was loaded with high payloads of efavirenz an antiretroviral drug for treating HIV dementia. Poloxamer F127, and mixed polymeric micelles containing 75% of T904 and 25% of F127 was employed with an attempt to determine the effect on size of the micelles as well as the drug payload. They compared intranasal administration of their formulation with intravenous administration; the result of their investigation shows four times bioavailability enhancement in the CNS for intranasal administration compared to intravenous which is as a result of direct migration of the nanomicelles to the olfactory region for onward delivery to the CNS. The size of the micelles ranged from 13.5nm to 247.3nm when the efavirenz was fully encapsulated.

2.4.5. Direct Drug Application into the Nasal Cavity

Direct drug application without any protective vessel has been demonstrated by various researchers for example, Deferoxamine (DFO) has been delivered using the noninvasive intranasal method of administration. Hanson et al. (2009) reported

that employing intranasal route to administer DFO resulted in higher brain uptake of DFO compare to intravenous administration, it also amount to reduction in systemic absorption, and subsequently resulted in prevention and treatment of stroke damage after middle cerebral artery occlusion in rats. Fine et al. determined whether intranasal administration of DFO would minimize loss of memory in the P301L mouse and how the treatment might affect AD neuropathology, their finding was that intranasal administration with DFO reduced both inflammation and oxidation which are the two phenomena associated with Alzhiemer's Disease (Fine et al., 2012).

Application of recombinant tissue plasminogen activator (tPA) to ischemic stroke has been carried out by Liu et al. (2012) using direct nose-to-brain approach because of the BBB issues and the associated side effect of the systemic pathway. Their study examined the therapeutic benefit of tPA when it is intranasally administered for direct CNS targeting for the treatment of stroke in rat model. Their result shows tPA content of 307 mg/ml at 30 min in the brain compare to 7 mg/ml measured 2 h after intravenous injection of tPA (10 mg/kg), signifying intranasal administration to be an effective method of delivering high molecular weight drugs for brain and spinal cord targeting (Liu et al., 2012)

Cocaine was intranasally and intravenously administered to male Sprague-Dawley rats by Chow et al (1999). The result of both routes of administration indicated similarity in concentration of cocaine in the brain. The concentration of cocaine in the olfactory lobe was investigated after 1 min of dosing and small fraction of the dose was found delivered in the olfactory bulb via the olfactory pathway, much of the cocaine have been trapped by the blood rich nasal mucosa for onward systemic delivery to the brain and CNS.

2.5. CONVENTIONAL NASAL DRUG DELIVERY DOSAGE FORMS

2.5.1. Nasal Drops

The purpose of using nasal drops is to instill the drugs inside the surface of the nasal cavity. Nasal Drops are the simplest and most convenient systems that have been developed for intranasal drug delivery. Aukema et al. have used nasal drops to deliver steroids into the middle meatus for the treatment of polyposis and chronic rhinosinusitis with fluticasone propionate (Aukema et al., 2005). Daley-Yates and Baker in their experiment tried to measure the bioavailability of Flutticasone Propionate administered as a nasal drops and also compare it to being administered as a nasal gel, it was observed that the formulation has low systemic bioavailability which is much lower than when administered as nasal gel (Daley-Yates and Baker, 2001). Nasal drops have been however reported to deposit human serum albumin in the nostrils better than nasal sprays (Patel, 2013). Nasal drops do not have dose precision which is an obvious shortcoming of the system. In addition liquid formulations are more easily emptied to the nasopharynx thereby showing quick clearance from nasal mucosa which is an impediment to sustained drug release (Alsarra et al., 2010).

2.5.2. Nasal Sprays

Nasal sprays function by the action of hand operated metered dose pumps and actuators to infuse a fine vapor into the nostril, they can therefore deliver exact dose from 25-200ul an advantage over nasal drop. Several nasal sprays have been developed over the years for drug delivery. Some of which are highlighted in Table 2.2. Chesnut III et al used Salmon calcitonin nasal spray at a dose of 200 IU daily to drastically reduce the threat of new vertebral fractures in postmenopausal women with osteoporosis (Chesnut III et al., 2000). Fluticasone nasal spray has been used to reduce the occurrence of pediatric obstructive apneas and hypopneas (Brouillette et al., 2001). Others include: Nicotine nasal spray for tobacco withdrawal (Blondal et al., 1999; Hjalmarson et al., 1994; Stapleton and Sutherland, 2011; Sutherland et al., 1992). Nicotine nasal spray for analgesic purposes (Yagoubian et al., 2011).

Table 2.2: Review of recent development in nasal sprays for delivery of therapeutic agents.

Therapeutic Agents	Functions	References
Nicotine	Tobacco withdrawal	(Blondal et al., 1999; Hjalmarson et al., 1994; Stapleton and Sutherland, 2011; Sutherland et al., 1992)
Salmon Calcitonin	Reduces new vertebral fractures in postmenopausal women with osteoporosis and in the treatment of Refractory Mania	(Chesnut III et al., 2000; Lee et al., 2011; Vik et al., 2013)
Fluticasone	reduces the occurence of pediatric obstructive apneas and hypopneas	(Brouillette et al., 2001)
Fentanyl pectin	Pain relief in the treatment of cancer	(Radbruch et al., 2012; Taylor et al., 2010)
Oxytocin	Treatment of Autistic or Asperger's Disorder	(Guastella et al., 2010)
Mometasone Furoate	Treatment of nasal polyps in children	(Chur et al., 2013)

2.5.3. Nasal Gels

Gelation occurs usually through polymers crosslinking by forming covalent bond known as chemical crosslinking or by non-covalent bonding and van der Waals forces known as physical crosslinking (Piechowiak et al., 2012). Gel formulations increase the contact time with the nasal mucosa and also increases efficiently the residence time of the therapeutic substances in the nasal mucosa. These advantages are dependent however on the type of polymers used. Other advantages include reduction of taste impact, reduction of leakages of the formulation from the anterior part and mucosa target for better absorption (Chaturvedi et al., 2011). Table 2.3 shows some of the recent development of nasal gel in delivering therapeutic agents through the nasal mucosa.

Table 2.3: Review of recent development in nasal gel for delivery of therapeutic agents

Therapeutic Agents	Functions	Polymers Used	References
Midazolam Hydrochloride	Treatment of epilepticus	Pluronic F127	(Basu and Bandyopadhyay, 2010)
Ondansetron Hydrochloride	Management of nausea and vomiting that is associated with cancer chemotherapy	Pluronic F127 and hydroxypropylcellulose	(Bhalerao et al., 2009)
Chlorpheniramine maleate	Antihistaminic drug	Sodium Carboxymethyl cellulose and Hydroxypropyl methylcellulose	(Soliman et al., 2010)
Ropinirole	Dopamine D2 agonist	chitosan and hydroxyl propyl methyl cellulose	(Khan et al., 2010)
Sumatriptan	Treament of migrane and severe headache	Carbopol 934P and Pluronic F127	(Majithiya et al., 2006)
Lorazepam	Treatment of status epileptics	Pluronic F127 and Chitosan	(Jose et al., 2013)
Curcumin	Anti-inflammatory, antioxidant, anti-tumoural and antimicrobial	polyethylene glycol 400 and Pluronic F127	(Chen et al., 2013)
Venlafaxine	Treatment of chronic depression	Methyl cellulose and Pluronic F127	(Pund et al., 2013)
Vinpocetine	Prevention of Azheimer's disease, ischemic stroke	Hydroxypropylmethylcellulose, methyl cellulose and Carboxymethyl Cellulose	(Badie, 2012)

2.5.4. Nasal Powders

The instability of therapeutic agents may inform the development of this delivery system, where solution and suspension dosage form may not be adequate to sustain the drug. Preservative is not required in the formulation and there is possibility of administration of larger doses of therapeutic agents. The suitability of powder for delivery of both peptide and non-peptide drugs has been established (Chaturvedi et al., 2011; Joshi and Misra, 2001). For nasal powder formulation to be efficient, factors such as aerodynamic properties, particle size, degree of irritancy of the formulation as well as the solubility of the therapeutic compounds must be considered. Nasal powder do not have metered dosage and causes nasal mucosa irritancy on application, these are however some of its disadvantages (Akhtar, 2012). Table 2.4 shows Review of some recent development in nasal powder for delivery of therapeutic agents.

Table 2.4: Review of recent development in nasal powder for delivery of therapeutic agents.

Therapeutic Agents	Functions	References
Anthrax vaccine	Prevention of Anthrax	(Wang et al., 2012)
Norwalk virus-like particles (NV VLP) Antigen	Prevention of norovirus infections	(Velasquez et al., 2011)
Tacrine hydrochloride	Treatment of Alzheimer's disease	(Saladini et al., 2013)
Desmopressin	Treatment of nocturnal enuresis	(Fransén et al., 2009)
Sumatriptan	Treatment of migraine	(Djupesland and Dočekal, 2010)
Zolmitriptan	Treatment of migraine	(Gavini et al., 2013)

2.6. THE USE OF SPECIALIZED INTRANASAL DRUG DELIVERY SYSTEMS

In the bid to find solution to the problem of BBB, specialized intranasal drug delivery systems have been developed by researchers to overcome the issue of bioavailability of therapeutic agents to the brain.

2.6.1. Liposomes

There are flexible and conventional liposomes which are differ by their high elastic fluid membranes that permit a number of molecules to pass across via the cellular membranes. (Elsayed et al., 2006; W. Li et al., 2012). Liposomes have several attractive features as pulmonary drug delivery systems particularly with respect to the controlled delivery. One of the alleged advantages of liposomes as a drug carrier is in their ability to effectively encapsulate small and large molecules (Alsarra et al., 2008; Tan et al., 2010) and alter auspiciously the pharmacokinetic profile of the encapsulated substance thereby providing selective and sustained pharmacological effects at the site of administration (Joshi and Misra, 2001). The control release profile of the encapsulated therapeutic agent in liposomes is difficult to manage, this may however be a major disadvantage of this system (Hearnden et al., 2012). Table 2.5 shows recent development in nasal liposomes drug delivery.

Table 2.5: Review of recent development in nasal liposomes for delivery of therapeutic agents.

Therapeutic Agents	Functions	References
Ovalbumin	Chelating agent	(Migliore et al., 2010)
hepatitis B surface antigen (HBsAG)	Vaccine	(Tiwari et al., 2011)
Galanthamine hydrobromide	Treatment of Alzheimer's disease	(W. Li et al., 2012)
Olanzapine	Treatment of schizophrenia	(Salama et al., 2012)
Rivastigmine	Treatment of Alzheimer's	(Arumugam et al., 2008; Mutlu et al., 2011)
Duloxetine	Treatment of depression	(M. I. Alam et al., 2012)

2.6.2. Microspheres

Microspheres are small spherical particles which are made up of macromolecular compounds of sizes of micrometer range usually from 1 to 1000 µm. Microspheres are matrix systems that are manufactured from basically natural and synthetic

polymers, drugs can then be incorporated into the matrix system by dispersion throughout the polymeric matrix. Microspheres have the ability to protect the drug from enzymatic degradation and are capable of prolonging the drug effect by sustained drug release. Table 2.6 shows some recent works done on microspheres as drug delivery system for nasal administration.

Table 2.6: Review of recent development in microspheres for nasal delivery of therapeutic agents.

Therapeutic Agents	Functions	Polymers Used	References
Rokitamycin	Antibiotics	Chitosan	(Gavini et al., 2011)
Rizatriptan Benzoate	Treatment of migraines	*Abelmoschus esculentus* polysaccharide	(Sharma et al., 2013)
Amlodipine Besylate	Treatment of hypertension	Polyvinyl Alcohol	(Swamy and Abbas, 2012)
Ondansetron Hydrochloride	Treatment of nausea and vomiting	Pectin	(Mahajan et al., 2012)
Lorazepam	Treatment of status epileptics	Pluronics PF-127 and PF-68	(Jose et al., 2012)
Valsartan	Treatment of hypertension	hydroxypropyl methylcellulose	(Pardeshi et al., 2012)

2.6.3. Nanoparticles

Nanotechnology is a very recent area of interest by researchers. Nanoparticles are colloidal solid particles with very small size in the nanometer range, usually from 1nm to 1000nm in diameter. Nanoparticulate drug delivery system through the systemic pathway possesses distinct advantages for delivery of drugs to the brain. However, the bioavailability of the therapeutics in the brain is still not satisfied (Hu et al., 2009; Lu et al., 2005; Xia et al., 2012). Intranasal drug delivery of nanoparticles absorb via the olfactory pathway will be a promising way of getting

drugs to the brain and CNS in general. Table 2.7 shows a summary of recent development in nanoparticles for intranasal delivery of therapeutic agents.

2.6.4. Microemulsions

Microemulsions are made up of oil phase, aqueous phase, surfactant and co-surfactant. Due to their lipophilic nature and their small size, microemulsion has been explored to be a good intranasal delivery system which efficiently improves drug absorption in the nasal mucosa. Microemulsion has advantage of being easy to produce compare to other delivery systems, because its production is mainly by mixing and stirring with magnetic stirrer or sonicator or by titration (Patel et al., 2013) and requires simple instruments and laboratory equipments. Microemulsion has been discovered to be a novel approach to improve water solubility of poor water soluble drugs and subsequently increase bioavailability (Mahajan and Rasal, 2013). Table 2.8 shows some of the recent work done using microemulsion as intranasal drug delivery system.

Table 2.7: Summary of recent development in nanoparticles for intranasal delivery of therapeutic agents.

Therapeutic Agents	Functions	Polymers Used	References
Insulin	Treatment of Alzheimer's disease	Glycopolymers. poly(3-acrylamidophenylboronic acid-ran-N-maleated glucosamine)	(Cheng et al., 2012; X. Zhang et al., 2012; Zheng et al., 2013)
NAPVSIPQ (Neuropeptide)	Treatment of Alzheimer's	Poly (ethylene glycol)-co-poly(ε-caprolactone)	(Liu et al., 2013)
Meloxicam	Treatment of rheumatoid arthritis (Anti inflammatory drug)	Polyvinylpyrrolidone	(Kürti et al., 2013)
Losartan Potassium	Treatment of Hypertension	Poly (lactic-co-glycolic acid) PLGA	(Verma et al., 2013)
Venlafaxine	Treatment of depression	Chitosan	(Haque et al., 2012)
Rivastigmine	Treatment of Alzheimer's Disease	Chitosan	(Fazil et al., 2012)
Bromocriptine	Treatment of Parkinson's disease	Chitosan	(Shadab et al., 2012)
Thymoquinone	Treatment of inflammatory disorder and cancer	Chitosan	(S. Alam et al., 2012)
Hepatitis B virus surface antigen (HBsAg)	Vaccine	*N,N,N*-Trimethyl chitosan	(Subbiah et al., 2012)
plasmid DNA	Vaccine	chitosan–sodium deoxycholate	(Cadete et al., 2012)
Clostridium botulinum type-A neurotoxin	Vaccine	Pullulan	(Nochi et al., 2010)
Ovalbumin (as model antigen)	Vaccine	N-trimethyl chitosan	(Bal et al., 2012)

Table 2.8: Summary of recent development in microemulsion for intranasal delivery of therapeutic agents.

Therapeutic Agents	Functions	References
Nimodipine	Treatment for cerebrovascular spasm, stroke and migraine	(Zhang et al., 2004)
Mirtazapine	Treatment of depression	(Thakkar et al., 2013)
Carbamazepine	Treatment of epilepsy	(Acharya et al., 2013)
Olanzapine	Treatment of schizophrenia	(Patel et al., 2013)
Diazepam	Treatment of anxiety disorders, alcohol withdrawal symptoms or muscle spasm	(Porecha et al., 2009)

2.6.5. Nanoemulsions

Nanoemulsions are thermodynamically stable and are stabilized by surfactants (Shafiq et al., 2007). They can be produced by simple emulsification method such as titration and by mixing oil, water, surfactant and co-surfactant together (Shafiq-un-Nabi et al., 2007). They are important vehicles for delivery of hydrophobic compounds, which make them an important intranasal drug delivery system. Due to their characteristic size and properties, which includes kinetic stability, they are very effective in encapsulating the drugs and successfully direct them towards the desired targets (Thiagarajan, 2011). They do not have toxic effect on human and animal cells due to their non-toxicity and non-irritancy (Aboofazeli, 2010) which are excellent properties that make them suitable for therapeutic purposes and good candidates for intranasal delivery system. Table 2.9 shows some of the therapeutic agents that have been recently designed for delivery via intranasal nanoemulsion.

Table 2.9: Review of recent development in nanoemulsion for nasal delivery of therapeutic agents.

Therapeutic Agents	Functions	References
Risperidone	Treatment of psychotic disorders	(Kumar et al., 2009, 2008a)
Olanzapine	Treatment of schizophrenia	(Kumar et al., 2008)
Safranal	Treatment of convulsive disorders	(Jain et al., 2012)
Rizatriptan benzoate	Treatment of migrane	(Bhanushali et al., 2009)

2.6.6. Iontophoretic Delivery

Lerner and coworkers (2004) investigated a method to increase the bioavailability and distribution of drug in the brain by employing iontophoresis as an intranasal delivery system to force the passage of drug from the nasal mucosa across to the brain employing an electric field. In their experiment, they charged up electrodes with drug and then applied it directly deep into the nasal neuro-epithelium of the rabbit, they then position a return electrode at the back of the rabbit's head. When electric current is applied, the charged drug molecules were forcefully driven across the nasal mucosa into the brain via the olfactory pathway. This method actually permits delivery of more therapeutics to the CNS compared to other methods. However, the method is cumbersome and highly invasive since the electrode has to be inserted deep into the nasal cavity potentially damaging the nasal mucosa.

2.7. CHALLENGES AND FUTURE TRENDS OF DIRECT NOSE-TO-BRAIN DELIVERY

There are several challenges facing direct nose to brain delivery. It has been recorded that drugs arrive at the CNS and the brain following nasal delivery, but the quantity of drugs recorded to have reached the brain is limited also the evidence of preferential brain delivery documented is limited. The dimension of the nasal cavity may also limit the dosage per time; the capacity of reaching sufficient

bio-distribution has not been established by this route of administration. Current intranasal delivery systems available cannot exploit the merits of nasal drug delivery maximally due to large amount of the dose been deposited at the anterior segment of the nose and thereby reducing drastically the amount of drugs that will eventually reach the olfactory region resulting in low bioavailability. The drug remaining at the surface of the nasal cavity may cause irritation and foul taste which may result in patient compliance problem.

Most nasal formulations are in form of liquid, powder or gel. Liquid formulation is limited by solubility, stability and dose volume. Powder and gel formulations may be faced with issues of stability, absorption across the mucosal epithelium cells, residence time and degradation. In general nasal drug delivery systems may face the problem of low bioavailability in the CNS and brain due to various factors. Enzymatic barriers which are amongst the limiting factors of drug absorption in the nasal epithelium are caused by the various enzymes such as carboxylesterases that subsist in considerable quantity in the nasal mucosa (Krishnamoorthy and Mitra, 1998). The presence of these enzymes may result in degradation of substances introduced into the nasal mucosa due to their metabolic actions and thereby stand as barrier for intranasal drug absorption into the olfactory epithelium. Enzyme inhibitors such as boroleucine and puromycin may be used to minimize enzymatic metabolism of protein and peptide drugs (Grassin-Delyle et al., 2012). Permeation through the nasal epithelium cells poses a challenge to intranasal drug delivery; drug administered via the nasal mucosa permeates by passive paracellular and active transcellular transport. Drug can also permeate by transport via intercellular tight junctions, transcytosis and carrier mediated transport (Arora et al., 2002). Low molecular weight and lipophilic drugs can permeate with ease across the nasal mucosa epithelium, but hydrophilic drugs and high molecular therapeutic agents such as peptide and protein have low permeability (Bahadur and Pathak, 2012) and therefore present challenges in intranasal delivery. The use of permeation enhancers and prodrugs has been employed to improve permeability in nasal drug delivery.

Mucociliary clearance is a vital defense mechanism of the respiratory system that protects the lung against noxious inhaled pathogens such as bacteria, allergens, virus, toxins and other undesirable substances (Fliegauf et al., 2013; Alagusundaram et al., 2010; Kanthakumar et al., 1994). When these substances reach the nasal mucosa, they adhere and dissolve in the mucus lining and are transported to the GIT through the nasopharynx for onward ejection into the GIT. This is the one of the fates of therapeutic agents introduced to the nasal cavity. The clearing mechanism reduces the transport of drugs to the CNS and brain through the olfactory pathway and also reduces the residence time of drugs in the nasal cavity. These factors contribute to limiting the bioavailability of therapeutics in the CNS. Mucocilliary clearance depends on the drug site deposition and deposition area also depend on parameters including mode of nasal administration, texture of the formulation, physicochemical properties of the drug and the velocity of the delivered particles [169]. The mucocilliary clearance problem can be overcome by using mucoadhesive polymers in formulating nasal drug delivery system. Alginate and Chitosan are good examples of mucoadhesive polymers that can be employed in formulation of nasal drugs. Chitosan has been used by various researchers (Fazil et al., 2012; Haque et al., 2012; Gavini et al., 2011) to increase the mucoadhesion of formulation in order to increase the residence time of the therapeutic agent in the nasal cavity. Poor physicochemical properties of the drugs and formulations may be another issue that needs to be addressed to achieve successful intranasal drug delivery.

The use of novel and specialized approaches such as nanoparticles, microspheres, liposomes mucoadhesive polymers to encapsulate and protect the drugs has been a way to enhance the bioavailability of drugs in the brain and CNS. Mechanisms of transport and absorption of drugs in the nasal epithelium is another issue to be considered, for example some of the solutes introduced to the nasal cavity follow the trigeminal route and major part of the solutes may be distributed to the orofacial tissues which may reduce bioavailability of drugs in the brain and the CNS as evidenced by the work of Johnson et al. Trigeminally innervated structures were found to have up to 20-fold higher tissue concentrations of lidocaine than the brain and blood following intranasal

administration of lidocaine to rats (Johnson et al., 2010). In addition, the nasal vasculature is undeniably another limiting factor to direct nasal mucosa delivery to the CNS and brain to treat neurogenerative diseases as it clears applied therapeutic agents into the system circulation for possible systemic delivery or elimination. This may be overcome by ensuring rapid movement of therapeutic agents to the olfactory region for onward delivery to the brain via the olfactory pathway.

Considering the mechanism involved in transporting the drug directly to the brain which depends on passive diffusion of the drugs to the olfactory epithelium before being transported to the brain, substantial part of the drugs may have found their way into the blood and then follow the systemic pathway thereby limiting the amount of drug that will follow the olfactory pathway for onward delivery to the CNS. This action ultimately reduces bioavailability to the brain and CNS. A formidable strategy is therefore desirable which will not only enhance the bioavailability of the drugs in brain and CNS (by the drugs going through the olfactory pathway) but ultimately ensuring timely and sustainable delivery to the brain and CNS within the shortest possible time in order to prevent drugs passing through the systemic pathway. Researchers are thus challenged to find an improved and better method of getting the drugs into the brain via the nasal mucosa in order to increase bioavailability of drugs in the brain by transportation and absorption going through the olfactory pathway instead of the systemic pathway.

2.8. CONCLUDING REMARKS

This chapter shows evidence of direct nasal mucosa to brain and CNS delivery, the importance of the intranasal route of administration and its great potential as a means of delivering therapeutic agents to the brain for the management of brain diseases that may not have been possible due to the BBB and other barriers. The nasal mucosa is very rich in blood vessels and capillaries for systemic delivery, the probability of the drugs administered intranasally getting absorbed into the

systemic pathway is very high, even though, only molecules permeable through BBB will eventually reach the brain.

All the researches enumerated in this chapter have employed the mechanism of passive diffusion that relies mainly on instillation of drug deep in the nasal cavity, physicochemical properties of the nasal and neuro-epithelia as well as gravity to penetrate the brain and CNS via the olfactory pathway. However, substantial quantities of drugs still go through the systemic pathway thereby reducing the quantity via the olfactory pathway. This is a challenge in the intranasal delivery of drugs as this action reduces the bioavailability of the drugs in the brain. Application of a 'driving force' that can propel the therapeutic agents directly to the brain after being administered through the nasal mucosa may be a promising way of increasing bioavailability and decrease the time drugs reach the CNS and brain for the treatment of neurogenerative diseases. This method could be achieved by employing the use of electroactive polymers in formulating intranasal drug delivery system with the aid of external stimuli such as electromagnetic force to propel non-invasively the drugs directly from the nose to CNS within shortest time in a sustainable manner. This could be proffered as a future advancement in intranasal drug delivery in the management of CNS diseases and brain disorder.

2.9. REFERENCES

Abbott, N.J., Patabendige, A.A.K., Dolman, D.E.M., Yusof, S.R., Begley, D.J., 2010. Structure and function of the blood–brain barrier. Neurobiol. Dis. 37, 13–25.

Aboofazeli, R., 2010. Nanometric-Scaled Emulsions (Nanoemulsions). Iran. J. Pharm. Res. 325–326.

Acharya, S.P., Pundarikakshudu, K., Panchal, A., Lalwani, A., 2013. Development of carbamazepine transnasal microemulsion for treatment of epilepsy. Drug Deliv. Transl. Res. 1–8.

Afifi, F., Al-Khalidi, B., Khalil, E., 2005. Studies on the in vivo hypoglycemic activities of two medicinal plants used in the treatment of diabetes in

Jordanian traditional medicine following intranasal administration. J. Ethnopharmacol. 100, 314–318.

Akhtar, M.A., 2012. A Novel Intranasal Drug Delivery System: Review. Nov. Sci. Int. J. Pharm. Sci. 1, 8.

Aktas, D., Kalcioglu, M.T., Kutlu, R., Ozturan, O., Oncel, S., 2003. The relationship between the concha bullosa, nasal septal deviation and sinusitis. Rhinology 41, 103–106.

Alagusundaram, M., Chengaiah, C., Gnanaprakash, K., Ramkanth, S., Chetty, C.M., Dhachinamoorthi, D., 2010. Nasal drug delivery system-an overview. Int J Res Pharm Sci 1, 454–465.

Alam, M.I., Baboota, S., Ahuja, A., Ali, M., Ali, J., Sahni, J.K., 2012. Intranasal administration of nanostructured lipid carriers containing CNS acting drug: Pharmacodynamic studies and estimation in blood and brain. J. Psychiatr. Res. 46, 1133–1138.

Alam, M.I., Baboota, S., Ahuja, A., Ali, M., Ali, J., Sahni, J.K., Bhatnagar, A., 2014. Pharmacoscintigraphic evaluation of potential of lipid nanocarriers for nose-to-brain delivery of antidepressant drug. Int. J. Pharm. 470, 99–106.

Alam, M.I., Beg, S., Samad, A., Baboota, S., Kohli, K., Ali, J., Ahuja, A., Akbar, M., 2010. Strategy for effective brain drug delivery. Eur. J. Pharm. Sci. 40, 385–403.

Alam, S., Khan, Z.I., Mustafa, G., Kumar, M., Islam, F., Bhatnagar, A., Ahmad, F.J., 2012. Development and evaluation of thymoquinone-encapsulated chitosan nanoparticles for nose-to-brain targeting: a pharmacoscintigraphic study. Int. J. Nanomedicine 7, 5705.

Alcalá-Barraza, S.R., Lee, M.S., Hanson, L.R., McDonald, A.A., Frey, W.H., McLoon, L.K., 2010. Intranasal delivery of neurotrophic factors BDNF, CNTF, EPO, and NT-4 to the CNS. J. Drug Target. 18, 179–190.

Al-Ghananeem, A.M., Saeed, H., Florence, R., Yokel, R.A., Malkawi, A.H., 2010. Intranasal drug delivery of didanosine-loaded chitosan nanoparticles for brain targeting; an attractive route against infections caused by AIDS viruses. J. Drug Target. 18, 381–388.

Alsarra, I.A., Hamed, A.Y., Alanazi, F.K., 2008. Acyclovir liposomes for intranasal systemic delivery: development and pharmacokinetics evaluation. Drug Deliv. 15, 313–321.

Alsarra, I.A., Hamed, A.Y., Alanazi, F.K., El Maghraby, G.M., 2010. Vesicular systems for intranasal drug delivery, in: Drug Delivery to the Central Nervous System. Springer, pp. 175–203.

Alves, J.L., 2014. Blood–brain barrier and traumatic brain injury. J. Neurosci. Res. 92, 141–147.

Andrews, G.P., Laverty, T.P., Jones, D.S., 2009. Mucoadhesive polymeric platforms for controlled drug delivery. Eur. J. Pharm. Biopharm. Off. J. Arbeitsgemeinschaft Pharm. Verfahrenstechnik EV 71, 505–518.

Arora, P., Sharma, S., Garg, S., 2002. Permeability issues in nasal drug delivery. Drug Discov. Today 7, 967–975.

Arumugam, K., Subramanian, G., Mallayasamy, S., Averineni, R., Reddy, M., Udupa, N., 2008. A study of rivastigmine liposomes for delivery into the brain through intranasal route. 58, 287–297.

Aryal, M., Arvanitis, C.D., Alexander, P.M., McDannold, N., 2014. Ultrasound-mediated blood–brain barrier disruption for targeted drug delivery in the central nervous system. Adv. Drug Deliv. Rev., Ultrasound triggered drug delivery 72, 94–109.

Aukema, A.A.C., Mulder, P.G.H., Fokkens, W.J., 2005. Treatment of nasal polyposis and chronic rhinosinusitis with fluticasone propionate nasal drops reduces need for sinus surgery. J. Allergy Clin. Immunol. 115, 1017–1023.

Badie, H., 2012. Bioadhesive Brain Targeted Nasal Delivery of an Ant ischemic Drug. Int. J. Pharm. Biol. Arch. 3, 1067-1076.

Bahadur, S., Pathak, K., 2012. Physicochemical and physiological considerations for efficient nose-to-brain targeting. Expert Opin. Drug Deliv. 9, 19–31.

Bal, S.M., Slütter, B., Verheul, R., Bouwstra, J.A., Jiskoot, W., 2012. Adjuvanted, antigen loaded N-trimethyl chitosan nanoparticles for nasal and intradermal vaccination: adjuvant-and site-dependent immunogenicity in mice. Eur. J. Pharm. Sci. 45, 475–481.

Basu, S., Bandyopadhyay, A.K., 2010. Development and characterization of mucoadhesive *in situ* nasal gel of midazolam prepared with Ficus carica mucilage. AAPS PharmSciTech 11, 1223–1231.

Begley, D.J., 1996. The Blood-brain Barrier: Principles for Targeting Peptides and Drugs to the Central Nervous System. J. Pharm. Pharmacol. 48, 136–146.

Bhalerao, A., Lonkar, S., Deshkar, S., Shirolkar, S., Deshpande, A., 2009. Nasal mucoadhesive *in situ* gel of ondansetron hydrochloride. Indian J. Pharm. Sci. 71, 711.

Bhanushali, R., Gatne, M., Gaikwad, R., Bajaj, A., Morde, M., 2009. Nanoemulsion based intranasal delivery of antimigraine drugs for nose to brain targeting. Indian J. Pharm. Sci. 71, 707.

Bleier, B.S., Kohman, R.E., Feldman, R.E., Ramanlal, S., Han, X., 2013. Permeabilization of the Blood-Brain Barrier via Mucosal Engrafting: Implications for Drug Delivery to the Brain. PloS One 8, e61694.

Blondal, T., Gudmundsson, L.J., Olafsdottir, I., Gustavsson, G., Westin, A., 1999. Nicotine nasal spray with nicotine patch for smoking cessation: randomised trial with six year follow up. BMJ 318, 285.

Brouillette, R.T., Manoukian, J.J., Ducharme, F.M., Oudjhane, K., Earle, L.G., Ladan, S., Morielli, A., 2001. Efficacy of fluticasone nasal spray for pediatric obstructive sleep apnea. J. Pediatr. 138, 838–844.

Buck, L., Axel, R., 1991. A novel multigene family may encode odorant receptors: a molecular basis for odor recognition. Cell 65, 175–187.

Buck, L.B., 2005. Unraveling the Sense of Smell (Nobel Lecture). Angew. Chem. Int. Ed. 44, 6128–6140.

Cadete, A., Figueiredo, L., Lopes, R., Calado, C.C.R., Almeida, A.J., Gonçalves, L.M.D., 2012. Development and characterization of a new plasmid delivery system based on chitosan–sodium deoxycholate nanoparticles. 3rd ESF-UB Conf. Nanomedicine 45, 451–458.

Chalbot, S., Zetterberg, H., Blennow, K., Fladby, T., Grundke-Iqbal, I., Iqbal, K., 2010. Cerebrospinal fluid secretory Ca< sup> 2 -dependent phospholipase A2 activity: A biomarker of blood–cerebrospinal fluid barrier permeability. Neurosci. Lett. 478, 179–183.

Chaturvedi, M., Kumar, M., Pathak, K., 2011. A review on mucoadhesive polymer used in nasal drug delivery system. J. Adv. Pharm. Technol. Res. 2, 215.

Cheng, C., Zhang, X., Xiang, J., Wang, Y., Zheng, C., Lu, Z., Li, C., 2012. Development of novel self-assembled poly (3-acrylamidophenylboronic acid)/poly (2-lactobionamidoethyl methacrylate) hybrid nanoparticles for improving nasal adsorption of insulin. Soft Matter 8, 765–773.

Chen, X., Zhi, F., Jia, X., Zhang, X., Ambardekar, R., Meng, Z., Paradkar, A.R., Hu, Y., Yang, Y., 2013. Enhanced brain targeting of curcumin by intranasal administration of a thermosensitive poloxamer hydrogel. J. Pharm. Pharmacol. 65, 807–816.

Chesnut III, C.H., Silverman, S., Andriano, K., Genant, H., Gimona, A., Harris, S., Kiel, D., LeBoff, M., Maricic, M., Miller, P., Moniz, C., Peacock, M., Richardson, P., Watts, N., Baylink, D., 2000. A randomized trial of nasal spray salmon calcitonin in postmenopausal women with established osteoporosis: the prevent recurrence of osteoporotic fractures study. Am. J. Med. 109, 267–276.

Chiappetta, D.A., Hocht, C., Opezzo, J.A., Sosnik, A., 2013. Intranasal administration of antiretroviral-loaded micelles for anatomical targeting to the brain in HIV. Nanomed. 8, 223–237.

Chur, V., Small, C.B., Stryszak, P., Teper, A., 2013. Safety of mometasone furoate nasal spray in the treatment of nasal polyps in children. Pediatr. Allergy Immunol. 24, 33–38.

Daley-Yates, P.T., Baker, R.C., 2001. Systemic bioavailability of fluticasone propionate administered as nasal drops and aqueous nasal spray formulations. Br. J. Clin. Pharmacol. 51, 103–105.

Dalpiaz, A., Ferraro, L., Perrone, D., Leo, E., Iannuccelli, V., Pavan, B., Paganetto, G., Beggiato, S., Scalia, S., 2014. Brain Uptake of a Zidovudine Prodrug after Nasal Administration of Solid Lipid Microparticles. Mol. Pharm.

Dhuria, S.V., Hanson, L.R., Frey, W.H., 2010. Intranasal delivery to the central nervous system: mechanisms and experimental considerations. J. Pharm. Sci. 99, 1654–1673.

Dhuria, S.V., Hanson, L.R., Frey, W.H., 2009. Intranasal drug targeting of hypocretin-1 (orexin-A) to the central nervous system. J. Pharm. Sci. 98, 2501–2515.

Djupesland, P., Dočekal, P., 2010. Intranasal sumatriptan powder delivered by a novel breath-actuated bi-directional device for the acute treatment of migraine: A randomised, placebo-controlled study. Cephalalgia 30, 933–942.

El-Gendy, S., Alsafy, M., 2010. Nasal and paranasal sinuses of the donkey: gross anatomy and computed tomography. J. Vet.Anat.Vol 3, 25–41.

Elsayed, M.M.A., Abdallah, O.Y., Naggar, V.F., Khalafallah, N.M., 2006. Deformable liposomes and ethosomes: Mechanism of enhanced skin delivery. Int. J. Pharm. 322, 60–66.

Eskandari, S., Varshosaz, J., Minaiyan, M., Tabbakhian, M., 2011. Brain delivery of valproic acid via intranasal administration of nanostructured lipid carriers: in vivo pharmacodynamic studies using rat electroshock model. Int. J. Nanomedicine 6, 363.

Fazil, M., Md, S., Haque, S., Kumar, M., Baboota, S., Ali, J., 2012. Development and evaluation of rivastigmine loaded chitosan nanoparticles for brain targeting. Eur. J. Pharm. Sci. 47, 6–15.

Fine, J., Baillargeon, A., Renner, D., Hoerster, N., Tokarev, J., Colton, S., Pelleg, A., Andrews, A., Sparley, K., Krogh, K., 2012. Intranasal deferoxamine improves performance in radial arm water maze, stabilizes HIF-1α, and phosphorylates GSK3β in P301L tau transgenic mice. Exp. Brain Res. 219, 381–390.

Fliegauf, M., Sonnen, A.F.-P., Kremer, B., Henneke, P., 2013. Mucociliary Clearance Defects in a Murine *In Vitro* Model of Pneumococcal Airway Infection. PloS One 8, e59925.

Fonollosa, J., Gutierrez-Galvez, A., Marco, S., 2012. Quality Coding by Neural Populations in the Early Olfactory Pathway: Analysis Using Information Theory and Lessons for Artificial Olfactory Systems. PloS One 7, e37809.

Fransén, N., Bredenberg, S., Björk, E., 2009. Clinical study shows improved absorption of desmopressin with novel formulation. Pharm. Res. 26, 1618–1625.

Gavini, E., Rassu, G., Ferraro, L., Beggiato, S., Alhalaweh, A., Velaga, S., Marchetti, N., Bandiera, P., Giunchedi, P., Dalpiaz, A., 2013. Influence of polymeric microcarriers on the in vivo intranasal uptake of an anti-migraine drug for brain targeting. Eur. J. Pharm. Biopharm. 83, 174–183.

Gavini, E., Rassu, G., Ferraro, L., Generosi, A., Rau, J.V., Brunetti, A., Giunchedi, P., Dalpiaz, A., 2011. Influence of chitosan glutamate on the in vivo intranasal absorption of rokitamycin from microspheres. J. Pharm. Sci. 100, 1488–1502.

Grassin-Delyle, S., Buenestado, A., Naline, E., Faisy, C., Blouquit-Laye, S., Couderc, L.-J., Le Guen, M., Fischler, M., Devillier, P., 2012. Intranasal drug delivery: an efficient and non-invasive route for systemic administration: focus on opioids. Pharmacol. Ther. 134, 366–379.

Griep, L.M., Wolbers, F., Wagenaar, B. de, Braak, P.M. ter, Weksler, B.B., Romero, I.A., Couraud, P.O., Vermes, I., Meer, A.D. van der, Berg, A. van den, 2013. BBB ON CHIP: microfluidic platform to mechanically and biochemically modulate blood-brain barrier function. Biomed. Microdevices 15, 145–150.

Groothuis, D.R., 2000. The blood-brain and blood-tumor barriers: a review of strategies for increasing drug delivery. Neuro-Oncol. 2, 45–59.

Guastella, A.J., Einfeld, S.L., Gray, K.M., Rinehart, N.J., Tonge, B.J., Lambert, T.J., Hickie, I.B., 2010. Intranasal Oxytocin Improves Emotion Recognition for Youth with Autism Spectrum Disorders. Dev. Inhib. Control Atten. - DeficitHyperactivity Disord. 67, 692–694.

Hanson, L.R., Frey, W.H., 2008. Intranasal delivery bypasses the blood-brain barrier to target therapeutic agents to the central nervous system and treat neurodegenerative disease. BMC Neurosci. 9, S5.

Hanson, L.R., Roeytenberg, A., Martinez, P.M., Coppes, V.G., Sweet, D.C., Rao, R.J., Marti, D.L., Hoekman, J.D., Matthews, R.B., Frey, W.H., 2009. Intranasal deferoxamine provides increased brain exposure and significant protection in rat ischemic stroke. J. Pharmacol. Exp. Ther. 330, 679–686.

Haque, S., Shadab, M., Fazil, M., Kumar, M., Sahni, J.K., Ali, J., Baboota, S., 2012. Venlafaxine loaded chitosan NPs for brain targeting: Pharmacokinetic and pharmacodynamic evaluation. Carbohydr. Polym. 89, 72–79.

Hearnden, V., Sankar, V., Hull, K., Juras, D.V., Greenberg, M., Kerr, A.R., Lockhart, P.B., Patton, L.L., Porter, S., Thornhill, M.H., 2012. New developments and opportunities in oral mucosal drug delivery for local and systemic disease. 2012 Ed. Collect. 64, 16–28.

Hinchcliffe, M., Illum, L., 1999. Intranasal insulin delivery and therapy. Adv. Drug Deliv. Rev. 35, 199–234.

Hjalmarson, A., Franzon, M., Westin, A., Wiklund, O., 1994. Effect of nicotine nasal spray on smoking cessation: a randomized, placebo-controlled, double-blind study. Arch. Intern. Med. 154, 2567.

Hu, K., Li, J., Shen, Y., Lu, W., Gao, X., Zhang, Q., Jiang, X., 2009. Lactoferrin-conjugated PEG–PLA nanoparticles with improved brain delivery: *In vitro and in vivo* evaluations. J. Controlled Release 134, 55–61.

Illum, L., 2004. Is nose-to-brain transport of drugs in man a reality? J. Pharm. Pharmacol. 56, 3–17.

Illum, L., 2000. Transport of drugs from the nasal cavity to the central nervous system. Eur. J. Pharm. Sci. 11, 1–18.

Jain, G., Pathan, S., Zaidi, S., Vohora, D., Kumar, N., Bhatnagar, A., Ahmad, F., Khar, R., 2012. Mucoadhesive Nanoemulsion of Safranal for the Treatment of Epilepsy. Planta Med. 78, P_112.

James Zinreich, S., Abidin, M., Kennedy, D.W., 1990. Cross-sectional imaging of the nasal cavity and paranasal sinuses. Endosc. Sinus Surg. 1, 94–98.

Johanson, C., Stopa, E., McMillan, P., Roth, D., Funk, J., Krinke, G., 2011. The Distributional Nexus of Choroid Plexus to Cerebrospinal Fluid, Ependyma and Brain Toxicologic/Pathologic Phenomena, Periventricular Destabilization, and Lesion Spread. Toxicol. Pathol. 39, 186–212.

Johnson, N.J., Hanson, L.R., Frey, W.H., 2010. Trigeminal pathways deliver a low molecular weight drug from the nose to the brain and orofacial structures. Mol. Pharm. 7, 884–893.

Jose, S., Ansa, C., Cinu, T., Chacko, A., Aleykutty, N., Ferreira, S., Souto, E., 2012. Thermo-sensitive gels containing lorazepam microspheres for intranasal brain targeting. Int. J. Pharm. 441, 516–526.

Jose, S., Ansa, C.R., Cinu, T.A., Chacko, A.J., Aleykutty, N.A., Ferreira, S.V., Souto, E.B., 2013. Thermo-sensitive gels containing lorazepam microspheres for intranasal brain targeting. Int. J. Pharm. 441, 516–526.

Joshi, A.S., Patel, H.S., Belgamwar, V.S., Agrawal, A., Tekade, A.R., 2012. Solid lipid nanoparticles of ondansetron HCl for intranasal delivery: development, optimization and evaluation. J. Mater. Sci. Mater. Med. 23, 2163–2175.

Joshi, M., Misra, A., 2001. Dry powder inhalation of liposomal Ketotifen fumarate: formulation and characterization. Int. J. Pharm. 223, 15–27.

Kanazawa, T., Akiyama, F., Kakizaki, S., Takashima, Y., Seta, Y., 2013. Delivery of siRNA to the brain using a combination of nose-to-brain delivery and cell-penetrating peptide-modified nano-micelles. Biomaterials 34, 9220–9226.

Kanthakumar, K., Cundell, D., Johnson, M., Wills, P., Taylor, G., Cole, P., Wilson, R., 1994. Effect of salmeterol on human nasal epithelial cell ciliary beating: inhibition of the ciliotoxin, pyocyanin. Br. J. Pharmacol. 112, 493–498.

Kaur, I.P., Bhandari, R., Bhandari, S., Kakkar, V., 2008. Potential of solid lipid nanoparticles in brain targeting. J. Controlled Release 127, 97–109.

Khan, S., Patil, K., Bobade, N., Yeole, P., Gaikwad, R., 2010. Formulation of intranasal mucoadhesive temperature-mediated *in situ* gel containing ropinirole and evaluation of brain targeting efficiency in rats. J. Drug Target. 18, 223–234.

Krishnamoorthy, R., Mitra, A.K., 1998. Prodrugs for nasal drug delivery. Adv. Drug Deliv. Rev. 29, 135–146.

Krol, S., 2012. Challenges in drug delivery to the brain: Nature is against us. J. Controlled Release 164, 145–155.

Kuhnline Sloan, C.D., Nandi, P., Linz, T.H., Aldrich, J.V., Audus, K.L., Lunte, S.M., 2012. Analytical and Biological Methods for Probing the Blood-Brain Barrier. Annu. Rev. Anal. Chem. 5, 505–531.

Kumar, M., Misra, A., Babbar, A., Mishra, A., Mishra, P., Pathak, K., 2008a. Intranasal nanoemulsion based brain targeting drug delivery system of risperidone. Int. J. Pharm. 358, 285–291.

Kumar, M., Misra, A., Mishra, A., Mishra, P., Pathak, K., 2008b. Mucoadhesive nanoemulsion-based intranasal drug delivery system of olanzapine for brain targeting. J. Drug Target. 16, 806–814.

Kumar, M., Pathak, K., Misra, A., 2009. Formulation and characterization of nanoemulsion-based drug delivery system of risperidone. Drug Dev. Ind. Pharm. 35, 387–395.

Kürti, L., Gáspár, R., Márki, Á., Kápolna, E., Bocsik, A., Veszelka, S., Bartos, C., Ambrus, R., Vastag, M., Deli, M.A., 2013. *In vitro* and in vivo characterization of meloxicam nanoparticles designed for nasal administration. Eur. J. Pharm. Sci. 50, 86–92.

Lam, C.H., Hansen, E.A., Janson, C., Bryan, A., Hubel, A., 2012. The characterization of arachnoid cell transport II: Paracellular transport and blood–cerebrospinal fluid barrier formation. Neuroscience 222, 228–238.

Langille, M., Walters, E., Dziegielewski, P.T., Kotylak, T., Wright, E.D., 2012. Frontal sinus cells: Identification, prevalence, and association with frontal sinus mucosal thickening. Am. J. Rhinol. Allergy 26, e107–e110.

Lee, S.L., Lawrence, X.Y., Cai, B., Johnsons, G.R., Rosenberg, A.S., Cherney, B.W., Guo, W., Raw, A.S., 2011. Scientific considerations for generic synthetic salmon calcitonin nasal spray products. AAPS J. 13, 14–19.

Lerner, E.N., van Zanten, E.H., Stewart, G.R., 2004. Enhanced delivery of octreotide to the brain via transnasal iontophoretic administration. J. Drug Target. 12, 273–280.

Li, L., Nandi, I., Kim, K.H., 2002. Development of an ethyl laurate-based microemulsion for rapid-onset intranasal delivery of diazepam. Int. J. Pharm. 237, 77–85.

Liu, Z., Jiang, M., Kang, T., Miao, D., Gu, G., Song, Q., Yao, L., Hu, Q., Tu, Y., Pang, Z., 2013. Lactoferrin-modified PEG-co-PCL nanoparticles for enhanced brain delivery of NAP peptide following intranasal administration. Biomaterials. 34, 3870–3881.

Liu, Z., Li, Y., Zhang, L., Xin, H., Cui, Y., Hanson, L.R., Frey II, W.H., Chopp, M., 2012. Subacute intranasal administration of tissue plasminogen activator increases functional recovery and axonal remodeling after stroke in rats. Neurobiol. Dis. 45, 804–809.

Li, W., Zhou, Y., Zhao, N., Hao, B., Wang, X., Kong, P., 2012. Pharmacokinetic behavior and efficiency of acetylcholinesterase inhibition in rat brain after

intranasal administration of galanthamine hydrobromide loaded flexible liposomes. Environ. Toxicol. Pharmacol. 34, 272–279.

Lu, C.-T., Zhao, Y.-Z., Wong, H.L., Cai, J., Peng, L., Tian, X.-Q., 2014. Current approaches to enhance CNS delivery of drugs across the brain barriers. Int. J. Nanomedicine 9, 2241–2257.

Lu, W., Zhang, Y., Tan, Y.-Z., Hu, K.-L., Jiang, X.-G., Fu, S.-K., 2005. Cationic albumin-conjugated pegylated nanoparticles as novel drug carrier for brain delivery. J. Controlled Release 107, 428–448.

Maggio, E.T., Pillion, D.J., 2013. High efficiency intranasal drug delivery using Intravail® alkylsaccharide absorption enhancers. Drug Deliv. Transl. Res. 3, 16–25.

Mahajan, H.S., Rasal, A.D., 2013a. Microemulsions for Nasal Drug Delivery Systems: An Overview. Int.J.Pharm. 5, 1825–1831.

Mahajan, H.S., Rasal, A.D., 2013b. Microemulsions for Nasal Drug Delivery Systems: An Overview. Int.J.Pharm. 5, 1825–1831.

Mahajan, H.S., Tatiya, B.V., Nerkar, P.P., 2012. Ondansetron loaded pectin based microspheres for nasal administration: *In vitro* and in vivo studies. Powder Technol. 221, 168–176.

Majithiya, R.J., Ghosh, P.K., Umrethia, M.L., Murthy, R.S., 2006. Thermoreversible-mucoadhesive gel for nasal delivery of sumatriptan. AAPS PharmSciTech 7, E80–E86.

Migliore, M.M., Vyas, T.K., Campbell, R.B., Amiji, M.M., Waszczak, B.L., 2010. Brain delivery of proteins by the intranasal route of administration: a comparison of cationic liposomes versus aqueous solution formulations. J. Pharm. Sci. 99, 1745–1761.

Misra, A., Ganesh, S., Shahiwala, A., Shah, S.P., 2003. Drug delivery to the central nervous system: a review. J Pharm Pharm Sci 6, 252–273.

Mistri, P.A., Patel, D.J., Prajapati, J.J., 2012. Intranasal Drug Delivery System: A Review. Int. J. Pharm. Innov. 2. 88-111.

Mistry, A., Stolnik, S., Illum, L., 2009. Nanoparticles for direct nose-to-brain delivery of drugs. Int. J. Pharm. 379, 146–157.

Mutlu, N.B., Degim, Z., Yilmaz, S., Essiz, D., Nacar, A., 2011. New perspective for the treatment of Alzheimer diseases: liposomal rivastigmine formulations. Drug Dev. Ind. Pharm. 37, 775–789.

Nag, S., Kapadia, A., Stewart, D.J., 2011. Review: Molecular pathogenesis of blood brain barrier breakdown in acute brain injury. Neuropathol. Appl. Neurobiol. 37, 3–23.

Napier, S.S., 2013. Nasal Cavities and Paranasal Sinuses, in: Histopathology Specimens. Springer, pp. 135–141.

Nochi, T., Yuki, Y., Takahashi, H., Sawada, S., Mejima, M., Kohda, T., Harada, N., Kong, I.G., Sato, A., Kataoka, N., 2010. Nanogel antigenic protein-delivery system for adjuvant-free intranasal vaccines. Nat. Mater. 9, 572–578.

Ozsoy, Y., Gungor, S., Cevher, E., 2009. Nasal delivery of high molecular weight drugs. Molecules 14, 3754–3779.

Padowski, J.M., Pollack, G.M., 2010. Examination of the ability of the nasal administration route to confer a brain exposure advantage for three chemical inhibitors of P-glycoprotein. J. Pharm. Sci. 99, 3226–3233.

Pardeshi, C.V., Rajput, P.V., Belgamwar, V.S., Tekade, A.R., 2012. Formulation, optimization and evaluation of spray-dried mucoadhesive microspheres as intranasal carriers for Valsartan. J. Microencapsul. 29, 103–114.

Patel, C.J., 2013. A Recent Review On Alternative System of Parenteral Delivery: Nasal Drug Delivery System. J. Drug Discov. Ther. 1, 12-18.

Patel, R.B., Patel, M.R., Bhatt, K.K., Patel, B.G., 2013. Formulation and Evaluation of Microemulsions-Based Drug Delivery System for Intranasal Administration of Olanzapine. Int. J. Biomed. Pharm. Sci. 7, 20–27.

Patel, S., Chavhan, S., Soni, H., Babbar, A., Mathur, R., Mishra, A., Sawant, K., 2011. Brain targeting of risperidone-loaded solid lipid nanoparticles by intranasal route. J. Drug Target. 19, 468–474.

Peter, J.W., 2003. The agger nasi cell: the key to understanding the anatomy of the frontal recess. Otolaryngol.--Head Neck Surg. 129, 497–507.

Piechowiak, M., Videcoq, A., Ferrando, R., Bochicchio, D., Pagnoux, C., Rossignol, F., 2012. Aggregation kinetics and gel formation in modestly concentrated suspensions of oppositely charged model ceramic colloids: a numerical study. Phys. Chem. Chem. Phys. 14, 1431–1439.

Porecha, S., shah, T., Jogani, V., Naik, S., Misra, A., 2009. Microemulsion based intranasal delivery system for treatment of insomnia. Drug Deliv. 16, 128–134.

Preetha, P., Priscilla, J., Padmavathi, R., Sitalakshmi, R., Bagavad, G., AS, S., 2013. The Effect of Ageing on Nasal Mucociliary Clearance in Women: A Pilot Study. ISRN Pulmonol. 2013.

Pringels, E., Callens, C., Vervaet, C., Dumont, F., Slegers, G., Foreman, P., Remon, J.P., 2006. Influence of deposition and spray pattern of nasal powders on insulin bioavailability. Int. J. Pharm. 310, 1–7.

Pund, S., Rasve, G., Borade, G., 2013. *Ex vivo* permeation characteristics of venlafaxine through sheep nasal mucosa. Eur. J. Pharm. Sci. 48, 195–201.

Radbruch, L., Torres, L.M., Ellershaw, J.E., Gatti, A., Lerzo, G.L., Revnic, J., Taylor, D., 2012. Long-term tolerability, efficacy and acceptability of fentanyl pectin nasal spray for breakthrough cancer pain. Support. Care Cancer 20, 565–573.

Radhika, B., Baloju, S., Chandrashekar Vemula, R.C., Swapna, K., Thati, M., 2011. Blood-Brain Barrier–Its Implication in Drug Transport: Novel Strategies in Drug Delivery to The Brain. Int. J. 1, 265–278.

Renner, D.B., Frey II, W.H., Hanson, L.R., 2012a. Intranasal delivery of siRNA to the olfactory bulbs of mice via the olfactory nerve pathway. Neurosci. Lett. 513, 193–197.

Renner, D.B., Frey II, W.H., Hanson, L.R., 2012b. Intranasal delivery of siRNA to the olfactory bulbs of mice< i> via the olfactory nerve pathway. Neurosci. Lett. 513, 193–197.

Renner, D.B., Svitak, A.L., Gallus, N.J., Ericson, M.E., Frey, W.H., Hanson, L.R., 2012c. Intranasal delivery of insulin via the olfactory nerve pathway. J. Pharm. Pharmacol. 64, 1709–1714.

Roth, L.J., Barlow, C.F., 1961. Drugs in the brain. Science 134, 22–31.

Saladini, B., Bigucci, F., Cerchiara, T., Gallucci, M.C., Luppi, B., 2013. Microparticles based on chitosan/pectin polyelectrolyte complexes for nasal delivery of tacrine hydrochloride. Drug Deliv. Transl. Res. 3, 33–41.

Salama, H.A., Mahmoud, A.A., Kamel, A.O., Hady, M.A., Awad, G.A., 2012. Phospholipid based colloidal poloxamer-nanocubic vesicles for brain targeting via the nasal route. Colloids Surf. B Biointerfaces. 100, 146–154.

Schlosshauer, B., Steuer, H., 2002. Comparative anatomy, physiology and *in vitro* models of the blood-brain and blood-retina barrier. Curr. Med. Chem.-Cent. Nerv. Syst. Agents 2, 175–186.

Shadab, M., Khan, R.A., Mustafa, G., Chuttani, K., Baboota, S., Ali, J., 2012. Bromocriptine loaded chitosan nanoparticles intended for direct nose to brain delivery: Pharmacodynamic, Pharmacokinetic and Scintigraphy study in mice model. Eur. J. Pharm. Sci. 48, 393–405.

Shafiq, S., Shakeel, F., Talegaonkar, S., Ahmad, F.J., Khar, R.K., Ali, M., 2007. Development and bioavailability assessment of ramipril nanoemulsion formulation. Eur. J. Pharm. Biopharm. 66, 227–243.

Shafiq-un-Nabi, S., Shakeel, F., Talegaonkar, S., Ali, J., Baboota, S., Ahuja, A., Khar, R.K., Ali, M., 2007. Formulation development and optimization using nanoemulsion technique: a technical note. AAPS Pharmscitech 8, E12–E17.

Shanmugam, S., Selvarajan, R., Thangiah, S., 2011. Drug resistance of Staphylococcus aureus in sinusitis patients. Int. J. Biosci. IJB 1, 63–71.

Sharma, N., Kulkarni, G.T., Sharma, A., Bhatnagar, A., Kumar, N., 2013. Natural mucoadhesive microspheres of Abelmoschus esculentus polysaccharide as a new carrier for nasal drug delivery. J. Microencapsul. 1–10.

Shawahna, R., Decleves, X., Scherrmann, J.-M., 2013. Hurdles with Using *In Vitro* Models to Predict Human Blood-brain Barrier Drug Permeability: A Special Focus on Transporters and Metabolizing Enzymes. Curr. Drug Metab. 14, 120–136.

Sherry Chow, H., Chen, Z., Matsuura, G.T., 1999. Direct transport of cocaine from the nasal cavity to the brain following intranasal cocaine administration in rats. J. Pharm. Sci. 88, 754–758.

Singh, A.K., Singh, A., Madhv, N., 2012. Nasal Cavity, a Promising Transmucosal Platform for Drug Delivery and Research Approaches from Nasal to Brain Targetting. J. Drug Deliv. Ther. 2, 22-23.

Soane, R., Frier, M., Perkins, A., Jones, N., Davis, S., Illum, L., 1999. Evaluation of the clearance characteristics of bioadhesive systems in humans. Int. J. Pharm. 178, 55–65.

Soliman, I.I., Soliman, N.A., Abdou, E.M., 2010. Formulation and stability study of chlorpheniramine maleate nasal gel. Pharm. Dev. Technol. 15, 484–491.

Stapleton, J.A., Sutherland, G., 2011. Treating heavy smokers in primary care with the nicotine nasal spray: randomized placebo-controlled trial. Addiction 106, 824–832.

Subbiah, R., Ramalingam, P., Ramasundaram, S., Kim, D.Y., Park, K., Ramasamy, M.K., Choi, K.J., 2012. < i> N, N, N-Trimethyl Chitosan Nanoparticles for Controlled Intranasal Delivery of HBV Surface Antigen. Carbohydr. Polym. 89, 1289–1297.

Sutherland, G., Stapleton, J.A., Russell, M.A.H., Jarvis, M.J., Hajek, P., Belcher, M., Feyerabend, C., 1992. Randomised controlled trial of nasal nicotine spray in smoking cessation. Orig. Publ. Vol. 2 Issue 8815 340, 324–329.

Swamy, N., Abbas, Z., 2012. Preparation and *In Vitro* Characterization of Mucoadhesive Polyvinyl Alcohol Microspheres Containing Amlodipine Besylate for Nasal Administration. Ind J Pharm Edu Res. 46, 52-58.

Tan, M.L., Choong, P.F., Dass, C.R., 2010. Recent developments in liposomes, microparticles and nanoparticles for protein and peptide drug delivery. Peptides 31, 184–193.

Taylor, D., Galan, V., Weinstein, S.M., Reyes, E., Pupo-Araya, A., Rauck, R., 2010. Fentanyl pectin nasal spray in breakthrough cancer pain. J Support Oncol 8, 184–190.

Thakkar, H., Patel, A., Chauhan, N., 2013. Intranasal mucoadhesive microemulsion of mirtazapine: Pharmacokinetic and pharmacodynamic studies. Asian J. Pharm. 7, 36-42.

Thiagarajan, B., 2013. Anatomy of Paranasal sinuses. ENT Sch. 2.

Thiagarajan, P., 2011. Nanoemulsions for drug delivery through different routes. Res. Biotechnol. 2, 1-13.

Tiwari, S., Verma, S.K., Agrawal, G.P., Vyas, S.P., 2011. Viral protein complexed liposomes for intranasal delivery of hepatitis B surface antigen. Int. J. Pharm. 413, 211–219.

Tong-un, T., Muchimapura, S., Phachonpai, W., Wattanathorn, J., 2010. Effects of Quercetin Encapsulated Liposomes via Nasal Administration: A Novel Cognitive Enhancer. Am. J. Appl. Sci. 7, 906–913.

Velasquez, L.S., Shira, S., Berta, A.N., Kilbourne, J., Medi, B.M., Tizard, I., Ni, Y., Arntzen, C.J., Herbst-Kralovetz, M.M., 2011. Intranasal delivery of Norwalk virus-like particles formulated in an *in situ* gelling, dry powder vaccine. Vaccine 29, 5221–5231.

Verma, A., Ratnawat, S., Gupta, A.K., Jain, S., 2013. PLGA Nanoparticles for Delivery of Losartan Potassium through Intranasal Route: Development and Characterization. IntJDrug Dev Res 5, 185–196.

Vik, A., Ravindran, A., Shiah, I., Wong, H., Walji, N., Lam, R.W., Yatham, L.N., 2013. A double-blind, placebo-controlled study of adjunctive calcitonin nasal spray in acute refractory mania. Bipolar Disord. 15, 359–364.

Vyas, T.K., Shahiwala, A., Marathe, S., Misra, A., 2005. Intranasal Drug Delivery for Brain Targeting. Curr. Drug Deliv. 2, 165–175.

Wang, S.H., Kirwan, S.M., Abraham, S.N., Staats, H.F., Hickey, A.J., 2012. Stable dry powder formulation for nasal delivery of anthrax vaccine. J. Pharm. Sci. 101, 31–47.

Weiglein, A., Anderhuber, W., Wolf, G., 1992. Radiologic anatomy of the paranasal sinuses in the child. Surg. Radiol. Anat. 14, 335–339.

Wolf, D.A., Hanson, L.R., Aronovich, E.L., Nan, Z., Low, W.C., Frey II, W.H., McIvor, R.S., 2012. Lysosomal enzyme can bypass the blood–brain barrier and reach the CNS following intranasal administration. Mol. Genet. Metab. 106, 131–134.

Xia, H., Gao, X., Gu, G., Liu, Z., Hu, Q., Tu, Y., Song, Q., Yao, L., Pang, Z., Jiang, X., 2012. Penetratin-functionalized PEG-PLA nanoparticles for brain drug delivery. Int. J. Pharm. 436, 840–850.

Yagoubian, B., Akkara, J., Afzali, P., Alfi, D.M., Olson, L., Conell-Price, J., Yeh, J., Eisig, S.B., Flood, P., 2011. Nicotine nasal spray as an adjuvant analgesic for third molar surgery. J. Oral Maxillofac. Surg. 69, 1316–1319.

Yasuda, K., Cline, C., Vogel, P., Onciu, M., Fatima, S., Sorrentino, B.P., Thirumaran, R.K., Ekins, S., Urade, Y., Fujimori, K., 2013. Drug

Transporters on Arachnoid Barrier Cells Contribute to the Blood–Cerebrospinal Fluid Barrier. Drug Metab. Dispos. 41, 923–931.

Zhang, Q., Jiang, X., Jiang, W., Lu, W., Su, L., Shi, Z., 2004. Preparation of nimodipine-loaded microemulsion for intranasal delivery and evaluation on the targeting efficiency to the brain. Int. J. Pharm. 275, 85–96.

Zhang, X., Wang, Y., Zheng, C., Li, C., 2012. Phenylboronic acid-functionalized glycopolymeric nanoparticles for biomacromolecules delivery across nasal respiratory. Eur. J. Pharm. Biopharm. 82, 76–84.

Zheng, C., Guo, Q., Wu, Z., Sun, L., Zhang, Z., Li, C., Zhang, X., 2013. Amphiphilic glycopolymer nanoparticles as vehicles for nasal delivery of peptides and proteins. Eur. J. Pharm. Sci. 49, 474-482.

CHAPTER 3

AN *IN VITRO* EVALUATION OF A CARMUSTINE-LOADED NANO-CO-PLEX FOR POTENTIAL MAGNETIC-TARGETED NOSE-TO-BRAIN DELIVERY

3.1. INTRODUCTION

Brain cancer is a life threatening disease that occurs when there is formation of abnormal cells within the brain, of which glioma is the most common (Killela et al., 2013). Despite the poor prognostic factors of malignant tumor, the quality of life of patients is seriously affected and may often lead to cognitive dysfunction (Omuro and DeAngelis, 2013). It was estimated that there would be about 23,000 new cases and over 15,000 deaths in 2015 in the United State alone due to brain cancer (Siegel et al., 2015). Several highly effective chemical and biological therapies have been researched to target brain tumors in order to improve its treatment. However, limited results have been achieved due to the difficulty of chemotherapeutics penetrating into the CNS due to the protective mechanism of the Blood Brain-Barrier (BBB). Radiotherapy and surgery are the alternative options that have been used both of which only provide temporary life extension (Hainfeld et al., 2013). The surgical technique is highly invasive and is challenged with excising tumor cells which may in fact affect normal brain cells. It is estimated that the 2-year survival rate is approximately 25% (Sullivan et al., 2014).

Carmustine (BCNU) is known to be an effective chemotherapeutic for the treatment of brain tumors (Qian et al., 2013). It is a nitrosourea compound which is highly lipophilic. It hydrolyzes *in vivo* to produce reactive metabolites which cause alkylation and crosslinking of DNA and RNA. It is known to inhibit repair and causes formation of high molecular complexes through de-novo purine synthesis (Dhakane and Ubale, 2012). Targeted delivery of BCNU to the brain has been challenged with bioavailability issues. The systemic route of drug administration is fraught with a short elimination half-life resulting in frequent administration leading to side effects such as hepatotoxicity and pulmonary fibrosis (Qian et al., 2013). Several drug delivery strategies have been developed to overcome these

challenges and improve the treatment of brain tumors. These include the use of polymers in various embodiments such as nanoparticles, micelles, microcapsules, copolymers, bioconjugation, microspheres and implants (Fattahi et al., 2013a, 2013b; Kim et al., 2009; Zhang et al., 2009; Xu et al., 2006; Painbeni et al., 1998). However, most of these approaches lack the ability to specifically target the tumor cells and instill adequate local concentrations of chemotherapeutic agents. Alternative strategies include the development of microelectromechanical systems (MEMS) devices (Li et al., 2005, 2004). MEMS devices function by a micro-reservoir releasing a specific dose of chemotherapeutics at the site of the tumor thereby improving local concentration and targeting ability. Biodegradable polymeric microchips (Grayson et al., 2003) are similar to MEMS in terms of multi-dose controlled release at the target site. However, these approaches are characterized by invasiveness, which is of major concern, especially during implantation of the devices. The most effective and well known approach is via localized delivery employing implants at the site of the tumor. Gliadel Wafer® (MGI Pharma, Bloomington, MN, U.S.A.) implants are currently approved for tumor resurrection, but high risk factors such as infection post implantation and brain abscess limit its use (McGovern et al., 2003).

Researchers are constantly looking for ideal strategies to overcome the above mentioned challenges. Magnetic targeting using magnetic nanoparticles (Yang et al., 2011) and molecular targeting employing ligands (Ren et al., 2012) are the two most studied approaches to combat the challenges of side-effects, low deposition of drugs at the target site and the spreading of chemotherapeutics to healthy organs of the body (Yang et al., 2011). Both strategies are quite efficient but are still fraught with low bioavailability issues since the mode of administration is still via the systemic pathway and will be limited by the BBB.

Intranasal drug delivery systems are more efficient in delivering therapeutic agents to the brain via the olfactory pathway. This method of administration has the advantages of circumventing the BBB, ease of administration, non-invasiveness, avoidance of the gastrointestinal tract and first pass metabolism, dose reduction and side-effect minimization (Mistri et al., 2012; Chalbot et al., 2010; Ozsoy et al.,

2009; Afifi et al., 2005). The integration of magnetic targeting with an intranasal drug delivery system may be an enhanced strategy of delivering chemotherapeutics to the brain tumor cells.

In this study we have successfully synthesized BCNU-loaded magnetized nanoparticles coated with a complex of Polyvinyl alcohol (PVA) conjugated to Polyethyleneimine (PEI) and FIuorecein isothiocyanate (FITC) referred to as a 'Nano-co-Plex', intended for intranasal delivery to the brain via the olfactory pathway. The magnetic Nano-co-Plex (with the aid of an external magnet) would be projected and guided to the brain following intranasal administration. The choice of PVA is to facilitate and achieve good mechanical strength and chemical stability after conjugation. Essentially, branched PEI was selected due to the number of amine groups which are chemo-specific in forming amide bonds. It has also been widely used as a DNA and gene carrier as it possesses excellent ability to bind and release DNA (Zhang et al., 2014; Huth et al., 2004). FITC was selected due to its excellent fluorescent attributes, and it has been widely used as dye for cell labeling (Pinheiro et al., 2013; Xu et al., 2012; Ge et al., 2009). The conjugation of these compounds to form the Nano-co-Plex that has high BCNU loading and release capacity as well as having the attribute of high magnetization with a cell labeling property is a novel approach for synthesizing an intranasal targeted drug delivery system for the management of brain tumors.

3.2. MATERIALS AND METHODS

3.2.1. Materials

Polyvinyl alcohol (PVA) (30kDa, 87−90% hydrolyzed), branched polyethylenimine (PEI) 1.8 kDa, iron (II) chloride tetrahydrate ($FeCl_2 \cdot 4H_2O$), iron (III) chloride hexahydrate ($FeCl_3 \cdot 6H_2O$), phosphate buffer solution (PBS) (pH=7.2), hydrochloric acid (HCl), sulphuric acid (H_2SO_4), N-hydroxysuccinimide (NHS), 1-ethyl-3 (3-dimethylaminopropyl) carbodiimide (EDC), FIuorescein isothiocyanate, epichlorohydrin, sodium hydrogen carbonate ($NaHCO_3$), sodium hydroxide (NaOH), dialysis tubing (Mw=10,000g/mol), carmustine (BCNU), chloroform, acetonitrile and deuterated water (D_2O). These chemicals were purchased from

Sigma-Aldrich Corp. (St. Louis, MO, USA). All other solvents and reagents were of analytical grade and were used as received. Deionized water was used in this experiment.

3.2.2. Preparation of the Iron Oxide Nanoparticles

Iron oxide nanoparticles were synthesized by dissolving 0.3mol of $FeCl_2 \cdot 4H_2O$ and 0.6mol of $FeCl_3 \cdot 6H_2O$ in 60mL aqueous medium to obtain 1:2 molar ratios of Fe^{2+} and Fe^{3+}. This mixture was added drop wise to 200mL of NaOH (0.4 M, pH=13) heated up at 75°C. This was done under continuous stirring condition while the mixture was being purged with N_2 gas to eliminate oxygen. This condition was maintained until dark precipitates of iron oxide nanoparticles were produced. The iron oxide nanoparticles so formed, were separated from the supernatant by centrifugation at 5,000 rpm for 30 minutes using an Eppendorf centrifuge 5804 (Hamburg, Germany). The precipitates were washed with deionized water purged with N_2 while under sonication (Sonics vibra cell, Newtown, CT, USA) for 30 minutes and subjected to centrifugation once again to separate the precipitates from the supernatant. The precipitates, which are magnetite nanoparticles, were then washed several times with deionized water and air dried.

3.2.3. Preparation of the Nano-co-Plex

In order to prepare the Nano-co-Plex for drug loading, it is necessary to first synthesize PVA chlorohydrin derivative (PVA-CH). PVA-CH was prepared by dissolving 500mg of PVA in water (5mL) at 80°C. Dilute H_2SO_4 (1M, 0.7mmol) was added to the solution after the PVA has completely dissolved followed by drop wise addition of 22.8mmol of epichlorohydrin. This mixture was stirred for 24 hours after which $5\%^{w}/_{v}$ $NaHCO_3$ was added to neutralize the mixture. Acetone was added to the mixture to precipitate out the chlorohydrins. The obtained PVA-CH was filtered, dissolved in 10mL of distilled water and then dialyzed against water for 2 days while changing the water every 12 hours. The product was subsequently freeze dried using Freezone 12 freeze drier (Labconco, Kansas City, USA).

FITC was included in order to investigate the cellular uptake and internalization characteristics of the Nano-co-Plex, and was conjugated by using the 1-ethyl-3 (3-dimethylaminopropyl) carbodiimide/N-hydroxylsuccinimide (EDC/NHS) coupling method. NHS (115mg) and 191.7mg of EDC were added to 40mL of PBS (pH=6) at 25°C. After stirring for 15 minutes, FITC (16.6mg) was added to the solution with continued stirring. Aqueous solutions of PEI (100mg, 10mg/mL) was then added sequentially to this solution and stirred for 2 hours.

PVA-CH (100mg) was dissolved in deionized water (10mL) at 70°C, and then an aliquot of FITC EDC/NHS/PEI previously prepared was added followed by addition of NaOH (4M, 5mL). The resulting mixture was stirred for 24 hours at 65°C. The synthesized magnetite nanoparticles were added and stirred for 24 hours. The resulting mixture was dialyzed against water for 48 hours followed by lyophilization. The lyophilized product was dispersed in deionized water and sonicated for 20 minutes. The particles were collected using a permanent magnet to separate them from the suspension while the supernatant was discarded. The particles were dried under vacuum at 40°C and are tagged Nano-co-Plex (NCP). This synthesis method was followed for samples prepared by changing the concentration percentage ratio of PVA and PEI in the formulation and are referred to as NCP-1, NCP-2 and NCP-3 with concentration percentage ratio of 70% PVA to 30% PEI, 50% PVA to 50% PEI and 30% PVA to 70% of PEI, respectively, as shown in Table 3.1.

Table 3.1: Formulation percentage ratio of conjugated polymers used

Samples	**NCP-1**	**NCP-2**	**NCP-3**
PVA Concentration (wt. %)	70	50	30
PEI Concentration (wt. %)	30	50	70

3.2.4. Determination of Structural Integrity of the BCNU-loaded Nano-co-Plex

3.2.4.1. Fourier Transform Infrared spectroscopy analysis of the BCNU-loaded Nano-co-Plex

Fourier Transform Infrared (FTIR) spectroscopy (Perkin-Elmer, Beaconsfield, BUCKS, UK) was employed to determine the structural modification of the nanoparticles used. FTIR spectra were obtained with samples subjected to pressure of 120 psi for 25 scans over a range of 4000-550cm^{-1}. FTIR was performed on the individual components (PVA, PEI, FITC) that were used to prepare the complex and the drug-loaded nanoparticles.

3.2.4.2. Nuclear Magnetic Resonance analysis of the Nano-co-Plex

The ^{1}H NMR was performed on PVA, PEI and the Polyplex employing NMR spectroscopy operating at 300MHz (Bruker Avance BioSpin, Germany). Each sample was dissolved in deuterated water (D_2O) with concentration of 15mg/mL. The spectra of each of the samples were obtained and analysed.

3.2.5. Thermal Stability and Quantitative Analysis of the Nano-co-Plex

The composition of the polymer coated iron oxide particles were ascertained out by employing thermal gravimetric analysis (TGA) (PerkinElmer, TGA 4000, Llantrisant, Wales, UK). The quantity of polymer coated on the iron oxide particles were determined by the TGA. The TGA was configured to starting temperature of 30°C and end temperature of 900°C under continuous flow of N_2. Samples were heated at a rate of 10°C per min. Thermograms were generated as percentage weight vs. temperature and analyzed using Pyris™ software (PerkinElmer, Llantrisant, Wales, UK).

3.2.6. Size and Stability Analysis of the BCNU-Loaded Nano-co-Plex

Nanoparticle size and size distribution profiles were generated using a ZetaSizer NanoZS (Malvern Instruments, Malvern, UK) instrument equipped with non-invasive backscatter technology set at an angle of 173°. The zeta potential of the synthesized nanoparticles was determined by exposing particles from each formulation independently to a controlled electric field and their mobility through Brownian motion was measured. This was achieved by a combination of Laser

Doppler Velocimetry and Phase Analysis Light Scattering at a maximum sample conductivity of 200mS/cm.

3.2.7. Determination of Size and Morphology of BCNU-Loaded Nano-co-Plex

The size and the morphology of the nanoparticles were visualized by employing a FEI Tecnai T12 transmission electron microscope operating at 120kV. Sample preparation was carried out by dispersing the particles in acetone and then ultrasonicated for 10 minutes using sonic vibra cell, (MO, USA). A drop of the dispersed sample was applied on a carbon coated copper grid placed on a filter paper for absorption of excess and acetone. The copper grid was allowed to air dry.

3.2.8. Determination of Magnetization Properties of the BCNU-Loaded Nano-co-Plex

Magnetic studies were performed employing a Quantum Design Superconducting Quantum Interference Device (SQUID) magnetometer (Quantum Design Inc., San Diego, CA). Approximately 30mg of samples were used per scan. The applied Magnetic Field (MF) ranged from -30,000Oe and 30,000Oe at room temperature.

3.2.9. Analysis of the Crystalline Structural Properties of BCNU-Loaded Nano-co-Plex

The XRD patterns were obtained utilizing a Rigaku 600 X-ray Diffractometer (RIGAKU, Inc., Tokyo, Japan) equipped with Cu-Kα radiation (λ=1.54056 Å). The diffractograms were obtained using the following parameters: Scan axis= Theta/2-Theta, scan range of 0°-90°, scan step of 0.1 and scan speed of 2.0°/min. The voltage and current was set to 40kV and 15mA respectively.

3.2.10. Establishment and Confirmation of the Interaction Profile Employing Computational Simulations

All modeling simulations were performed using HyperChem™ 8.0.8 Molecular Modeling Software (Hypercube Inc., Gainesville, FL, USA) and ChemBio3D Ultra 11.0 (CambridgeSoft Corporation, Cambridge, UK). The 3D structures of PVA and PEI were archetyped using ChemBio3D Ultra in their syndiotactic stereochemistry.

The structures of FITC and BCNU were constructed with natural bond angles in HyperChem 8.0.8. The models were primarily energy-minimized using the MM+ Force Field algorithm and the resulting structures were once again energy-minimized using the AMBER 3 (Assisted Model Building and Energy Refinements) Force Field algorithm. The conformer having the lowest energy was used to develop the molecular complexes. A complex of one polymer molecule with another was assembled by parallel disposition and the energy-minimization was repeated to generate the final molecular complex models: PEI-PVA; PEI-FITC; and PEI-BCNU. Full geometrical optimization was conducted in vacuum employing the Polak–Ribiere Conjugate Gradient method until an RMS gradient of 0.001kcal/mol was reached.

3.2.11. Determination of the Loading Capacity and Efficiency of BCNU within the Nano-Co-Plex

The BCNU loading was carried out in the dark by dispersing 5mg of NCP-1 in 5mL aqueous BCNU solution (drug concentration=0.1mg/mL). The mixture was sonicated for 30 min at 10 °C and then shaken in a rotary shaker (Rotavapor® RII, Büchi Labortechnik AG, Flawil, Switzerland) at 200rpm at 10°C for 6 hours to facilitate BCNU uptake. Magnetite nanoparticles were removed from the solution every 30 minutes by employing a permanent magnet. The optical density of residual BCNU was immediately measured at 230nm by using high performance liquid chromatography (HPLC) (Waters, Milford, Massachusetts, USA). The HPLC system was equipped with a Waters symmetry300™ C18 5 µm, 4.6 x 250mm column, a UV-detector and a Waters binary HPLC pump. 3:7 ($^{v}/_{v}$) mixtures of acetonitrile and deionized water was used as the mobile phase with a flow rate of 1.0mL/min, at wavelength of 230nm, in order to calculate the amount of BCNU adsorbed on the nanoparticles. Nanoparticles were redispersed in the buffer solution after each measurement for further BCNU adsorption. This exercise was repeated until there were no further changes in the concentration of BCNU indicating loading capacity had reached saturation point. The BCNU-loaded NCP (BCNU-NCP) obtained were then magnetically separated and freeze dried. This procedure was repeated for NCP-2 and NCP-3.

3.2.12. Determination of the *In Vitro* Drug Release Profile of BCNU released from the BCNU-Loaded Nano-co-Plex

The release study was carried out by dispersing the dried BCNU-loaded NCP in 5mL PBS pH 7.4 and incubating at 37°C in an orbital shaker incubator (YIHDER, Taiwan). At fixed incubation times, the BCNU-loaded nanoparticles were separated using a permanent magnet from the solution washed with deionized water. The separated nanoparticles were lyophilized employing Freezone 12 freeze drier (Labconco, Kansas City, USA), the lyophilized product was then dissolved in chloroform followed by addition of mixtures of acetonitrile and deionized water in ratio 3:7 $^{v}/_{v}$. The chloroform from the mixtures was removed employing rotary evaporator (Rotavapor® RII, Büchi Labortechnik AG, Flawil, Switzerland). The polymers were then deposited on the side of the reaction vessel. The resultant solution was quickly analysed for BCNU employing HPLC. The released quantity of BCNU was calculated by determining the difference between the total amount of drug loaded and the amount obtained from HPLC result analysis. The entire drug release procedure was carried out for BCNU-NCP-1, BCNU-NCP-2 and BCNU-NCP-3.

3.2.13. Cytotoxicity Analysis, Cellular Uptake and Internalization of the BCNU-Loaded Nano-co-Plex

3.2.13.1. Cytotoxicity studies via 3-(4,5-dimethylthiazole-2-yl)-2,5-diphenyl tetrazolium bromide assay on the conventional BCNU and BCNU-loaded Nano-co-Plex

The human glioblastoma cell line (A172) was employed in this study. The cell line was obtained from Cellonex, (Johannesburg, South Africa). The cells were grown in a 9:1 mixture of Dulbecco's modified Eagle's medium (DMEM) with 5% L-glutamine and fetal bovine serum (FBS) (Cellonex, Johannesburg, South Africa), supplemented with 1% penicillin-streptomycin (Sigma-Aldrich; St. Louise, MO, USA) in a T-25 culture flask (Sigma-Aldrich; St. Louise, MO, USA) after which the cell line was expanded to large T-175 (175 cm2) culture flasks. The culture grew in a T-175 flask containing growth media (DMEM and 10% FBS) in an incubator (RS Biotech Galaxy, Irvine, UK) set at 37°C and 5% CO_2, with media changed every 48 hours. Cultured cells were dissociated from the culture flask with 0.25% trypsin

and then neutralized with Dulbecco's phosphate buffer saline (DPBS); the cells were quickly centrifuged at 1000 rpm for 5 minutes at room temperature. The cells were collected and then dispersed in 15mL of DMEM and 10% FBS. Cell counting was carried out by trypan blue dye exclusion employing a hemocytometer. The BCNU-loaded Nano-co-Plex was exposed to UV light for disinfection overnight prior to inoculation. The experimental cells were seeded at a concentration of $1.0x10^4$cells/well into each well of a 96-well plate, in 180µL of DMEM and 10% FBS medium/well. The plates were then incubated at 37°C and 5% CO2 overnight to allow cells adhesion to the bottom of the plates. Seven plates (A-G) were employed in this experiment, each plate contained similar contents and represented incubation times of 0, 4, 8, 16, 24, 48 and 72 hours, respectively. The wells in each plate were divided into 6 groups with predetermined quantities of BCNU-loaded Nano-co-Plex and conventional BCNU added to each well as depicted in Table 3.2. After incubation, each plate was removed according to the respective time of incubation for assay.

Table 3.2: DPBS, NCP, BCNU-NCP and BCNU contents distribution in each plate

Group	**Number of well used**	**Contents added to each well**	**BCNU quantity in each well (µg)**
Control	15	20µL of DPBS	0
NCP	15	20µL of DPBS and 0.5mg of NCP (drug free Nano-co-Plex)	0
BCNU-NCP-1	15	20µL of DPBS and 0.5mg of BCNU-NCP-1	46
BCNU-NCP-2	15	20µL of DPBS and 0.5mg of BCNU-NCP-2	77
BCNU-NCP-3	15	20µL of DPBS and 0.5mg of BCNU-NCP-3	88
BCNU	15	20µL of DPBS and 0.088mg of BCNU	88

The cell viability was measured by using the 3-(4,5-dimethylthiazole-2-yl)-2,5-diphenyl tetrazolium bromide (MTT) assay. Each well was injected with 20µL of MTT solution (5mg/mL) in DPBS (pH 7.4) and further incubated for 4 hours. The media and the unreacted MTT were then carefully aspirated from each well leaving behind the formazan products. The formazan precipitate was then dissolved with 150mL of 100% dimethyl sulfoxide (DMSO) (Sigma Chemical Co., St. Louis, MO, USA) and the optical density of the solution measured with a microplate reader (FilterMax™ F5 Multi-Mode Microplate Reader, Molecular Devices, USA) at 570nm. The number of viable cells is directly proportional to the quantity of formazan products formed as quantified by the microplate reader. The results are presented as cell viability (CV) percentage (mean ± standard deviation); the percentage of viable cells was therefore calculated using Equation 3.1.

$$CV\ (\%) = \frac{absorbance\ value\ of\ treated\ cells}{absorbance\ \ value\ of\ control\ (untreated)\ cells} \qquad \textbf{Equation 3.1}$$

3.2.13.2. Cellular uptake and internalization studies of the BCNU-loaded Nano-co-Plex

The cellular uptake and internalization studies of BCNU-NCP were carried out using the human glioblastoma A172 cell line. Six 24-well plates divided into 2 groups of three well-plates were used in this experiment. A172 cells were cultured as described in Section 2.13.1. Cells were seeded at a concentration of 5 x 10^4cells/well in 24-well plates (Sigma-Aldrich; St. Louise, MO, USA) and incubated for 24 hours at 37°C and 5% CO_2. After 24 hours, the well plates were then divided into 2 groups, group 1 consist of 3 well plates which were fixed with 0.1 Tesla neo disc magnets (Magnetech, Capetown, South Africa) positioned under the well plates. Group 2 comprised of three well plates which did not have magnets attached to them. Preliminary studies showed that the magnet used has no effect on the growth of the cells (data not included). The cells in the two groups were incubated with BCNU-NCP-1, BCNU-NCP-2 and BCNU-NCP-3, respectively, at concentration of 0.5mg/mL at 37°C for a period of 1 hour. The media was

removed from each well and washed 5 times in DPBS in order to rid the cells of nanoparticles that were not internalized by the cells. The cells were then visualized under a Confocal Laser Scanning Microscope (CLSM, Leica Microsystems, Wetzlar, Germany).

3.3. RESULTS AND DISCUSSION

3.3.1. Synthesis of the BCNU-Loaded Nano-co-Plex

In this study, we have achieved the synthesis of an anti-cancer drug-loaded nanoparticulate delivery system with superparamagnetic properties and cell labeling capability which can accommodate a high drug payload with the ability to respond to external MF intended for targeted delivery of drug to brain tumor following intranasal administration. Figure 3.1 shows the schematic of the synthesis of BCNU-loaded Nano-co-Plex. The magnetite was synthesized following the precipitated procedure of the combination of iron II and iron III salts in the ratio 1:2 at high pH under N_2 gas to yield magnetite. PVA and PEI have been conjugated by utilizing the chemistry of the epoxidation reaction wherein PVA was reacted with epichlorohydrin in acidic medium to form a PVA chlorohydrin derivative (PVA-CH) by opening up the epoxide ring. Low molecular weight branched PEI was carefully selected for this work because of its non-toxic attributes to cells as opposed to the high molecular weight PEI. Conjugation of low molecular weight branched PEI with FITC was achieved by following NHS coupling chemistry. The addition of this conjugate (PEI-FITC) to PVA-CH at high pH formed a polymer complex (Polyplex) which *in situ* with the magnetite resulted in the coating of the magnetite nanoparticles with the Polyplex. The coated magnetite so obtained (Nano-co-Plex) was then loaded with BCNU to obtain the formulation.

The mechanism of the conjugation of PVA with PEI is based on the replacement of the chlorine atom in the PVA-CH derivative by the amine group of the PEI after the opening of the epoxide ring forming a direct covalent bond between carbon and the nitrogen atom of the PVA-CH derivative and the amine group of the PEI. It has been established that branched PEI has numerous primary and secondary amine

groups (McBain et al., 2007). FITC can form amide bonds with PEI and can also form a thiourea covalent bond between the NH_2 group of PEI and the isothiocyanate (–N=C=S) group of FITC (Pinheiro et al., 2013). It therefore means that PVA as well as FITC are covalently attached to the amine groups of the branched PEI. The mechanism of the coating of the magnetite by the Polyplex may have been through hydrogen bonding between the OH groups of PVA and the positively charged surface of the iron oxide core of the nanoparticles (Kayal and Ramanujan, 2010). Furthermore, the amine group on the PEI chain may bind tightly to the surface of the magnetite via donation of a pair of non-bonding electrons of N_2 atom to an empty orbital of magnetite ion (Xu et al., 2012). PEI is a cationic polymer; its presence allows the complex to be positively charged. This attribute allowed BCNU, which is a negatively charged compound, to undergo electrostatic interaction with the complex and thereby formed a van der Waals bond between its molecules and the amine group of PEI. Coulomb forces may also contribute to the binding. The formation of hydrogen bonding is also possible between the N atom of BCNU and the OH group of PVA which may further strengthen the bonding of BCNU into the matrix.

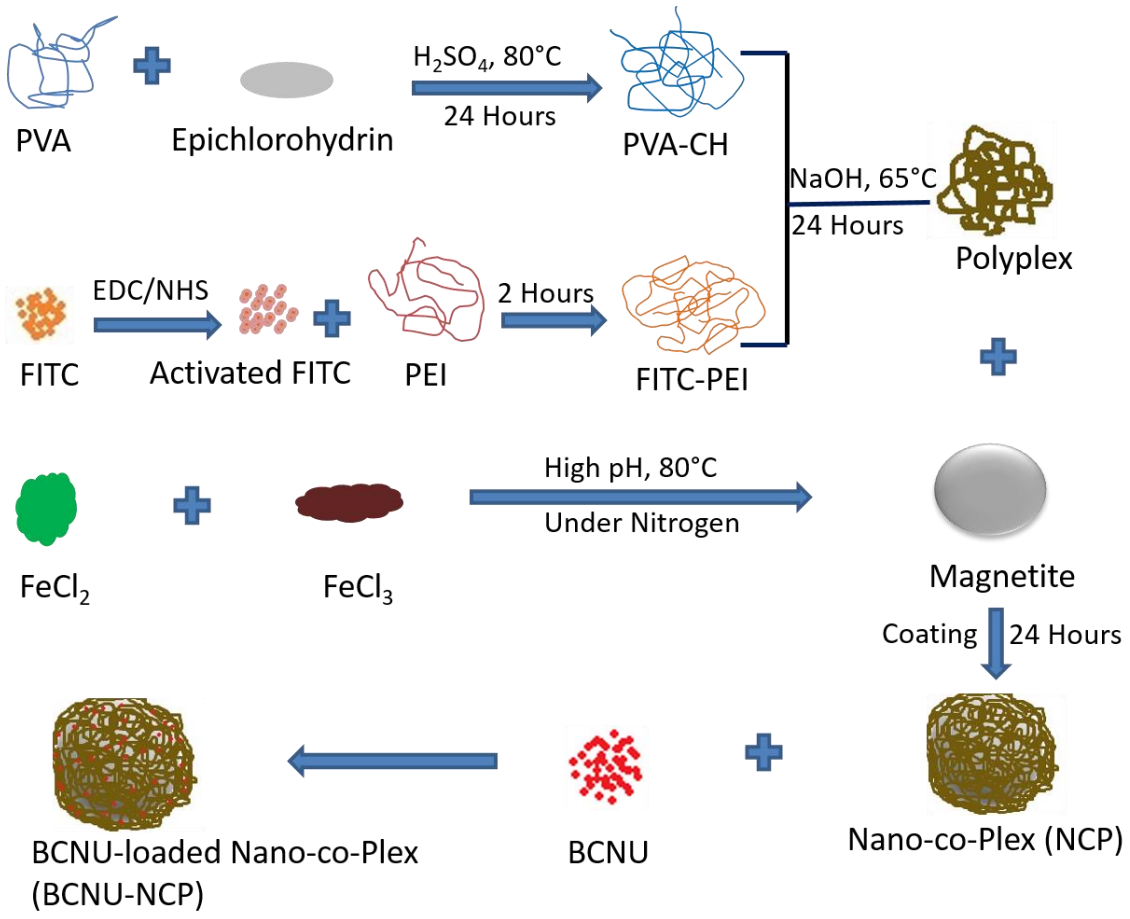

Figure 3.1: Schematic of the synthesis of BCNU-loaded Nano-co-Plex.

3.3.2. Assessment of the Structural Modifications of the BCNU-Loaded Nano-co-Plex

3.3.2.1. Structural modification assessment via Fourier Transform Infrared spectroscopy

The FTIR spectra of the synthesized magnetite, native PVA and PEI and FITC are shown in Figure 3.2a, b, c and d respectively. The low frequency band at 575cm^{-1} indicates Fe-O symmetry stretching vibration of the synthesized magnetite (Ma et al., 2007). For PVA, the O-H stretching band at 3289cm^{-1} and C-H stretching band at 2910 were observed (Kayal and Ramanujan, 2010; Raju et al., 2007). The strong absorption peak at 1579cm^{-1} corresponds to the amine group of PEI (Wang et al., 2006). The intense absorption band observed at 2004cm^{-1} is the characteristic band for –N=C=S of FITC (N. Zhang et al., 2012).

FTIR spectra of BCNU, NCP and BCNU-NCP are shown in Figure 3.2e, f and g, respectively. In Figure 3.2e the spectra of BCNU shows its native peaks of N-H, and C-Cl stretching vibration at 3350cm^{-1} and 621cm^{-1}, respectively. In Figure 3.2f, the spectra of NCP, there is still the presence of the Fe-O stretching vibration (567cm^{-1}), in addition to this, there are characteristic peaks of PVA, PEI and FITC. The peak around 3400cm^{-1} on the magnetite skeleton represents OH and it has shifted to 3215cm^{-1} in Figure 3.2f, suggesting that Polyplex was chemisorbed into the magnetite surface. The broad peak observed at 3216cm^{-1} is associated with N-H symmetric vibration of the amine group in PEI and overlapping O-H stretching of the PVA molecule arising from the intermolecular hydrogen bonds. The peak at 2811cm^{-1} is the C-H stretching from the PVA alkyl group while the band at 1449cm^{-1} and 1094cm^{-1} are CH_2 stretching and C-O-C stretching, respectively (Mansur et al., 2008). The peak at 1297cm^{-1} represents a C-N stretching vibration; this basically indicated the formation of a carbon-nitrogen bond as a result of the cleavage of the carbon chlorine bond from the epoxide chain and the amine group of PEI. This further confirmed the covalent bond between PVA and PEI molecules.

The peak at 1559cm^{-1} represents N-H stretching vibration of an amide an indication of the formation of amide group (Duan et al., 2012) from the reaction of the carboxylic acid group of FITC amine group of the PEI thus confirming the presence of FITC in the complex. The disappearance of the absorption band of N=C=S at 2004cm^{-1} in Figure 3.2f and 2g suggested the formation of thiourea bond, which further confirmed the presence of FITC. Figure 3.2g is the absorption spectra of BCNU-NCP, here in addition to the peaks in Figure 3.2f, there are peaks at 1375cm^{-1} and 621cm^{-1} representing the N=O stretching vibration and C-Cl stretching vibration of the BCNU compound, respectively. These peaks confirmed that BCNU was adsorbed within the complex and held in place by electrostatic forces such as hydrogen bonding and van der Waals force within the matrix of the polymeric coating complex.

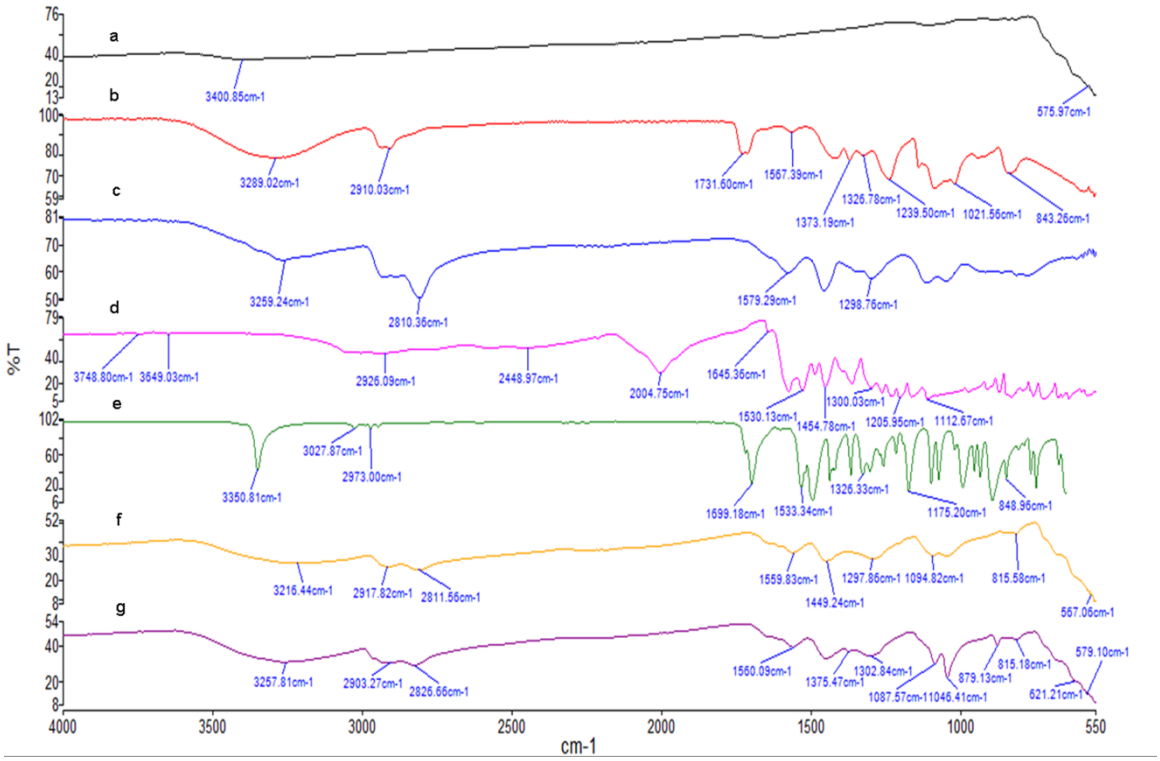

Figure 3.2: FTIR spectra of a) synthesized magnetite, b) native PVA, c) native PEI, d) native FITC, e) BCNU, f) NCP-3 and g) BCNU-NCP-3.

3.3.2.2. Structural modification assessment via Nuclear Magnetic Resonance analysis

The 1H NMR was carried out on the PVA, PEI and Polyplex in order to further confirm the PVA- PEI conjugation. The 1H NMR results are displayed in Figure 3.3. The methylene (CH_2) and methine (CH) groups of PVA are visible at about 1.70 and 4.03 ppm, respectively, in the 1H-NMR spectrum, as shown in Figure 3.3a. The 1H-NMR spectrum of branched PEI (Figure 3.3b) shows characteristic peaks of methylene signals from 2.61-2.38 ppm. Due to samples being recorded in D2O, the NH2 peaks were not observed due to deuterium exchange. The Polyplex, which comprises both PVA and PEI, is formed by crosslinking of PEI and PVA. When PEI is crosslinked to PVA, the proton spectrum shows methylene resonance at 3.14 ppm which is indicative of -NH-CH2-CH-OH-; the new NH-CH2 bond is visualized only in the spectrum of the Polyplex, and it is highlighted as shown in Figure 3.3c. The NMR spectrum further suggested the conjugation of PEI

to PVA. From the integration obtained from the NMR spectra, the conjugation ratio is estimated to be ~4:1 PEI to PVA in the Polyplex.

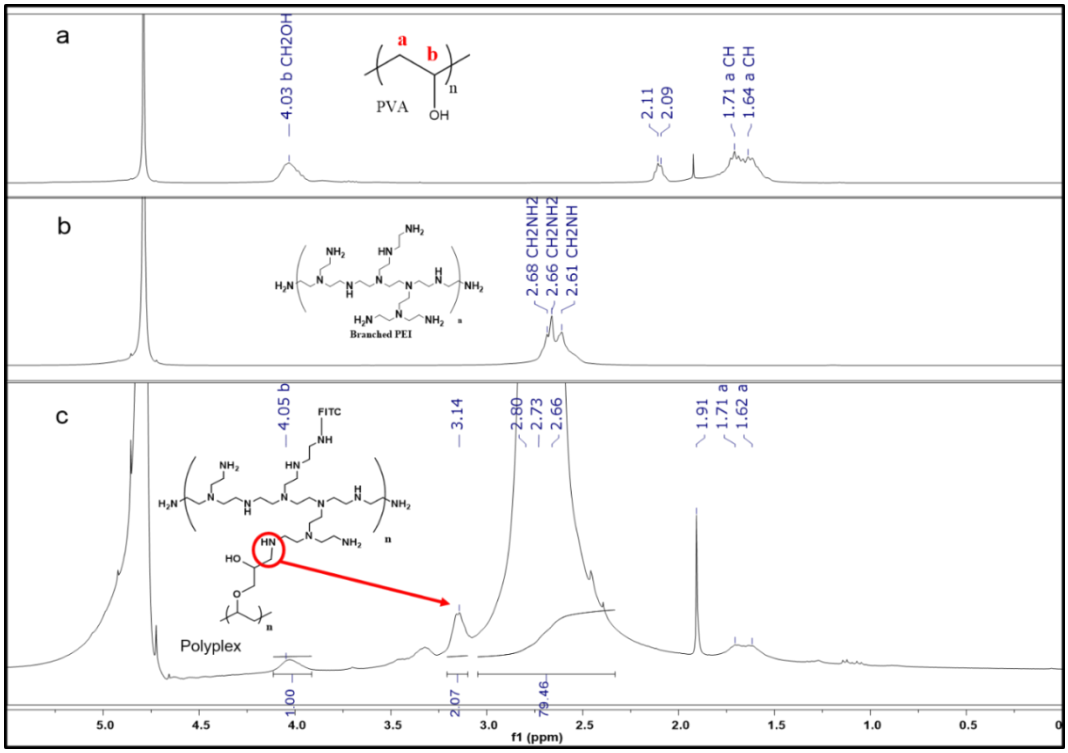

Figure 3.3: ^{1}H NMR spectra of (a) PVA, (b) PEI and (c) Polyplex. The red circle and arrow indicating the new NH-CH_2 bond formed by the conjugation of PEI and PVA at peak 3.14 ppm.

3.3.3. Morphology and Particle Size of the BCNU-Loaded Nano-co-Plex

The TEM micrographs of the uncoated nanoparticles and the drug loaded nanoparticles, BCNU-NCP-1, BCNU-NCP-2 and BCNU-NCP-3, are shown in Figure 3.4a, b, c and d, respectively. The average size of the uncoated magnetite is about 30±6nm while that of drug-loaded nanoparticles average about 45±8nm. The increase in size may be attributed to the polymer coating; this is supported by the result obtained from the zetasizer and further confirmed by TGA. The size of the nanoparticles is very important in the formulation; the smaller the size of the drug loaded particles the more they can quickly migrate through the cells as they are being attracted by the external magnetic force applied. The morphology of the synthesized magnetite shows spherically and hexagonally shaped particles. The

drug loaded nanoparticles are also of these shapes even after coating as observed in Figure 3.4. It is imperative for this shape to be maintained as this is one of the parameters that assists the drug-loaded particles in being propelled by a smooth upward movement through to the cancer cells (Trewyn et al., 2008). The hexagonal shape may assist the nanoparticles to possess a better penetrating ability into the cancer cells by utilizing the angular sections as contact points for access.

The TEM results revealed that the surface of the synthesized magnetite is smooth in comparison to the coated nanoparticles; this may be attributed to various components of the conjugated complex. The rough surface may also help to keep the drug molecules anchored to the polymer complex. The size of our drug-loaded Polyplex coated magnetite is within the range of those that have been previously reported in the literature (Chertok et al., 2010; Kayal and Ramanujan, 2010; McBain et al., 2007; Roque et al., 2009; Yang et al., 2011) but with a different shape. The variation in sizes observed in our nanoparticles compared to that found in the literature may have been due to the differences in the components of the coated materials, the mode of coating, synthesis, and preparation techniques used to mention just a few. The size obtained by us is deliberate as we require sizes that are moderate, i.e. not too large and not too small. The nanoparticles should not be too large so as to have easier penetration and movement of the nanoparticles through the cells to the target tumor site. Larger magnetic nanoparticles have high tendency of aggregating thereby resulting in poor tumor accumulation because they may not be able to extravasate into the interstitial space of the brain tumor cells (Zhang et al., 2009). Additionally, the nanoparticles should not be too small in order to optimize loading capacity of BCNU as well as to have an optimum magnetization effect; it has been reported that extremely small magnetic nanoparticles have poor accumulation ability at the target tumor site because the magnetic forces may not be able to overcome the Brownian motion forces (Yavuz et al., 2006). Therefore, the average particle size obtained in this study was uniform and consistent which offered an advantage of the drug-loaded magnetic coating being evenly distributed on the magnetite after loading.

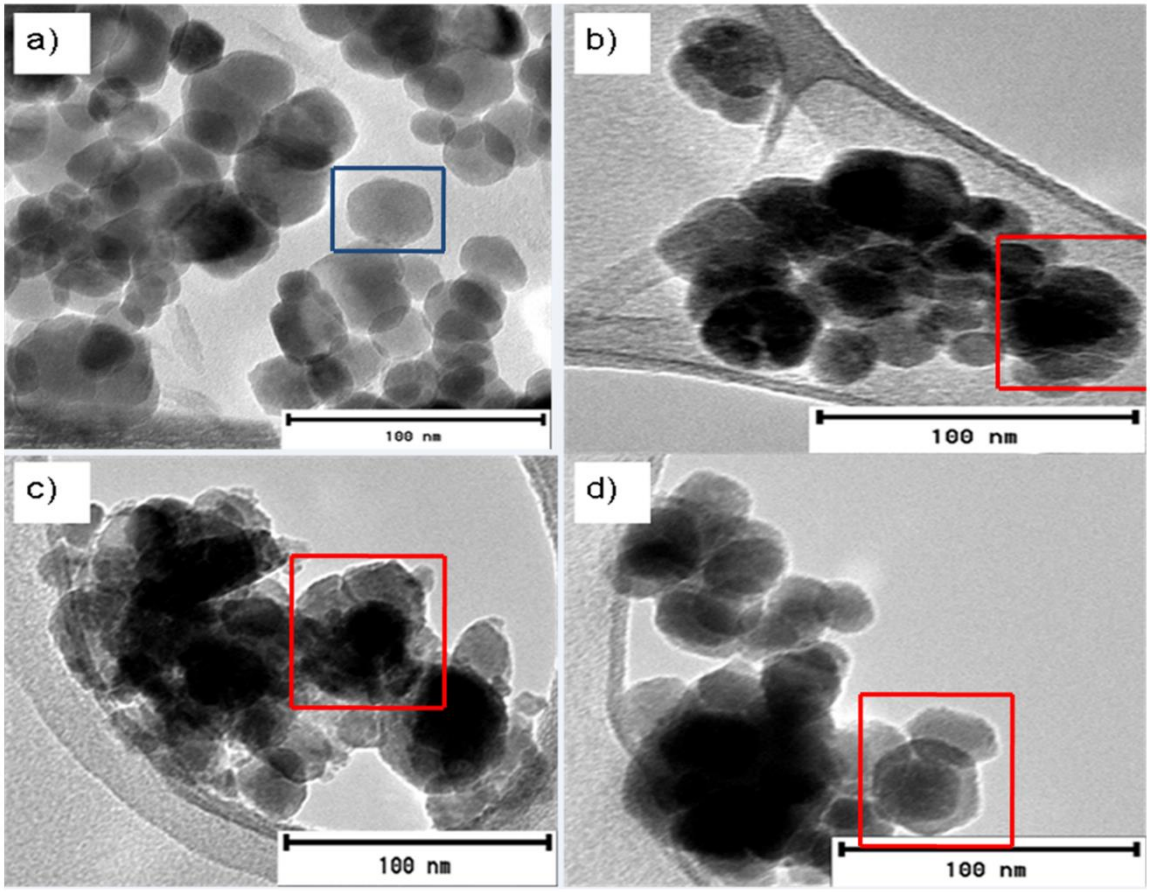

Figure 3.4: TEM image of a) Uncoated magnetite, b), c) and d) BCNU-loaded Nano-co-Plex (BCNU-NCP-1, BCNU- NCP-2 and BCNU- NCP-3 respectively). The blue box in a) indicates uncoated particle while the red boxes in b), c) and d) indicate coated particles.

3.3.4. Size Distribution and Zeta Potential Analysis of the BCNU-Loaded Nano-co-Plex

The hydrodynamic sizes of the uncoated and coated magnetite obtained from the zetasizer are 35±6nm and 45±8nm, respectively which are slightly more than the size obtained from the TEM. This difference may be attributed to the absorption of liquid by the nanoparticles during the analysis bearing in mind that TEM analysis uses solid samples. The zeta potential of the synthesized magnetite was +10.1±1mV while that of Nano-co-Plex was +32±2mV and that of BCNU-loaded Nano-co-Plex was +21±2mV, as shown in Figure 3.5. The synthesized magnetite has the lowest zeta potential while the coated nanoparticles have the highest of +32±2mV. The reason for this is due to the polymeric coating which contains

cationic PEI which added to the overall charge of the coated magnetite. On the other hand, the drug loaded nanoparticles have zeta potential of +21±2mV which is a reduction in zeta potential from the nanoparticles without the drug, the reason for this is due to the fact that BCNU is an overall negatively charged molecule; (Hua et al., 2011), its interaction with the cationic polymeric complex resulted in the reduction of the positive charges on the overall charges of the formulation. The high zeta potential suggested that the particles are not clustering together and are therefore arranged relatively individually. The resultant high positive charges on the particles means there will be repulsion of the particles towards themselves, thereby reducing considerably nanoparticles agglomeration.

It is important to note that despite concerns, previous studies in the literature have shown that a positive zeta potential of nanoparticles have no notable cytotoxic effect on normal cells (Merhi et al., 2012). Furthermore, tumor cells have negatively charged surface (Márquez et al., 2004), therefore the use of positively charged nanoparticles will allow enhanced binding to tumor cells and provide better cell uptake and internalization (Liu et al., 2013).

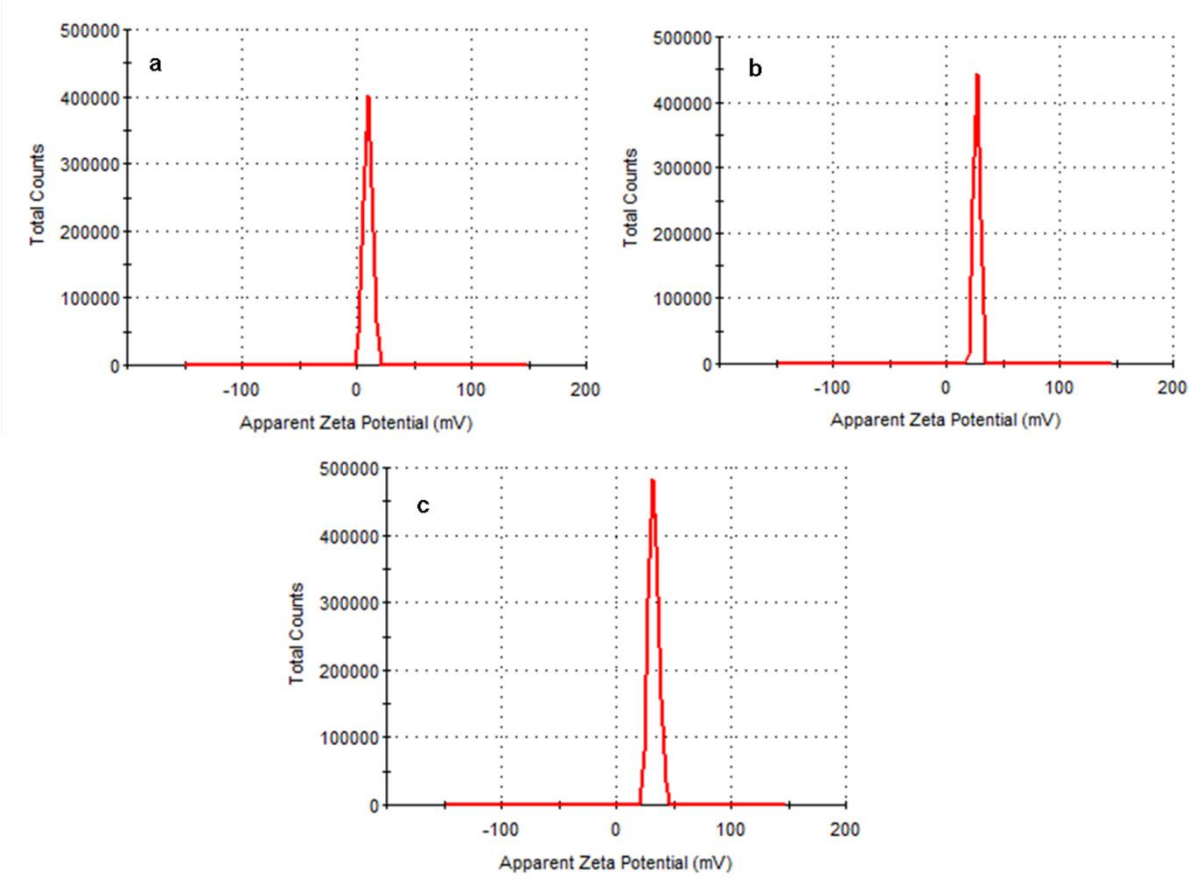

Figure 3.5: Zeta potential of a) synthesized magnetite b) Nano-co-Plex (NCP-3) and c) BCNU-loaded Nano-co-Plex (BCNU-NCP-3).

3.3.5. Assessment of the Crystalline Structural Properties of the BCNU-Loaded Nano-co-Plex

Figure 3.6 shows the XRD results in 3D. The results confirmed the crystalline nature of both the coated and uncoated particles. The characteristic peaks obtained for the synthesized magnetite at 2θ are 29.4°, 34.7°, 42.5°, 52.9°, 56.4°, and 62.0°. The peaks obtained for NCP-1, NCP-2 and NCP-3 are similar to that of the magnetite. Overlapping of the spectra is observed due to similar peak values of the coated samples with the magnetite, the difference is however in the intensity of the peaks. At 2θ=29.4°, NCP-3 has the least intensity while the magnetite has the highest intensity; this is attributed to degree of coating of the magnetite, the more coating the less intensity obtained. It is interesting, however, to note that despite the coating of the magnetite with the polymeric complex, the coated nanoparticles still maintain the crystalline property of the magnetite.

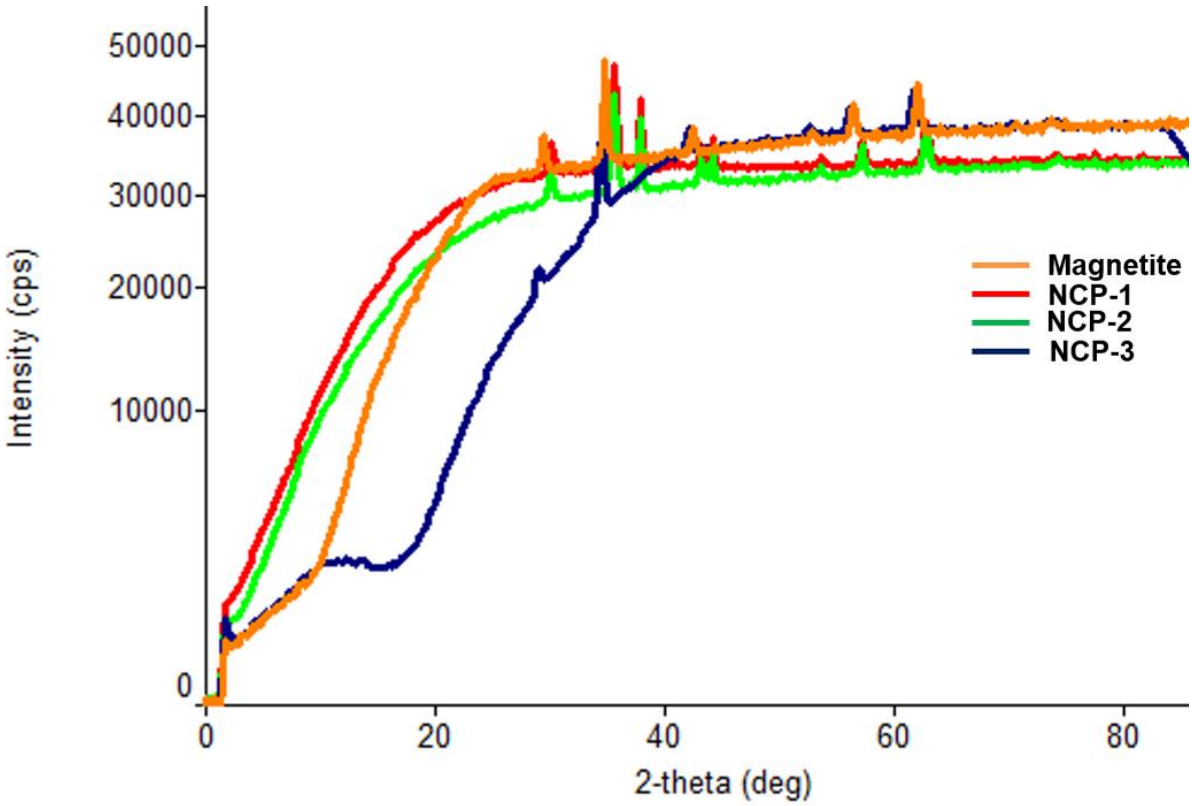

Figure 3.6: XRD spectra of uncoated Magnetite and Nano-co-Plex (NCP-1, NCP-2 and NCP-3).

3.3.6. Assessment of the Thermal Stability and Quantitative Analysis of the Nano-co-Plex

TGA was employed to evaluate the thermal stability as well as the weight loss of the coated magnetite nanoparticles. Figure 3.7 depicts the weight loss against temperature curves of uncoated and coated magnetite nanoparticles which was heated up to 900°C. The quantity of coatings onto the magnetite nanoparticles was determined by TGA. The result of the TGA firstly confirmed the presence of the coating as evidenced from the % weight loss of the formulation at 450°C, and secondly indicated the % weight of the drug-loaded coated complex and that of the magnetite in the formulation. Table 3.3 shows the percentage weight loss of BCNU-NCP-1, BCNU-NCP-2 and BCNU-NCP-3 to be 9.5%, 18.5% and 32% respectively. It was clear that a maximum of 32% of the drug-loaded Nano-co-Plex was coated on the magnetite as can be observed from the TGA curve, this therefore leaves approximately 68% magnetite content in the formulation

indicating a high magnetization capability which was consistent with the high saturated magnetization value obtained from the SQUID measurement. The complete degradation at 450°C of the complex leaves the magnetite nanoparticles as residue above this temperature. There is no significant weight loss in the TGA curve of uncoated magnetite at temperature as high as 900°C. The weight loss from 100 to 200°C may be attributed to the loss of water and the dehydration reaction of OH groups in PVA chains in the complex.

Table 3.3: Percentage weight loss of the synthesized magnetite and the various formulations.

Formulations	Weight loss (%)
Magnetite	0.1
NCP-1	9.5
NCP-2	18.5
NCP-3	32.0

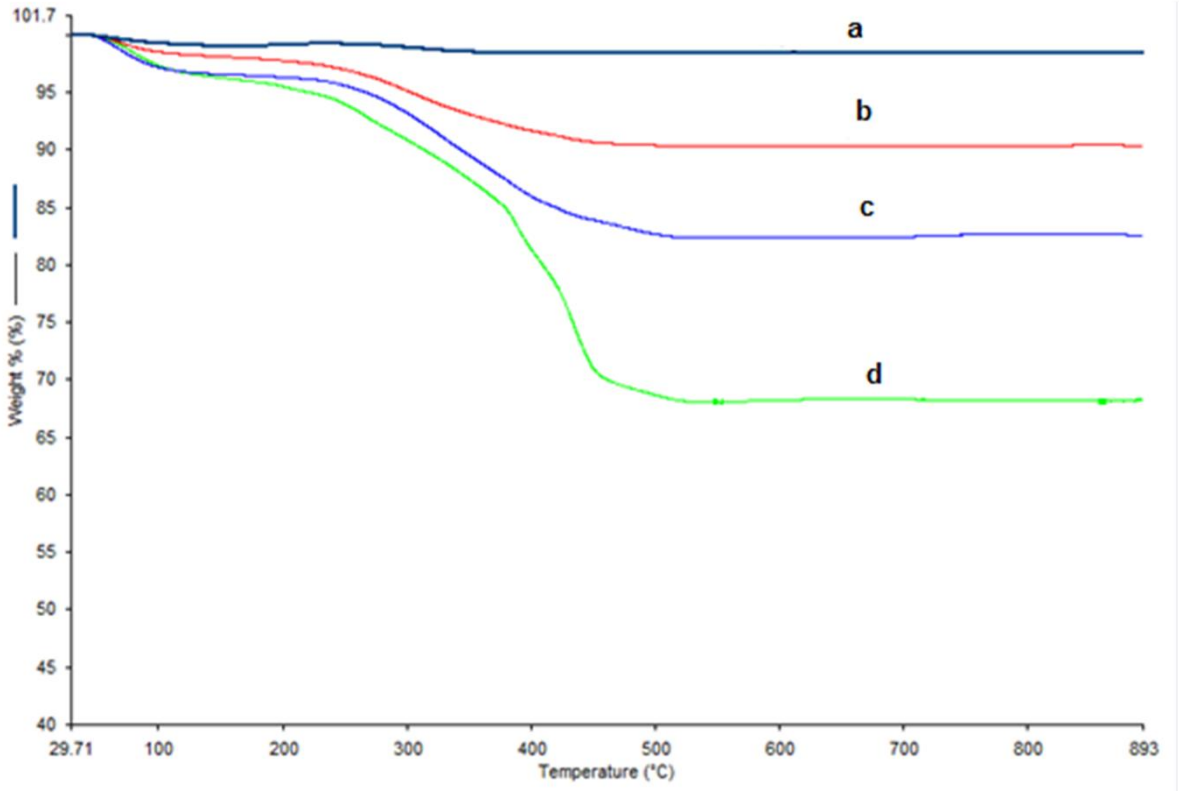

Figure 3.7: TGA thermograms of a) uncoated magnetite and Nano-co-Plex b) NCP-1, c) NCP-2 and d) NCP-3.

3.3.7. Assessment of Attraction Sensitivity of the BCNU-Loaded Nano-co-Plex to an External Magnetic Field

The goal of this study is designing a formulation which has sufficient magnetization in order to enable the drug loaded polymeric coated nanoparticles to be quickly projected to the CNS via the olfactory pathway and subsequently be guided to the site of the tumor on application of external MF for targeted delivery of BCNU. It is therefore important for the design of the formulation to be of high magnetization capacity. Figure 8 shows the magnetization results which indicated saturated magnetization (Ms) of 87emu/g, 78emu/g, 65emu/g and 61emu/g for magnetite, NCP-1, NCP-2 and NCP-3, respectively. All the four samples exhibited superparamagnetic properties as evidenced by the absence of remanence in the hysteresis curve in Figure 3.8. These superparamagnetic properties are an indication that the sizes of the particles are in the nano range and possess single magnetic domain characteristics (Sánchez et al., 2004).

The limited spatial extent thus achieved with the magnetic particles is responsible for the relatively low observed fields required to saturate these materials, which is an efficient approach in confining the magnetic species and to avoid long-range magnetic exchange interactions from producing magnetic ordering or memory effects. This property makes the formulation a good candidate for biomedical applications as the nanoparticles are not magnetic before application of external MF and are immediately deprived of magnetization after the external MF has been removed. Moreover, as demonstrated in Figure 3.8, even cycling of the MF leaves no remanent magnetization. The nanoparticles only exhibit magnetization in the presence of a MF.

It can be observed from the curves that the Ms of the coated nanoparticles is lower than that of the synthesized magnetite, the reason for this decrease in Ms is attributed to the coating of the magnetite which reduced the effect of the MF on NCP-1, NCP-2 and NCP-3. Another reason is the overall quantity (relative mass amount) of magnetite in the samples, which decreases from NCP-1 to NCP-3. This result supported those obtained from the TGA regarding the weight loss of the samples when subjected to thermal analysis; the more the polymeric coating the

less the effect of magnetization on the nanoparticles. NCP-3, which has more coating as seen earlier, therefore has the lowest magnetization capability. It is demonstrated that all the three samples surveyed in Figure 3.8 become near-fully saturated and magnetized in relatively small fields. This means that the magnetic-species impregnated substances studied here are amenable to be reproducibly manipulated under applied fields as low as 5000 Oe, and again fully released after termination of the location process. We note that a field of this magnitude amounts to as little as one third to one half the field intensity produced by modern neodymium-iron-boride permanent magnets.

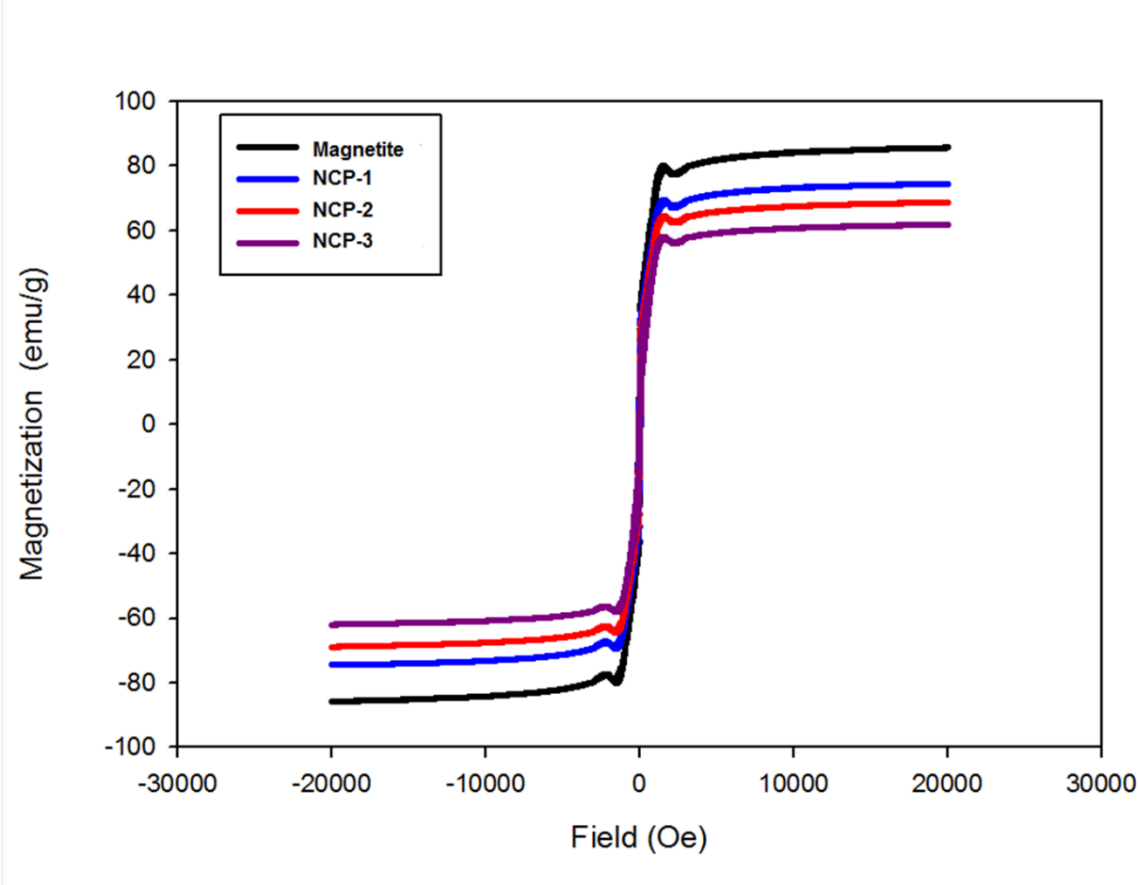

Figure 3.8: Magnetization curve of the synthesized magnetite and that of the Nano-co-Plex (NCP-1, NCP-2 and NCP-3) measured at 25°C showing the hysteresis loop.

3.3.8. BCNU Loading into the Nano-co-Plex

The BCNU loading profile of NCP was studied and the loading profile is shown in Figure 3.9; the loading profile showed initial rapid adsorption of BCNU into the NCP after which the rate of adsorption was reduced and finally reached a saturation value of 93.54µg, 154.92µg and 176.82µg for NCP-1, NCP-2 NCP-3, respectively after 6 hours of loading. The loading of BCNU into the Nano-co-Plex is time dependent as the drug loaded increases with time for the three samples; saturation point is obtained after 6 hours of loading. From the result, a higher PEI content in the formulation resulted in higher BCNU loading. This may be attributed to the binding of the BCNU molecules to the PEI molecule since the PEI contains a high number of amine groups which are positively charged and could display high electrostatic interaction with the negatively charged BCNU through the amine group in the chains of PEI. It can be inferred that, the more the free amine groups available, the greater the drug binding capacity. All the formulations containing high PEI contents loaded more BCNU. The high and rough surface area may have also contributed to the binding of the drugs to the complex. From the result analysis, it can be deduced that for each milligram of NCP, there is approximately 93.54µg, 154.92µg and 176.82µg of BCNU loaded into it, respectively. The highest loading percentage of BCNU to NCP was approximately 17.7% ($^{w}/_{w}$).

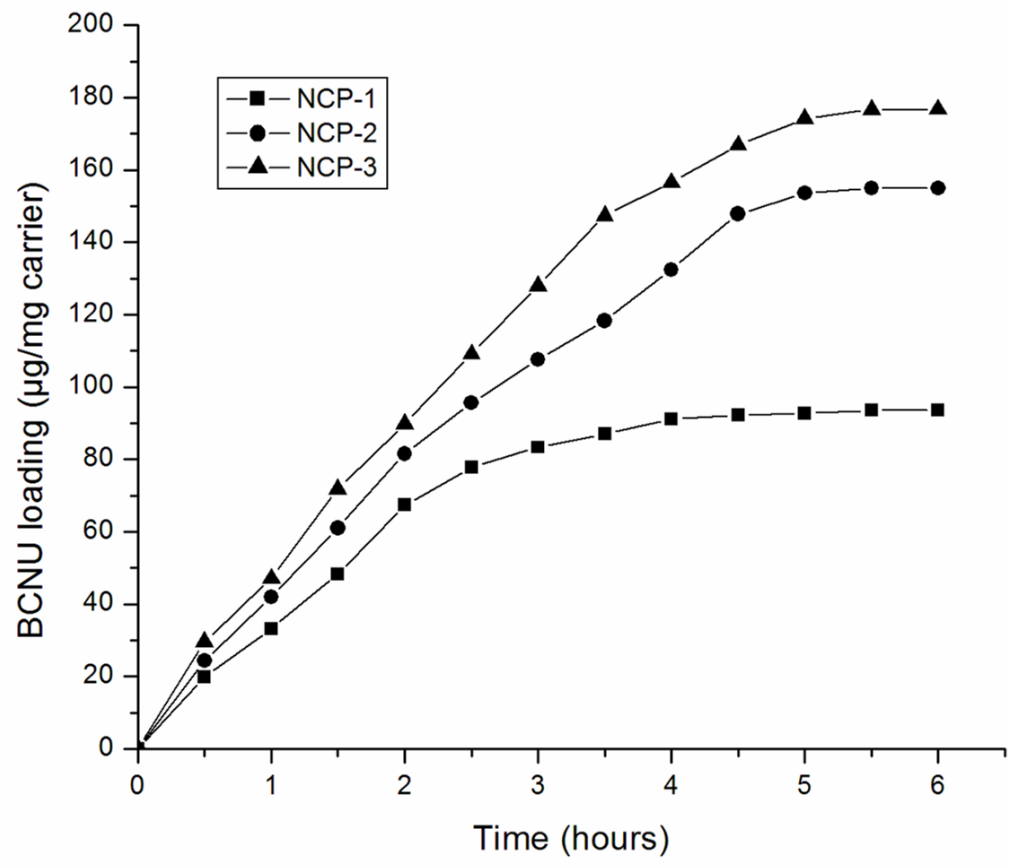

Figure 3.9: BCNU loading profile of Nano-co-Plex (NCP-1, NCP-2 and NCP-3).

3.3.9. Assessment of the *In Vitro* Drug Release Profile of BCNU from the Nano-co-Plex

BCNU is widely known to be unstable to light and it has a melting point of about 32°C (Xu et al., 2006). This is the reason why the loading experiment has to be performed in the dark and at low temperature. In order to get accurate data, we therefore obtained the release quantity not by taking the reading from the released drug in the buffer solution but by determining what was left in the drug-loaded nanoparticles employing HPLC. The release profiles of BCNU in the three preparations (BCNU-NCP-1, BCNU-NCP-2 and BCNU-NCP-3) are shown in Figure 3.10. The release profiles showed a rapid release of BCNU in the first 10 hours after which it decreased and then plateaued. The profiles also indicated an increase in release of BCNU with an increase in the quantity of drug loaded in the sample. BCNU-NCP-1 which has loading capacity of 93.45µg release maximum of 30.2% of its drug content after 72 hours, while BCNU-NCP-2 with loading capacity of 154.92µg released 56.9% and BCNU-NCP-3 with loading capacity of

173.82µg released 78.8% of its drug content after 72 hours. The drug release profiles can be explained by the interactions between the drug molecules and the polymeric complex which were not as a result of covalent bonding but electrostatic forces such as van der Waals bonding which are weak bonds and can be broken in buffer solution at 37°C as the polymer complex holding the BCNU degrades or erodes. The release could also be explained by the diffusion rule which indicated that the higher the concentration the higher the rate drug is diffused into the environment. The drug release profiles were observed to follow Fick's law of diffusion for monolithic systems. The drug release also depends on the erosion of the polymeric matrix, as the polymeric complex remains in the buffer solution; the matrix degrades, thus releasing the drugs into the environment as the electrostatic force holding the drugs in the matrix are being reduced due to polymeric matrix erosion. This implies that the drug could be released from the polymeric matrix depending on the degradation and erosion rate of the Polyplex in the buffer.

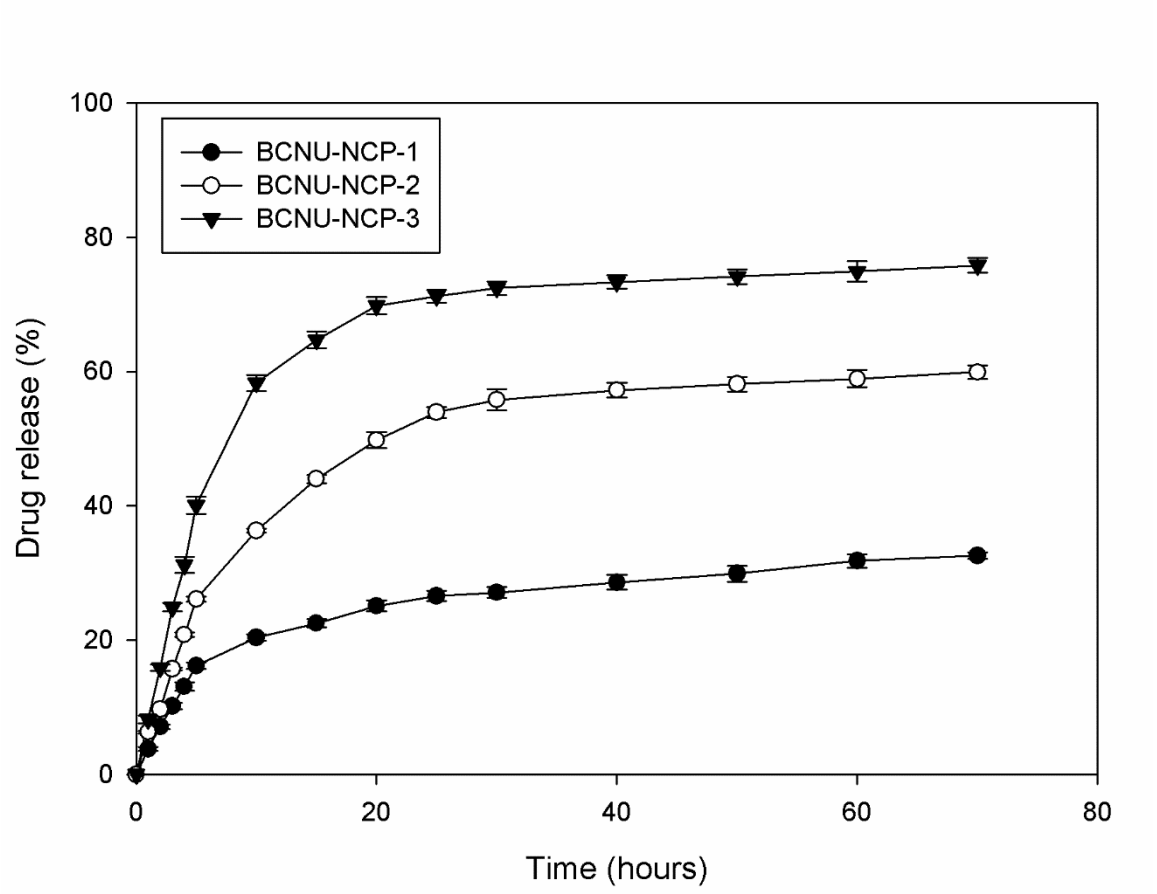

Figure 3.10: *In vitro* release profile of BCNU-loaded Nano-co-Plex (NCP-1, NCP-2 and NCP-3).

3.3.10. Establishment and Confirmation of the Interaction Profile Employing Computational Simulations

Aside from the various covalent bonds formed by the reactions of the polymer moieties during the conjugation, there are other non-bonding interactions that enhance the stability of the polymer complex. To further confirm the molecular interaction between the polymer segments that constitute the Polyplex, computational simulation mechanics was employed. Figure 3.11a, b and c showed the interaction profiles of PEI/PVA, PEI/FITC and PEI/BCNU, respectively. It was observed that intermolecular hydrogen bonding occurred between the hydroxyl group of the PVA and the amine group of the PEI in which the N in PEI is the hydrogen bonding donor and the O in the PVA the acceptor. Likewise, in the PEI/FITC interaction profile the amine group of the PEI is the donor and the carboxylic group in the FITC is the acceptor. The same explanation goes for the PEI/BCNU interaction profile. There is also evidence of van der Waals and electrostatic forces observed due to the ionic properties of the components of the Polyplex. BCNU is an overall negatively charged compound and it is capable of undergoing electrostatic interaction with the positively charged PEI through its nitro group and the amine group of PEI, this is in agreement with the result obtained from the FTIR. These non-bonding interactions in the form of hydrogen bonding, van der Waals and electrostatic forces, which is as a result of bond stretching, bond angle and torsional contributions, further account for the stability of the Polyplex formation.

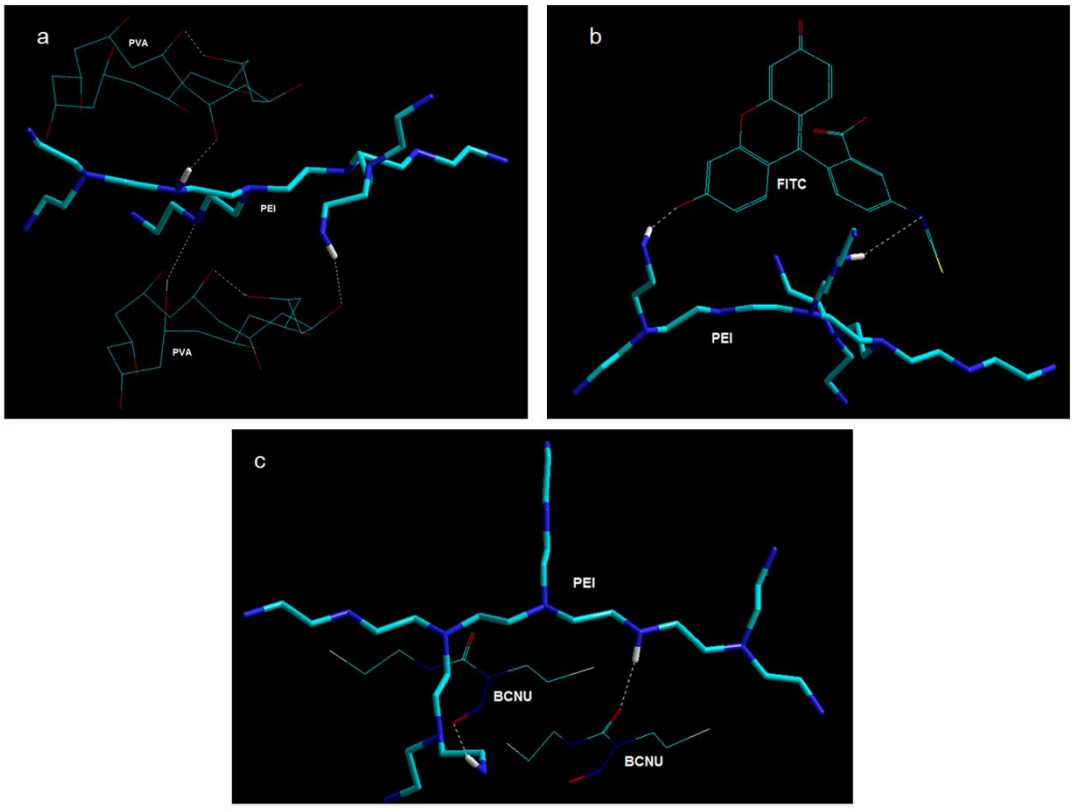

Figure 3.11: Computational simulations of interaction profile of a) PVA and PEI, b) FITC and PEI and c) BCNU and PEI. The color codes for various elements are as follows: Carbon=cyan, Nitrogen=blue, Oxygen=red, Sulphur=yellow and Hydrogen=white.

3.3.11. Assessment of the Cytotoxicity and Cellular Uptake of the BCNU-Loaded Nano-co-Plex

3.3.11.1. Cytotoxicity studies of the BCNU-loaded Nano-co-Plex

The results of the MTT assay displaying the percentage of cell viability against time of incubation, which was used to measure the cytotoxicity of the BCNU-loaded Nano-co-Plex, are displayed in Figure 3.12. The results showed that the NCP which is drug-free did not have any significant cytotoxicity on human glioblastoma cells as the cell viability percentage was ~96% after 72 hours. BCNU-NCP-1, BCNU-NCP-2 and BCNU-NCP-3 displayed cytotoxicity to human glioblastoma cells with cell viability percentage reaching 49.8%, 19.4% and 7.3%, respectively. This highlights the low toxicity of the Nano-co-Plex delivery system; cytotoxicity is attributed the BCNU. BCNU-NCP-3 showed the highest cytotoxicity

towards the human glioblastoma cells. The result of the conventional BCNU cytotoxicity at 88ug/mL showed that the cell viability percentage went as low as 30.1% at 24 hours of incubation after which the cell viability percentage began to increase gradually to 33.9% after 72 hours. The increase in the viability percentage might be due to the instability of the BCNU which could affect its potency and therefore could no longer cause apoptosis nor inhibit the proliferation of the human glioblastoma cells. These results therefore showed the superiority of BCNU-NCP compared to the conventional drug. The graph revealed that for the period of 72 hours BCNU-NCP-3 continued to release drug into the cells in its potent form while the conventional drug lost its potency after 24 hours. The ability of BCNU-NCP-3 to continuously release BCNU may be attributed to NCP's protective and stabilizing property as BCNU is embedded in the matrix of the Polyplex while it erodes gradually, and thereby overcoming the BCNU disadvantage of short half-life and instability. These results exhibited the efficacy of the BCNU-loaded Nano-co-Plex. The results obtained are also in agreement with the release profile of BCNU-loaded Nano-co-Plex as previously discussed (Figure 3.10). Comparing the release profile of BCNU-NCP-1, BCNU-NCP-2 and BCNU-NCP-3 which achieved 30.2%, 52.9% and 78.8% release, respectively after 72 hours, it was established that the *in vitro* release profile corresponded to the cytotoxicity levels of the drug-loaded NCP observed in the studies.

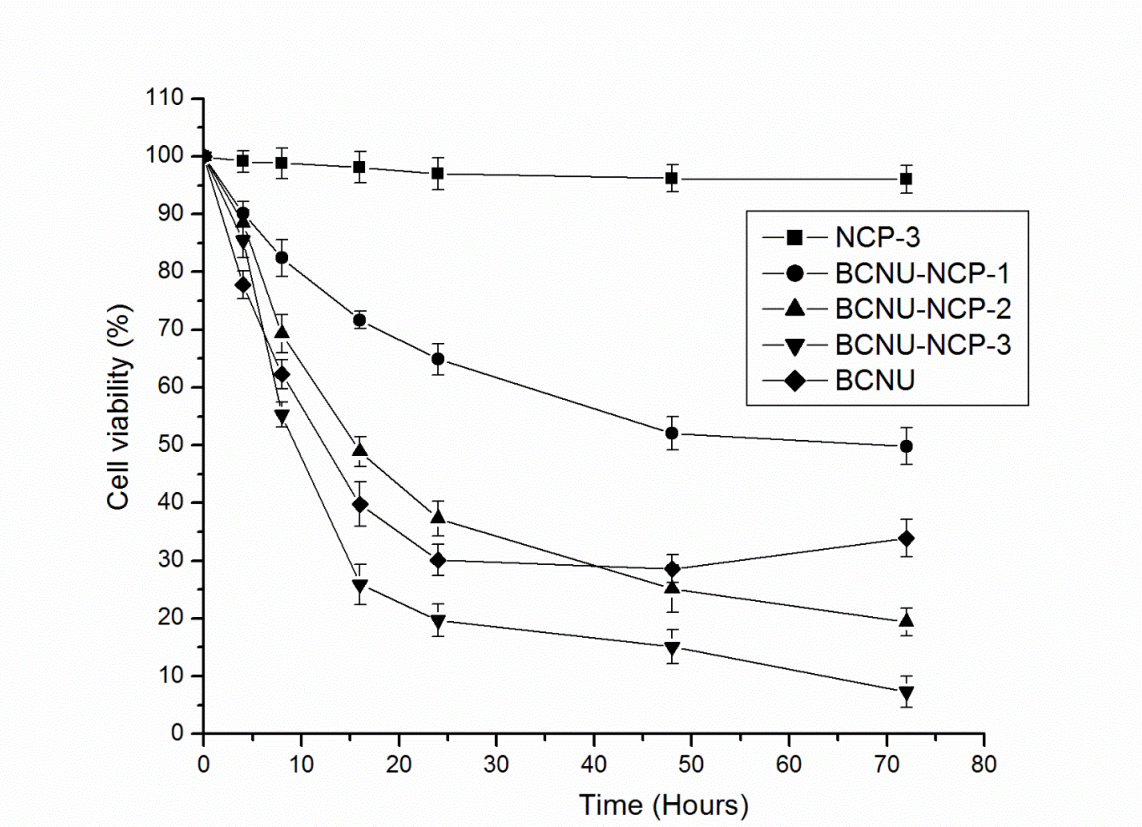

Figure 3.12: Cell viability of human glioblastoma A172 cell line treated with BCNU-NCP-1, BCNU-NCP-2, BCNU-NCP-3 and BCNU incubated at 37°C for 72 hours.

3.3.11.2. Cellular uptake and internalization of the BCNU-loaded Nano-co-Plex

The BCNU-loaded Nano-co-Plex consists of FITC of which its primary function is to label the nanoparticles in order to investigate the cellular uptake and internalization characteristics of the Nano-co-Plex. The results obtained after incubation of 0.5mg/mL of BCNU-loaded Nano-co-Plex for a period of 1 hour are displayed in Figure 3.13. The results showed qualitative analysis using fluorescent images for the group that were incubated with and without application of magnets. The group that were incubated with the application of magnets showed more uptake as displayed by high fluorescent intensity compared to the group without application of magnets. BCNU-NCPs possess magnetic property and thus in the presence of external MF, the nanoparticles are attracted towards the magnet, this action increases the mobility of the nanoparticles towards the internalization of the particles into the cells. There is therefore indication that more

BCNU-NCPs internalized more in the presence of external magnet at a given time in comparison with those without magnets. These results were an indicative of more cellular uptake of the BCNU-NCP and magnetic targeting to the A170 cells.

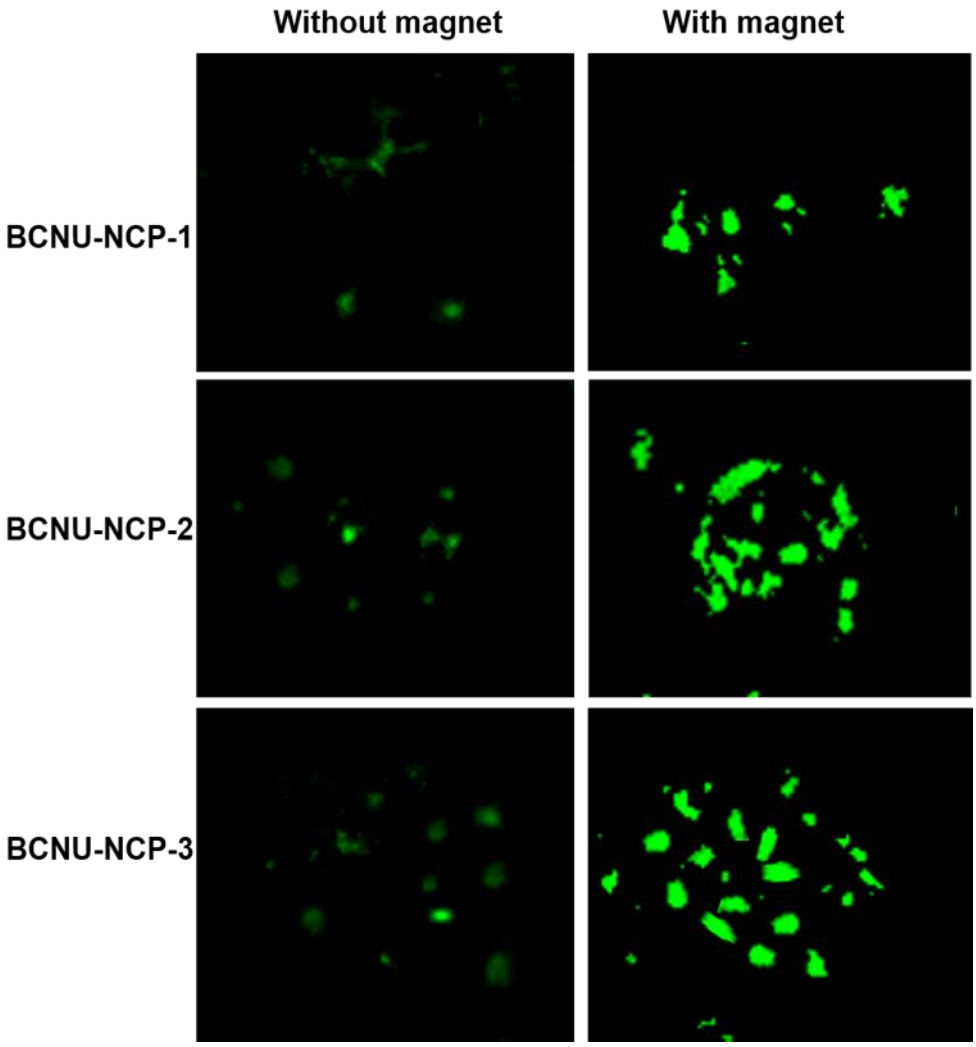

Figure 3.13: Fluorescent microscopy analysis of human glioblastoma A172 cell line treated with BCNU-NCP-1, BCNU-NCP-2 and BCNU-NCP-3 incubated at 37°C for 2 hours without and with application of magnet.

3.4. CONCLUDING REMARKS

Magnetite nanoparticles were synthesized and successfully coated with Polyplex that was prepared as a nanocarrier for BCNU loading. Both the nanocarrier and the BCNU-loaded Nano-co-Plex possess fluorescent ability for cell labeling and were characterized and confirmed to possess high magnetization. The magnetic

studies also showed the superparamagnetic properties of the formulation which is an attribute of successful magnetic targeted delivery devices. The average size of the Nano-co-Plex was ~35nm as indicated by TEM and also confirmed by the zetasizer analysis. The TGA results confirmed the coating and the quantity of the polymer complex on the magnetite. FTIR and NMR confirmed the conjugation of PVA, PEI as well as FITC in the Nano-co-Plex; it also confirmed the adsorption of BCNU onto the Nano-co-Plex. The loading capacity of the synthesized Nano-co-Plex was found to be efficient for BCNU. The release profiles indicated a sustainable release of BCNU and up to 75% of drug released after 72 hours. Magnetic targeting and internalization cell studies revealed enhanced uptake and internalization of BCNU-loaded Nano-co-Plex in HG cells in the presence of an external MF. Due to the size, high payload of drug, as well as high magnetization attribute of the formulation, it may be a suitable magnetic targeted intranasal drug delivery system for delivering BCNU to brain tumors. Magnetic drug targeting via the nasal route may therefore be a promising method of delivering drugs to the brain.

3.5. REFERENCES

Afifi, F., Al-Khalidi, B., Khalil, E., 2005. Studies on the *in vivo* hypoglycemic activities of two medicinal plants used in the treatment of diabetes in Jordanian traditional medicine following intranasal administration. J. Ethnopharmacol. 100, 314–318.

Chalbot, S., Zetterberg, H., Blennow, K., Fladby, T., Grundke-Iqbal, I., Iqbal, K., 2010. Cerebrospinal fluid secretory Ca^{2+}-dependent phospholipase A2 activity: A biomarker of blood–cerebrospinal fluid barrier permeability. Neurosci. Lett. 478, 179–183.

Chertok, B., David, A.E., Yang, V.C., 2010. Polyethyleneimine-modified iron oxide nanoparticles for brain tumor drug delivery using magnetic targeting and intra-carotid administration. Biomaterials 31, 6317–6324.

Dhakane, V.D., Ubale, M.B., 2012. A Validated Stability-Indicating HPLC Related substances method for Carmustine in bulk drug. Elixir Int. J. 50, 10383–10386.

Duan, X., Xiao, J., Yin, Q., Zhang, Z., Mao, S., Li, Y., 2012. Amphiphilic graft copolymer based on poly(styrene-co-maleic anhydride) with low molecular weight polyethylenimine for efficient gene delivery. Int. J. Nanomedicine 7, 4961–4972.

Fattahi, P., Borhan, A., Abidian, M.R., 2013. Characterization of the size, shape, and drug encapsulation efficiency of PLGA microcapsules produced via electrojetting for drug delivery to brain tumors, in: 2013 6th International IEEE/EMBS Conference on Neural Engineering (NER). Presented at the 2013 6th International IEEE/EMBS Conference on Neural Engineering (NER), pp. 953–956.

Fattahi, P., Borhan, A., Abidian, M.R., 2013. Microencapsulation of Chemotherapeutics into Monodisperse and Tunable Biodegradable Polymers via Electrified Liquid Jets: Control of Size, Shape, and Drug Release. Adv. Mater. 25, 4555–4560.

Ge, Y., Zhang, Y., He, S., Nie, F., Teng, G., Gu, N., 2009. Fluorescence Modified Chitosan-Coated Magnetic Nanoparticles for High-Efficient Cellular Imaging. Nanoscale Res. Lett. 4, 287–295.

Grayson, A.C.R., Choi, I.S., Tyler, B.M., Wang, P.P., Brem, H., Cima, M.J., Langer, R., 2003. Multi-pulse drug delivery from a resorbable polymeric microchip device. Nat. Mater. 2, 767–772.

Hainfeld, J.F., Smilowitz, H.M., O'Connor, M.J., Dilmanian, F.A., Slatkin, D.N., 2013. Gold nanoparticle imaging and radiotherapy of brain tumors in mice. Nanomed. 8, 1601–1609.

Hua, M.-Y., Liu, H.-L., Yang, H.-W., Chen, P.-Y., Tsai, R.-Y., Huang, C.-Y., Tseng, I.-C., Lyu, L.-A., Ma, C.-C., Tang, H.-J., Yen, T.-C., Wei, K.-C., 2011. The effectiveness of a magnetic nanoparticle-based delivery system for BCNU in the treatment of gliomas. Biomaterials 32, 516–527.

Huth, S., Lausier, J., Gersting, S.W., Rudolph, C., Plank, C., Welsch, U., Rosenecker, J., 2004. Insights into the mechanism of magnetofection using PEI-based magnetofectins for gene transfer. J. Gene Med. 6, 923–936.

Kayal, S., Ramanujan, R.V., 2010. Doxorubicin loaded PVA coated iron oxide nanoparticles for targeted drug delivery. Mater. Sci. Eng. C 30, 484–490.

Killela, P.J., Reitman, Z.J., Jiao, Y., Bettegowda, C., Agrawal, N., Diaz, L.A., Friedman, A.H., Friedman, H., Gallia, G.L., Giovanella, B.C., Grollman, A.P., He, T.-C., He, Y., Hruban, R.H., Jallo, G.I., Mandahl, N., Meeker, A.K., Mertens, F., Netto, G.J., Rasheed, B.A., Riggins, G.J., Rosenquist, T.A., Schiffman, M., Shih, I.-M., Theodorescu, D., Torbenson, M.S., Velculescu, V.E., Wang, T.-L., Wentzensen, N., Wood, L.D., Zhang, M., McLendon, R.E., Bigner, D.D., Kinzler, K.W., Vogelstein, B., Papadopoulos, N., Yan, H., 2013. TERT promoter mutations occur frequently in gliomas and a subset of tumors derived from cells with low rates of self-renewal. Proc. Natl. Acad. Sci. 110, 6021–6026.

Kim, J.O., Kabanov, A.V., Bronich, T.K., 2009. Polymer micelles with cross-linked polyanion core for delivery of a cationic drug doxorubicin. J. Controlled Release, Sixth International Nanomedicine and Drug Delivery Symposium 138, 197–204.

Liu, X., Huang, N., Li, H., Jin, Q., Ji, J., 2013. Surface and Size Effects on Cell Interaction of Gold Nanoparticles with Both Phagocytic and Nonphagocytic Cells. Langmuir 29, 9138–9148.

Li, Y., Duc, H.L.H., Tyler, B., Williams, T., Tupper, M., Langer, R., Brem, H., Cima, M.J., 2005. *In vivo* delivery of BCNU from a MEMS device to a tumor model. J. Controlled Release 106, 138–145.

Li, Y., Shawgo, R.S., Tyler, B., Henderson, P.T., Vogel, J.S., Rosenberg, A., Storm, P.B., Langer, R., Brem, H., Cima, M.J., 2004. *In vivo* release from a drug delivery MEMS device. J. Controlled Release 100, 211–219.

Ma, H., Qi, X., Maitani, Y., Nagai, T., 2007. Preparation and characterization of superparamagnetic iron oxide nanoparticles stabilized by alginate. Int. J. Pharm. 333, 177–186.

Mansur, H.S., Sadahira, C.M., Souza, A.N., Mansur, A.A.P., 2008. FTIR spectroscopy characterization of poly (vinyl alcohol) hydrogel with different hydrolysis degree and chemically crosslinked with glutaraldehyde. Mater. Sci. Eng. C, Proceedings of the Symposium on Nanostructured Biological Materials, V Meeting of the Brazilian Materials Research Society (SBPMat) 28, 539–548.

Márquez, M., Nilsson, S., Lennartsson, L., Liu, Z., Tammela, T., Raitanen, M., Holmberg, A.R., 2004. Charge-dependent targeting: results in six tumor cell lines. Anticancer Res. 24, 1347–1351.

McBain, S.C., Yiu, H.H.P., Haj, A.E., Dobson, J., 2007. Polyethyleneimine functionalized iron oxide nanoparticles as agents for DNA delivery and transfection. J. Mater. Chem. 17, 2561–2565.

McGovern, P.C., Lautenbach, E., Brennan, P.J., Lustig, R.A., Fishman, N.O., 2003. Risk Factors for Postcraniotomy Surgical Site Infection after 1,3-Bis (2-Chloroethyl)-1-Nitrosourea (Gliadel) Wafer Placement. Clin. Infect. Dis. 36, 759–765.

Merhi, M., Dombu, C.Y., Brient, A., Chang, J., Platel, A., Le Curieux, F., Marzin, D., Nesslany, F., Betbeder, D., 2012. Study of serum interaction with a cationic nanoparticle: Implications for *in vitro* endocytosis, cytotoxicity and genotoxicity. Int. J. Pharm., Special Issue: Drug Delivery and Imaging in Cancer 423, 37–44.

Mistri, P.A., Patel, D.J., Prajapati, J.J., 2012. Intranasal Drug Delivery System: A Review. Int. J. Pharm. Innov. 2, 88-111.

Omuro A, DeAngelis LM, 2013. Glioblastoma and other malignant gliomas: A clinical review. JAMA 310, 1842–1850.

Ozsoy, Y., Gungor, S., Cevher, E., 2009. Nasal delivery of high molecular weight drugs. Molecules 14, 3754–3779.

Painbeni, T., Venier-Julienne, M.C., Benoit, J.P., 1998. Internal morphology of poly(d,l-lactide-co-glycolide) BCNU-loaded microspheres. Influence on drug stability. Eur. J. Pharm. Biopharm. 45, 31–39.

Pinheiro, P.C., Daniel-da-Silva, A.L., Tavares, D.S., Calatayud, M.P., Goya, G.F., Trindade, T., 2013. Fluorescent Magnetic Bioprobes by Surface Modification of Magnetite Nanoparticles. Materials 6, 3213–3225.

Qian, L., Zheng, J., Wang, K., Tang, Y., Zhang, X., Zhang, H., Huang, F., Pei, Y., Jiang, Y., 2013. Cationic core–shell nanoparticles with carmustine contained within O6-benzylguanine shell for glioma therapy. Biomaterials 34, 8968–8978.

Raju, C.L., Rao, J.L., Reddy, B.C.V., Brahmam, K.V., 2007. Thermal and IR studies on copper doped polyvinyl alcohol. Bull. Mater. Sci. 30, 215–218.

Ren, J., Shen, S., Wang, D., Xi, Z., Guo, L., Pang, Z., Qian, Y., Sun, X., Jiang, X., 2012. The targeted delivery of anticancer drugs to brain glioma by PEGylated oxidized multi-walled carbon nanotubes modified with angiopep-2. Biomaterials 33, 3324–3333.

Roque, A.C.A., Bicho, A., Batalha, I.L., Cardoso, A.S., Hussain, A., 2009. Biocompatible and bioactive gum Arabic coated iron oxide magnetic nanoparticles. J. Biotechnol. 144, 313–320.

Sánchez, R.D., Ramos, C.A., Rivas, J., Vaqueiro, P., López-Quintela, M.A., 2004. Ferromagnetic resonance and magnetic properties of single-domain particles of Y3Fe5O12 prepared by sol–gel method. Phys. B Condens. Matter, Proceedings of the Workshop “At the Frontiers of Condensed Matter”. Magnetism, Magnetic Materials, and their Applications 354, 104–107.

Siegel, R.L., Miller, K.D., Jemal, A., 2015. Cancer statistics, 2015. CA. Cancer J. Clin. 65, 5–29.

Sullivan, J.P., Nahed, B.V., Madden, M.W., Oliveira, S.M., Springer, S., Bhere, D., Chi, A.S., Wakimoto, H., Rothenberg, S.M., Sequist, L.V., Kapur, R., Shah, K., Iafrate, A.J., Curry, W.T., Loeffler, J.S., Batchelor, T.T., Louis, D.N., Toner, M., Maheswaran, S., Haber, D.A., 2014. Brain Tumor Cells in Circulation Are Enriched for Mesenchymal Gene Expression. Cancer Discov. 4, 1299–1309.

Trewyn, B.G., Nieweg, J.A., Zhao, Y., Lin, V.S.-Y., 2008. Biocompatible mesoporous silica nanoparticles with different morphologies for animal cell membrane penetration. Chem. Eng. J., Porous Inorganic Materials for Biomedical Applications 137, 23–29.

Wang, F., Chatterjee, D.K., Li, Z., Zhang, Y., Fan, X., Wang, M., 2006. Synthesis of polyethylenimine/NaYF4 nanoparticles with upconversion fluorescence. Nanotechnology 17, 5786.

Xu, W., Park, J.Y., Kattel, K., Ahmad, M.W., Bony, B.A., Heo, W.C., Jin, S., Park, J.W., Chang, Y., Kim, T.J., Park, J.A., Do, J.Y., Chae, K.S., Lee, G.H., 2012. Fluorescein-polyethyleneimine coated gadolinium oxide nanoparticles as T1 magnetic resonance imaging (MRI)–cell labeling (CL) dual agents. RSC Adv. 2, 10907.

Xu, X., Chen, X., Xu, X., Lu, T., Wang, X., Yang, L., Jing, X., 2006. BCNU-loaded PEG–PLLA ultrafine fibers and their *in vitro* antitumor activity against Glioma C6 cells. J. Controlled Release 114, 307–316.

Yang, H.-W., Hua, M.-Y., Liu, H.-L., Huang, C.-Y., Tsai, R.-Y., Lu, Y.-J., Chen, J.-Y., Tang, H.-J., Hsien, H.-Y., Chang, Y.-S., Yen, T.-C., Chen, P.-Y., Wei, K.-C., 2011. Self-protecting core-shell magnetic nanoparticles for targeted, traceable, long half-life delivery of BCNU to gliomas. Biomaterials 32, 6523–6532.

Yang, X., Hong, H., Grailer, J.J., Rowland, I.J., Javadi, A., Hurley, S.A., Xiao, Y., Yang, Y., Zhang, Y., Nickles, R.J., Cai, W., Steeber, D.A., Gong, S., 2011. cRGD-functionalized, DOX-conjugated, and 64Cu-labeled superparamagnetic iron oxide nanoparticles for targeted anticancer drug delivery and PET/MR imaging. Biomaterials 32, 4151–4160.

Yavuz, C.T., Mayo, J.T., Yu, W.W., Prakash, A., Falkner, J.C., Yean, S., Cong, L., Shipley, H.J., Kan, A., Tomson, M., Natelson, D., Colvin, V.L., 2006. Low-Field Magnetic Separation of Monodisperse Fe3O4 Nanocrystals. Science 314, 964–967.

Zhang, H., Gao, F., Liu, L., Li, X., Zhou, Z., Yang, X., Zhang, Q., 2009. Pullulan acetate nanoparticles prepared by solvent diffusion method for epirubicin chemotherapy. Colloids Surf. B Biointerfaces 71, 19–26.

Zhang, L., Li, Y., Yu, J.C., Chen, Y.Y., Chan, K.M., 2014. Assembly of polyethylenimine-functionalized iron oxide nanoparticles as agents for DNA transfection with magnetofection technique. J. Mater. Chem. B 2, 7936–7944.

Zhang, L., Yu, F., Cole, A.J., Chertok, B., David, A.E., Wang, J., Yang, V.C., 2009. Gum Arabic-Coated Magnetic Nanoparticles for Potential Application in Simultaneous Magnetic Targeting and Tumor Imaging. AAPS J. 11, 693–699.

Zhang, N., Ding, E., Feng, X., Xu, Y., Cai, H., 2012. Synthesis, characterizations of dye-doped silica nanoparticles and their application in labeling cells. Colloids Surf. B Biointerfaces 89, 133–138.

CHAPTER 4

DEVELOPMENT OF THE *IN SITU* THERMOSENSITIVE ELECTRO-RESPONSIVE MUCOGEL FOR INCORPORATION OF THE BCNU-LOADED NANO-CO-PLEX

4.1. INTRODUCTION

The attribute of direct connection of nasal mucosa to the central nervous system (CNS) may assist delivery of therapeutic agents directly from the nasal mucosa to the CNS, thereby overcoming the problem of BBB, increasing the bioavailability of drugs to the CNS. Amongst the several intranasal dosage forms such as drops, sprays, gels and powders; a gel formulation has the most advantages, due to its ability to increase residence time of the formulation in the nasal mucosa (Chaturvedi et al., 2011). Gel formulations may also act as a protective embodiment for therapeutic agents against enzymatic degradation. To exploit the advantages of a gel and overcome its challenges in clinical use (Wu et al., 2007), a thermosensitive polymer such as Pluronic F127 (F127) was used in the formulation. F127 is a non-ionic, hydrophilic triblock copolymer of polyoxyethylene and polyoxyproylene (PEO-PPO-PEO). This copolymer exhibits thermo-reversible properties, remaining as a liquid at low temperature and forms a gel at physiological temperature. The copolymer molecules aggregate into spherical micelles containing a dehydrated hydrophobic PPO core and outer shell of hydrated swollen PEO chains. In aqueous medium, the micellar nature has been demonstrated to be suitable for incorporating drugs as well as for sustained release of bioactive agents (Akash et al., 2014).

Inclusion of mucoadhesive polymers may result in effective intranasal gel formulations with prolonged residence time. Chitosan (CS) is a natural polymer that has been widely used in pharmaceutical industries and its mucoadhesive property has been well researched (Baltzley et al., 2014; Saladini et al., 2012; Patil and Sawant, 2011). Thus, CS can be employed in formulating an intranasal gel in conjunction with hydroxylpropyl methylcellulose (HPMC), which also possesses

significant mucoadhesion (Fahmy, 2012). Thus, innovative approaches for controlling the release of therapeutic agents from the gel in a controlled and predetermined quantity for a fixed period of time, by applying an external electrical stimulus to modulate drug-loaded release can be explored. This was achieved by including an electro-active polymer (EAP) into the formulation. Examples of such polymers are polyaniline (PANI) (Kumar et al., 2012; Soni et al., 2012; Tsai et al., 2011), polypyrrole (PPy) (Shi et al., 2014; Stewart et al., 2014) and polythiophene (PT) (Imae et al., 2014). Among these EAPs, PANI has been given much attention due to its intrinsic electro conducting abilities and its application in numerous areas of technological advancement which include fields of artificial muscles (García-Gallegos et al., 2016), rechargeable batteries (Li et al., 2012; Xiao et al., 2012), microwave technologies (Cheng et al., 2015; Wang et al., 2015), biosensors (Özcan and Aydin, 2016) and drug delivery systems (Shokry et al., 2015; Tsai et al., 2011).

In this study, a novel biocompatible and biodegradable Thermosensitive Electro-Responsive Mucogel (TERM) made from a combinatorial blending of CS, HPMC, PF127 and PANI, developed with the ability for a prolong residence time in the nasal mucosa. Carmustine (BCNU)-loaded Nano-co-Plex (BCNU-NCP) was then incorporated into the TERM to form the “Nanogel Composite”, a delivery system which is a liquid at room temperature but forms gel at physiological temperature for ease of administration via intranasal route and can be electro modulated for controlled release of drug upon application of an external electric field. This study further explores the prospect of electro-actuation of the gel in an “on-off” drug release kinetics by means of an electrical switching for the control of drug within the nasal mucosa for onward delivery to the brain. The formulation was optimized employing a design of experiment (DOE), with the aid of a box-behnken experimental design software.

4.2. MATERIALS AND METHODS

4.2.1. Materials

Pluronic F127 (Mw=12,600g/mol), medium Mw chitosan (CS) (Mw=400,000g/mol), polyaniline (PANI) (Mw=20,000g/mol), hydroxylpropyl methylcellulose (HPMC), acetic acid, polyvinyl alcohol (PVA) (30kDa, 87−90% hydrolyzed), branched polyethylenimine (PEI) 1.8 kDa, iron (II) chloride tetrahydrate ($FeCl_2 \cdot 4H_2O$), iron (III) chloride hexahydrate ($FeCl_3 \cdot 6H_2O$), hydrochloric acid (HCl), sulphuric acid (H_2SO_4), N-hydroxysuccinimide (NHS), 1-ethyl-3(3-dimethylaminopropyl) carbodiimide (EDC), fluorescein isothiocyanate, epichlorohydrin, sodium hydrogen carbonate ($NaHCO_3$), sodium hydroxide (NaOH), dialysis tubing (Mw=10,000g/mol) and carmustine (BCNU) were purchased from Sigma-Aldrich (St. Louis, MO, USA). Double deionized water was obtained from a Milli-Q water purification system (Milli-Q, Millipore, Billerica, MA, U.S.). All other reagents used were of analytical grade and were employed as purchased.

4.2.2. Preparation of the Thermosensitive Electro-Responsive Mucogel

The TERM was prepared by solubilizing 20g of Pluronic F127 (F127) in 100mL of deionized water by stirring continuously for 1 hour. Partial solubility of the mixture was observed. The solution was then placed in an ice bath for another 1 hour after which the turbid solution was stored in a refrigerator at 4°C. A clear and transparent solution was observed after 24 hours of storage. CS (2g) was dissolved in 100mL of 1%$^{v}/_{v}$ acetic acid. F127 and CS blend was prepared by slowly adding CS solution to the F127 solution and stored in an ice bath for 4 hours. PANI (0.2%$^{w}/_{w}$) was then added to the mixture for a further 4 hours. HPMC (1%$^{w}/_{w}$) was lastly added to the final mixture. HCl (0.1mL, 0.1M) was then added to the mixture, resulting in a greenish-blue appearance. The sample was then stored at -80ºC over night, thawed at room temperature and then kept at 4ºC for further application.

4.2.3. Preparation of Carmustine-Loaded Nano-co-Plex

The carmustine (BCNU)-loaded Nano-co-Plex (NCP) was prepared as described in Chapter 3, Sections 3.2.2, 3.2.3 and 3.2.11.

4.2.4. Incorporation of the Carmustine-Loaded Nano-co-Plex into the Thermosensitive Electro-Responsive Mucogel

BCNU-loaded NCP (5mg) was added to 1mL of TERM and stirred for 1 hour for homogenization at 4ºC. The resultant blend, “Nanogel Composite” was then stored in a refrigerator at 4ºC for further application.

4.2.5. Optimization Studies Employing a Box-Behnken Experimental Design for the Nanogel Composite

A Box-Behnken Experimental Design was applied guided through a 3-factor, 3-level quadratic design employing Minitab Statistical Software, V15 (Minitab Inc., State College, PA, U.S.). Three formulation independent variables were considered viz, the concentration of F127 (15-25%$^{w}/_{w}$), CS (0.1-0.6%$^{w}/_{w}$) and PANI (0.1-0.8%$^{w}/_{w}$). The lower and upper limits of the independent variables obtained after the preliminary studies are presented in Table 4.1. HPMC (1%$^{v}/_{v}$) was constant in all the formulations. The design generated 15 formulations which are listed in Table 4.2. Response surface analysis was carried out on all the variables. Surface and contour plots were generated from the responses which were based on the Box-Behnken template to visualize the data in terms of the effect of the formulation variables on the response factors of the formulation.

Table 4.1: Lower and upper limits of the variables employed for the Box- Behnken design.

Polymers	Lower limits (%$^{w}/_{w}$)	Upper limits (%$^{w}/_{w}$)
F127	15	25
CS	0.1	0.6
PANI	0.1	0.8

Table 4.2: Series of formulations statistically generated by the Box–Behnken design.

Formulation	CS (% w/w)[a]	F127 (% w/w)[b]	PANI (%w/w)[c]
1	0.1	20	0.8
2	0.6	20	0.1
3	0.6	15	0.45
4	0.35	25	0.8
5	0.35	20	0.45
6	0.1	25	0.45
7	0.35	25	0.1
8	0.1	15	0.45
9	0.1	20	0.1
10	0.6	25	0.45
11	0.35	20	0.45
12	0.6	20	0.8
13	0.35	15	0.1
14	0.35	20	0.45
15	0.35	15	0.8

[a]chitosan concentration, [b]pluronic F127 concentration, [c]polyaniline concentration

4.2.6. Determination of Structural Modification and Chemical Interaction of the Nanogel Composite

The structural modification and chemical interaction between the polymers of the Nanogel Composite were carried out on the lyophilized gel formulation, as well as native polymers. FTIR Spectroscopy (PerkinElmer Spectrum 100, Beaconsfield, United Kingdom) over a range of 4000–550cm-1 was employed. The structural integrity was also elucidated by obtaining the XRD patterns of the Nanogel Composite and the native polymers employing a Rigaku 600 x-ray diffractometer (RIGAKU, Inc., Tokyo, Japan) equipped with Cu-Kα radiation (λ=1.54056 Å). The diffractograms were obtained using the parameters listed in Table 4.3. Integrated X-ray Diffraction software (PDXL 2.1, Rigaku, Tokyo, Japan) was used to analyze the results obtained.

Table 4.3: X-ray diffraction parameters

Parameter	Settings
Soller (inc.)	2.5°
Incident Height Slit (IHS)	10mm
Divergence Slit (DS)	1.25°
Solar Slit (SS)	13mm
Soller (rec.)	2.5°
Receiving Slit (RS)	13mm
Filter	None
Monochromater	None
Voltage	40kV
Current	15mA
Step	0.1°
Speed	2°/minute
Scan axis	Theta/2-Theta
Scan range	0°-90°
Scan mode	Continuous

4.2.7. Determination of the Mucoadhesive Behavior of the Nanogel Composite

Mucoadhesion study was carried out on all the 15 Nanogel Composite formulations by employing 0.5%$^{w}/_{v}$ solution of mucin in simulated nasal buffer solution. The Nanogel Composite (20mg/1.5mL) was dispersed in the buffer solution. The mixture was vigorously shaken and homogenized at 34°C for 2 hours. The dispersions were then centrifuged at 5,000rpm for 10 minutes to pellet the Gel-Mucin Complex. The supernatant was collected and used for free mucin content analysis. The quantity of mucin adsorbed onto the gel was the difference between the total quantity of mucin added and the free mucin content in the supernatant. The concentration of free mucin in the solution, after 6 hours was determined by UV spectrophotometry at a wavelength of 201nm (IMPLEN Nanophotometer™, Implen GmbH, München Germany). A calibration curve was prepared by using a series of known concentrations (0.1–1.0 mg/mL) of mucin in PBS (pH 6.0) as the standard.

4.2.8. Determination of Gelation Temperature of the Nanogel Composite

Gelation temperature was measured using two methods. The first method was by visual inspection as described elsewhere by Majithiya and co-workers (2006).

Briefly, 1mL samples of each formulation was measured and placed in transparent 5mL vials with a magnetic bar. These vials were then placed in a water bath that was heated from temperature of 20°C. The temperature of the water bath was increased at the rate of 1°C/minute while under magnetic stirring. The temperature was recorded when the magnetic bar stopped moving due to an increase in viscosity signifying the gelation temperature. The test-tube inverted approach (Chung et al., 2005) was also used as part of the visual method to support the magnetic bar method. The gelation temperature was measured at a point at which the formulation no longer flowed when the vial was tilted at any angle. Each formulation was tested 3 times. The second method was evaluation by rheological analysis. This was undertaken by carrying out temperature ramp experiments, employing a thermostatically controlled (UTC-MARS II), Modular Advanced Rheometer System (ThermoHaake MARS Thermo Fischer Scientific, Karlsuhe, Germany) fitted with a cone and plate geometry with a diameter of 3.5 cm and cone angle of 1° (sensor C35/1°) Ti at a temperature range of 20–40°C.

4.2.9. Determination of the Electrical Conductivity of the 15 Nanogel Composite Formulations

Electrical conductivity was assessed on the Nanogel Composite formulations employing a TDSTest™ Kit Model WD-35661-70 (Oakton instruments, Vernon Hills, IL, USA). The Nanogel Composite (5mL) was placed in a 50mL buffer solution (pH 6) and electrodes were applied onto the gel surface. The conductivity of the gel was recorded for all 15 formulations. This was performed in triplicate.

4.2.10. *In vitro* Determination of the Release Profiles of the 15 Nanogel Composite Formulations upon Application of an Electrical Stimulation

BCNU-NCP release was evaluated by the dialysis method (Zaki et al., 2007). The dialysis tubing cellulose membrane (Mw=12,000-14,000g/mol, Sigma-Aldrich, Steinhelm, Germany) was first immersed in a warm deionized water so as to remove the glycerol and sulphide from the tubing. Each formulation containing (5mg/mL) BCNU concentration was placed in the dialysis tubing while the two ends of the tubing were sealed, this was then immersed in a dissolution vessel containing 50mL of PBS (pH 6) dissolution medium, the temperature was kept at

34±1°C, with speed of rotation maintained at 50rpm. Electrical stimulation was carried out by applying a Potential Difference (PD) of 5V using a potentiostat/galvanostat (PGSTAT302N, Autolab, Utrecht, Netherlands). This was performed by placing a platinum electrode as the cathode and a gold electrode as the anode on the dialysis tube containing the Nanogel Composite in the buffer medium. Aliquots of 2mL were withdrawn from the release medium at time intervals of 1 hour. In order to maintain sink conditions, fresh PBS of 2mL was replaced into the released medium. Sampling was undertaken prior and after each application of electrical stimulation. The amount of BCNU-loaded Nano-co-Plex released is quantified by determining the amount of iron content in the withdrawn solution. Figure 4.1 illustrates the electro-simulation setup.

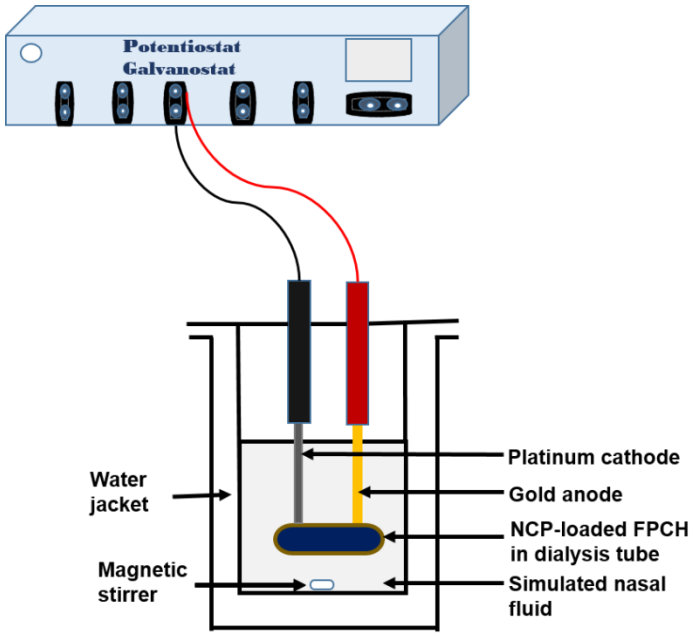

Figure 4.1: A schematic diagram depicting the electro-stimulation *in vitro* release experimental setup.

4.2.10.1. Quantitative analysis of the BCNU-loaded Nano-co-Plex released from the Nanogel Composite

This experiment was performed to determine the quantity of BCNU-loaded NCP that was released when 5V of PD was applied on the Nanogel Composite. The release of BCNU-loaded NCP from the Nanogel Composite was then determined by calculating the amount of iron contents in the released medium. This is due to

iron being the core of the BCNU-loaded NCP. Iron content was determined by using Wang and Edgar's method (Wang and Acosta, 2013). Briefly, a sample of 0.5mL was taken from the aliquot withdrawn prior and after the application of electric stimulation. This sample was then added to 7.5mL of 6N HCl in a 50mL beaker for 24 hours. This procedure was to solubilize all the iron species in the solution. The iron present in the solution was in the form of Fe^{3+} (Ferric chloride) with a yellowish-red color due to oxidation in the presence of HCl and the exposed air. A UV spectroscopy (IMPLEN Nanophotometer™, Implen GmbH, München, Germany) was used to measure the absorbance at 450nm. A calibration curve was generated from standard samples by dissolving 0.1mg-1mg of iron oxide nanoparticles in 7.5mL of 6N HCl and 0.5mL of deionized water for 24 hours. The quantity of iron was determined from the calibration curve.

4.2.11. *Ex Vivo* Evaluation of Mucoadhesive Strength of the Nanogel Composite

A texture analyzer (TA) (TA.XT plus, Stable Microsystems, Surrey, UK) was employed to determine the mucoadhesive strength of the Nanogel Composite. This was performed by measuring the force required to detach nasal mucosa membrane from each of the formulation. Freshly excised rabbit nasal membrane was attached to the upper probe of the instrument. The Nanogel Composite (1mL) was placed below the platform inside a temperature controlled compartment (34±1°C). The upper probe fixed with the rabbit nasal tissue was then lowered in order to establish contact with the surface of the Nanogel Composite. The exposed nasal mucosal membrane surface area was 0.785cm2. Measurement settings were displayed in Table 4.4. These measurements were repeated 5 times for each of the formulation, (N=5). Mucoadhesive strength was calculated from the generated force-distance curve as the peak detachment force (F_{det}) measured in Newton (N) and work of adhesion ($Ш_{adh}$) in Joules (J). The peak detachment force was taken as the maximum force needed for detaching the matrix formulation from the tissue while the work of adhesion was calculated as the area under the Force-Distance curve (Adeleke et al., 2015).

Table 4.4: The parameter settings for the mucoadhesion analysis of the Nanogel Composite.

Parameters	Settings
Pre-Test Speed	1mm/sec
Test Speed	0.5mm/sec
Post-Test Speed	1mm/sec
Trigger Type	Force
Trigger Force	0.05N
Applied Force	0.5N
contact force	0.001N
Contact Time	2min
Return Distance	10mm

4.2.12. Evaluation of the Thermal Behavior of the Optimized Nanogel Composite

Differential scanning calorimetry (DSC 1 STARe system, Mettler Toledo, Schwerzenbach, Switzerland) was employed to analyze the thermal behavior of the Nanogel Composite and the native polymers. The native polymers and the Nanogel Composite were subjected to a heating gradient, ranging from 0-300°C at a rate of 5°C per minute under innert conditions. Thermal gravimetric analysis (TGA) (PerkinElmer, TGA 4000, Llantrisant, Wales, UK), was also employed to further elucidate the thermal stability of the Nanogel Composite. The TGA was configured at a starting temperature of 30°C and end temperature of 900°C under continuous flow of nitrogen. Samples were heated at a rate of 10°C/min. Thermograms were generated as percentage weight vs. temperature. All results were analyzed using Pyris™ software (PerkinElmer, Llantrisant, Wales, UK).

4.2.13. Determination of Surface Morphology and Porosity of the Optimized Nanogel Composite

4.2.13.1. Scanning Electron Microscopy

The TERM and the optimized Nanogel Composite were lyophilized in order to assess the morphological characteristics of the formulation. Samples were sputter-coated using gold compound (EPI sputter coater) (SPI ModuleTM sputter-coater and control unit, West Chester, PA, USA), which was mounted on an aluminum spud. After coating the samples for 120s, under helium gas conditions, the

samples were analyzed using a FEI ESEM Quanta 400F (FEITM, Hillsboro, OR, USA) electron microscope, employing an electron acceleration charge of 20kV, to produce high resolution images of the particles.

4.2.13.2. Determination of the porosity profile of the Nanogel Composite

Porositometric analysis was carried out on the lyophilized optimized Nanogel Composite in order to evaluate pore size and the surface area of the optimized formulation employing a porositometric analyzer (Micrometrics ASAP 2020, Norcross, GA, USA). A sample of Nanogel composite (100mg) was placed in the sample tube and a glass filler rod was inserted into the sample tube to reduce the total free space volume in the tube, thereby speeding up the degassing process. The nanogel then went through the degassing stage to eliminate residual moisture and contaminants in the sample. The second stage involved the transfer of the tube to the analysis port for pore size, volume and surface area measurement in accordance with the BET and BJH models. The measurements were carried out with the parameters shown in Table 4.5.

Table 4.5: Porositometry parameters employed in the measurement of TERM/Nanogel Composite

Parameters	**Target/Rate**
Evacuation rate (mm Hg/s)	50
Temperature ramp rate (°C/min)	10
Target temperature (°C)	40
Hold temperature (°C)	30
Hold time (min)	900
Hold pressure for evacuation and heating phase (mm Hg/s)	100

Monolayer capacity of the gel was determined by using the BET linear equation (Equation 4.1) (Calvo et al., 1995).

$$\frac{1}{W[\left(\frac{Po}{P}\right)-1]}=\frac{1}{WmC}+\frac{C-1}{Wm}\left(\frac{P}{Po}\right) \qquad \textbf{Equation 4.1}$$

Where W is the quantity of nitrogen gas absorbed at the relative pressure of P/Po

Wm was the monolayer capacity and C is the constant which is related to the difference between the molar free energy of absorption of the first layer and the liquefaction layer.

Using the molecular cross-sectional value, A_m, the surface area was determined from the monolayer capacity applying Equation 4.2 and 4.3 (Ramburrun et al., 2015).

$$As(BET) = Wm \times L \times Am \qquad \textbf{Equation 4.2}$$

$$as(BET) = \frac{As(BET)}{m} \qquad \textbf{Equation 4.3}$$

where As(BET) and as(BET) are the total and specific surface areas, respectively of the absorbent of mass, m, and L is the Avogadro constant.

4.2.14. Rheological Analysis of the Optimized Nanogel Composite

Rheological studies of the optimized Nanogel Composite were carried out to measure and assess various rheological parameters of the Nanogel Composite in comparison to the native polymer F127. This was achieved by employing a thermostatically controlled (UTC-MARS II), Modular Advanced Rheometer system (ThermoHaake MARS Rheometer, Thermo Fischer Scientific, Karlsuhe, Germany) fitted with a cone and plate geometry with a diameter of 3.5cm and cone angle of 1° (sensor C35/1°) Ti. The parameter settings used for the rheological analysis are provided in Table 4.6. During the temperature ramp experiment, the cone and the plate were covered with a solvent trap to prevent the samples from drying up which might be due to solvent evaporation. The frequency employed was the frequency at which the yield value was obtained.

Table 4.6: The parameter settings for the rheological analysis of Nanogel Composite and F127.

Tests	Parameters				
	Shear Rate (s^{-1})	**Shear Stress (Pa)**	**Time (s)**	**Frequency (Hz)**	**Temperature (°C)**
Shear Viscosity	0.00-200		180		34
Yield Stress		0.200-200	200		34
Oscillatory Stress Sweep		0.200-200		0.1, 1, 10	34
Oscillatory Frequency Sweep				50.0-0.05	34
Creep and Recovery Test			60-180		34
Temperature Ramp				1	20-40

4.2.15. Evaluation of the Electro-activity of the Optimized Nanogel Composite

Electro-activity of the Nanogel Composite was determined by carrying out cyclic voltammetry on the Nanogel Composite. This was achieved by the adapted method of Tsai and coworkers (Tsai et al., 2011). Briefly, the Nanogel Composite was first homogenized in PBS (pH 6.0) which was the conducting solvent for 5 minutes, followed by 3 minutes ultrasonication (Vibra-Cell™, Sonics® Sonics & Material Inc., Newtown, CT, U.S.). Nitrogen gas was passed through the solution obtained for purging. Galavanometer (PGSTAT302N, Autolab, Utrecht, Netherlands), a three-electrode system with a saturate Ag/AgCl (3.0 M KCl) as the reference electrode, a platinum wire as the auxiliary electrode, and a 5mm glassy carbon electrode as the working electrode were employed for the analysis. A scan rate of $0.1Vs^{-1}$ was applied.

4.2.16. *In Vitro* Drug Release Analysis from the Optimized Nanogel Composite on the Application of an Electrical Stimulation

In vitro drug release analysis from the optimized Nanogel Composite was performed as detailed in Section 4.2.10. The quantity of BCNU in the aliquot of the BCNU-NCP was carried by extracting the BCNU using dichloromethane (DCM) as reported by Levin and coworkers (1978). This was then analyzed employing the Ultra Performance Liquid Chromatography (UPLC).

4.2.16.1.Quantitative determination of the BCNU-loaded Nano-co-Plex released from the optimized Nanogel Composite

The BCNU-loaded Nano-co-Plex released from the optimized Nanogel Composite was determined by calculating the amount of iron content in the released solution as described in Section 4.2.10.1.

4.3. RESULTS AND DISCUSSION

4.3.1. Preparation of the Thermosensitive Electro-Responsive Mucogel and the Nanogel Composite

In order to prepare a suitable nasal formulation that will have the advantage of ease of administration, the formulation should possess the ability of being a sol at room temperature and transitions to a gel at nasal mucosa temperature (sol-gel-sol phase transition). The Nanogel Composite was prepared by blending together F127 and CS, HPMC and PANI. F127 represented the thermosensitive portion of the formulation, the CS and the HPMC represented the mucoadhesion portion of the formulation while PANI was the electroactive moiety of the formulation. Results of the preliminary studies showed that a lower limit of 15, 0.1 and 0.1%$^{w}/_{w}$ for F127, CS and PANI respectively and upper limits of 25, 0.6, and 0.8%$^{w}/_{w}$ for F127, CS and PANI respectively were limits outside of which no meaningful formulation can be achieved. Addition of 1%$^{w}/_{w}$ HPMC was constant throughout the preliminary tests. HPMC was employed to increase viscosity, adjust the gelation temperature and most importantly prevent leakage of incorporated therapeutic agent.

It was observed that the gelation temperature increased with the addition of CS and decreased when HPMC was added. The reason for the increase in gelation temperature with the addition of CS may be due to the acetic acid used in solubilizing the CS, which tends to weaken the H-bonds between the tightly packed configurations of the F127 gel thus disorientating the well-packed micelle arrangement (Zaki et al., 2007). The decrease in gelation temperature on addition of HPMC may be due to an increase of the viscosity of the solution provided by the addition of the HPMC. It was observed that the gelation temperature of all the resulting formulations during the preliminary tests were between 20°C and 35°C, since the temperature of nasal mucosa is between 32°C and 35°C (Basu and Bandyopadhyay, 2010), any gelling temperature between 26°C to 34°C will be suitable.

4.3.2. Evaluation of Box–Behnken experimental design optimization

The lower and upper limits were applied using the Box–Behnken experimental design to generate the 15 formulations. These formulation variables were evaluated for their responses to mucoadhesion, conductivity and drug release upon application of electric stimulation. The responses from the 15 formulations are shown in Table 4.7. The application of this design was based on developing an optimized Nanogel Composite that has the ability to release desired amount of drug upon application of a specific voltage to the formulation in an ‘‘on–off’’ pulsatile drug release pattern with the aim of acquiring quality statistically scientific significance.

Response surface analysis results generated by the Minitab Statistical Software revealed the correlation of the data with the response elements of the formulation. The residual and surface plots were generated from the response data. Residual plots were used to evaluate the differences in the fitted and the observed responses, and how best the outcome fits the regression. From Figure 4.2, it can be observed that the residual plot indicated a near perfect regression. The surface plots explicate the relationship existing between one response and two factors while keeping the third factor constant. Figure 4.3 shows the surface plots of the 3 responses. The average release per cycle versus concentration of PANI and CS

showed the corresponding values of PANI and CS concentration for the maximum release per cycle achieved. Further, the maximum value of conductivity and mucoadhesion responses were displayed in the plots with the corresponding values of the variables. The optimal formulation for the three responses was derived by employing desirability function. The formulation was optimized for maximum mucoadhesion and 10% average drug release per cycle. Figure 4.4 shows the result of the optimization by the desirability function, in relation to the quantity of the independent variables required to obtain the optimized formulation. The optimized formulation was achieved by using 0.36, 16.8 and 0.40%$^{w}/_{w}$ of CS, F127 and PANI respectively while keeping the concentration of HPMC at 1%$^{w}/_{w}$.

Table 4.7: Formulations and their corresponding responses

Variables				**Responses**		
Formulation Number	**CS (%)**	**F127 (%)**	**PANI (%)**	**Conductivity (mS/cm) SD≤0.1012**	**Mucin adsorbed (mg) SD≤0.03**	**Average release per cycle (%), SD≤3.50**
1	0.1	20	0.8	1.7921	0.05	13.67
2	0.6	20	0.1	0.0611	0.39	4.55
3	0.6	15	0.45	1.2386	0.31	10.03
4	0.35	25	0.8	1.1097	0.11	12.43
5	0.35	20	0.45	1.8699	0.18	8.11
6	0.1	25	0.45	0.4581	0.06	6.05
7	0.35	25	0.1	0.0314	0.2	4.78
8	0.1	15	0.45	2.4997	0.08	9.18
9	0.1	20	0.1	0.1533	0.09	4.56
10	0.6	25	0.45	0.8806	0.29	5.21
11	0.35	20	0.45	1.8698	0.18	8.04
12	0.6	20	0.8	1.2156	0.24	11.24
13	0.35	15	0.1	0.276	0.21	4.76
14	0.35	20	0.45	1.8679	0.18	8.09
15	0.35	15	0.8	2.1283	0.12	15.82

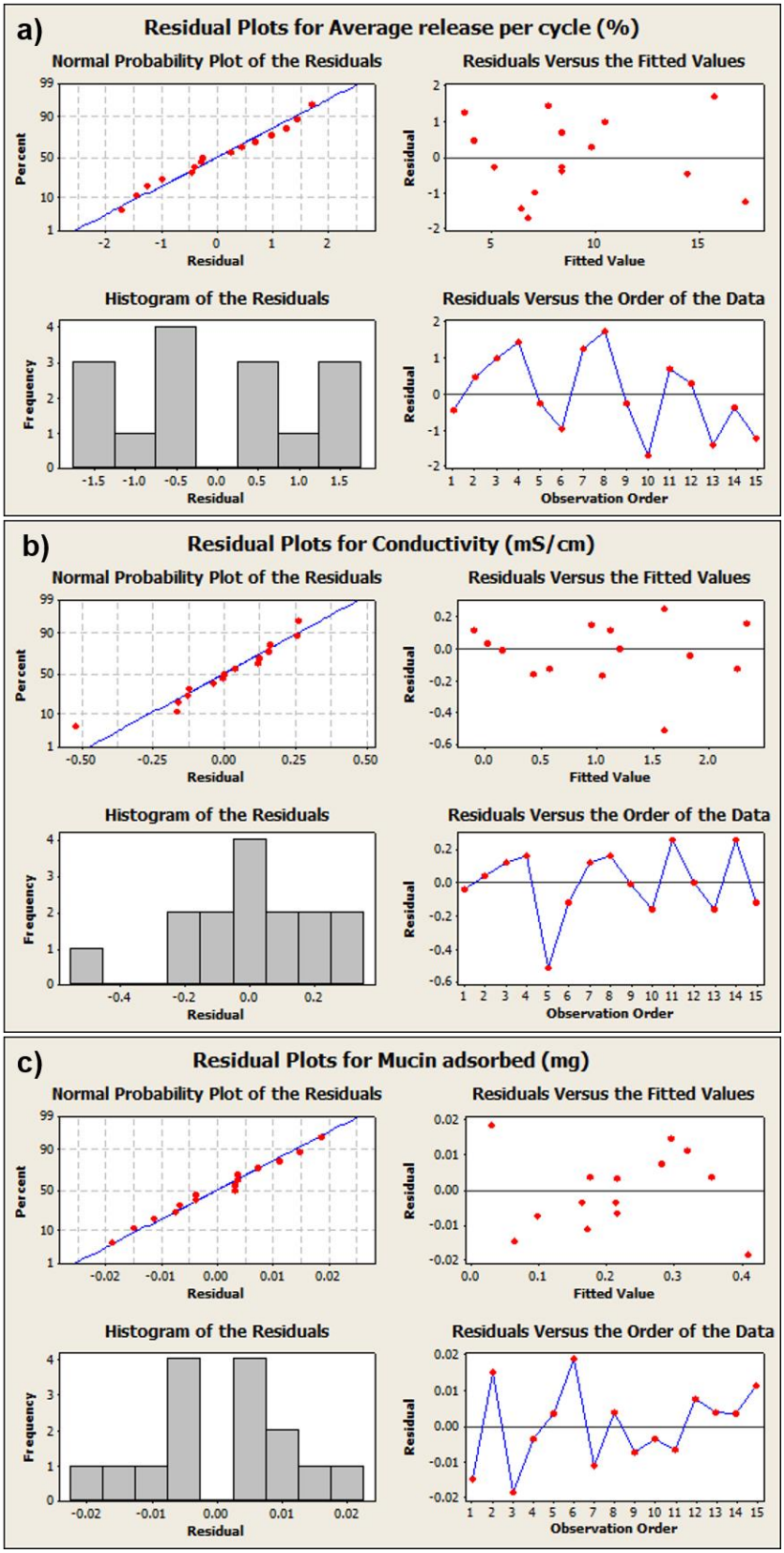

Figure 4.2: Residual plots of (a) average release per cycle, (b) conductivity and (c) mucoadhesion.

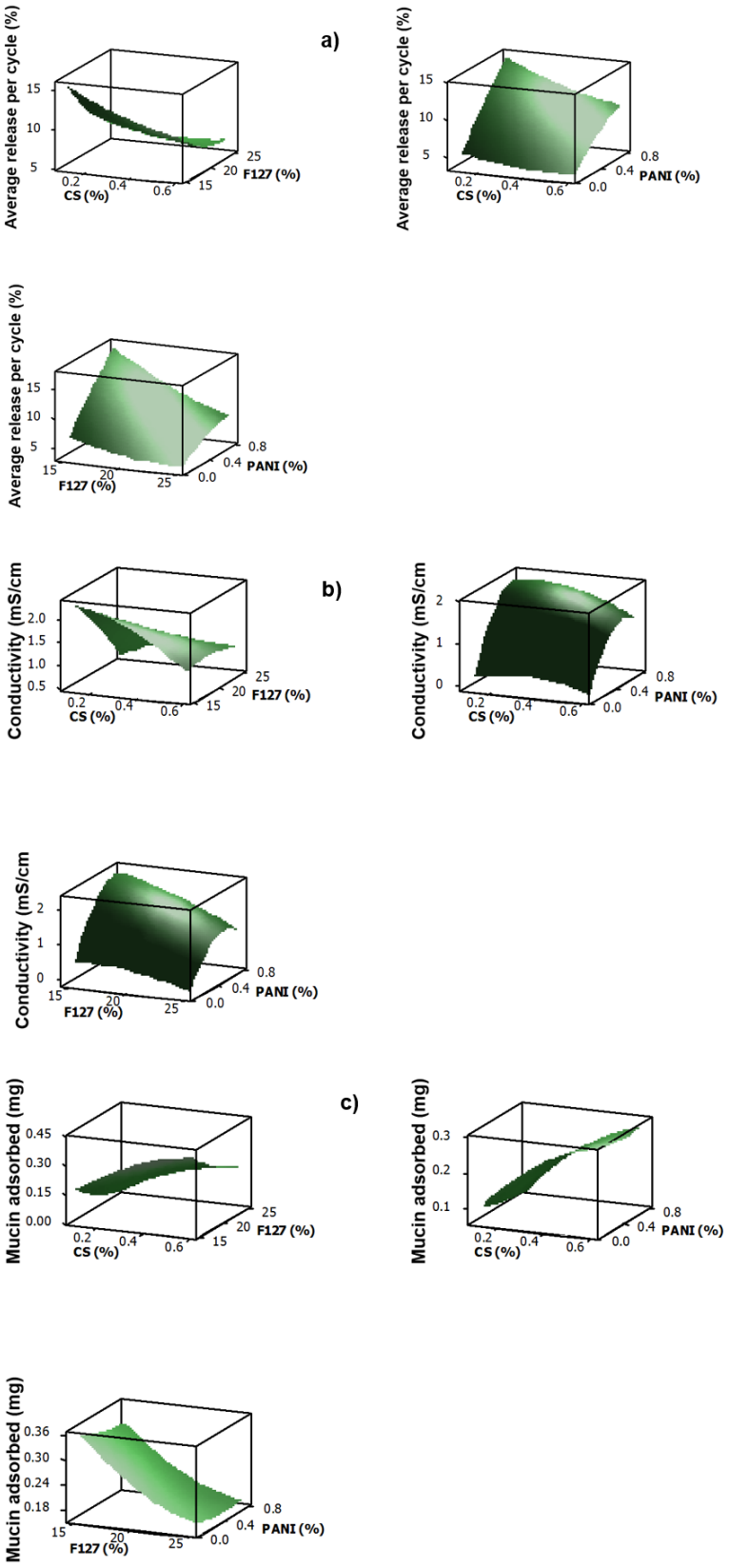

Figure 4.3: Response surface plots showing the effects of F127, CS and PANI on (a) electro-responsive drug release, (b) conductivity and (c) mucoadhesion.

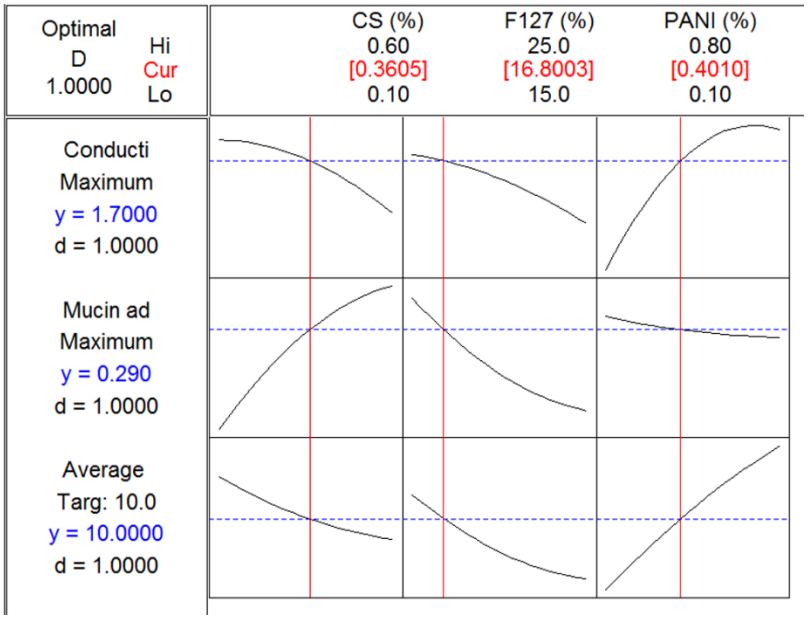

Figure 4.4: Response Optimization output plot by desirability function with the values of independent variables and predicted values of the responses of Nanogel Composite.

4.3.3. Assessment of the Mucoadhesive Behavior of the Nanogel Composite

The results of the mucoadhesive behavior of the Nanogel Composite are displayed in Figure 4.5. The nasal formulation is considered to be effective if it can have a long resident time in the nasal cavity. The nasal mucosa has a clearing mechanism that does not permit therapeutic compounds to reside for long in the mucosa; they are easily cleared away by the mucociliary clearance which is a natural defensive mechanism. It is therefore pertinent to formulate therapeutic agent that can adhere considerably tight to the mucosal wall to keep the administered formulation in the mucosa. From the experiment, the amount of mucin adsorbed by each formulation is indicative of the mucoadhesive capacity of the formulation. The results showed the amount of mucin adsorbed by the gel in each of the formulation. The amount of mucin adsorbed is therefore directly proportional to the degree of mucoadhesion of the formulation. The results obtained indicated that formulation 2 has the highest percentage amount of adsorbed mucin value (0.39mg), signifying the degree of mucoadhesion being the highest in this formulation compared to the other formulations in the design. This formulation, however, is observed to contain the highest concentration of CS and a low concentration of PANI. Furthermore, formulation 1 has the lowest adsorbed

amount of mucin (0.05mg) which also indicated lowest degree of mucoadhesion. This formulation contained low concentration of CS and high concentration of PANI in comparison to the other formulations. This outcome showed clearly that CS exhibits the mucoadhesion property and it is the moiety that is responsible for the mucoadhesive nature of the gel, while PANI did not contribute to the mucoadhesion. Furthermore, the results indicated that the greater the concentration of PANI in the formulation, the less the degree of mucoadhesion. It can be deduced from the results that, the higher the concentration of CS, the higher the degree of mucoadhesion. The results obtained also demonstrated that CS, which is a cationic polymer, has the ability to bind through electrostatic interaction with the mucus and the charged mucosal surface (Kondiah et al., 2013). CS is solely responsible for the ionic interaction forming strong electrostatic bonds with the mucus of the nasal cavity thereby prolonging the residence time of the formulation in the nasal cavity.

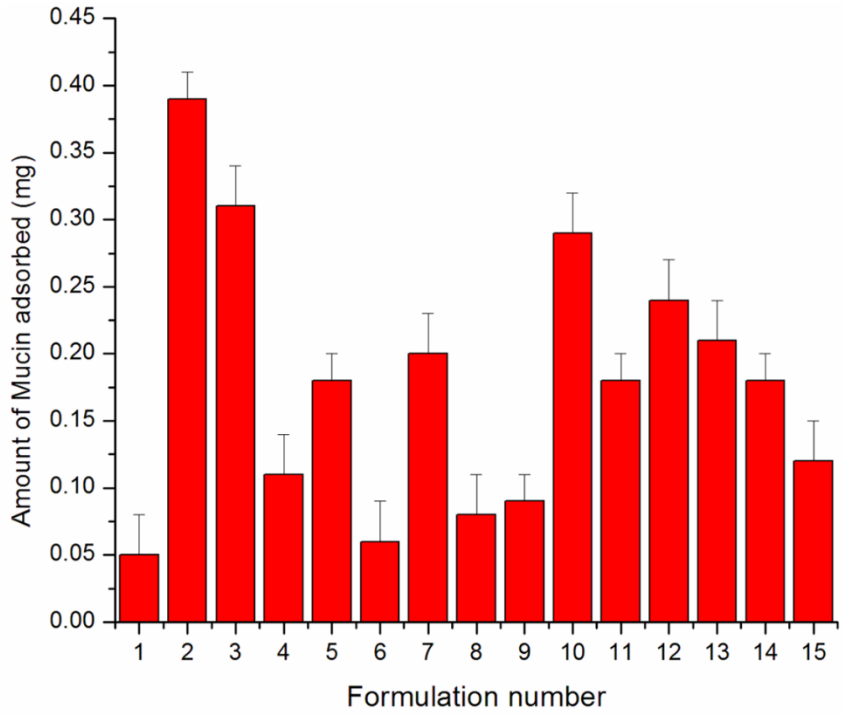

Figure 4.5: Percentage of mucin adsorbed by the 15 formulations.

4.3.4. Assessment of the Gelation Temperature

The gelation temperatures of all the 15 formulations are shown in Table 4.8. The mechanism of gelation can be explained by the change in the number of micelles formed with change in temperature. As the temperature increases, so does the number of formed micelles thereby leading to a tightly packed micelle formations and entanglements, the solution thus becomes immobile which results in gel formation (Majithiya et al., 2006). Furthermore, gelation may be brought about by the conformational alterations in the orientation of the CH_3- groups in the PPO side chains, which is the micellar core, coupled with dehydration of the micelles (Cabana et al., 1997). Furthermore, from Table 4.8, the gelation temperature was observed to increase as the quantity of CS in the formulation increases, this is due to the hydrophilic properties of CS which interfered with the hydrophobic interaction of F127 (Chung et al., 2005). Formulation 3 has the highest gelation temperature which stands at 32°C while formulation 6 has the lowest gelation temperature of 21.5°C. The gelation temperature values obtained from the rheological experiment are very close to those observed with visual inspection methods as shown in Table 4.8.

Table 4.8: Gelation temperature of the 15 formulations

	Gelation temperature (ºC)	
Formulation number	**Rheological determination (N=3)**	**Visual inspection (N=3)**
1	22.5±0.11	24±0.82
2	28±0.05	30.3±0.47
3	32±0.08	31.7±0.94
4	25±0.1	26.3±0.47
5	27.5±0.05	29.3±0.47
6	21.5±0.1	22±0.82
7	22±0.06	23±1.41
8	23.5±0.12	24.3±0.94
9	20±0.1	21.7±0.94
10	24±0.05	24±0.82
11	27±0.1	28.7±0.94
12	29.5±0.06	31.3±1.25
13	23±0.1	24.3±0.47
14	27.5±0.12	28±0.82
15	26±0.5	28.3±1.25

4.3.5. Electro-Responsiveness of the Nanogel Composite via Electric Conductivity Assessment

The electrical conductivity of the 15 Nanogel Composite formulations was investigated in order to evaluate their electro-responsive behavior when electric current is passed through them. Figure 4.6 shows the results of the conductivity test; the formulation with the most electrical conductivity is formulation 12 with a value of 27.8±1.8mS/cm. This formulation contained the highest concentration of PANI. Formulation 9 was found to have the lowest conductivity value; this formulation contained the lowest concentration of PANI of all the formulations. These results signify that PANI is responsible for the conductivity of the Nanogel Composite. The emeraldine base of PANI is highly conductive when doped with HCl, thus enhancing the conductivity of the formulation. The conductivity property of the Nanogel Composite is directly proportional to the ability to respond to electrical stimulation. It is therefore pertinent to infer that the higher the concentration of PANI in the Nanogel Composite, the higher the conductivity and subsequently the higher the response when electric stimulation is applied to it. The electrical stimulation is the key to the release of drug from the Nanogel Composite. Therefore, in order to modulate the release of drug incorporated in the Nanogel Composite, the electrical properties of the Nanogel Composite must be given adequate attention.

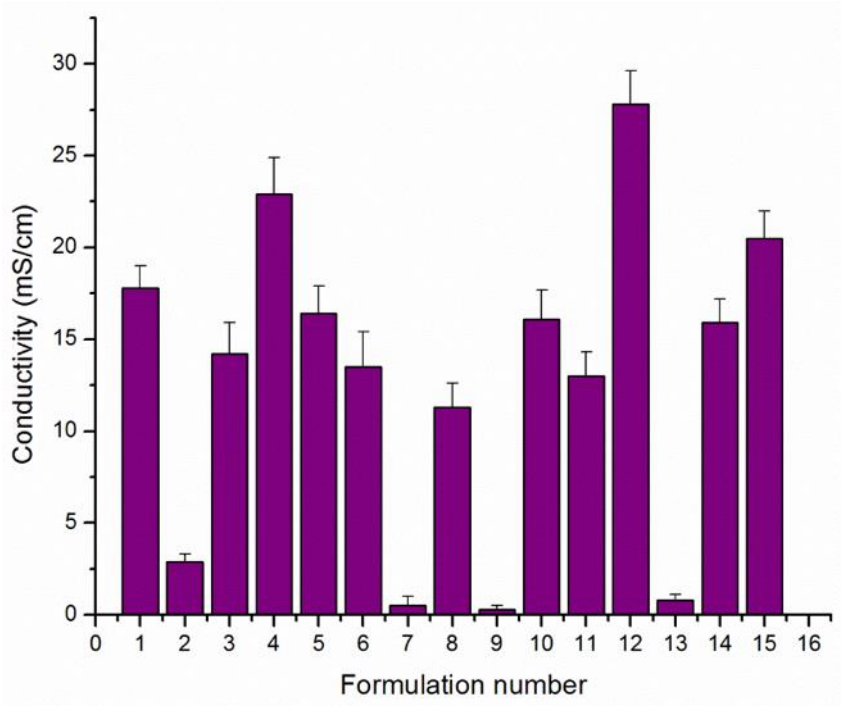

Figure 4.6: Electrical conductivity of the 15 formulations of the Nanogel Composite

4.3.6. *In Vitro* Assessment of Release Behavior of the 15 Nanogel Composite Formulations on Application of Electrical Stimulation

The purpose of developing an electro-responsive system is to ensure that it releases therapeutic agent that is incorporated into it on application of electrical stimulation. The *in vitro* drug release carried out was to assess the electro-actuated release of BCNU-NCP from the Nanogel Composite upon application of electric stimulation. The preliminary studies revealed that a potential of 5V is adequate to invoke release of BCNU-NCP from the Nanogel Composite. The release studies were carried out using 5V potential difference for all the formulations. All the formulations released BCNU-NCP upon application of electrical stimulation. Figure 4.7 shows the release profile of BCNU-NCP for all the 15 formulations. Formulations 15, 1, 4 and 12 demonstrated average release percentage of 15.82%, 13.67%, 11.89% and 11.24% respectively. These formulations contained the highest concentration of PANI relative to the concentration of the other native polymers in each of the formulation. This confirms that PANI is the moiety that is responsible for the release of BCNU-NCP from the Nanogel Composite, with the release being proportional to the

concentration of PANI in the formulations. The mechanism of release may be explained by the electrical conducting characteristics of PANI. During the application of electrical stimulation, hydrolysis of water occured which tend to protonate the NH group of the PANI. The PANI molecules are thereby excited within the nanogel matrix and thus transport the PANI molecules towards the cathode. This action may therefore lead to disruption of the H-bonding holding the matrix together as a result of this; the micellar structure of the nanogel begins to dismantle and the nanogel begins to erode, subsequently resulting in the release of the BCNU-loaded NCP in the matrix system of the gel. It may therefore be inferred that the release of BCNU-loaded NCP was due to the matrix erosion when electrical stimulation was applied. It is envisaged that disintegration of the Nanogel Composite occurred by surface erosion during the migration of the PANI moiety towards the cathode. The release was found to follow zero-order kinetics. Furthermore, the release profile demonstrated a pulsatile “on-off” switchable release upon electro-actuation as seen in Figure 4.7.

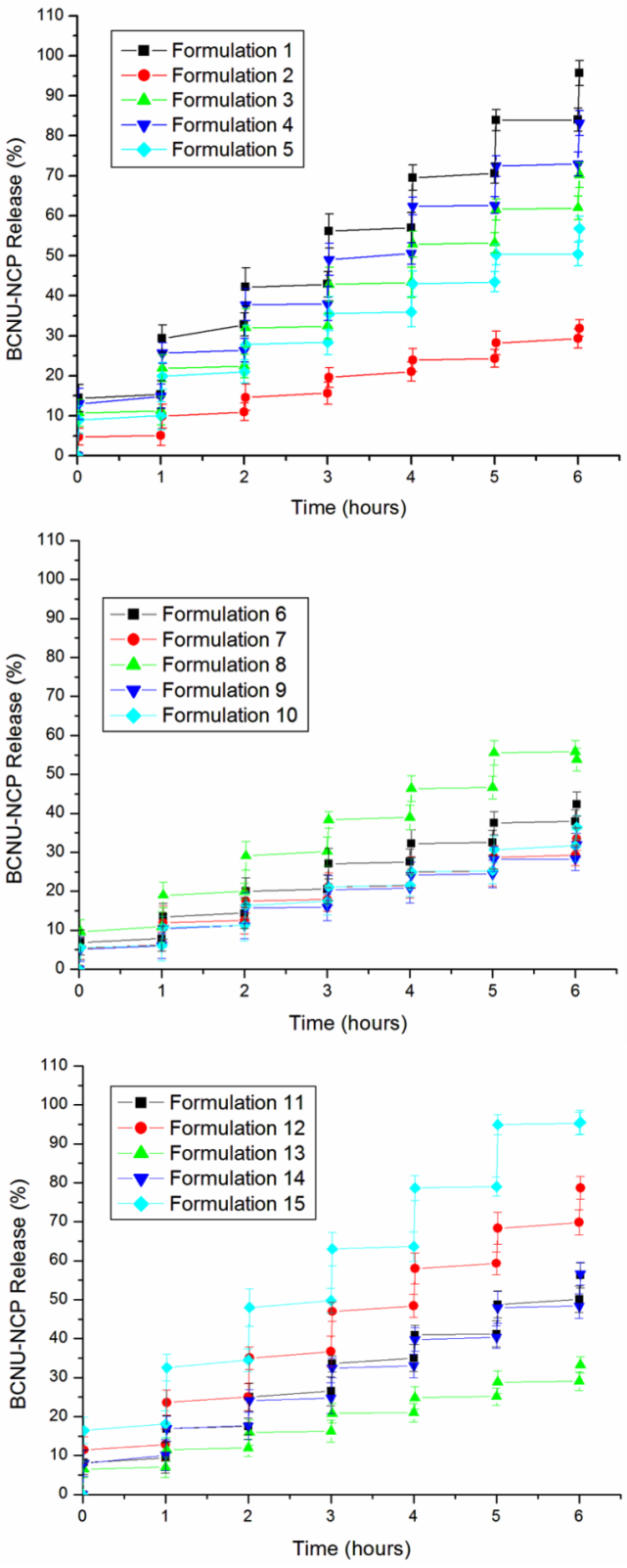

Figure 4.7: BCNU-NCP release profiles in simulated nasal fluid (pH 6.0) for Formulations 1-15.

4.3.7. *Ex vivo* Mucoadhesion Analysis

The mucoadhesive strengths of the 15 formulations were measured by *ex vivo* analysis. The average maximum detachment force in Newton and work of adhesion in mJ were determined from the peak and Area under the curve (AUC), respectively, of the Force-Distance profiles as presented in Figure 4.8 and Figure 4.9. Formulation 2 demonstrated the highest value of 0.622±0.013N while formulation 1 displayed the lowest value of 0.076±0.007N. Likewise, the work of adhesion for formulation 2 was the highest with value of 0.2855±0.00997mJ, while formulation 1 demonstrated the lowest with value of 0.02488±0.00521mJ as illustrated in Figure 4.9. The major factor which is responsible for these observations can be attributed to the concentration of CS present in the formulation. Formulations with high concentration of CS are more mucoadhesive than those containing low CS concentration. The NH_3^+ group of CS of the formulation has the ability to crosslink with the carboxylic group of mucin in the mucus of the nasal mucosa to form a polymer network and thereby strengthening the bonds holding them together. These results are in agreement with the chemical analysis performed using the reaction of mucin with the formulation as explained in Section 4.3.3.

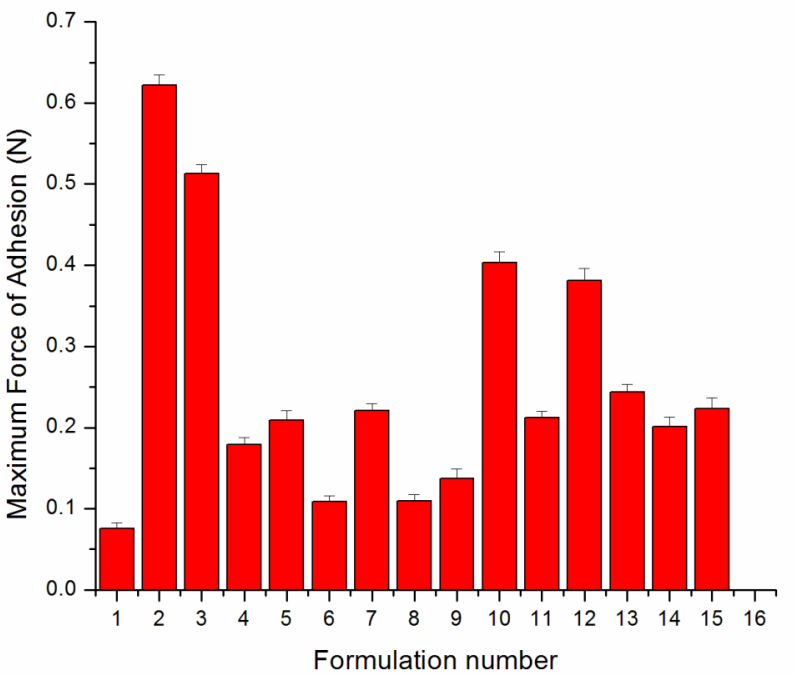

Figure 4.8: Tensile detachment measurement displaying Maximum force of adhesion of the Nanogel Composite formulations from rabbit nasal mucosal tissue wetted with simulated nasal buffer at pH 6.0 (SD≤ 0.015; N=5).

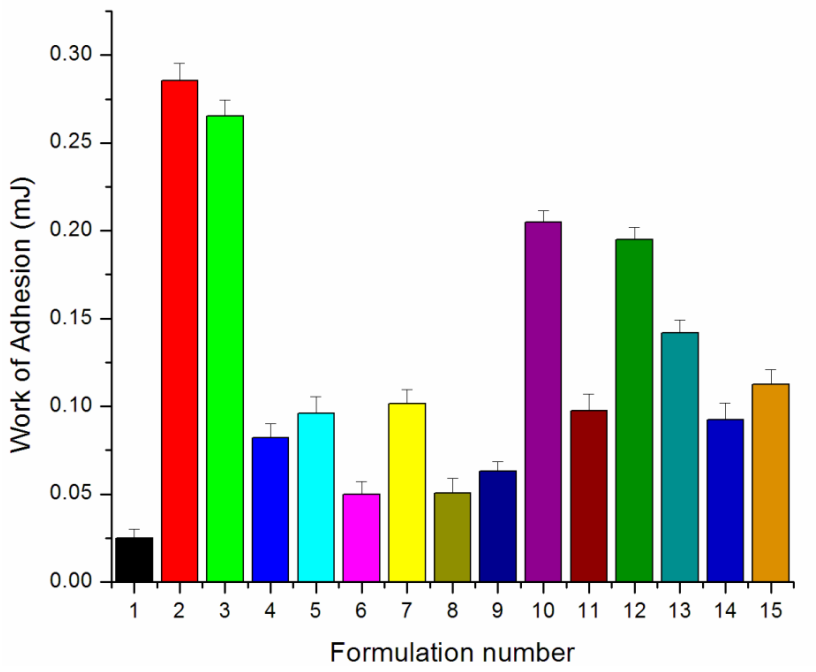

Figure 4.9: The total work of adhesion for removing Nanogel Composite from rabbit nasal mucosal tissue wetted with simulated nasal buffer at pH 6.0 (SD≤ 0.00997; N=5).

4.3.8. Assessment of the Structural Modification of the Optimized Nanogel Composite

4.3.8.1. Assessment of the structural modification employing Fourier Transmission Infrared spectroscopy

The structural integrity of TERM and Nanogel Composite were assessed employing FTIR. Figure 4.10 depicts the FTIR spectra of the native polymers that were employed in formulating the Nanogel Composite. The native polymers displayed their unique characteristics absorption peaks at various bands; these are summarized in Table 4.9.

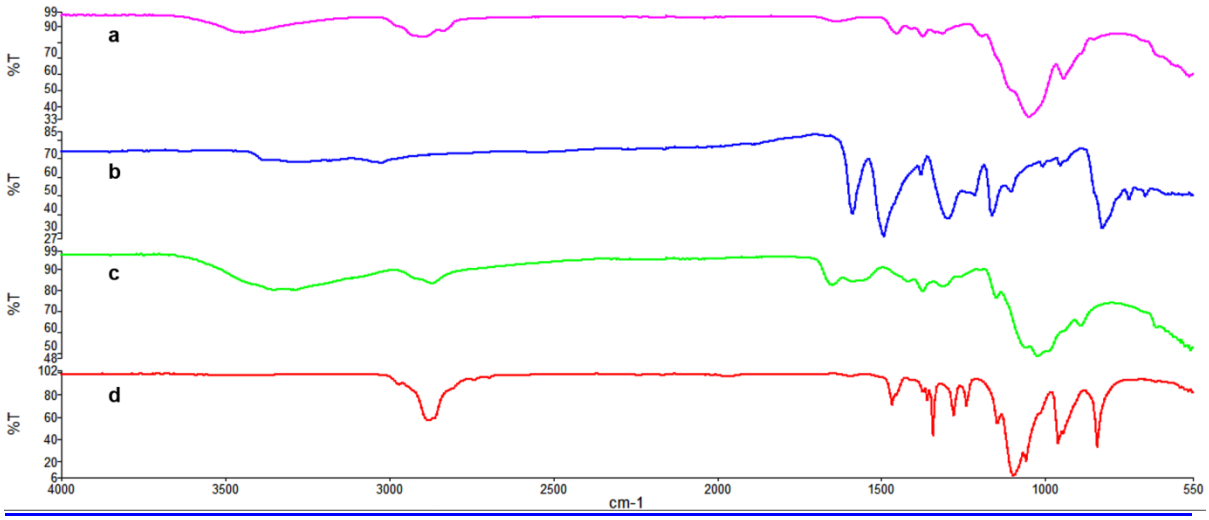

Figure 4.10: FTIR spectra of a) HPMC, b) PANI, c) CS and d) F127.

Table 4.9: FTIR spectra of HPMC, PANI, CS and F127 showing their major characteristic native bands.

Samples	IR bands (cm^{-1})	Description	References
HPMC	3442	O-H stretching vibrations	(Sahoo et al., 2012)
	2900	C-H stretching vibrations	
	1635	Cyclic rings stretching vibrations	
	1453	Asymmetric bending vibrations of methoxy group	
	1373	Cyclic anhydride	
	1050	C-O-C stretching vibrations	
PANI	1589	N=Q=N ring stretching vibrations	(Trchová et al., 1999)
	1379	N-B-N ring stretching vibrations	
	1297	C-N stretching vibrations	
	1153,1103, 825	C-H bending vibrations	
CS	3400–3500	amino group	(Sionkowska et al., 2004)
	3288	O-H stretching vibrations	
	2890	CH_3 stretching vibrations	
	1651	C=O stretching vibrations	
	1587	NH bending vibrations	
	1373	NH- bending vibrations	
F127	2877	Aliphatic C-H stretching vibrations	(Karolewicz et al., 2014)
	1466	Aliphatic C-H bending vibrations	
	1341	O-H bending vibration	
	1097	C-O stretching vibrations	

Q and B represent abbreviations for quinoid and benzenoid moieties in PANI polymers respectively.

Figure 4.11 displays the FTIR spectra of F127, the TERM, and Nanogel Composite. F127 exhibits 2 distinct strong bands at 2877cm^{-1} which corresponds

to aliphatic C-H stretching, and strong peak at 1097cm^{-1} which corresponds to the C-O stretching vibrations as depicted in Figure 4.11a. These two distinct strong bands are also present in TERM and Nanogel Composite. Figure 4.11b shows the spectrum of TERM, in addition to the peaks observed in F127, there are other additional peaks at 3323cm^{-1}, 3182cm^{-1}, 3959cm^{-1}, and 2626 cm^{-1}. These peaks represent the absorption band of other excipients that were present in the formulation. This confirms the difference in physicochemical features of TERM in comparison to that of the F127 and Nanogel Composite. The spectrum of Nanogel Composite is very similar to that of TERM; however, it is worth noting that there is a distinct difference in the intensity of C-H band observed at 2880cm^{-1} amongst the three spectra. The highest intensity of the peak was observed for F127 followed by TERM and then the Nanogel Composite as highlighted in Figure 4.11. This phenomenon can be explained in terms of the H-bond interaction of F127 with CS, PANI and HPMC in the blend; the C-H bond is synonymous to the polyoxypropylene block of F127, the more functional groups capable of forming H-bonding with it the less the intensity of the peak generated. In this case CS and HPMC, they can form H-bonding including van der Waals bonds with F127. Furthermore, the broad band observed at 3323cm^{-1} is evidence of H-bonding that is formed due to the interaction of the F127 with the other excipients in the formulation. Infrared spectroscopy is known to be a highly effective method for investigating H-bonding interactions in polymer blend systems (Chu et al., 2013). It is pertinent to therefore note that there is no chemical conjugation or covalent bonding within the components that made up the Nanogel Composite. The stability of the gel is solely dependent on the interactions of the functional groups of the polymers to form non-ionic bod such as H-bonding, electrostatic interaction and van der Waals forces.

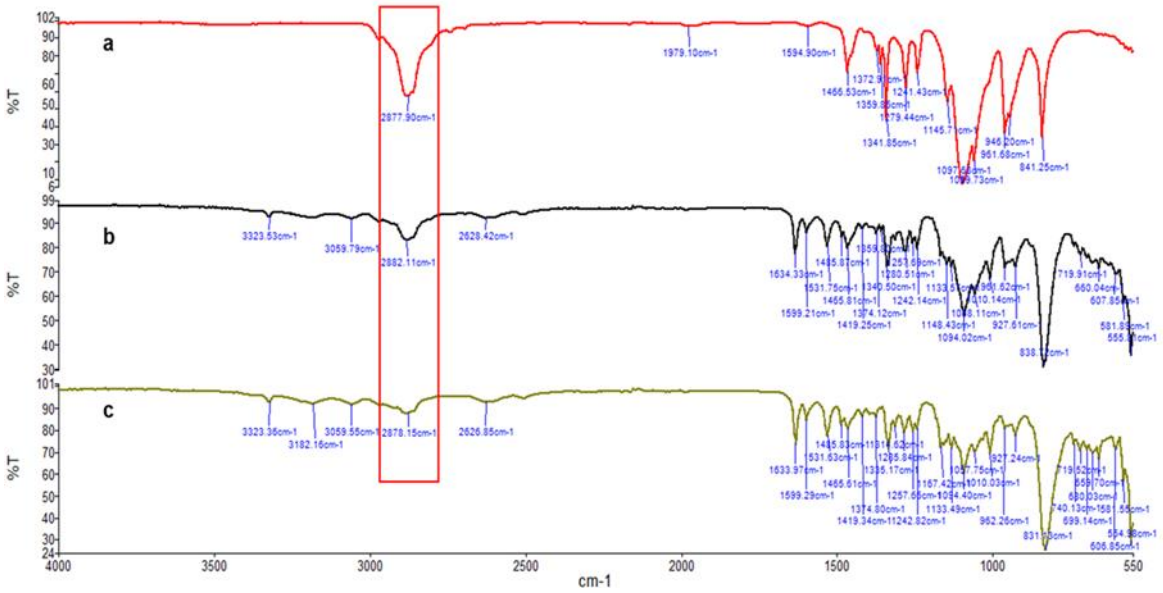

Figure 4.11: FTIR spectra of a) F127, b) TERM and c) Nanogel Composite

4.3.8.2. Assessment of structural integrity by XRD spectroscopy

To further validate the structural integrity of Nanogel Composite, XRD analysis was performed to investigate the crystallinity of the formulation. Figure 4.12 shows the XRD of the Nanogel Composite, CS, PANI and HPMC. F127 spectrum displayed a high degree of crystallinity as evidenced by the intensity of the peaks at 2θ=19.5° and 23.6°. The intensity of these peaks is, however, being reduced drastically in the spectrum of the Nanogel Composite with shifts in the 2θ position to 17.9° and 22.1°. This shift in 2θ position can be explained by the polymer-polymer interactions of the excipients due to the polymer blending. The CS, PANI and HPMC exhibit semi-crystalline features as evidenced by their broad peaks at 9.8° and 19.17° for CS, 20.2° for PANI and 18.7° for HPMC. Their semi-crystallinity may be responsible for the low intensity and shift in the 2θ value observed in the spectrum of the Nanogel Composite.

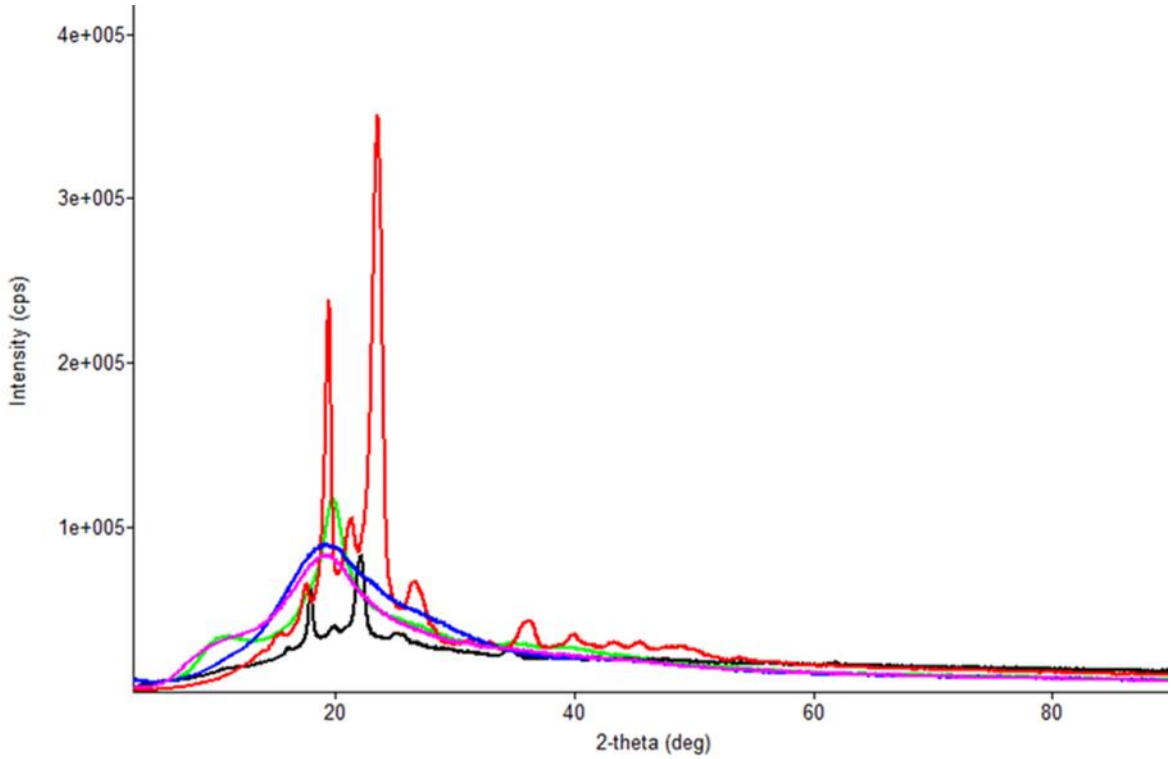

Figure 4.12: XRD spectra of the Nanogel Composite (black), F127 (red), CS (green), PANI (blue) and HPMC (purple).

4.3.9. Evaluation of the Thermal Stability of the Optimized Nanogel Composite

Thermogravimetric analysis (TGA) was performed in order to investigate the thermal stability of the formulation and to compare the thermogram obtained with that of the native polymers that constitute the Nanogel Composite. Figure 4.13 shows the thermograms of the Nanogel Composite, F127, CS, HPMC and PANI. It can be seen that the Nanogel Composite begins to decompose at temperature of 220°C, F127 at 240°C, CS at 280°C, HPMC at 320°C while PANI demonstrated significant decomposition at 380°C. The decomposition curve of the Nanogel Composite demonstrated gradual decomposition up to 40%, following complete decomposion at 390°C; whereas, F127 was seen to decompose from 240°C to 360°C. The variation in decomposition of Nanogel Composite and the native polymers, signifies the unique thermal property of the Nanogel Composite. To further explicate the thermal behavior of Nanogel Composite, DSC evaluation was carried out; Figure 4.14 shows the DSC thermogram of Nanogel Composite, F127, CS, PANI and HPMC. The melting point of the Nanogel Composite reflected at

60°C. F127 exhibits a melting point at 56°C, highlighting the slightly enhanced thermal stability of the Nanogel Composite compared to its native polymer. This observation correlates with the result obtained from the TGA analysis. The endothermic curve of F127 is sharper and steeper than that of the Nanogel Composite; this may be attributed to the retardation of heat flow due to the presence of the other polymers in the composite.

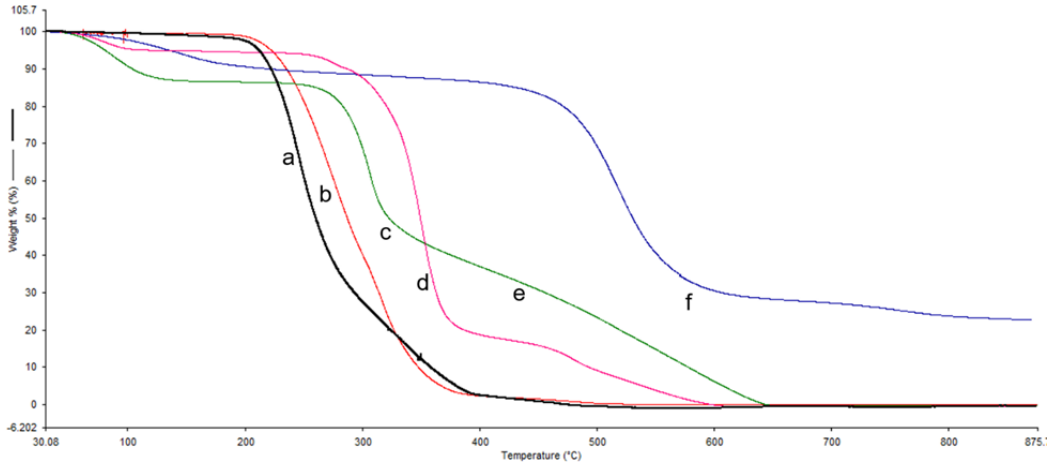

Figure 4.13: TGA thermograms of a) Nanogel Composite, b) F127, c) CS, d) HPMC and f) PANI.

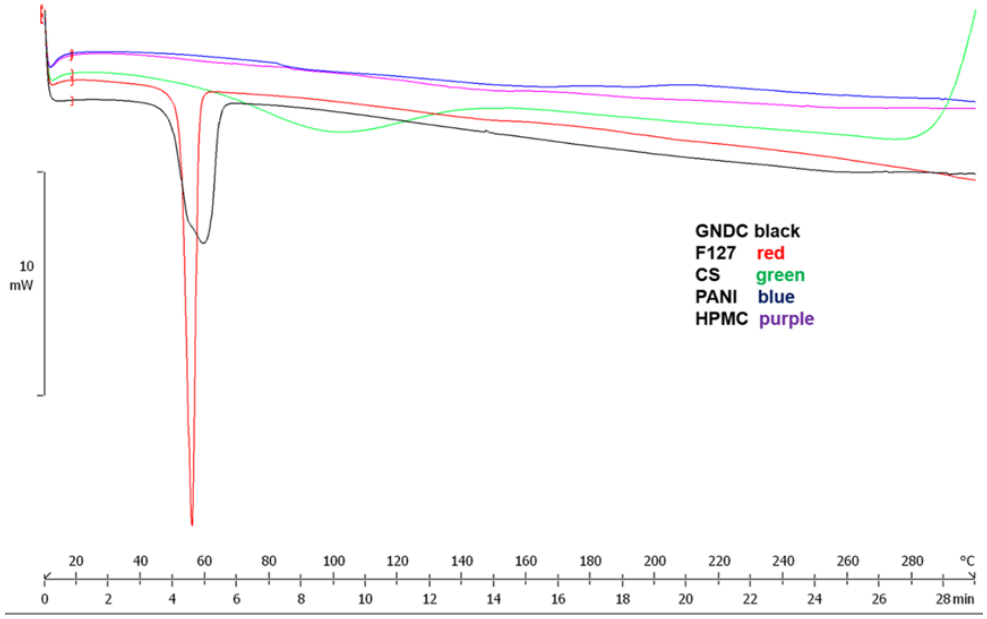

Figure 4.14: DSC thermogram of Nanogel Composite (black), F127 (red), CS (green), PANI (blue) and HPMC (purple).

4.3.10. Assessment of the Surface Morphology and Porosity of the Nanogel Composite

The samples of TERM, Nanogel Composite before and after application of electrical stimulus were lyophilized and the lyophilized samples were viewed under SEM and compared with the native polymers that constitute the Nanogel Composite in order to evaluate their surface morphology. Figure 4.15 illustrates the SEM images obtained from the native polymers. Figure 4.15a, b, c and d depict the surface morphology of F127, CS, HPMC and PANI respectively. Figure 4.16a depicts the surface morphology of the TERM while Figure 4.16b shows the cross sectional view of TERM. There are pores in the morphological structure of TERM as it is also made clear by the cross sectional view. The formation of these pores allows the incorporated nanoparticles to be embedded into the gel matrix. Figure 4.16c shows the surface morphology of the Nanogel Composite before application of electrical stimulation, the image shows little or no visible pores as it was envisaged that most of the pores may have been filled with the nanoparticles. Figure 4.16d depicts the morphology of the Nanogel Composite after application of electrical stimulation and 5 released cycles**.** Numerous pores observed was due to the release of the nanoparticles occupying the sample, upon electro-actuation,

were released creating large and numerous pores in the matrix of the residual Nanogel Composite.

This observation is supported by the results obtained from the porositometric analysis as shown in Figure 4.17. Figure 4.17 shows the isotherm linear plots of TERM, the Nanogel Composite before and after application of electrical stimulation for 6 released cycles. For the plots, a type IV isotherm with type H1 hysteresis loop was observed. Brunauer–Emmett–Teller (BET) and Barrett-Joyner-Halenda (BJH) adsorption and desorption profiles were employed to characterize the pore size by using the technique of relative adsorption of N_2 gas. This was used to evaluate the pore size, pore volume and surface area for the TERM and the Nanogel Composite before and after application of electrical stimulation in order to correlate the outcome of the porosity to the results obtained for both the SEM and electro-modulation drug release cycle.

The analysis of the porosity based on the BET and BJH characteristics observed is shown in Table 4.10. The Table shows evidence of the TERM having a pore size and volume greater than that of the Nanogel Composite before electro-actuation, however, Nanogel Composite after electro-actuation exhibited higher pore size, volume and surface area values than the TERM and Nanogel Composite before electro-actuation. These results supported the observations of the SEM analysis. This is a good attribute that makes TERM a good candidate for nanoparticle loading and subsequent release of the incorporated nanoparticles when electrical stimulation is applied.

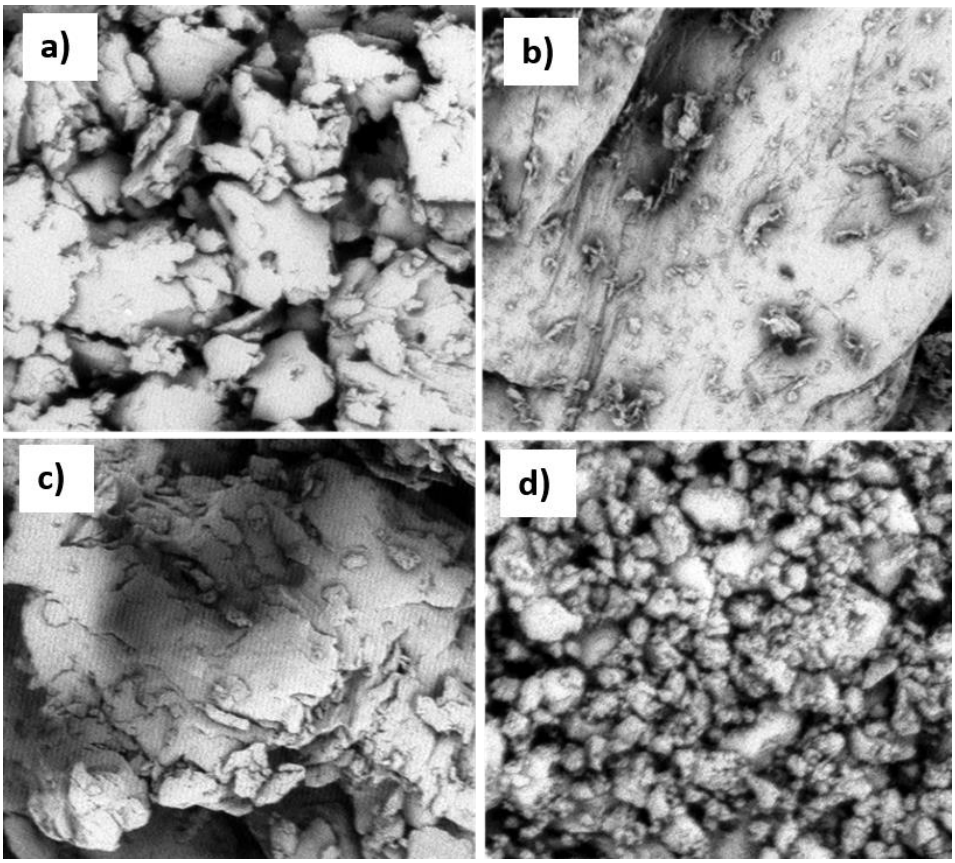

Figure 4.15: SEM images of native a) F127, b) CS, c) HPMC and d) PANI. Magnification=740x.

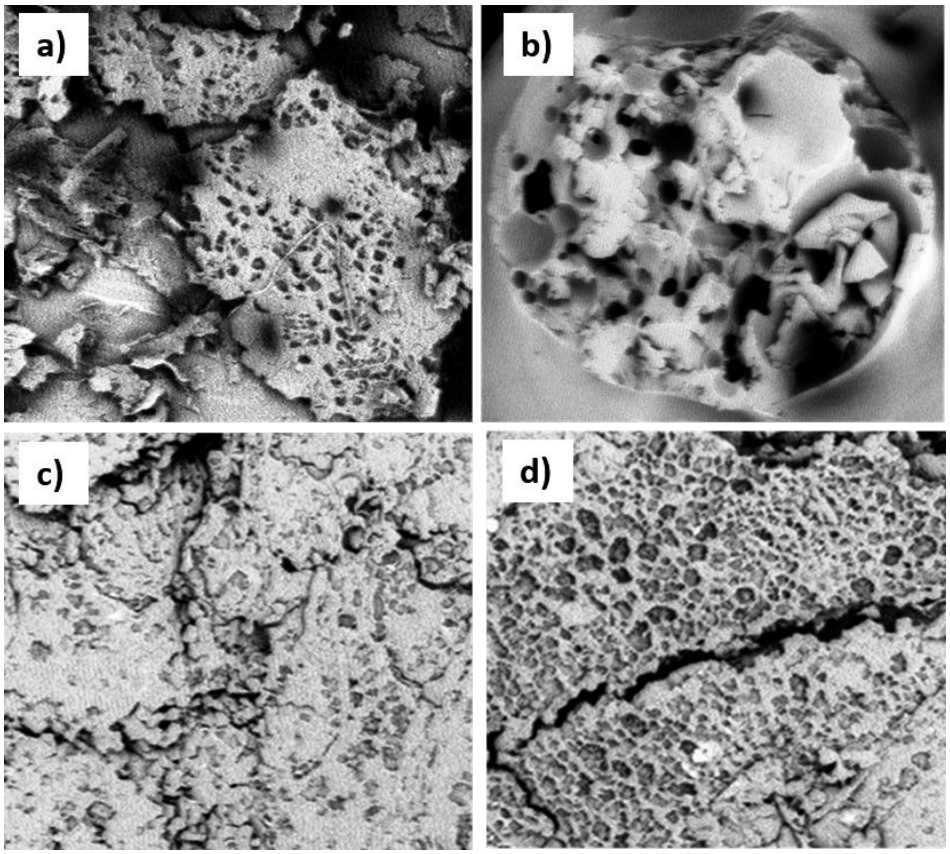

Figure 4.16: SEM images of a) TERM b) cross section view of TERM, c) Nanogel Composite before application of electrical stimulation and d) Nanogel Composite after application of electrical stimulation and 5 released cycle. Magnification=740x.

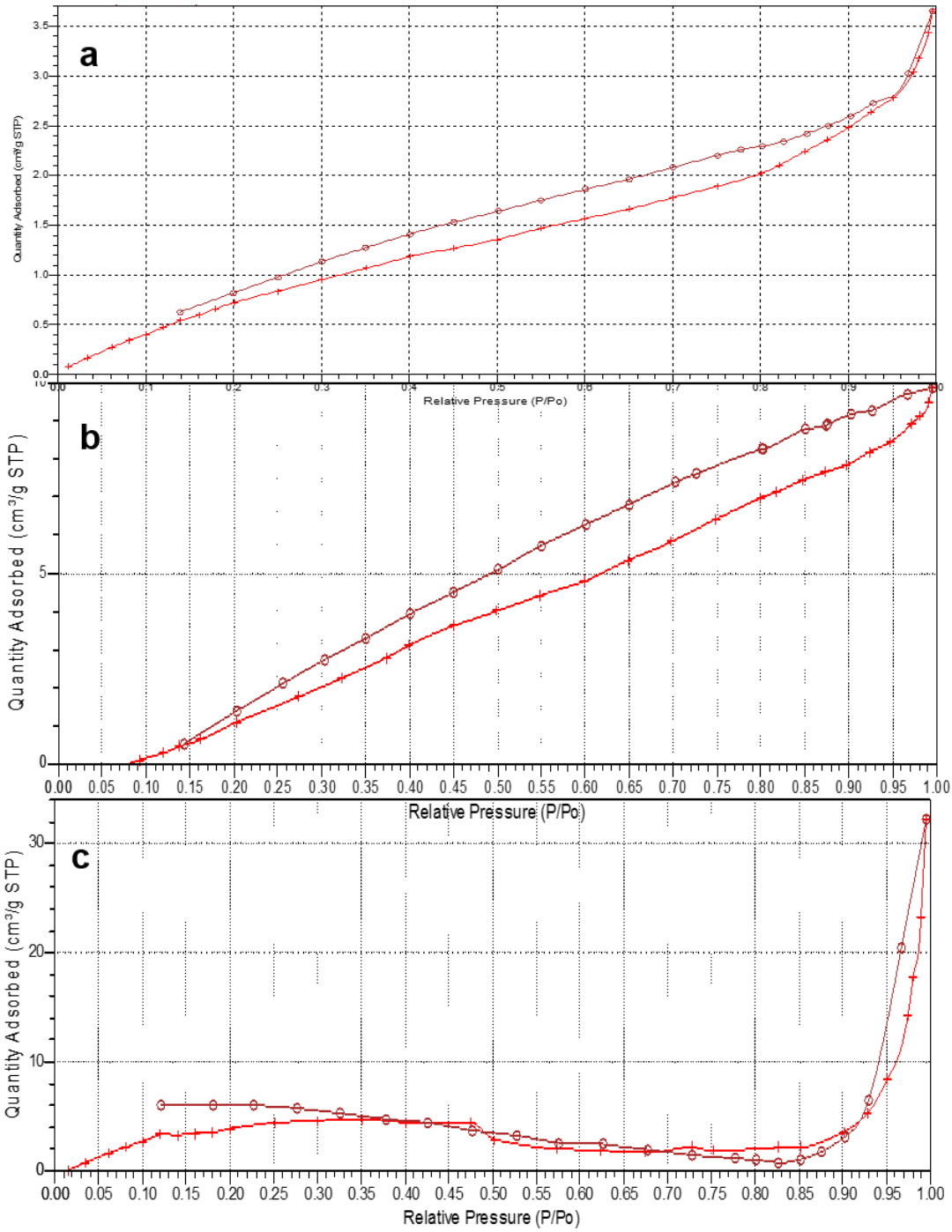

Figure 4.17: Isotherm linear plots of a) TERM, b) Nanogel Composite before application of electrical stimulation and c) Nanogel Composite after application of electrical stimulation. (N_2 adsorption in red and desorption in burgundy color).

Table 4.10: Results of the porosity analysis of the TERM and the Nanogel Composite

Parameter	TERM	Nanogel Composite before electrical stimulation	Nanogel Composite after electrical stimulation
Surface Area			
Single point surface area (m^2/g)	2.5204	1.8090	13.5209
BET Surface Area (m^2/g)	4.5176	0.8913	19.1719
t-Plot External Surface Area (m^2/g)	6.6994	1.177	26.2364
BJH Adsorption cumulative surface area of pores between 17.000 Å and 3000.000 Å diameter (m^2/g)	3.489	1.9413	14.013
BJH Desorption cumulative surface area of pores between 17.000 Å and 3000.000 Å diameter (m^2/g)	4.2747		5.5164
Pore Volume			
Single point adsorption total pore volume of pores less than 798.210 Å diameter at P/Po=0.975135248 (cm^3/g)	0.004702	0.001379	0.022153
BJH Adsorption cumulative volume of pores between 17.000 Å and 3000.000 Å diameter (cm^3/g)	0.005369	0.001394	0.051699
BJH Desorption cumulative volume of pores between 17.000 Å and 3000.000 Å diameter (cm^3/g)	0.005386	0.001342	0.049943
Pore Size			
Adsorption average pore width (4V/A by BET) (Å)	41.6362	19.2247	46.2190
BJH Adsorption average pore diameter (4V/A) (Å)	61.549	9.894	147.579
BJH Desorption average pore diameter (4V/A) (Å)	50.396	8.509	362.138

4.3.11. Assessment of Gelation Temperature of the Optimized Nanogel Composite

The gelation temperature is the temperature at which there is a transition of liquid phase to solid phase (sol-to-gel phase transition). Visual inspection showed that the magnetic stirrer stopped rotating at temperature of 28±1°C for the magnetic bar method while 29±1°C was observed for the test-tube inverted method. Figure 4.18a and Figure 4.18b illustrate the visual inspection before gelation and after gelation with the test tube inverted method.

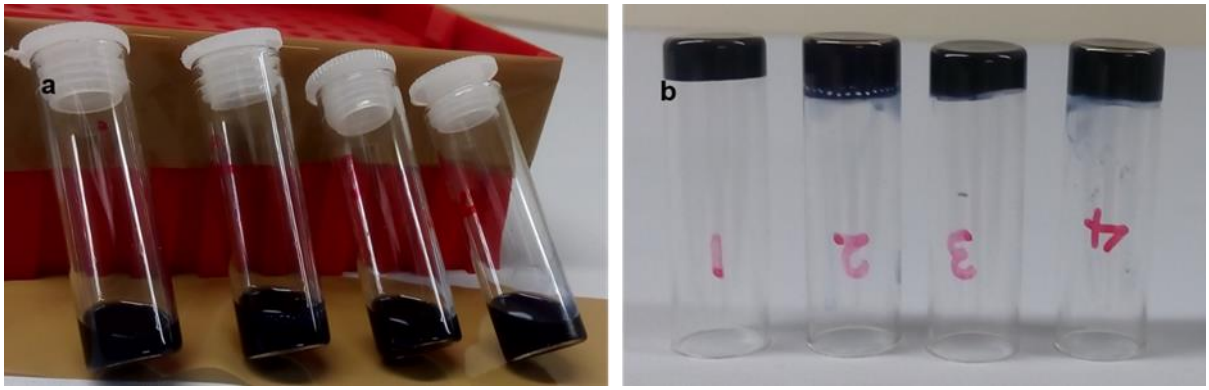

Figure 4.18: Test tube inverted method for the determination of gelation temperature, a) before gelation at room temperature and b) immediately after gelation at 29±1°C.

4.3.12. Assessment of Rheological Properties of the Nanogel Composite

The rheological behavior of polymers used in devising drug delivery systems can have a great influence on both *in vitro* and *in vivo* behaviours of the systems. Factors such as polymer characteristics, temperature, concentration pH, modification combinations, ions and additives may affect the rheological properties of the drug delivery devices. It is therefore pertinent to carry out the rheological investigation on the Nanogel Composite. The results of the rheological evaluation are depicted in Figure 4.19-Figure 4.24.

4.3.12.1. Shear viscosity

The basic viscosity of the optimized Nanogel Composite against the native polymer F127 shows that for both, the viscosity was observed to decrease as the

shear rate increased, this phenomenon is said to follow the non-Newtonian flow pattern (Ngwuluka et al., 2013). The Nanogel Composite and the F127 both displayed shear thinning characteristics classifying them as pseudoplastic however, from Figure 4.19; it is revealed that the shear viscosity of Nanogel Composite is more than that of F127 at every shear rate, observed at the same concentrations. As the shear rate increases, the viscosity decreases; the loss of viscosity may be due to the tightly bounded micelles of the polymers tendency to begin to loosen up and thereby dismantling the crosslinking of the entangled micelle arrangements of the PEO-PPO-PEO in the structure of the polymer.

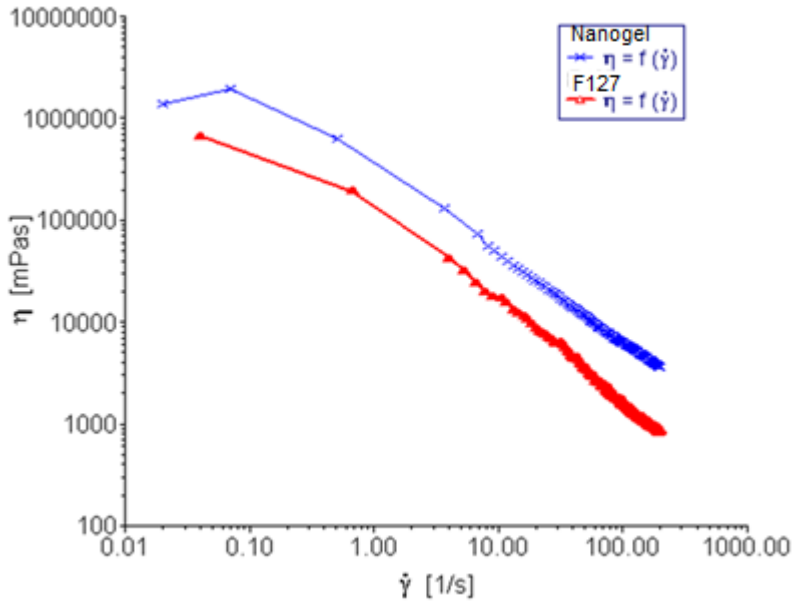

Figure 4.19: Rheogram of viscosity as a function of shear rate of Nanogel Composite and F127.

4.3.12.2. Yield stress

The yield stress of a compound is the point at which the substance begins to flow freely due to deformation of its intrinsic structure. It is apparent that below the yield stress point the compound has the characteristics of a solid substance and above this point the liquid characteristics of the substance is exhibited. It is important therefore to measure the yield stress of the optimized Nanogel Composite and F127 in order to determine the yield values which provide the insight on their yield which is a direct influence on the type and strength of the matrix formed in

comparison to the native polymer. Figure 4.20 shows the stress yield rheogram of both the Nanogel Composite and F127 which represents the plot of shear (γ) versus shear stress (τ). The apparent yield values for TERM and F127 were 113.0Pa and 31.13Pa respectively. These values were calculated employing RheoWin software PC version 3. The yield value of Nanogel Composite is clearly greater than that of F127, this may be due to the increase in internal strength of the Nanogel Composite as the addition of the excipients such as CS, PANI and especially HPMC may have increased the interaction and cohesiveness of the molecular structure of the Nanogel Composite over F127 at the experimental temperature of 34°C and thereby increasing the mechanical strength and enhancing the physicomechanical characteristics of the Nanogel Composite over F127.

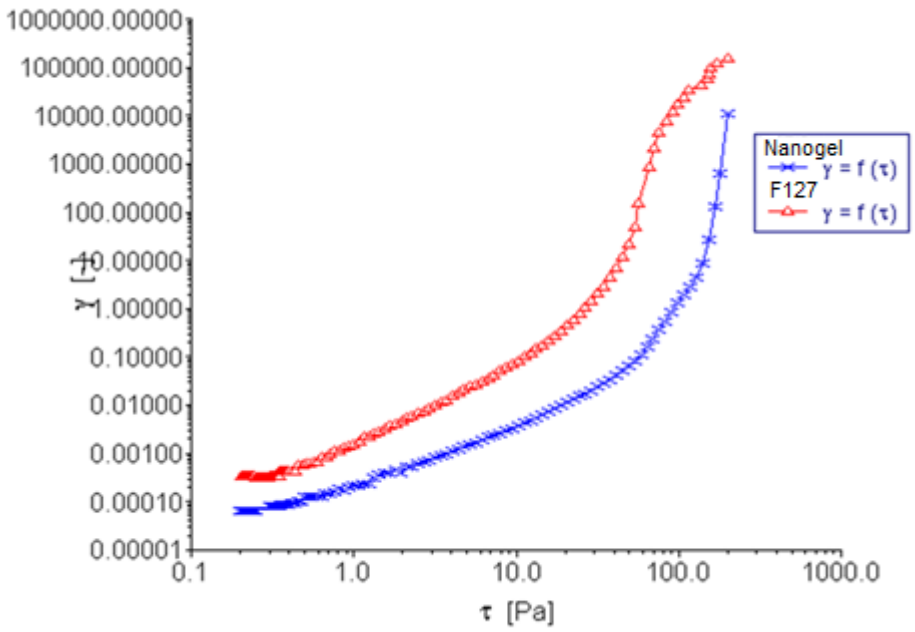

Figure 4.20: Rheogram of Yield stress of Nanogel Composite and F127.

4.3.12.3. Oscillation stress sweep

The viscoelastic region of the optimized Nanogel Composite and F127 was determined by using oscillation stress sweep method. The viscoelastic property is a measure of the mechanical strength of the polymers which have a direct consequence on the manner the polymer behaves during electrical actuation and subsequently drug release kinetics. This measurement is frequency dependent;

frequencies of 0.1, 1 and 10 Hz were used. The elastic modulus also known as storage modulus G' represents the elasticity of a material while loss modulus G″ represents the viscosity of a material. Intra and intermolecular crosslinking within a polymer network may be related to the elastic modulus properties of the polymer (Moura et al., 2007). In this case, the PEO's chains in the micellar layer enable the formation of a tighter structure in the Nanogel Composite than the F127, which is an indication of a display of a higher elastic modulus G' with a corresponding increase in its mechanical strength. Figure 4.21 shows the oscillation stress sweep of both TERM and F127 depicting the elastic modulus G' as a function of shear stress at a frequency of 0.1 Hz. The G' value observed in TERM compared to F127 may be explained by the induced transformation of intramolecular interaction further contributed by the HPMC to form the complex.

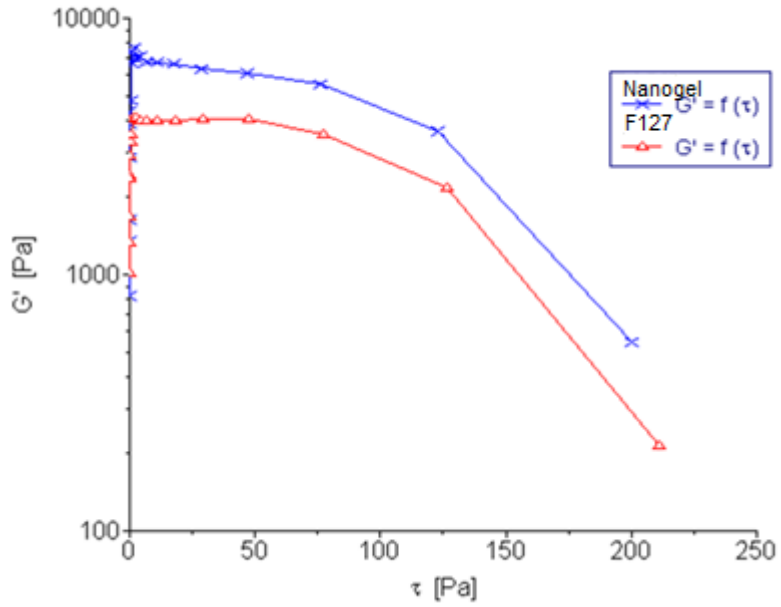

Figure 4.21: Rheogram of oscillation stress sweep of Nanogel Composite and F127.

4.3.12.4. Frequency sweep

Structural elucidation of a material in an entangled, crosslinking or three dimensional network states such as gel, paste or liquid may be determined by employing the oscillation frequency sweep rheological method. Figure 4.22 shows the rheogram of the optimized Nanogel Composite against the native polymer

F127, depicting elastic and loss moduli (G' and G") against the angular frequency (ω). Both the elastic and loss moduli were observed to increase with increase in angular frequency (ω). In case of the Nanogel Composite, the loss modulus is higher than the elastic modulus at a very short angular frequency, after which the elastic modulus became higher after the crossover point. This phenomenon was observed at very short angular frequency. The implication of this is that the Nanogel Composite behaved as an elastic material for the most part of the test and therefore exhibited a solid-like characteristic. On the contrary from Figure 4.22, F127 exhibited a higher loss modulus than the elastic modulus until the angular frequency was about 150 rad/s, when crossover took place. This indicated that for most part of the test F127 behaved like a viscous liquid and therefore exhibited liquid-like characteristics. We can therefore conclude that the Nanogel Composite possesses enhanced structural ability compared to F127 and may therefore be suitable for an electrical-pulsatile controlled drug release device.

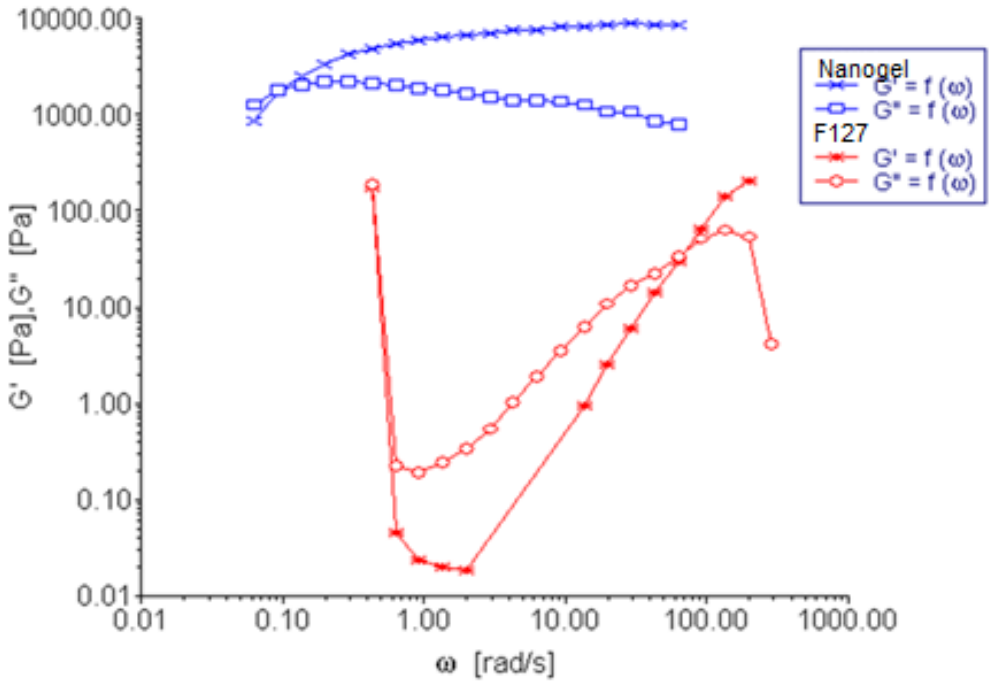

Figure 4.22: Frequency sweep rheogram of Nanogel Composite and F127.

4.3.12.5. Creep recovery test

The creep recovery test was used to further assess the elasticity of the polymers on application and removal of the applied stress. After deformation, materials may retract or spring back to its original position or shape. The results of this test may help in evaluating the subsequent behavior of materials on release of stress. The ability of the material to spring back after the removal of the stress is an indication of the elasticity of the material. Figure 4.23 shows the creep recovery test of both the optimized Nanogel Composite and F127, where J (1/Pa) is plotted against time (s). Both the Nanogel Composite and F127 showed elastic deformation and possess the ability to recover when the stress was removed. However, the recovery time for the Nanogel Composite is shorter than that of F127 on application of the same load and from the graph, it can be deduced that the Nanogel Composite has more ability to recoil and restore back to its original position than F127. This also supports the higher elasticity of the Nanogel Composite over the F127.

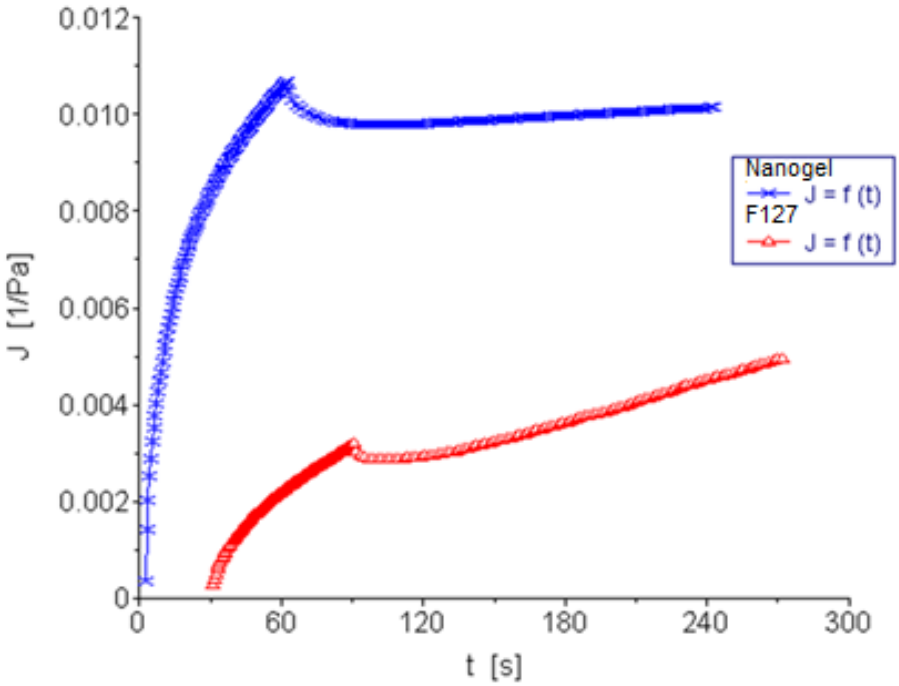

Figure 4.23: Rheogram of creep recovery test for the Nanogel Composite and F127.

4.3.12.6. Temperature ramp analysis

The temperature ramp is used to evaluate the change in the properties of a material on temperature variance. This method can be used to determine the gelation temperature of materials by observing the temperature at which there is a drastic change or movement in the sol-gel properties of the materials. Figure 4.24 shows the temperature ramp rheograms of the optimized Nanogel Composite and F127 where viscosity is plotted against temperature. The experiment was carried out at a temperature range of 20 to 40±1ºC. The Nanogel Composite is seen to have a gelling temperature of 27.5±0.5ºC while F127 has a gelling temperature of 21±0.5ºC. The gelling temperature was graphically determined as the temperature at which the curve of the apparent viscosity against temperature starts to plateau. Furthermore, the gelling temperature can equally be determined by plotting G' and G" against temperature. The temperature at the crossover point is taken as the gelling temperature as illustrated in Figure 4.25. the crossover point where the curve of G' crosses the curve of G" is that point where there is a significant phase transition from sol-to-gel state.

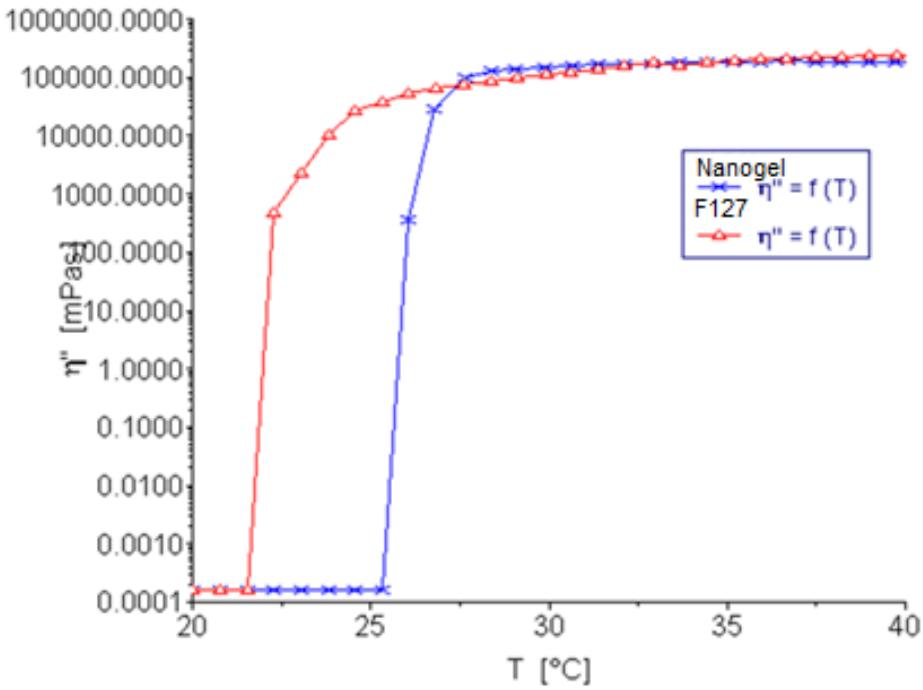

Figure 4.24: Rheogram of temperature ramp of Nanogel Composite and F127.

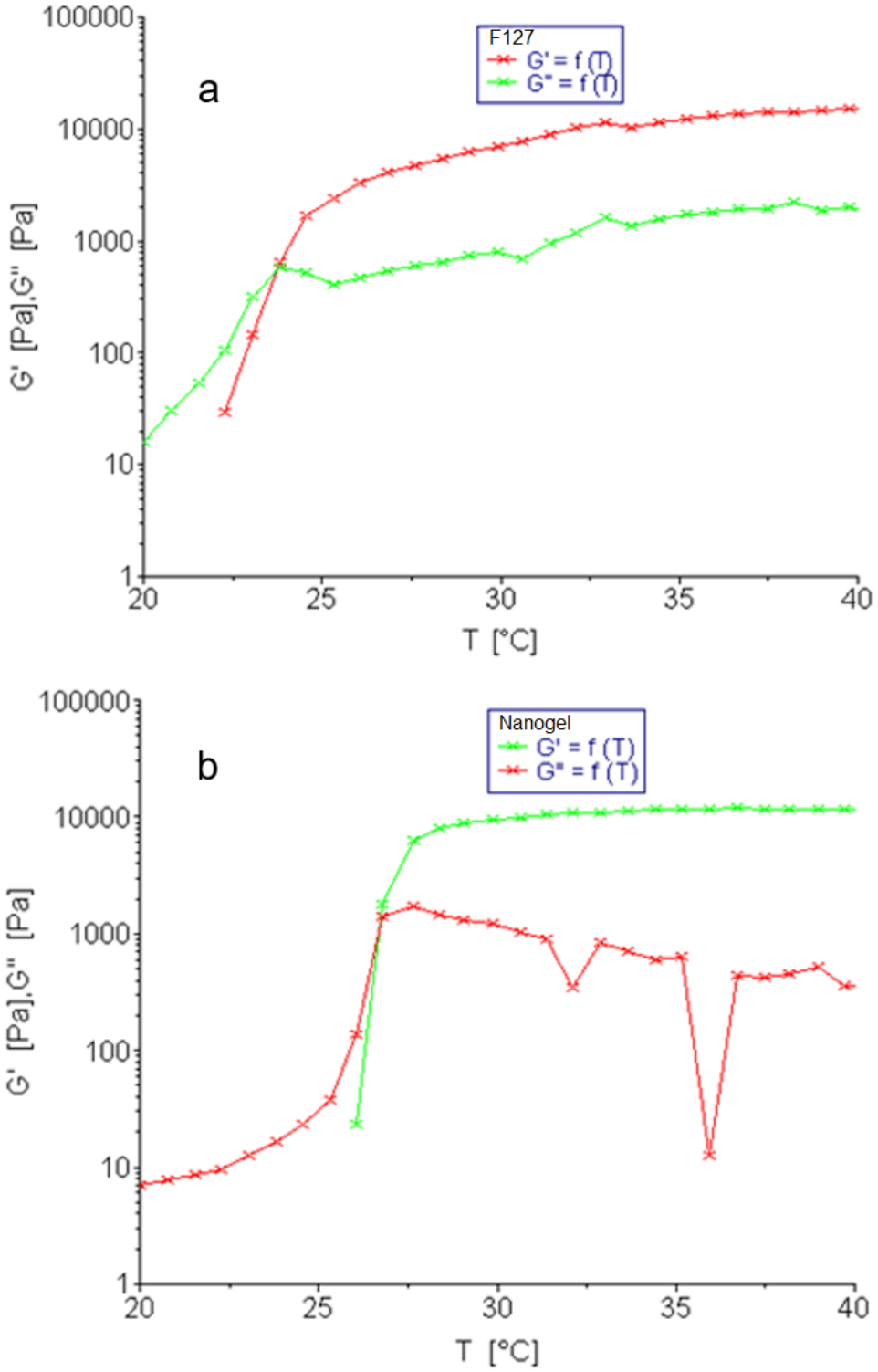

Figure 4.25: Rheogram showing G'G" plot against temperature for a) F127 and b) Nanogel Composite

4.3.13. Assessment of the Electro-active Properties of the Nanogel Composite Employing Cyclic Voltammetric Analysis

In order to assess an electro-responsive formulation, it is important to determine if the formulation has an element of redox properties. Cyclic voltammetry (CV) is used to assess the oxidation-reduction reactions of the formulation; this enables analysis of the movement and exchange of ions in the media. The results of the measurements for the Nanogel Composite are illustrated in Figure 4.26 where Figure 4.26a depicts the voltammogram of PANI and Figure 4.26b the voltammogram of Nanogel Composite. It can be observed from the two voltammograms that there is similarity between them. However, the important parameter to look for in a cyclic voltammetric analysis is the peak potentials, the PANI exhibits two oxidation peak potentials at 1.10V and 1.45V while it exhibits 3 reduction peak potentials at 0.5V, 0.7V and -0.83V. For the Nanogel Composite, the peaks observed are similar with a slight shift in oxidation and reduction peaks to 1.42V, 0.85V; reduction peaks are 0.5, 0.7, and -0.83V. The significant difference was actually in the output current generated. The output current for PANI Voltammogram is 1.5mA and 0.6mA for oxidation and reduction, respectively. While that of Nanogel Composite is 0.6mA and -0.4mA for oxidation and reduction respectively.

PANI is known to exist in three forms, the emeraldine, pernigrinline and leucoemeraldine (Weerakoon et al., 2012). Figure 4.27 shows the three forms of PANI and their transition and reversible states. The first peak may be corresponded to the inter conversion between pernigraniline and emeraldine, the second peak may be associated with formation of benzoquinone and hydroquinone which may be due to the breakdown of the polymer chain during electrolysis (Kannusamy and Sivalingam, 2013) while the third reduction peak observed may be due to the PANI emeraldine salt being electronically reduced to PANI leucoemeraldine base. The whole redox activity is, however, reversible in both PANI and Nanogel Composite.

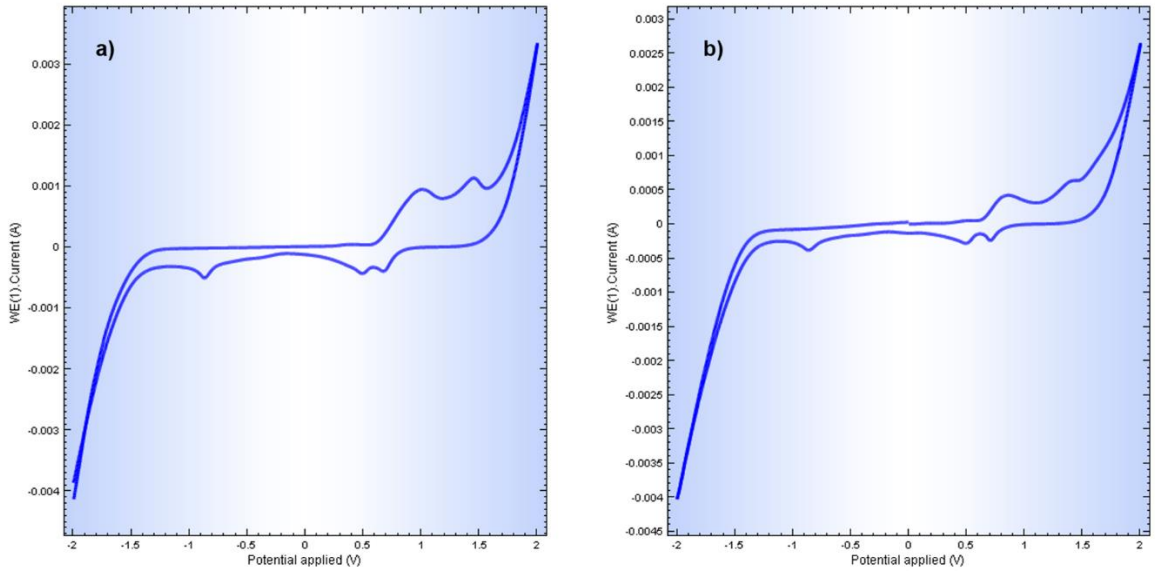

Figure 4.26: Voltammogram of a) PANI and b) Nanogel Composite

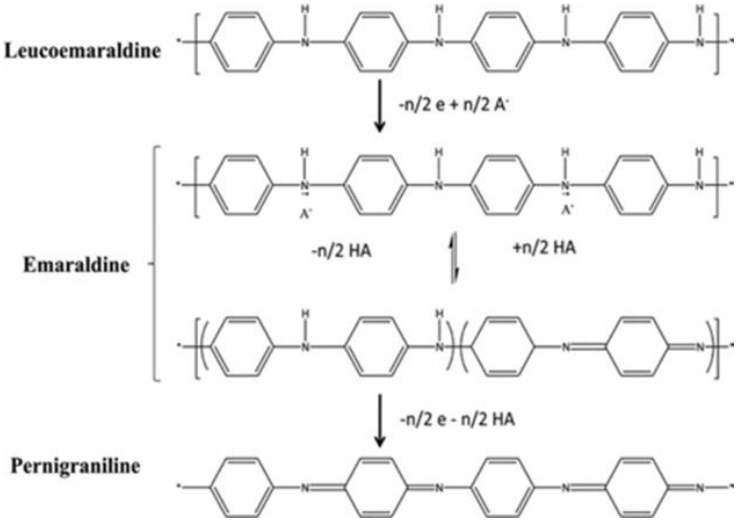

Figure 4.27: The three forms of PANI showing their transition and reversible states

4.3.14. Assessment of the *In Vitro* Drug Release Analysis of the Optimized Nanogel Composite on Application of Electrical Stimulation

It is necessary to evaluate the release capability of Nanogel Composite on application of electrical stimulation. Preliminary studies revealed that the Nanogel Composite did not release significant quantity of BCNU-NCP if electrical stimulation was not applied, but upon application of electrical stimulation

substantial drug is released as demonstrated in Figure 4.28. Various studies have shown that mucoadhesive polymers retard drug-release in a gel formulation (Ravi et al., 2015; Zaki et al., 2007). The addition of CS therefore slows down the drug release. Furthermore, the addition of HPMC has the ability to retard the drug release substantially when blended with F127 (Desai and Blanchard, 1998), this is a major and important reason for including this polymer into the formulation as the release of drug without electrical stimulation is not desired. The combination of the retardation ability of both CS and HPMC is responsible for the insignificant release of drugs without the application of electrical stimulation. The *in vitro* release of BCNU-NCP from the optimized formulation is illustrated in Figure 4.28. The formulation was optimized to release 10% of BCNU-NCP loaded in the Nanogel Composite on electrical stimulation, applying 5V of potential. The results obtained from the release studies showed that the average release percentage of BCNU-NCP upon application of 5V electrical stimulation for 1 minute per cycle is 10.24%. This value is very close to the desired percentage release of 10% for the optimized formulation.

BCNU concentration from the released BCNU-NCP was further analysed, the release profile obtained was similar to that of the BCNU-NCP release profile. Figure 4.29 shows the release profile of the BCNU from the NCP over 6 hours.

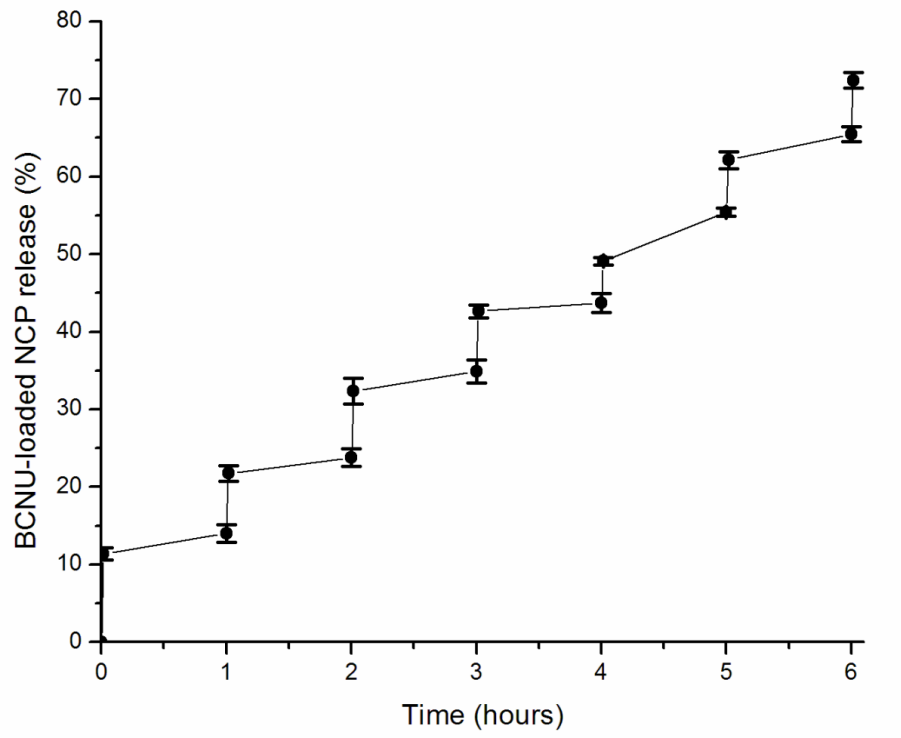

Figure 4.28: BCNU-NCP release profile in simulated nasal fluid (pH 6.0).

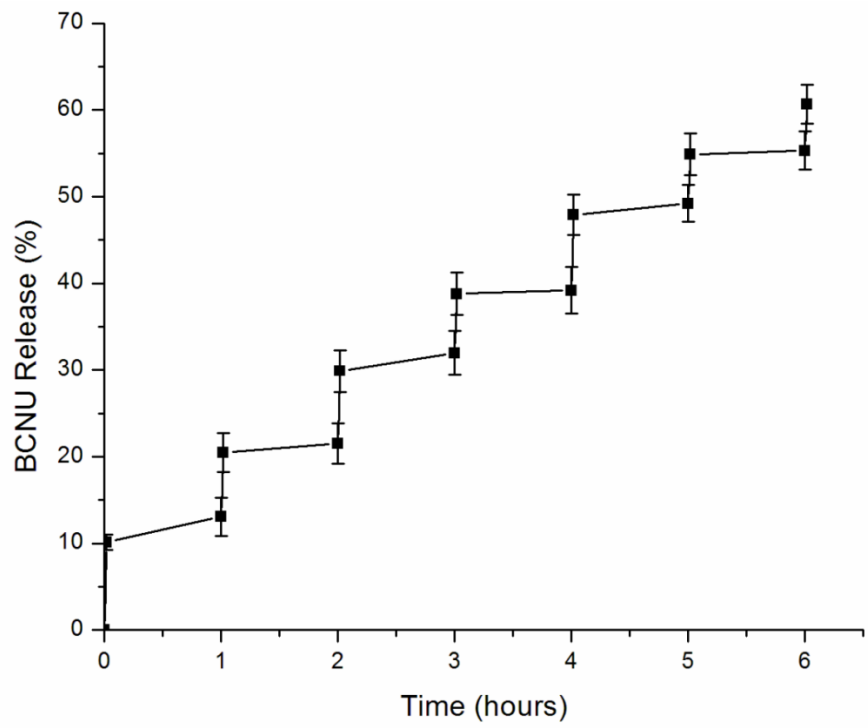

Figure 4.29: *In vitro* BCNU release profile from the BCNU-NCP for a period of 6 hours

4.4. CONCLUDING REMARKS

A novel biocompatible and biodegradable thermosensitve electro-conductive mucoadhesive gel was prepared by blending Pluronic F127, CS, HPMC and PANI. BCNU-loaded Nano-co-Plex was incorporated into the polymer matrix to form a Nanogel Composite. The Nanogel Composite was optimized using the Box–Behnken experimental design. The lower and upper limits was used to generated 15 Nanogel Composite formulations in which conductivity, mucoadhesion and electro-actuation drug release were the responses undertaken to generate the optimal formulation. This formulation was characterized using FTIR, XRD, TGA, DSC, SEM, rheological, cyclic voltammetric and porositometric analyses to assess the physicochemical properties of the formulation. A thermally-stable gel with suitable rheological and mucoadhesion properties was formulated. Results revealed a Nanogel Composite that possesses porous matrix and was found to have the ability to undergo redox reaction which allows response to ES. The formulation was prepared to form an *in situ* gel at a temperature of 27.5±0.5°C. The release profile of the formulation when ES was applied demonstrated a desired 10.28% release of nanoparticles per release cycle. This formulation may therefore be a suitable candidate for use as an intranasal drug delivery system that can be modulated to deliver therapeutic agents to the brain via electro-actuation in an “on-off” drug release kinetics by means of an external ES for a controlled nose-to-brain delivery.

4.5. REFERENCES

Adeleke, O.A., Choonara, Y.E., Toit, L.C. du, Kumar, P., Pillay, V., 2015. *In Vitro*, *Ex Vivo* and In Silico Mechanistic Elucidation of the Performance of an Optimized Porosity-Controlled Multi-Elemental Transbuccal System. Pharm. Res. 32, 2384–2409.

Akash, M.S.H., Rehman, K., Chen, S., 2014. Pluronic F127-Based Thermosensitive Gels for Delivery of Therapeutic Proteins and Peptides. Polym. Rev. 54, 573–597.

Baltzley, S., Mohammad, A., Malkawi, A.H., Al-Ghananeem, A.M., 2014. Intranasal Drug Delivery of Olanzapine-Loaded Chitosan Nanoparticles. AAPS PharmSciTech 15, 1598–1602.

Chaturvedi, M., Kumar, M., Pathak, K., 2011. A review on mucoadhesive polymer used in nasal drug delivery system. J. Adv. Pharm. Technol. Res. 2, 215-222.

Cheng, J., Zhao, B., Zheng, S., Yang, J., Zhang, D., Cao, M., 2015. Enhanced microwave absorption performance of polyaniline-coated CNT hybrids by plasma-induced graft polymerization. Appl. Phys. A 119, 379–386.

Fahmy, R.H., 2012. Statistical Approach for Assessing the Influence of Calcium Silicate and HPMC on the Formulation of Novel Alfuzosin Hydrochloride Mucoadhesive-Floating Beads as Gastroretentive Drug Delivery Systems. AAPS PharmSciTech 13, 990–1004.

García-Gallegos, J.C., Martín-Gullón, I., Conesa, J.A., Vega-Cantú, Y.I., Rodríguez-Macías, F.J., 2016. The effect of carbon nanofillers on the performance of electromechanical polyaniline-based composite actuators. Nanotechnology 27, 015501.

Imae, I., Mashima, T., Sagawa, H., Komaguchi, K., Ooyama, Y., Harima, Y., 2014. *In situ* conductivity measurements of polythiophene partially containing 3,4-ethylenedioxythiophene and 3-hexylthiophene. J. Solid State Electrochem. 19, 71–76.

Kumar, N.A., Choi, H.-J., Shin, Y.R., Chang, D.W., Dai, L., Baek, J.-B., 2012. Polyaniline-Grafted Reduced Graphene Oxide for Efficient Electrochemical Supercapacitors. ACS Nano 6, 1715–1723.

Li, G.-C., Li, G.-R., Ye, S.-H., Gao, X.-P., 2012. A Polyaniline-Coated Sulfur/Carbon Composite with an Enhanced High-Rate Capability as a Cathode Material for Lithium/Sulfur Batteries. Adv. Energy Mater. 2, 1238–1245.

Özcan, H.M., Aydin, T., 2016. A new PANI biosensor based on catalase for cyanide determination. Artif. Cells Nanomedicine Biotechnol. 44, 664–671.

Patil, S.B., Sawant, K.K., 2011. Chitosan microspheres as a delivery system for nasal insufflation. Colloids Surf. B Biointerfaces 84, 384–389.

Saladini, B., Bigucci, F., Cerchiara, T., Gallucci, M.C., Luppi, B., 2012. Microparticles based on chitosan/pectin polyelectrolyte complexes for nasal delivery of tacrine hydrochloride. Drug Deliv. Transl. Res. 3, 33–41.

Shi, Y., Pan, L., Liu, B., Wang, Y., Cui, Y., Bao, Z., Yu, G., 2014. Nanostructured conductive polypyrrole hydrogels as high-performance, flexible supercapacitor electrodes. J. Mater. Chem. A 2, 6086–6091.

Shokry, H., Vanamo, U., Wiltschka, O., Niinimäki, J., Lerche, M., Levon, K., Linden, M., Sahlgren, C., 2015. Mesoporous silica particle-PLA–PANI hybrid scaffolds for cell-directed intracellular drug delivery and tissue vascularization. Nanoscale 7, 14434–14443.

Soni, S.N., Bajpai, J., Bajpai, A.K., 2012. Investigation of electroactive behaviour of polyaniline containing polyelectrolyte nanocomposite membranes. Nanosci. Methods 1, 164–182.

Stewart, E., Kobayashi, N.R., Higgins, M.J., Quigley, A.F., Jamali, S., Moulton, S.E., Kapsa, R.M.I., Wallace, G.G., Crook, J.M., 2014. Electrical Stimulation Using Conductive Polymer Polypyrrole Promotes Differentiation of Human Neural Stem Cells: A Biocompatible Platform for Translational Neural Tissue Engineering. Tissue Eng. Part C Methods 21, 385–393.

Trchová, M., Stejskal, J., Prokeš, J., 1999. Infrared spectroscopic study of solid-state protonation and oxidation of polyaniline. Synth. Met., International Conference on Science and Technology of Synthetic 101, 840–841.

Tsai, T.-S., Pillay, V., Choonara, Y.E., Du Toit, L.C., Modi, G., Naidoo, D., Kumar, P., 2011. A Polyvinyl Alcohol-Polyaniline Based Electro-Conductive Hydrogel for Controlled Stimuli-Actuable Release of Indomethacin. Polymers 3, 150–172.

Wang, L., Huang, Y., Li, C., Chen, J., Sun, X., 2015. Hierarchical composites of polyaniline nanorod arrays covalently-grafted on the surfaces of graphene@Fe3O4@C with high microwave absorption performance. Compos. Sci. Technol. 108, 1–8.

Wu, J., Wei, W., Wang, L.-Y., Su, Z.-G., Ma, G.-H., 2007. A thermosensitive hydrogel based on quaternized chitosan and poly(ethylene glycol) for nasal drug delivery system. Biomaterials 28, 2220–2232.

Xiao, L., Cao, Y., Xiao, J., Schwenzer, B., Engelhard, M.H., Saraf, L.V., Nie, Z., Exarhos, G.J., Liu, J., 2012. A Soft Approach to Encapsulate Sulfur: Polyaniline Nanotubes for Lithium-Sulfur Batteries with Long Cycle Life. Adv. Mater. 24, 1176–1181.

CHAPTER 5

EX VIVO EVALUATION OF THE *IN SITU* NANOGEL COMPOSITE

5.1. INTRODUCTION

Several therapeutic agents introduced into the nasal mucosa migrate into the systemic circulation rather than traversing directly to the brain (Fortuna et al., 2014; Lewis et al., 2012). This is due to the blood rich vessels in the nasal mucosa causing the therapeutic agents to face the challenge of the BBB (Tabatabaei et al., 2015). There is evidence of nose-to-brain drug delivery most of which has been reviewed in Chapter 2 of this thesis. However, the probability of the therapeutic agents administered via the intranasal route reaching the systemic circulation is higher than the drug getting to the olfactory bulb for nose-to-brain delivery. This is due to slow movement of the therapeutic agents as the drug migrates and transverses across the nasal epithelial mucosa to the olfactory region (Grassin-Delyle et al., 2012). Those that get to the brain do so by migrating through the nasal epithelial tissue to the olfactory region and subsequently to the CSF and brain.

The mechanism of transport depends solely on therapeutic agent's physicochemical characteristics, passive diffusion and gravity (Lin et al., 2005). This poses a major challenge to nose-to-brain drug delivery as bioavailability of drug is substantially reduced. However, an effective nose-to-brain formulation should be able to migrate to the olfactory region as quickly as possible in order to increase bioavailability of drug in the brain as any delay causes the therapeutic agents to be absorbed through the systemic pathway and may significantly reduce bioavailability due to drugs recirculating back to face the challenges of the BBB. An enhanced transportation of the therapeutic agents to the brain through the olfactory pathway will be an advantage.

BCNU-NCP are magnetic nanoparticles which are paramagnetic and therefore respond to Magnetic Field (MF). It is therefore important to evaluate the

permeability of BCNU-NCP through the nasal tissues with or without MF to observe the effect of a MF on the permeation and transportation of the nanoparticles across the nasal epithelial tissue. This chapter is based on the *ex vivo* evaluation of the Nanogel Composite by studying the mechanism by which the Nanogel Composite releases therapeutic agents on application of Electric Stimulation (ES) and how the released BCNU-NCP permeate through the nasal tissues of rabbit. Furthermore, the effect of a MF on the permeation was examined to compare the permeability of BCNU-NCP in the presence and absence of external MF. The nasal tissue of rabbit was employed for this assessment. Several researchers have used the nasal tissue of rabbits to evaluate the permeability of active compounds across the nasal epithelia membrane (Ohtake et al., 2003; Maitani et al., 1992).

5.2. MATERIALS AND METHODS

5.2.1. Materials

Pluronic® F127 (Mw=12,600g/mol), medium molecular weight chitosan (CS) (Mw=400,000g/mol), polyaniline (PANI) (Mw=20,000g/mol), sodium hydroxide, hydroxylpropyl methylcellulose (HPMC), acetic acid, these chemicals were purchased from Sigma-Aldrich, (Steinhelm, Germany). Double deionized water was obtained from a Milli-Q water purification system (Milli-Q, Millipore, Billerica, MA, U.S.). All other reagents used were of analytical grade and were employed as purchased.

5.2.2. Preparation of the Nanogel Composite

The preparation of the Nanogel Composite was carried out as described in Chapter 4, Sections 4.2.2, 4.2.3, and 4.2.4.

5.2.3. *Ex Vivo* Evaluation of the Nanogel Composite

5.2.3.1. Preparation of the rabbit nasal tissue for permeation studies

These studies were performed according to method adapted from Kubo et al. (1994). Ringer solution was prepared by mixing 154mM of sodium chloride,

5.64mM of potassium chloride, 2.16mM of calcium chloride, 11.10mM of dextrose and 2.38mM of sodium bicarbonate in 1000mL of deionized water and the pH adjusted to 6.0. The nasal mucosa tissues used in these experiments were obtained from a New Zealand White rabbit. Prior approval was obtained from the University of the Witwatersrand Animal Ethics Committee. The rabbit was euthanized with an appropriate dose of sodium pentobarbitone. The nasal septum was carefully removed from the bone block and immersed and adequately rinsed in an ice-cold Ringer's solution previously prepared. Two pieces of the nasal mucosa were stripped with care using forceps and surgical scissors from the nasal mucosa ready for the permeation studies.

5.2.4. *Ex Vivo* Evaluation of Mucoadhesive Strength of the Nanogel Composite

A Texture Analyzer (TA) (TA.XT plus, Stable Microsystems, Surrey, UK) was employed to determine the mucoadhesive strength of the formulations. This was undertaken by measuring the force required to detach nasal mucosa membrane from each of the formulations. Freshly excised rabbit nasal membrane was attached to the upper probe of the instrument; a 1mL of Nanogel Composite was placed below the platform inside a temperature controlled compartment. The temperature was regulated to 34±1°C. The upper probe containing the membrane was then lowered at a speed of 10mm/min to touch the surface of the gel. A force of 0.1N was applied for 2 minutes to ascertain intimate contact with the gel. The exposed nasal mucosa membrane surface area was 0.785cm^2.

5.2.5. Determination of the Permeation Capability of the BCNU-Loaded Nano-co-Plex across Rabbit Nasal Tissue

One of the important aspects of this work is to investigate how rapidly the nanoparticles released from the gel migrate from the nasal mucosa through the nasal epithelial tissue, to the olfactory region for subsequent delivery to the brain. Thus *ex vivo* permeation studies would give a better assessment of the permeation of the formulation through nasal tissue. Furthermore, the use of electric and magnetic fields would be assessed to see the effect of these parameters on the release and subsequent transportation of drug across the nasal

epithelial tissue. The permeation studies were performed by employing the experimental setup illustrated in Figure 5.1. The diffusion cells used were a side-by-side type. This apparatus consists of donor and receptor half-cells of 12mL volume capacity. The choice of this apparatus was due to the use of a bar magnet that was positioned at the receiver compartment in order to evaluate the effect of MF on the permeation of the nanoparticles. The apparatus was equipped with a stirrer on each compartment and the system was connected to a thermostat controlled water jacket maintaining a temperature of 34±1°C. The apparatus was then mounted on an agitator to aid mixing. The tissue thickness was measured using a micrometer; the tissue was then mounted on a glass disc with round hole of 5mm diameter with the mucosal surface facing the donor compartment and the serosal side facing the receptor compartment. This was then placed in between the donor and the receptor compartments of the diffusion cell apparatus which contained pre-warmed PBS (pH 6) at 34±1°C to mimic nasal mucosa physiological conditions. The nasal mucosa was equilibrated in the PBS solution for 1 hour to achieve electrophysiological steady state.

The optimized formulation containing (5mg/mL) drug concentration was transferred onto the mounted nasal tissue. The whole system was maintained at 34±1°C. The formulation solidified immediately after being transferred into the donor compartment containing the nasal tissue. ES of PD (5V) was applied at time points of 0.5, 1, 2, 4, 6, 8, 16, 20 and 24 hours, applied using a potentiostat/galvanostat (PGSTAT302N, Autolab, Utrecht, Netherlands). A permanent magnet of 0.4 Tesla was placed at 1cm from the receiver compartment after each electrical application. Aliquot samples (1mL) were withdrawn and replaced with the same quantity of fresh pre-warmed PBS. Sampling was carried out prior and after each ES. The amount of BCNU-NCP permeated was quantified by determining the amount of iron contents in the withdrawn solution as iron formed the core of the BCNU-NCP. All experiments were repeated 3 times. The whole procedure was repeated with ES but no application of the permanent magnet and without both electrical and magnetic stimulation. This was done in order to evaluate the effect of ES as well as MF on the permeation characteristics

of the formulation. Table 5.1 summarizes the assessment procedures that were employed for the permeation studies.

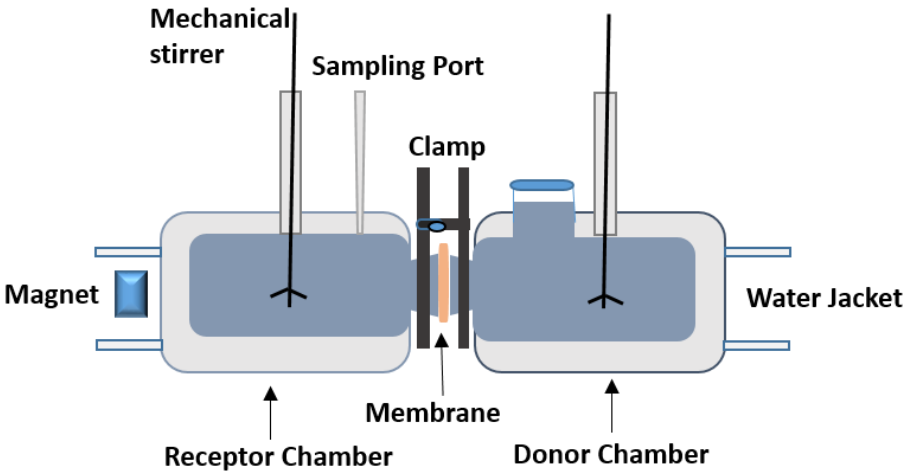

Figure 5.1: Schematic diagram of side-by-side diffusion cell.

Table 5.1: Assessment procedures used in the permeation studies

Test	Formulation	Application of Electro-stimulation	Application of Magnetic Field
1	Nanogel Composite	None	No
2	Nanogel Composite	Yes	No
3	Nanogel Composite	Yes	Yes

5.2.5.1. Quantitative analysis of the BCNU-loaded Nano-co-Plex permeated through the rabbit nasal epithelial tissue from the Nanogel Composite

BCNU-loaded Nano-co-Plex permeated through the nasal epithelia tissue of rabbit was determined by following the procedure described in Chapter 4, Section 4.2.10.1.

5.2.5.2. Evaluation of BCNU-loaded Nano-co-Plex permeability

The BCNU-NCP permeability was calculated by ascertaining the cumulative diffusion of BCNU-NCP per unit area of the nasal tissue. The steady state flux (Js) was calculated from the slope of the linear section of the line obtained after plotting the amount of drug permeating nasal epithelium per unit area (mg/cm^2)

against time (h) as shown in Equation 5.1 and the permeation coefficient P calculated using Equation 5.2.

$$Js = \frac{Qs}{AT}$$ **Equation 5.1**

$$P = \frac{Js}{Cd}$$ **Equation 5.2**

Where Js is the flux (mg/cm^2/h), Qs is the amount of drug (mg), A is the area (cm^2), T is the time interval (h), P permeability coefficient (cm/h) and Cd is the initial concentration (mg/mL) of the sample in the donor compartment.

Enhancement ratios (ER) of BCNU-NCP permeation through rabbit nasal mucosa were calculated based on P values, according to Equation **5.3**

$$ER = \frac{P(Nanogel\ Composite\ with\ ES\ and\ MF)}{P(Nanogel\ Composite\ without\ ES\ and\ MF)}$$ **Equation 5.3**

Where P(Nanogel Composite with ES and MF) is the permeability coefficient of BCNU-NCP when there is application of electric and magnetic fields, and P(Nanogel Composite without ES and MF) is the permeability coefficient when there is no application of electric and magnetic fields.

5.2.5.3. Evaluation of the effect of magnetic field on cytotoxicity of the BCNU-loaded Nano-co-Plex on human glioblastoma A170 cells

The effect of MF on cytotoxicity of BCNU-NCP was evaluated by employing the human glioblastoma cell line (A170) and following the method used in Chapter 3, Section 3.2.13.1 with slight modification. Briefly, two sets of seven plates (A-G) and (H-N) were employed in this experiment, each plate contained similar contents and represented incubation times of 0, 4, 8, 16, 24, 48 and 72 hours, respectively for the two sets. The well in each first set of plates was divided into 4 groups (1-4) which were Control, NCP, BCNU-NCP and BCNU group respectively. The second set of seven plates contains only 1 group (group 5), which is group BCNU-NCP (with the application of MF). Predetermined quantities of BCNU-NCP and conventional BCNU were added to each well as depicted in Table 5.2. The plates

were incubated for the time of incubation they represented. The second set of plates (H-N) was fixed with 0.1 Tesla neo disc magnets (Magnetech, Capetown, South Africa) positioned under the well plates. After incubation, each plate was removed according to the respective time of incubation for assay. The contents distributions in each plate are displayed in Table 5.2. The cell viability was measured as described in Chapter 3, Section 3.2.13.1.

Table 5.2: Distribution of DPBS, NCP, BCNU-NCP and BCNU contents in individual plate.

Group	Number of well used	Contents added to each well	BCNU quantity in each well (µg)
Control	15	20 µL of DPBS	0
NCP	15	20 µL of DPBS and 0.5mg of NCP (drug free Nano-co-Plex)	0
BCNU	15	20 µL of DPBS and 0.088mg of BCNU	88
BCNU-NCP	15	20 µL of DPBS and 0.5mg of BCNU-NCP-3	88
BCNU-NCP (with application of a Magnetic Field)	15	20 µL of DPBS and 0.5mg of BCNU-NCP-3	88

5.3. RESULTS AND DISCUSSION

5.3.1. *Ex Vivo* Evaluation of Mucoadhesive Strength of the Optimized Nanogel Composite

The attachment or adherence of a polymeric material to a mucosal membrane, such as nasal mucosa, can be referred to as mucoadhesion. A nasal drug delivery formulation should ideally possess good mucoadhesive characteristics in order to be retained within the nasal cavity for a prolonged period of time to exert the desired delivery of drug to the brain. The process of mucoadhesion between a polymeric system and a mucosal surface is facilitated by ionic bonding, covalent bonding, hydrogen bonding, electrostatic forces, such as van der Waals forces, hydrophobic interactions and chain interlocking (Zaman et al., 2015). The degree

of interaction between the formulation and the mucosal surface is also dependent on the viscosity of the mucus on the surface of the mucosal membrane, the degree of chain entanglement within the formulation and the water contents. CS and HPMC have been carefully selected to prepare the Nanogel Composite due to their mucoadhesive properties. The mucoadhesion is the average maximum detachment force (MDF) and was determined from the peak of the Force-Distance profiles generated by textural profiling for the Nanogel Composite. The optimized formulation exhibited a MDF of 0.53±0.07N and work of adhesion of 0.27±0.056mJ. These results suggest that the Nanogel Composite possessed desirable adhesive properties and this could be attributed to the ability of the selected polymers to form H-bonds with the mucosal membrane upon hydration with nasal solution on the surface of the mucosa, which resulted in gelling of the formulation.

5.3.2. Calibration Curve of Iron

A calibration curve for iron was constructed in PBS (pH 6; 34°C), using a known series of concentrations (0.1mg/mL-1mg/mL) of iron, the observed absorbance plotted against the known concentration of iron using a UV-Vis at 450nm is displayed in the calibration curve of iron depicted in Figure 5.2.

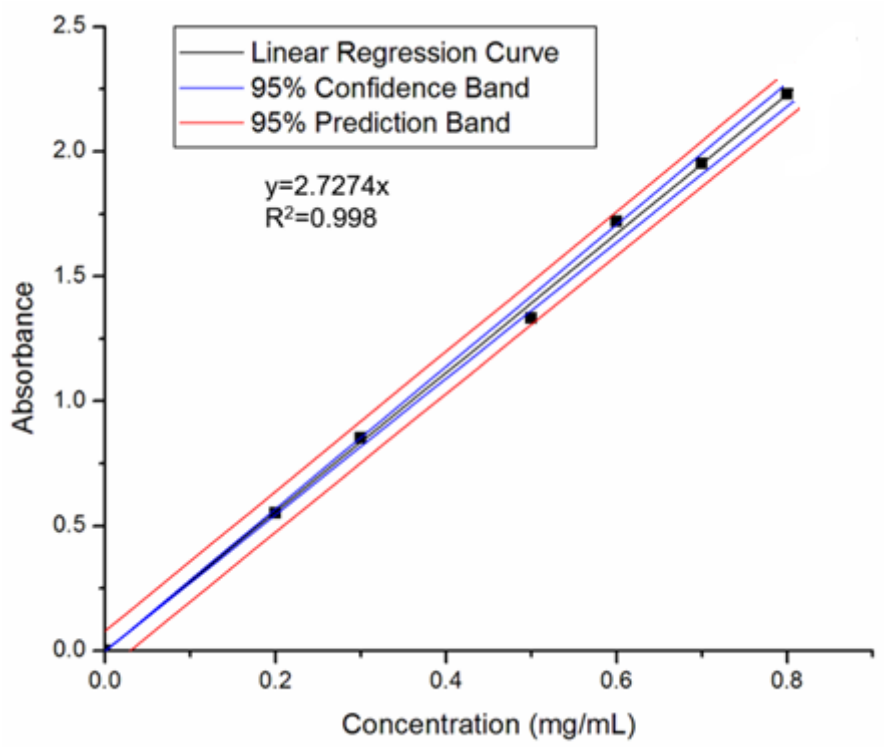

Figure 5.2: Calibration curve of iron

5.3.3. Assessment of the Permeation of the BCNU-Loaded Nano-co-Plex across the Rabbit Nasal Tissue

The permeation of the BCNU-NCP is based firstly on the release of the BCNU-NCP from the Nanogel Composite followed by BCNU-NCP transportation across the nasal epithelial tissue to the receiver compartment through the nasal epithelial tissue. Figure 5.3 shows the plot of the cumulative BCNU-NCP permeation against time for the permeation studies. Figure 5.3 shows the cumulative permeation curve of BCNU-NCP released and permeated with application of ES and MF, ES only, and without application of both ES and MF, respectively. The results showed that the sample with the application of ES and MF displayed the highest quantity of BCNU-NCP permeation across the nasal epithelial tissue, followed by the sample with application of ES but no MF, and the least is the sample with no application of ES.

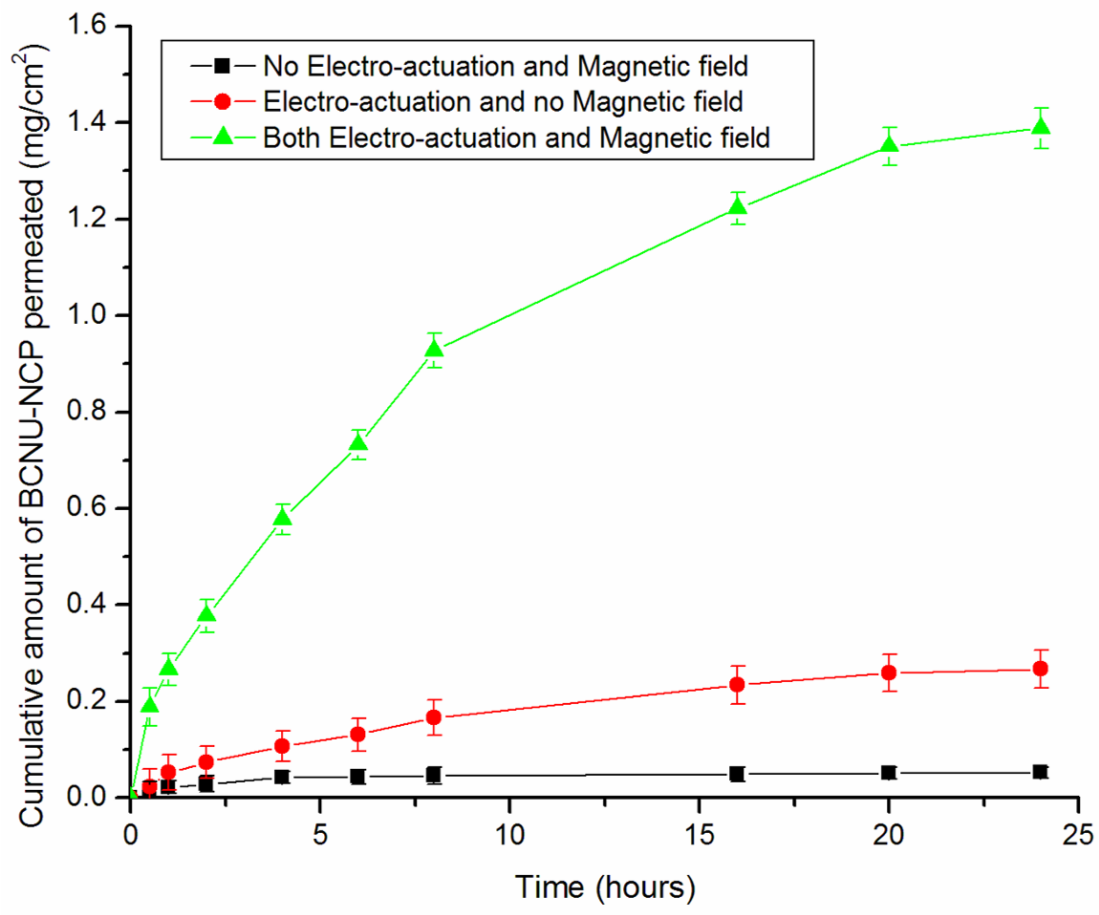

Figure 5.3: Permeation curve showing the cumulative amount of BCNU-NCP Permeated across the nasal epithelial tissue of rabbit at 34±1°C in a diffusion cell. Data are expressed as mean ± SD (N=3).

The flux, which determines the amount of molecules that permeated through nasal epithelial tissue and the permeability coefficient, which is a measure of the distance traveled by the drug molecules per unit time (Adeleke et al., 2015), were calculated and displayed in Table 5.3. The results revealed that the BCNU-NCP flux and permeability coefficient for the sample with the application of MF were $1.4177x10^{-2}$±$1.7245x10^{-3}$ and $5.6709x10^{-3}$, respectively. These results displayed extensive synergistic and efficient permeation due to the application of the MF. The BCNU-NCP are magnetic nanoparticles and they have the ability to respond to MF; they are therefore quickly transported across the nasal epithelia tissue due to the high magnetization properties of the nanoparticles. This thereby enhanced the permeation of the nanoparticles and thus increases bioavailability of BCNU-NCP at the receptor compartment. For the sample with only application of ES where there was no application of MF, the curve displayed an increase in

permeation as the time increased; in this case, the BCNU-NCP flux and permeability coefficient were $1.4177x10^{-2}\pm1.7245x10^{-3}$ and $5.6709x10^{-3}$, respectively. The BCNU-NCP was released on electro-actuation but the nanoparticles were transported across the nasal epithelium tissue unaided and thus the mode of transportation was by passive diffusion following the concentration gradient across the nasal epithelium tissue. The BCNU-NCP flux and permeability coefficient for the sample without the application ES were $2.7654x10^{-3}\pm7.0929x10^{-4}$ and $1.1062x10^{-3}$, respectively. This sample displayed the lowest values and this can be explained by the fact that there was no application of ES to trigger the release of the BCNU-loaded NCP, the little amount of BCNU-loaded NCP released and permeated might have been attributed to those nanoparticles that adhered onto the surface of the Nanogel Composite that eventually migrated into the diffusion medium. This further confirmed that nanoparticles release is also based on electro-actuation of the Nanogel Composite.

The enhancement ratio was calculated and the results are displayed in Table 5.3. The results revealed that the enhancement ratio when comparing the sample without both the application of ES and MF to when there is application of ES only, was approximately 5-fold in terms of permeability and approximately 86-fold for the sample with the application of MF. Furthermore, the enhancement ratio when comparing formulation with the application electric field only to that of application of both ES and MF was approximately 5-fold across the nasal epithelial tissue. It is therefore evident from these results that MF application greatly enhances the permeability of BCNU-NCP across the nasal epithelial tissue and will indeed permit rapid transport of nanoparticles across the nasal epithelial tissue to the olfactory region of the nasal mucosa for onward delivery to the CNS in order to circumvent the BBB and enhance bioavailability of therapeutics in the brain.

Table 5.3: Flux, Permeability coefficient and Enhancement ratio for permeation of BCNU-NCP through the nasal tissue of New Zealand white rabbit.

Formulation	Flux, Js ($mg.cm^{-2}.h^{-1}$)	Permeability Coefficient, P	Enhancement ratio*	Enhancement ratio**
Nanogel Composite (No application of ES and MF)	$2.7654x10^{-3}$ $\pm 7.0929x10^{-4}$	$1.1062x10^{-3}$	-	-
Nanogel Composite (with application of ES and MF)	$1.4177x10^{-2}$ $\pm 1.7245x10^{-3}$	$5.6709x10^{-3}$	5.13	-
Nanogel Composite (with application of both ES and MF)	$7.3681x10^{-2}$ $\pm 1.6912x10^{-3}$	$2.9472x10^{-2}$	85.63	5.20

*The enhancement ratio is based on the permeation of Nanogel Composite without the application of Electro-actuation and a magnetic field.

**The enhancement ratio is based on the permeation of Nanogel Composite without application of a magnetic field.

5.3.4. Assessment of the Magnetic Field Influence on the Cytotoxicity of BCNU-Loaded Nano-co-Plex on Human Glioblastoma A170 Cells

The effect of the MF on the cytotoxicity of BCNU-NCP was evaluated by employing human glioblastomer A170 cell lines. The results revealed that BCNU-NCP with application of magnet demonstrated greater toxicity towards glioblastomer A170 cells than when there was no application of magnet as shown in Figure 5.4. These results demonstrated remarkably the effect of the magnet in enhancing the internalization of the nanoparticles by attracting them towards the A170 cells.

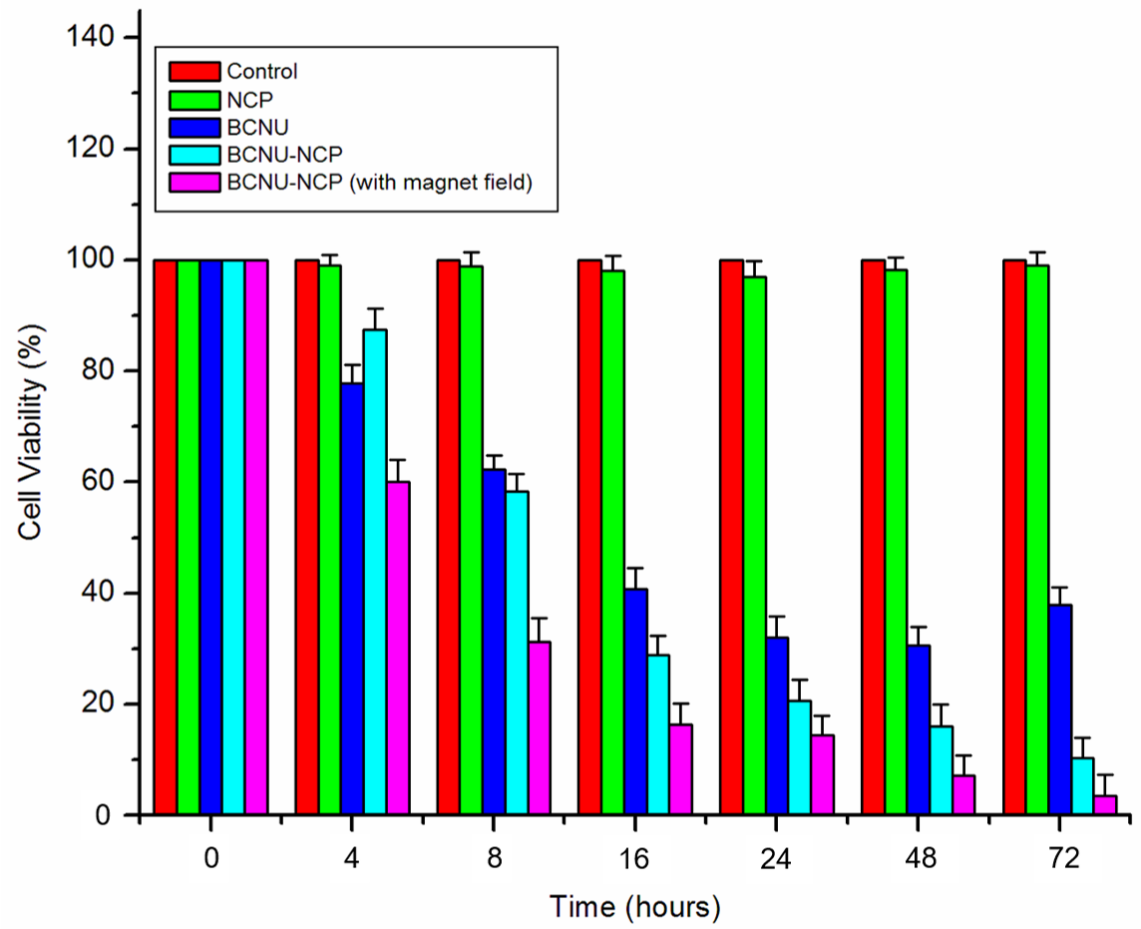

Figure 5.4: effect on toxicity of human glioblastoma A172 cell line showing the control treatment, treated with NCP, BCNU, BCNU-NCP and BCNU-NCP (with magnetic field) incubated at 37°C for 72 hours.

5.4. CONCLUDING REMARKS

The *ex vivo* investigation further demonstrated the efficacy of the nanoparticles being released from the Nanogel Composite when ES is applied. The released nanoparticles were found to permeate across the rabbit nasal epithelial tissue as revealed by the results. Furthermore, the permeation of the nanoparticles was found to be enhanced by the application of a MF as seen from the permeation coefficient values. This study therefore proves that this novel delivery system is practicable with significant potential and the study can therefore be taken further to an *in vivo* investigation in a suitable animal model which will be further discussed in detail int the next Chapter.

5.5. REFERENCES

Adeleke, O.A., Choonara, Y.E., Toit, L.C. du, Kumar, P., Pillay, V., 2015. *In Vitro, Ex Vivo* and *In Silico* Mechanistic Elucidation of the Performance of an Optimized Porosity-Controlled Multi-Elemental Transbuccal System. Pharm. Res. 32, 2384–2409.

Fortuna, A., Alves, G., Serralheiro, A., Sousa, J., Falcão, A., 2014. Intranasal delivery of systemic-acting drugs: Small-molecules and biomacromolecules. Eur. J. Pharm. Biopharm. 88, 8–27.

Grassin-Delyle, S., Buenestado, A., Naline, E., Faisy, C., Blouquit-Laye, S., Couderc, L.-J., Le Guen, M., Fischler, M., Devillier, P., 2012. Intranasal drug delivery: an efficient and non-invasive route for systemic administration: focus on opioids. Pharmacol. Ther. 134, 366–379.

Kubo, H., Hosoya, K.-I., Natsume, H., Sugibayashi, K., Morimoto, Y., 1994. *In vitro* permeation of several model drugs across rabbit nasal mucosa. Int. J. Pharm. 103, 27–36.

Levin, V.A., Kabra, P.A., Freeman-Dove, M.A., 1978. Relationship of 1,3-bis(2-chloroethyl)-1-nitrosourea (BCNU) and 1-(2-chloroethyl)-3-cyclohexyl-1-nitrosourea (CCNU) pharmacokinetics of uptake, distribution, and tissue/plasma partitioning in rat organs and intracerebral tumors. Cancer Chemother. Pharmacol. 1, 233–242.

Lewis, A.L., Jordan, F., Illum, L., 2012. CriticalSorb^{TM}: enabling systemic delivery of macromolecules via the nasal route. Drug Deliv. Transl. Res. 3, 26–32.

Lin, H., Yoo, J.-W., Roh, H.-J., Lee, M.-K., Chung, S.-J., Shim, C.-K., Kim, D.-D., 2005. Transport of anti-allergic drugs across the passage cultured human nasal epithelial cell monolayer. Eur. J. Pharm. Sci. 26, 203–210.

Maitani, Y., Asano, S., Takahashi, S., Nakagaki, M., Nagai, T., 1992. Permeability of Insulin Entrapped in Liposome through the Nasal Mucosa of Rabbits. Chem. Pharm. Bull. (Tokyo) 40, 1569–1572.

Ohtake, K., Maeno, T., Ueda, H., Natsume, H., Morimoto, Y., 2003. Poly-L-Arginine Predominantly Increases the Paracellular Permeability of Hydrophilic Macromolecules Across Rabbit Nasal Epithelium *in Vitro*. Pharm. Res. 20, 153–160.

Tabatabaei, S.N., Girouard, H., Carret, A.-S., Martel, S., 2015. Remote control of the permeability of the blood–brain barrier by magnetic heating of nanoparticles: A proof of concept for brain drug delivery. J. Controlled Release 206, 49–57.

Zaman, M., Sajid, N., Rehman, A.U., 2015. Gastrointestinal Mucosa: The Target Site of Mucoadhesive Microspheres, A Review. Adv. Polym. Technol. 1–8. doi:10.1002/adv.21550.

CHAPTER 6

IN VIVO EVALUATION OF THE OPTIMIZED NANOGEL COMPOSITE

6.1. INTRODUCTION

The drug release behavior of the Nanogel Composite has been extensively determined *in vitro*. However, *in vitro* evaluations of a novel drug delivery system may provide valid information regarding the drug release properties; they cannot completely simulate *in vivo* conditions. Therefore, *in vivo* studies still need to be conducted to obtain significant pharmacokinetic data. The use of an *in vivo* model offers greater pharmacokinetic and pharmacodynamic accuracy as well as a more realistic clinical extrapolation. The use of rabbits in neuroscience may be a suitable option for comparing experimental modelling of human brain diseases as the larger animal allows for multiple sampling in the same animal and relatively accurate results compared to smaller laboratory animals such Sprague Dawley Rats (Traystman, 2003). The entrance into the nasal cavity of the rabbit is larger in comparison to that of the rat and may therefore enable ease of administration of the formulation (Bojsen-Moller and Fahrenkrug, 1971). In addition, euthanasia of rabbits to obtain CSF at each time interval may not be necessary due to the larger rabbit model having a larger CSF volume.

The use of electrodes and magnetic headband would also be more appropriate in rabbit model than smaller animal model. Furthermore, the use of electrodes in intranasal drug delivery to the brain has been successfully carried out by Lerner and co-workers (2004) using New Zealand White Rabbit. Electrotherapy has been carried out by Vaiman and co-wrokers (2004) for the treatment of nasal valve collapse. Additionally, Wan-Ching Ho (2015) employed ES on the nose to treat nasal polyps and allergic rhinitis. The acquisition of *in vivo* data from the formulation is essential to corroborate the feasibility of the novel delivery system in human patients. The *in vivo* studies were therefore carried out employing New Zealand white rabbits to evaluate the release behaviour of the Carmustine-loaded Nano-co-Plex (BCNU-NCP) from the Nanogel Composite upon the application of

ES on the nose of the rabbit and to assess the effect of an external MF on the released BCNU-NCP transportation across the nasal epithelial tissue towards the olfactory pathway for onward nose-to-brain delivery of the BCNU-NCP. Furthermore, the release of BCNU was determined by calculating the quantity of BCNU released in CSF, brain and the blood of the rabbit after intranasal administration and to establish the influence of ES in releasing the BCNU-NCP in an “on-off” pulsatile fashion. It is essential to also conduct a thorough toxicity study through histopathological evaluation on the nasal epithelial tissues exposed to the formulation and the placebo in comparison to the control.

6.2. MATERIALS AND METHODS

6.2.1. Materials

New Zealand White rabbits (2-2.5 kg) were acquired from the Central Animal Service (CAS), University of the Witwatersrand (Wits), Galantmine (Gal) and carmustine (BCNU) were purchased from Sigma-Aldrich (Steinhelm, Germany). The UPLC chromatographic separations were performed with a SunFire^{TM} C18 column (3.5µm, 4.6x75mm) (Waters, Milford, MA, USA) auto sampler and 515 oval pumps. Double de-ionized water was used (Milli- Q, Millipore, Johannesburg, South Africa). UPLC solvents were of UPLC grades and all other reagents used are of analytical grades and of the highest purity. All drugs and their respective dosages as administered to the rabbits are provided in Table 6.1. Ketamine, Xylazine, Buprenorphine, Carprofen, Isoflurane, Oxygen, Procaine and Sodium pentobarbitone were provided by the CAS (Wits).

Table 6.1: Details of drugs, anesthetics, analgesics and other medicinal or experimental substances used, including the doses and routes of administration

Drug/Substance	Route	Dose	Frequency
Nanogel Composite	IN	0.5mg/kg	once
Carmustine	IV	1mg/kg	once
Ketamine	IM	50mg/kg	once
Xylazine	IM	5mg/kg	once
Buprenorphine	IM	0.05mg/kg	When necessary
Carpofen	IM	4mg/kg	When necessary
Isoflurane	Inhalation	2%	once
Oxygen	Inhalation	12%	once
Procaine	Topical	0.5%	When necessary
Sodium pentobarbitone	IP	100mg/kg	once

IN=Intranasal, IV=Intravenous, IM=Intramuscular and IP=Intraperitoneal

6.2.2. Animal Ethics Clearance

Animal ethics clearance for these *in vivo* studies was obtained from the Animal Ethics Screening Committee (AESC) of the University of the Witwatersrand. Ethics Clearance Number 2015/05/C (Appendix D).

6.2.3. Preparation and Sterilization of Nanogel Composite

Preparation of Nanogel Drug Composite (Nanogel Composite) was carried out as described in Chapter 4, Sections Chapter 4, Sections 4.2.2, 4.2.3, and 4.2.4. The Nanogel Composite was sterilized by exposing the formulation to UV light overnight in an aseptic and sterile environment.

6.2.4. *In Vivo* Experimental Studies

In vivo studies to evaluate the release of BCNU loaded Nano-co-Plex from the Nanogel Drug Composite on application of ES and Magnetic MF and further evaluation of the BCNU release kinetics from the Nano-co-Plex were carried out.

6.2.4.1. Pilot studies for determining the workability and suitability of the application of electric stimulation and magnetic field.

The purpose of this pilot study was to demonstrate the workability and suitability of the Nanogel Composite using New Zealand white rabbits. It was to also examine the mode of administration and the effects of the application of the external electric and magnetic stimuli on the rabbit model. The three rabbits approved for the Pilot

study arrived at CAS. The rabbits were weighed on arrival and on the day of the procedure. The weight was recorded according to Table 6.2. The animals were monitored and fed with rabbit food and water. The rabbits were closely monitored and found to be generally healthy.

Table 6.2: Weight of the three rabbits on day of arrival and a day prior to procedure.

Rabbits	1	2	3
Weight on arrival (kg)	2.30	2.40	2.15
Weight on procedure day (kg)	2.30	2.50	2.19

6.2.4.1.1. Preparation of the dosage forms of the Nanogel Composite and the conventional BCNU

The sterilized optimized formulation (Nanogel Composite) was prepared and sterilized as described in Section 6.2.3. In order to compare Nanogel Composite to the conventional drug currently on the market so as to evaluate the superiority of the Nanogel Composite in terms of their drug release kinetics, the BCNU intravenous injection (IV) from the market was prepared by aseptically weighing accurately 5mg of BCNU and then dissolved it in 5mL of sterile 10% ethanol solution to make a concentration of 1mg/mL.

6.2.4.1.2. Experimental procedures for the pilot study

The rabbits were sedated before dosing by injecting ketamine (50mg/kg) and xylazine (5mg/kg) into the marginal vein of the rabbit's ear. Nanogel Composite (200µL, 0.5mg/kg) was intranasally administered into the nasal cavity of the rabbit using a 1mL syringe with rubber needle attached, to instil 100µL into each nostril. ES of 5V potential difference was applied for a period of 1 minute using electrodes from a potentiostat/galvanostat (PGSTAT302N, Autolab, Utrecht, Netherlands) on the nose of the rabbits after dosing as shown in Figure 6.1a. A magnetic headband equipped with 0.4 Tesla magnetic strength, (Magnetech, Capetown, South Africa) was placed on the rabbit's head as shown in Figure 6.1b. The rabbit was then left to recover from the sedation with careful observation. The rabbits were returned

back to the cage after full recovery. Fluid sampling was carried out prior and after ES at predetermined time interval. Blood samples (2mL) were collected through the marginal vein of the left ear following the procedure highlighted in Section 6.2.4.2.4 as depicted in Figure 6.5f, followed by CSF (125µL) withdrawal by cisternal puncture through the foramen magnum as detailed in Section 6.2.4.2.5 as shown in Figure 6.5g. Each rabbit in each group was subjected to 2 sampling timelines. Sampling time points were 0, 0.5, 1, 2, 4, 6, 8, 16, 20 and 24 hours. The rabbits were then humanely euthanized after the second sampling timeline and the brain removed and placed in 10% phosphate buffered formalin for drug concentration studies.

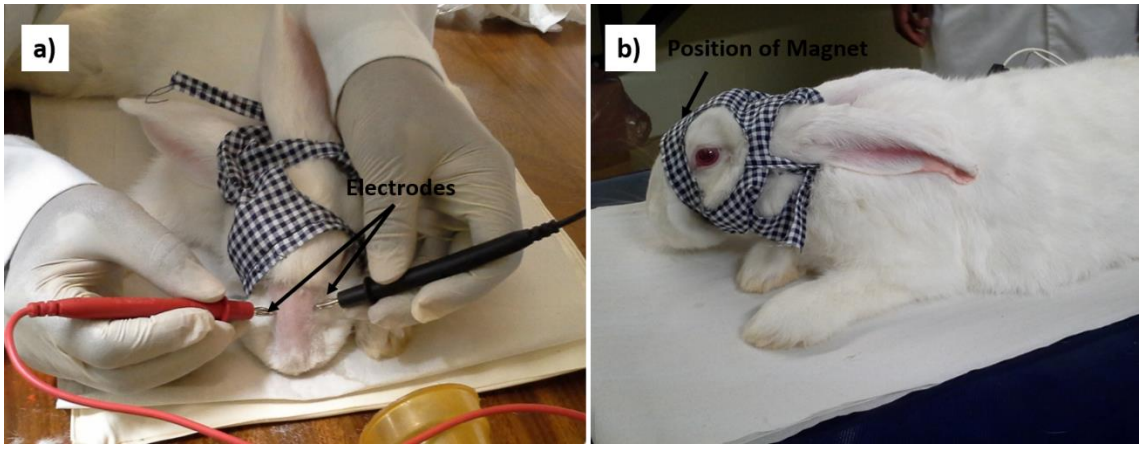

Figure 6.1: Digital images of a) application of electric stimulus on the nose and b) Magnetic Headband fitted on the head of the rabbit.

6.2.4.1.3. Pilot studies design

The three rabbits were distributed into three groups, one rabbit per group. The time point was randomly chosen for this pilot study.

Group 1: This group was the experimental group. The experimental procedure detailed in Section 6.2.4.1.2 was followed. Fluid sampling was carried out at 1 hour and 6 hours for the purpose of the pilot study.

Group 2: This group was the control group to examine the effect of electrical and magnetic stimulations. There was no application of both ES and MF. Fluid sampling was carried out at 2 hours and 8 hours for the purpose of this pilot study.

Group 3: This group was intended to be used to obtain pharmacokinetic and pharmacodynamics data for comparison purposes and *in vivo* proof of concept.

A dose of 1mL of BCNU prepared as stipulated in Section 6.2.4.1.1 was intravenously injected into the rabbit through the marginal ear vein. Fluid Sampling was carried out at 1 hour after dosing.

6.2.4.2. In vivo experimental design and procedure for the studies

6.2.4.2.1. Habituation of the experimental animals (New Zealand White Rabbits)

The rabbits were purchased and transported from certified suppliers. Appropriate pre-transportation handling, loading, journeying and unloading at the Central Animal services (CAS), University of the Witwatersrand, were accomplished according to CAS standard operating procedures (SOPs). On arrival at CAS the rabbits were habituated, weighed and assessed for any signs of disease, injury or distress and then socialized accordingly before the experimental procedures were conducted (Zhang et al., 2015). Animals were housed at room temperature with a 12-hour light/dark cycle (light from 6am to 6pm), and were fed a standard rabbit diet with water available ad libitum as shown in Figure 6.2.



Figure 6.2: A digital image depicting the conditions under which the rabbits were housed in a vivarium according to ARVO Resolution guidelines.

6.2.4.2.2. Experimental design

A total of 105 New Zealand White Rabbits were approved for these studies inclusive of the pilot studies. The rabbits were randomly assigned to 4 groups of 25 rabbits per group. Each group is subdivided into 5 groups per 2 time points. The experimental design and the assignment of the rabbits into the groups including the outline summary of the *in vivo* studies are illustrated in Figure 6.3.

Group 1 (Placebo): Drug free Nanogel Composite was administered to the 25 rabbits in this group. There was application of magnetic headband equipped with 0.4 Tesla magnet and ES application using electrodes with a potential difference of 5V on the nose of the rabbit. This group was used for comparison purposes against the experimental groups to evaluate pharmacokinetic and pharmacodynamics data.

Group 2 (Positive control): Nanogel Composite was administered to all the rabbits in this group but there was no application of electrodes on the nose and no application of a magnetic headband. This group was used as control to observe the effect of ES and MF on drug release and onward movement of nanoparticles to the brain through the nasal cavity.

Group 3 (Experimental group): Nanogel Composite was administered to all the rabbits in this group. There was application of electrodes on the nose and application of a magnetic headband. This group was used to obtain pharmacokinetic and pharmacodynamics data for comparison purposes and *in vivo* proof of concept.

Group 4 (Negative control): BCNU was intravenously administered to all the rabbits in this group. There was no application of electrodes on the nose and no application of a magnetic headband. This group was used to compare the pharmacokinetic and pharmacodynamics properties of the current drug on the market, as well as administration method with that of the nasal Nanogel Composite formulations. BiCNU is the market leader product and was used for comparison purposes.

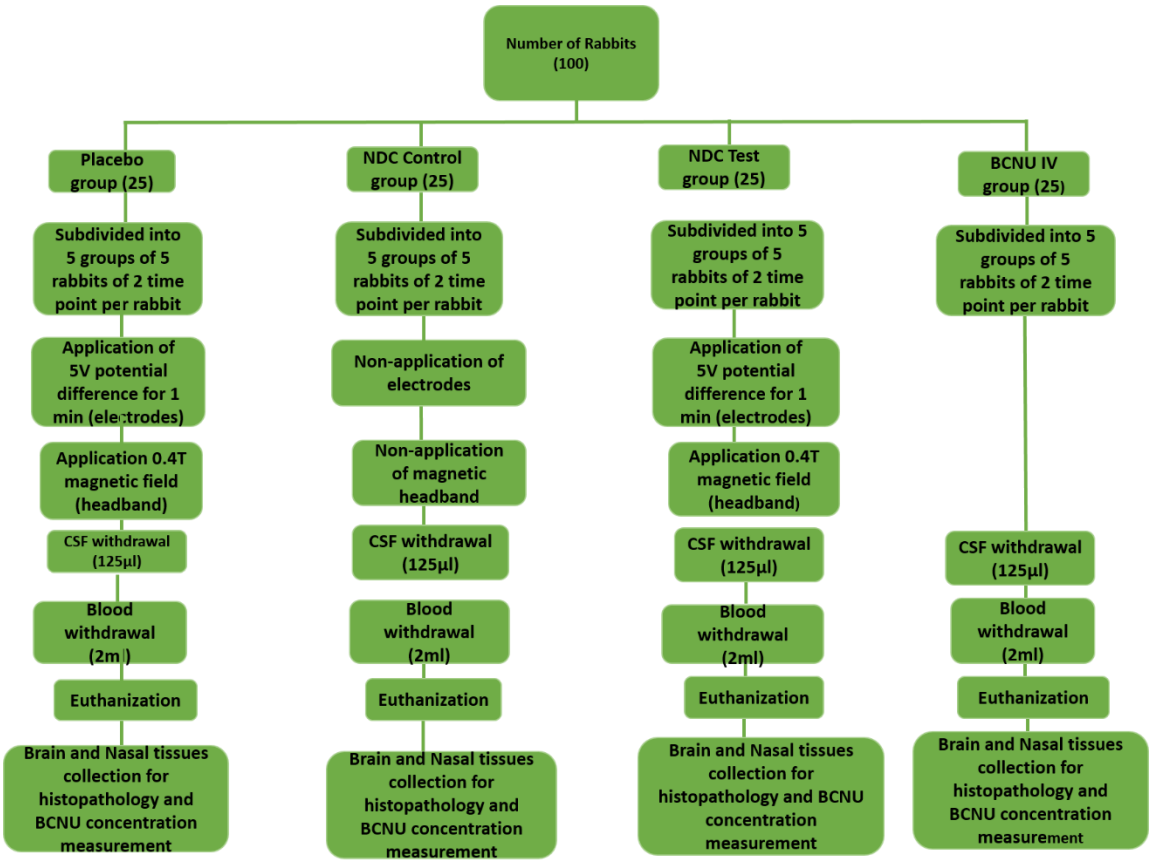

Figure 6.3: Schematic diagrams showing the outline summary of the *in vivo* animal studies.

6.2.4.2.3. Blood sample collection

The rabbits were anesthetized prior to blood sample withdrawal. Blood samples (2mL) were withdrawn directly from the marginal ear vein of the rabbits. Each rabbit in this study were subjected to only 2 sampling timepoints. Sampling time points were 0, 0.5, 1, 2, 4, 6, 8, 16, 20 and 24 hours. The withdrawn blood samples were immediately placed in heparinized tubes to prevent clotting. The blood samples were centrifuged at 5000rpm and the supernatant was transferred into 2mL Eppendorf tubes and stored in the -80 °C freezer for further analysis.

6.2.4.2.4. Cerebrospinal fluid sample collection

The rabbit was anaesthetized prior to the procedure. The back of the neck of the rabbit was shaved in order to have access to the occipital protuberance and the cranial margins areas of the rabbit. A 23-gauge needle was inserted approximately midway between these two points in order to have access to the cisterna magna

through the foramen magnum. The needle was slowly inserted and directed towards the nose of the rabbit, the needle penetrated the dura and the subarachnoid membranes with a slight “pop” felt confirming the puncturing of the cisterna magna. Appearance of CSF at the hub of the needle confirmed correct placement of the needle, the CSF drip from the needle and a 1mL syringe was used to slowly aspirate 125µL of CSF. The needle was gently removed and a mild pressure was applied at the needle exit point for about 15 seconds. The CSF was quickly transferred into an Eppendorf tube and stored in -80°C freezer. This procedure is illustrated in Figure 6.4. The reason for staggering the sampling points as well as using the 5 rabbits in all the sub-groups was due to the inability of rabbits to provide more than 2 sampling time points per day. The CSF sampling time point was therefore limited to 2 per rabbit and was well spread so as to give the rabbits enough recovery time.

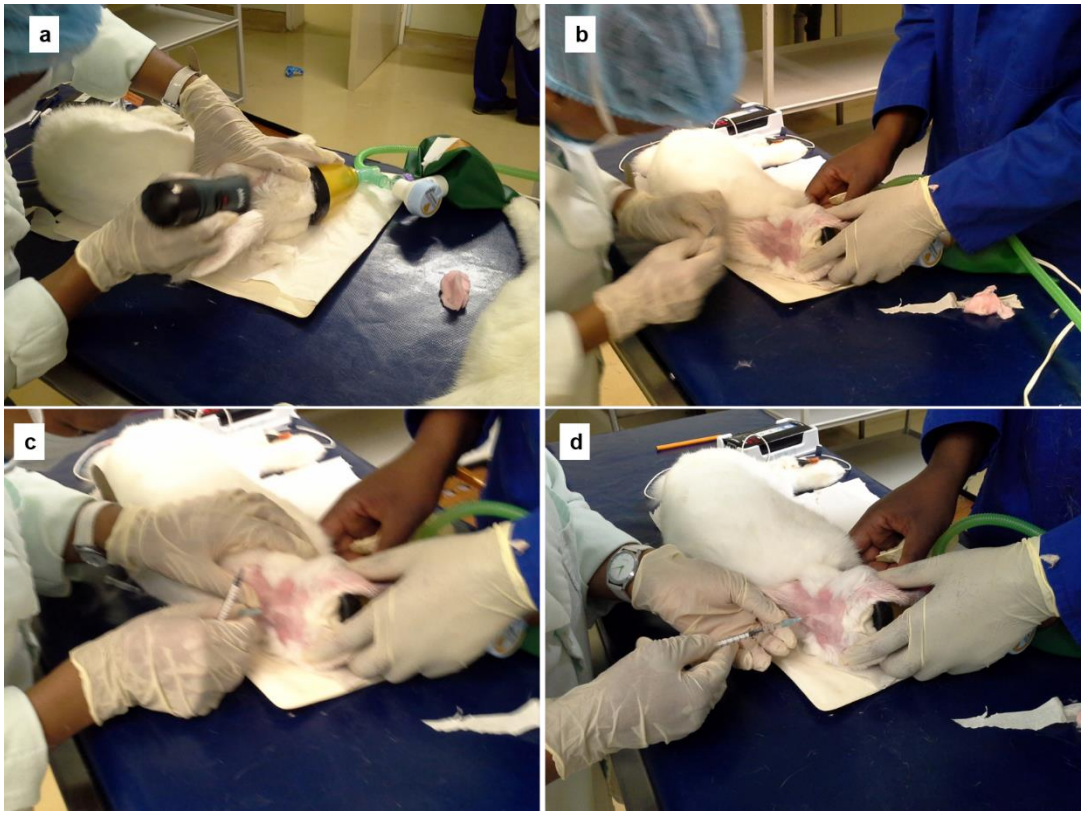

Figure 6.4: Digital images of the procedure for withdrawing CSF from the rabbit showing a) shaving of the back of the neck of rabbit, b) shaved area, c) insertion of needle directed towards the nose of the rabbit and d) the withdrawal of CSF with the aid of 1mL syringe).

6.2.4.2.5. Brain tissue collection

The rabbits were humanely euthanized, and the brains were removed. The extraction of BCNU from the brain tissue was performed by a modified method used by Ved and Kim (2011). Briefly, the brain tissue was homogenized employing a VDI-12 homogenizer at 20,000rpm for 15 minutes, 1mL of 1.25%($^{v}/_{v}$) absolute ethanol in diethyl ether was added to 100mg of the brain sample and further homogenized for 2 minutes. The resultant tissue homogenate was then centrifuged at 5000rpm for 20 minutes. The supernatant was measured for BCNU contents, using the extraction methods provided in Section 6.2.5.2 followed by UPLC analysis.

6.2.4.2.6. Experimental procedure for the in vivo studies

The optimized Nanogel Composite delivery system was compared to the conventional drug currently in the market to evaluate the superiority of the new systems in terms of their drug release kinetics. Furthermore, a placebo (drug-free) system was administered to compare results. The experimental procedure for each group is elaborated below.

Group 1 (Placebo)

There were 25 rabbits in this group which were subdivided into 5 groups per 2 time points. Rabbits were sedated before dosing by injecting ketamine (50mg/kg) and xylazine (5mg/kg), into the marginal vein of the rabbit's ear. Nanogel Composite (200µL, 0.5mg/kg) without BCNU-NCP was intranasally administered into the nasal cavity of the rabbit using a 1mL syringe with rubber needle attached to it to instil 100µL into each nostril. ES of 5V potential difference was applied for 1 minute using electrodes from a potentiostat/galvanostat (PGSTAT302N, Autolab, Utrecht, Netherlands) on the nose of the rabbits after dosing as shown in Figure 6.1a. A magnetic headband equipped with 0.4 Tesla magnetic strength was placed on the rabbit's head as shown previously in Figure 6.1b. Fluid Sampling was carried out prior and after ES at predetermined time. Blood samples (2mL) were collected through the marginal vein of the left ear following the procedure highlighted in Section 6.2.4.2.4 as depicted in Figure 6.5f, followed by CSF (125µL) withdrawal by cisternal puncture through the foramen magnum as detailed

in Section 6.2.4.2.5. and shown in Figure 6.5g. Sampling time points were 0, 0.5, 1, 2, 4, 6, 8,16, 20 and 24 hours. The rabbits were then humanely euthanized after the second sampling timeline and the brain removed and placed in 10% phosphate buffered formalin for drug concentration studies.

Group 2 (Positive control)

The same procedure detailed for group 1 above was applied to this group with the exception of the dosing formulation. Nanogel Composite (200µL, 0.5mg/kg) was intranasally administered, with no application of electrical and magnetic stimulation.

Group 3 (Experimental group)

The same procedure detailed for group 1 was applied to this group. The Nanogel Composite (200µL, 0.5mg/kg) was intranasally administered.

Group 4 (Negative control)

In this group, 1mL of BCNU prepared as stipulated in Section 6.2.4.1.1 was intravenously injected very slowly into the rabbits through the marginal ear. There was no application of electric and magnetic stimulation. All standard procedures as in group 1 were followed.



Figure 6.5: Photographic evidence of (a) Housing of the rabbits (b) preparation for surgery with anesthetization (c) intravenous dosing (d) intranasal dosing e) application of ES (f) blood withdrawal (g) CSF withdrawal (h) administration of oxygen after dosing and sampling (i) rabbit recovering from sedation.

6.2.5. Quantitative Chromatographic Determination of BCNU in Plasma, CSF and the Brain Tissue of Rabbit

Detection and quantification of BCNU in the plasma, CSF and brain samples was carried out on a Waters Acuity™ Ultra Performance Liquid Chromatography (UPLC) (Waters Corporation, Milford, Massachusetts, USA). This was made up of a binary solvent manager, a sample manager and fitted with a photodiode array detector (PAD) synchronously controlled using the Waters Empower 2 software. A SunFire™ C18 column (3.5µm, 4.6X75mm) (Waters, Milford, MA, USA) auto sampler and 515 oval pumps was used to detect and separate BCNU.

6.2.5.1. Development of a method for sample analysis employing Ultra Performance Liquid Chromatography

UPLC was technique utilized to determine the concentrations of the drugs in the biological fluid retrieved at different time points through the identification of peaks. A method for the detection and determination of BCNU was investigated involving the selection of appropriate mobile phases, flow rate, wavelength and injection volume. The mobile phase employed was a mixture of Acetonitrile (ACN) and water. An isocratic method with the ratio of 70:30 (ACN:Water) proved to be the most suitable. Table 6.3 shows the parameters employed while galantamine was chosen as the internal standard for the quantification analysis. Mobile phases were prepared and filtered through 0.22µm Millipore filters and placed in the machine with the appropriate solvent flow lines placed in the two mobile phases. The initial step to UPLC analysis is priming the machine which includes washing of the pumps and lines. Two types of washing occurred, a weak wash (90%$^{v}/_{v}$ double de-ionised water and 10%$^{v}/_{v}$ ACN) and a strong wash (90%$^{v}/_{v}$ ACN and 10%$^{v}/_{v}$ double de-ionized water). Once the priming process was completed, the column was equilibrated to the selected separation method.

Table 6.3: UPLC parameters employed for the determination of BCNU concentration

Parameters	**Conditions**
Mobile phase	ACN and Water (70:30) isocratic gradient
Flow rate	0.5mL/min
Injection volume	2µL
Wavelength	230nm
Column temperature	40ºC
Sample temperature	25ºC

6.2.5.2. Extraction of BCNU from rabbit plasma and CSF for UPLC analysis

An effective liquid-liquid extraction method was developed and applied to BCNU in the rabbit plasma. The frozen experimental plasma samples were thawed at room temperature and allowed to environmentally equilibrate. The samples were then centrifuged at 5000rpm for 15 minutes. Centrifugation was repeated twice in order to release any drug present in the tissues. The supernatant was isolated and

0.2mL of the supernatants was transferred into Eppendorff tubes. The IS in 10% ethanol Gal; (100µL, 0.2mg/mL) was added to each tube, and the tubes were vortexed for 30s. A liquid-liquid phase extraction methodology was employed in extracting the drugs from the studied rabbit plasma. To each of the tube, 0.3mL of 1.25%($^{v}/_{v}$) absolute ethanol in diethyl ether was added. The tubes were vortexed for 30s and then centrifuged at 5000rpm for 20 minutes. The supernatant (ethanol-diethyl ether layer) was then transferred to clean vials and was air dried at room temperature leaving dry residues containing the drugs in the vials. The residues were then reconstituted with 0.5mL of the UPLC mobile phase (Acetonitrile/Water in ratio 70:30). The solution was filtered through a 0.22µm Cameo Acetate membrane filter (Millipore Co., Bedford, MA, USA) into Waters® Certified UPLC vial for analysis. The same procedure was performed for the CSF samples and the supernatant samples collected from the brain, as carried out in Section 6.2.4.2.5 of this chapter. Measurements were conducted on all the samples from each time point (N=5).

6.2.5.3. Validation of liquid-liquid extraction procedure

The precision and accuracy of the extraction process was determined by repeating the extraction procedure performed in Chapter 6, Section 6.2.5.2 on 3 consecutive days to allow for the determination of inter-day precision and accuracy (N=3 for each day) and intra-day variability consisting of multiple injections of samples during a 24-hour period (N=3). Accuracy was estimated using the mean percentage error, based upon differences between actual and predicted concentrations. The precision, expressed as a percentage, was evaluated by calculating the intra- and inter-day variability coefficients of variation (Boon et al., 2006). The extraction process was further validated by the use of the IS (Gal), the peak area of the Gal should always be similar in every sample as a constant quantity is always utilized. The extraction yield percentage was calculated by comparing the peak areas obtained from the extracted BCNU in the plasma (AUC_{plasma}) to the peak areas obtained from BCNU extraction from standard solutions ($AUC_{standard}$) of the same concentration using Equation 6.1.

$$Yield\ (\%) = \frac{AUCplasma}{AUCstandard} \times 100$$ **Equation 6.1**

6.2.5.4. Preparation of calibration curve

Stock solutions of BCNU were prepared by dissolving 20mg of BCNU in 100mL of 10% ethanol. Dilutions were made from fresh stock prepared the same day and kept at low temperature because of degradation. Spiking solutions with concentrations spanning between 0.02 and 0.1mg/mL were prepared from stock solution of BCNU prepared at concentration of 0.2mg/mL by diluting the stock solution with deionized water. Gal was selected during preliminary study as the suitable Internal Standard (IS). A stock solution of Gal was prepared at concentration of 0.2mg/mL. In order to prepare standard solutions for generating a standard curve for BCNU in the plasma, BCNU spiking solutions (0.1mL) and the IS (0.1mL) were added to Eppendorf tubes, each of which contained 0.2mL of blank rabbit plasma thawed previously and then centrifuged (Optima® LE-80K, Beckman, USA) at 5,000rpm for 15 minutes. A liquid-liquid phase extraction methodology was employed in extracting both BCNU and Gal added from the blank rabbit plasma to prepare a calibration curve. To each calibration standard, 0.3mL of 1.25%($^{v}/_{v}$) absolute ethanol in diethyl ether was added. The tubes were vortexed for 30s and then centrifuged at 5000rpm for 20 minutes. The supernatant (ethyl alcohol-diethyl ether layer) was then transferred to a clean vial and was air dried at room temperature, leaving dry residues containing the drug samples in the vials. The residues were then reconstituted with the UPLC mobile phase (Acetonitrile/Water). The solution was filtered through a 0.22µm Cameo Acetate membrane filter (Millipore Co., Bedford, MA, USA) into Waters® Certified UPLC vial for analysis. The same procedure was performed for the CSF samples. The ratio of the area under the curve (AUC) for the peaks between BCNU and the IS was plotted against the concentration of the standard solutions to generate the calibration curve. A linear curve was constructed from five calibration standards.

6.2.5.5. Determination of BCNU-NCP in the brain tissue employing Field Emission Electron Probe Micro Analyzer (FE EPMA)

The presence of BCNU-NCP in the brain was confirmed by evaluating the presence of iron oxide nanoparticles in the brain through the detection of iron content in the brain sample employing Field Emission Electron Probe Micro Analyzer (FE EPMA). Samples of the brain obtained from the euthanized rabbit were homogenized for 15 minutes, the homogenate was vacuum dried at 40°C. Sample of the dried brain was placed on aluminum stubs with the aid of a carbon tape. The sample was sputter-coated with gold-palladium and then loaded into the FE EPMA for analysis.

6.2.5.6. Histopathological Evaluation of the Nasal Mucosa of the Rabbits

Samples of the nasal tissues of the rabbits were randomly taken from each group and sent to IDEXX laboratory for histopathological examination and analysis. The nasal mucosa of the rabbits was excised and quickly transferred into neutral buffered formalin. The nasal tissues were decalcified for 12 hours in rapid decal solution (sulphuric and hydrochloric acid) to allow for cutting and section while maintaining anatomical integrity of the nasal turbinate and mucosa. The formalin fixed tissue samples were then blocked and processed overnight in the automatic tissue processor as per standard operating procedure. The produced wax blocks were then sectioned on a microtome to produce 5-6µm sections which were then stained in an automated Haemotoxylin and Eosin (H&E) stainer (IdexxSA-APSOP-205).

6.3. RESULTS AND DISCUSSION

6.3.1. Pilot Study to Assess the Effect of Electric Stimulation, Magnetic Headband and Fluid Sampling on the Rabbits

The pilot study was designed to observe the effects of the ES and the MF application on the safety and wellbeing of the rabbits during the experimental period as well as to perfect the experimental procedure. The sampling frequency was also of concern especially the collection of CSF from the rabbit. The outcome of the pilot study for Group 1 was successful. This is the group that demonstrated

the full application of the drug delivery system. The intranasal dosing, the magnetic headband and the application of the ES were all carried out successfully without any difficulty. The fluid sample collections went easily and without any hindrance. Sample collections were carried out successfully at 2 timepoints (1 and 6 hours). Group 2 was also successful as there was no problem during anaesthetization, dosing and fluid collection procedures. This group serves as control in demonstrating the effect of the magnetic headband and the electric stimulus applied. Sample collections were carried out successfully at 2 timelines (2 and 8 hours). The rabbit in group 3 died after IV administration of the conventional BCNU. The cause of death was not clear. The cause of death may however be attributed to different issues and complications as a result of the administration of the IV injection, or it may be due to one or more of the numerous side effects of BCNU.

BCNU is an antineoplastic cancer chemotherapeutic which works by blocking the growth of cancer cells. Some of the side effects of BCNU are nausea, vomiting, diarrhoea, gastrointestinal upset, nephrotoxicity, oral ulcers, alopecia and bone marrow suppression. The rate at which the IV was administered may also be a contributing factor according to the literature (Joshi et al., 2007), IV dosing of BCNU in rabbit should be administered at a very slow rate. The concentration of the dosage as well as the quantity may also be a contributing factor. However, comparing the concentration and the quantity of the dose administered in this case to that obtained from the literature (Joshi et al., 2007; Liu et al., 1983), possibility of overdose may be rule out as the right dosage was administered. The solution proffered to this problem was to administer the IV at a very slow rate. Group 3 was then repeated with an additional rabbit approved by the AESC for the purpose. This time, IV injection was slowly administered to the rabbit. Rabbits were closely monitored before and after the procedure. Blood and CSF were collected twice at different time points from the rabbit. The pilot study was carried out successfully with the novel drug delivery system, without any discomfort to the rabbits during dosing, application of both electric and magnetic stimulation, as well as sample collection procedures. The pilot study provided a useful experience and familiarization of procedures which were applied in the main study.

6.3.2. Drug Extraction, UPLC Method Validation and Assay Procedure

Figure 6.6a and Figure 6.6b shows high resolution chromatographic peaks of the analyte (BCNU) and the internal standard (Gal) as obtained by the UPLC-PDA. The analysis revealed two separated and defined peaks (wavelength 230nm) at the respective retention times of 1.90 and 15.28 minutes for Gal and BCNU, respectively, as depicted in Figure 6.6c.

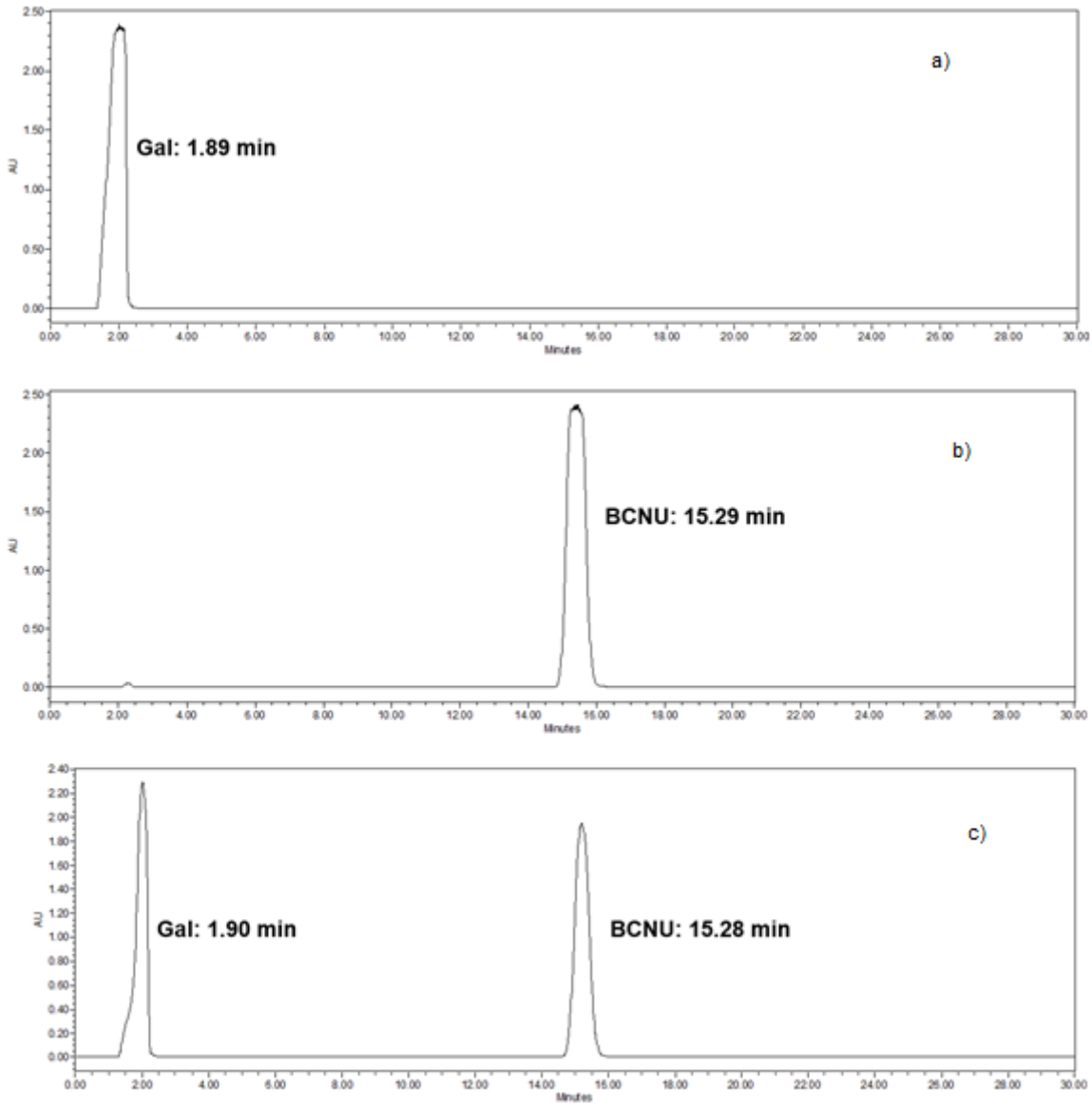

Figure 6.6: Typical chromatogram displaying a) the spiking plasma separation of the Gal, b) BCNU and c) the separation of both Gal and BCNU after plasma extraction.

Figure 6.7 shows the chromatographic peaks of BCNU and Gal at 230nm after CSF extraction, with their respective retention times of 1.20 and 16.49 minutes. These retention times are very similar to those obtained from the plasma analysis. Figure 6.6 and Figure 6.7 further revealed that there was no change in the retention time when the analyte and the IS were spiked in plasma and CSF individually and when they were spiked in plasma and CSF together. This observation proved the UPLC method adopted to be a suitable and appropriate method for analysing the drug in the samples. The mean recovery percentage of BCNU from the plasma and CSF samples during the liquid-liquid phase extraction implemented was calculated by comparing the peak areas of both low and high extraction calibration standards to those of aqueous standards. Validation of the extraction method indicated that the mean coefficient of variation in the intra-day and inter-day precision and accuracy was determined to be 0.46% and 0.38%, respectively. The results of the extraction procedure of the spiked blank plasma and CSF samples revealed a mean recovery (N=5) range of 91.2-95.7% (SD≤3.48), these results were found to be satisfactory. The generated calibration curve for BCNU is displayed in Figure 6.8.

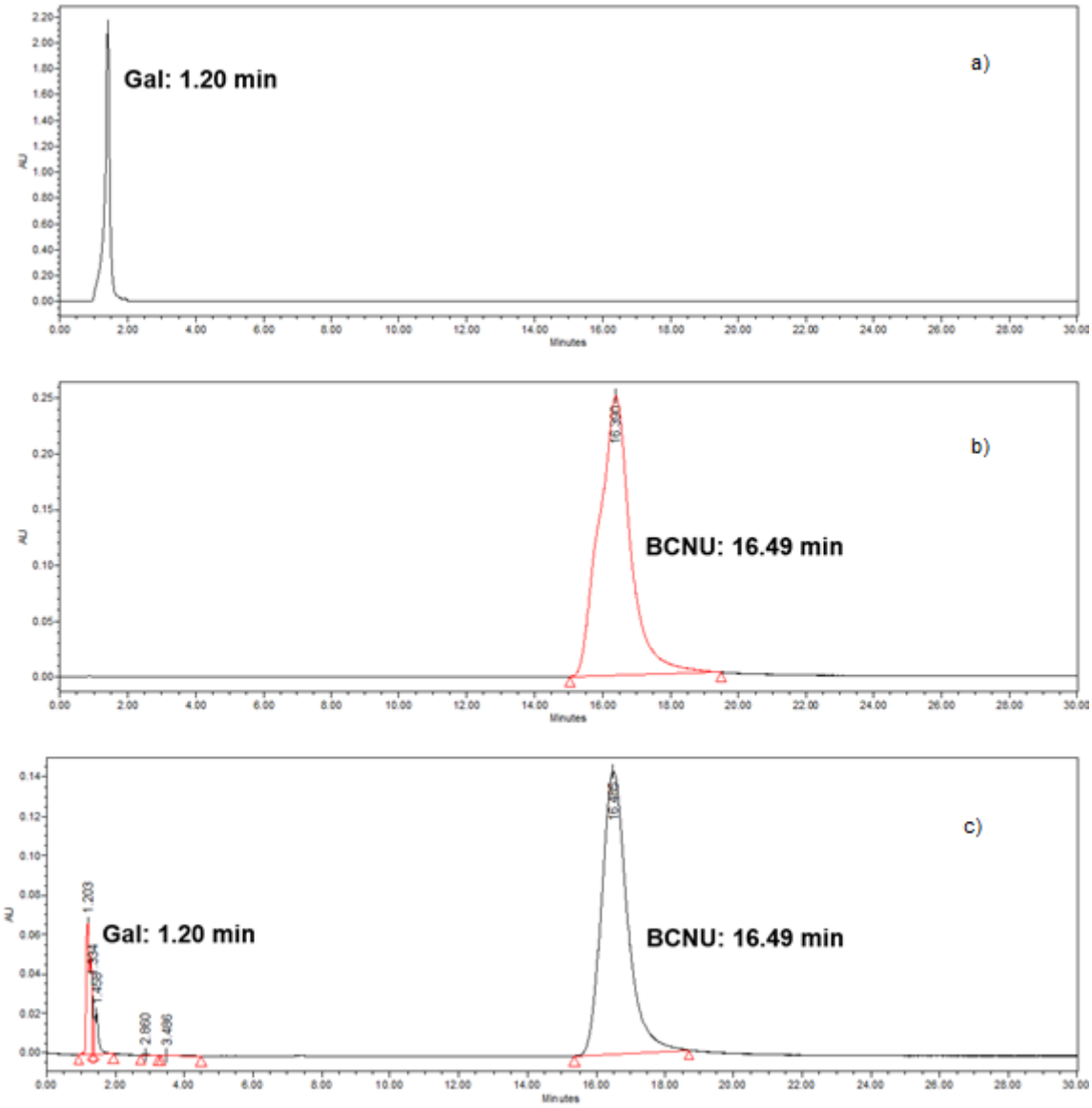

Figure 6.7: Typical chromatogram depicting a) the spiking CSF separation of the Gal, b) BCNU and c) the separation of both Gal and BCNU after CSF extraction.

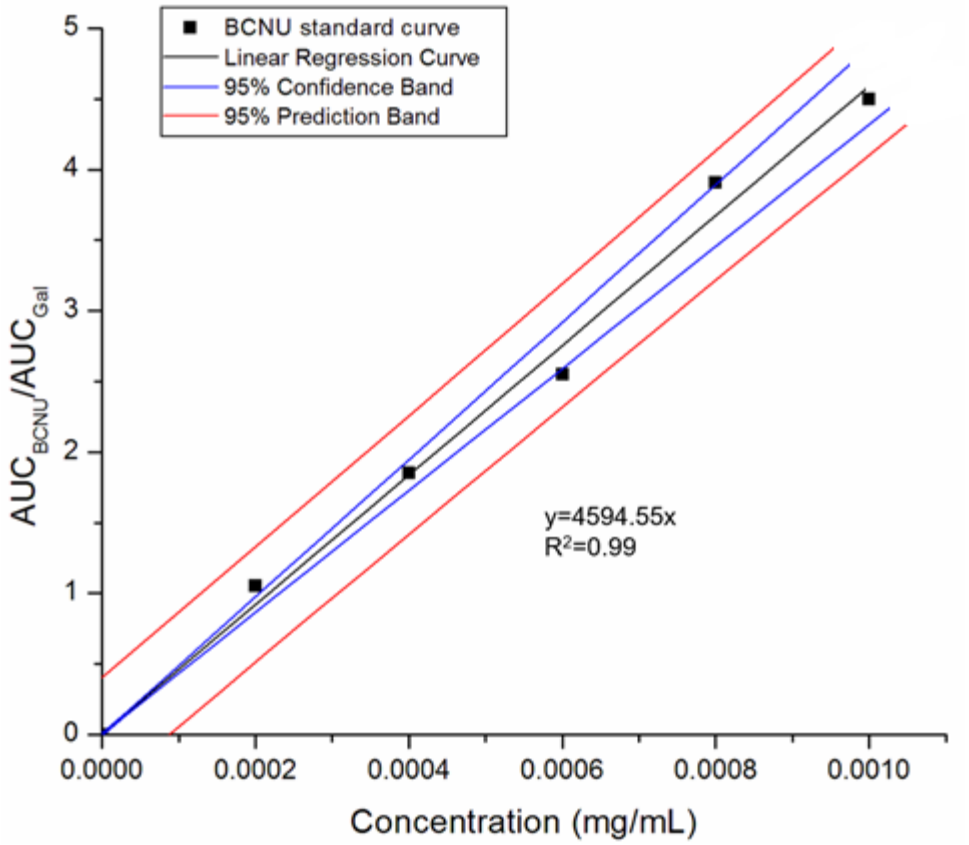

Figure 6.8: Calibration curve of BCNU at 230nm.

6.3.3. Concentration of BCNU in the blood, CSF and brain tissue of the rabbit model

The concentration of BCNU in plasma, CSF and brain were computed using the calibration curve generated from the area under the curve of BCNU/Gal ($AUC_{BCNU/Gal}$) with reference to the calibration curve. Figure 6.9 shows the Mean BCNU concentration-time profile in plasma simultaneously compared after IV injection, IN administration with and without application of ES and MF. The curve displayed a high concentration of BCNU in the plasma for IV administration compared to IN administration with or without the application of ES and MF. The C_{max} for BCNU after 30 minutes of IV and IN administration (with and without application of ES and MF) are 0.5843, 0.0789 and 0.0199µg/mL, respectively. The plasma concentration of BCNU was slowly diminishing until around 6 hours when the concentration became nil. The plasma concentration of BCNU for IN administration of Nanogel Composite with application of ES shows a steady low and high display of concentration peaks, this is due to the electro-actuation which

brought about release of BCNU-NCP which increases BCNU concentration in the plasma and reduces to minimum when there is no application of ES, this occurs in an “on-off” pulsatile fashion. However, with IN administration of BCNU-NCP, the plasma concentrations of BCNU were more than 10 times lower than following IV. The plasma concentration of IN administration of Nanogel Composite without the application of ES shows the lowest plasma concentration, there is insignificant release of BCNU-NCP; this is due to non-application of ES to release the BCNU-NCP.

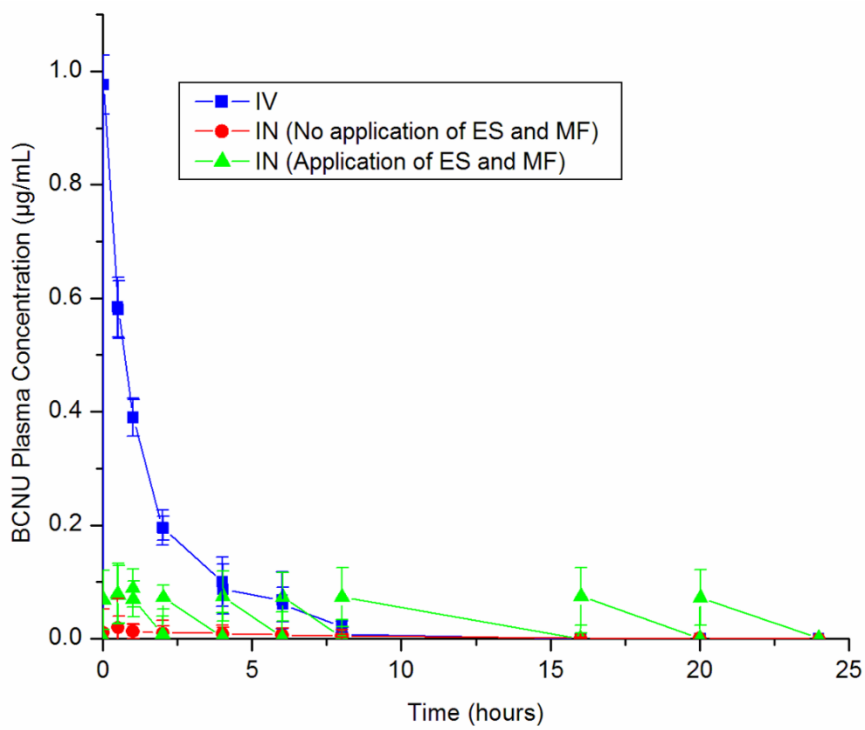

Figure 6.9: Mean BCNU concentration-time profile in plasma after IV injection of the conventional BCNU, IN administration of Nanogel Composite without application of ES/MFand IN administration of Nanogel Composite with the application of ES/MF (SD≤ 0.053; N=5 at each time point).

The BCNU concentration-time profile in CSF after IV injection, IN administration (with and without ES and MF application) is displayed in Figure 6.10. It can be observed that the concentration of BCNU in CSF is the highest for IN administration with the application of both ES and MF. A steady state profile can be observed for this administration with an “on-off” pulsatile switching. The average release of BCNU in the CSF per electro-actuation was observed to be 0.2819µg/mL. The BCNU-NCP was released upon electro-actuation. The released

BCNU-NCP was rapidly transported to the CSF with the aid of the MF through the olfactory pathway to increase the BCNU concentration at each pulsatile release of the nanoparticles from the Nanogel Composite brought about by the ES. The IV and the IN without ES and MF application have the lowest concentration. For the IV, the BCNU has to pass to the CSF through the systemic pathway, this pathway is challenged by Blood CSF Barrier (BCB), which tends to block the drug from passing into the CSF and thereby drastically reducing bioavailability in the CSF, however some of the drugs were able to cross to the CSF as seen in the profile curve. For the profile of IN without the application of ES and MF, there was insignificant concentration of BCNU in comparison to when there is application of ES. This may be explained by the fact that BCNU-NCP is not being significantly released due to non-application of ES. Figure 6.11 shows the percentage of BCNU released in the CSF for IN when there is application of ES and MF. The profile illustrated the concentration of BCNU in the CSF for over a 24-hour period.

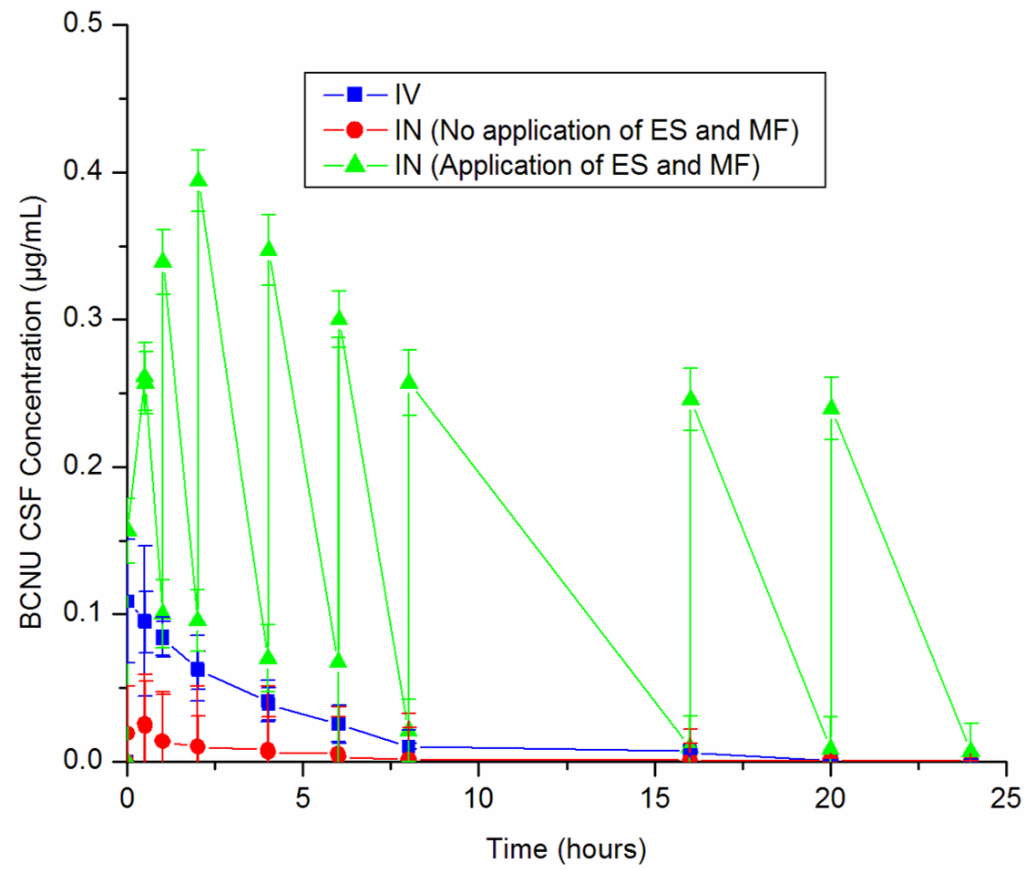

Figure 6.10: Mean BCNU concentration–time profile in CSF after IV injection of conventional BCNU, IN administration of Nanogel Composite without application of ES and IN administration of Nanogel Composite with the application of ES and MF at 1mg/kg dose in rabbits. (SD≤ 0.051; N=5 at each time point).

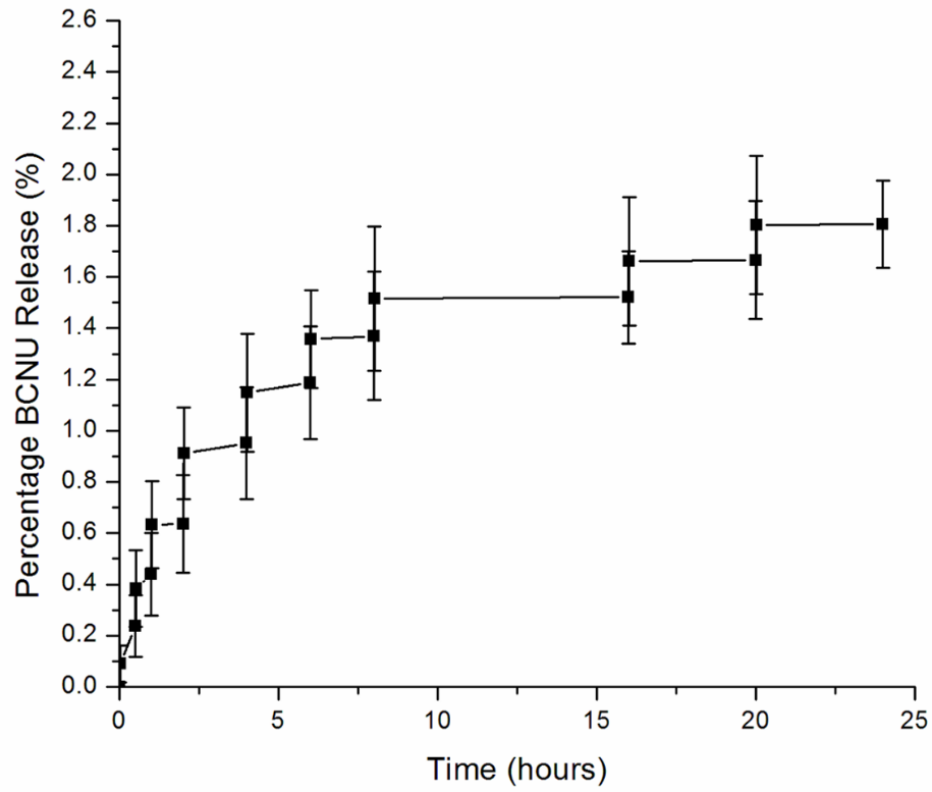

Figure 6.11: Percentage of BCNU released in CSF following IN administration. (SD≤ 0.051; N=5 at each time point).

The BCNU concentration-time profile in brain tissue after IV injection, IN administration (with and without ES and MF application) is shown in Figure 6.12. Here, the concentration of BCNU for IN administration with the application of ES and MF displayed the highest concentration in the brain; this mechanism is similar to that explained in the CSF profile. The average concentration of BCNU in the brain per electro-actuation was 0.1968µg/g. It can be seen from the concentration-time profile that the C_{max} of 0.00776µg/mL BCNU for IV was attained in less than 2 min after IV and gradually diminishes to nil. The concentration of BCNU for IN administration of Nanogel Composite with application of ES and MF was approximately constant through the duration of 24 hours. This is advantageous because the BCNU was available in the brain with increased bioavailability. The brain concentration of BCNU for the IN without application ES is the lowest and it is insignificant in comparison to when there is application of ES and MF.

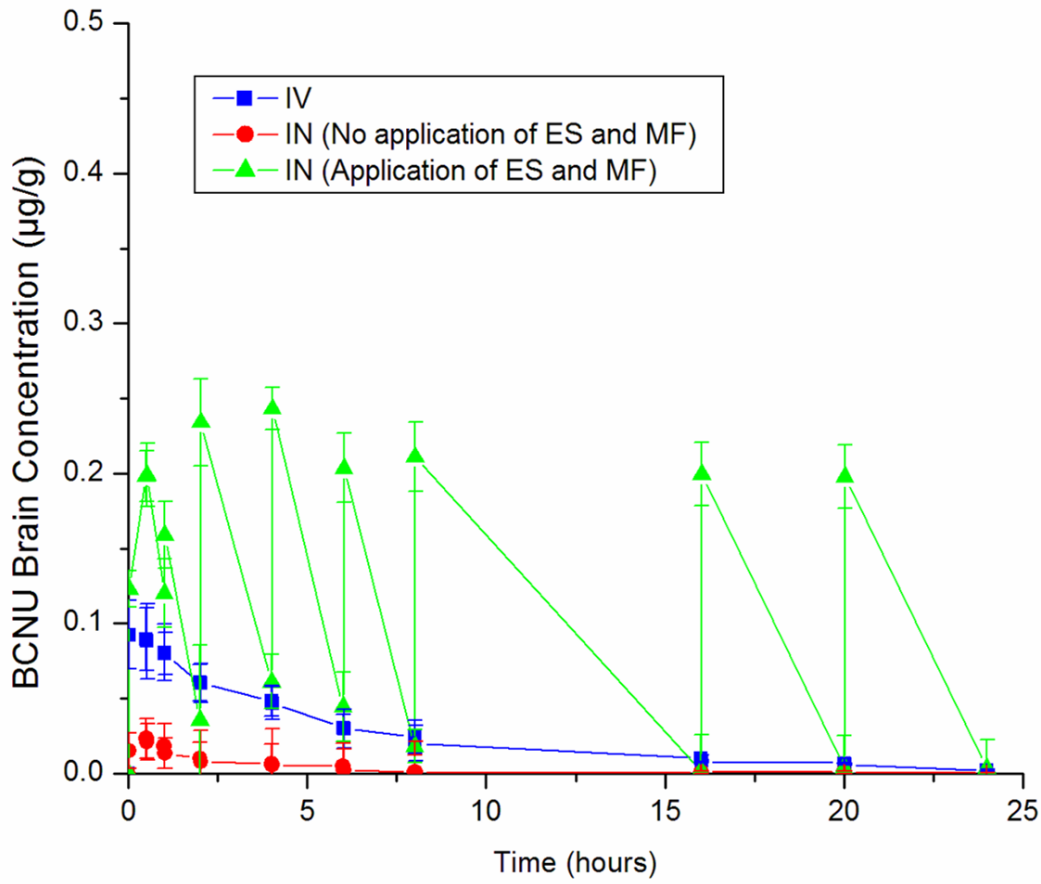

Figure 6.12: Mean BCNU concentration–time profile in Brain after IV injection of the conventional BCNU, IN administration of Nanogel Composite without application of ES and IN administration Nanogel Composite with the application of ES and MF at 1mg/kg dose in rabbits. (SD≤ 0.05; N=5 at each time point).

One of the important reasons for these *in vivo* studies is to identify the superiority of the novel Nanogel Composite over the conventional BCNU available on the market, to prove that IN administration of Nanogel Composite with the application of ES and MF, may aid in increasing bioavailability of BCNU in the brain and CNS through an “on-off" pulsatile controlled release of therapeutics for a direct nose-to-brain drug delivery. In order to prove this concept, comparison of BCNU concentration in plasma, CSF and brain tissue was further examined and analyzed when the mode of administration is IV, IN with or without ES and MF. Figure 6.13 shows the BCNU concentration in Plasma, CSF and brain tissue after IV injection for a period of 24 hours. From the results, it can be observed that the concentration of BCNU is the highest in the plasma with a concentration approximately 9-fold more compared to that of CSF and brain. The implication of this is that less drug is getting into the the CSF and brain; this may be due to the

BBB which prevents drugs from penetrating the brain, thereby providing low bioavailability of BCNU in the brain, thereby providing low bioavailability of BCNU in the brain. However, IN administration of Nanogel Composite with application of ES and MF demonstrated a high concentration of BCNU in the CSF and the brain as shown in Figure 6.14. The BCNU concentration in the CSF, brain and plasma are 0.2571µg/mL, 0.199µg/g and 0.0078µg/mL after 30 minutes, respectively, and 0.2395µg/mL, 0.1979µg/g and 0.0072µg/mL after 24 hours respectively.

Figure 6.15 depicts the BCNU concentration in the plasma, CSF and brain tissue after lN administration without the application ES and MF. The results are 0.0078µg/mL, 0.0087µg/mL and 0.0076µg/g in plasma, CSF and brain, respectively. These values are considered to be low in comparison to the values obtained when ES and MF were applied, this can be explained by taking into consideration the ability of Nanogel Composite to release BCNU-NCP only if there is application of ES and in this case there was none. Therefore, the insignificant quantity of BCNU-NCP released was due to the BCNU-NCP that were leached out from the surface of the Nanogel Composite. This observation also confirms the effectiveness of the electro-actuation in releasing the BCNU-NCP from the Nanogel Composite on application of ES.

The aim of this novel drug delivery system is to enhance drug bioavailability to the brain; our device shows that BCNU reaches the brain in much higher quantity and displayed efficient bioavailability compared to the conventional BCNU. Furthermore, there is a steady concentration of BCNU in the CSF and brain at an appropriate level throughout the duration of 24 hours. Figure 6.16 further clarifies the superiority of the novel delivery system as it illustrates the BCNU concentration in CSF and the brain following IV administration of the conventional BCNU and IN administration of Nanogel Composite with the application of ES and MF. The results demonstrated that the novel drug delivery system has the ability to keep the concentration of BCNU constant through the 24-hour duration as compared to the conventional drug which diminishes with time. The average BCNU concentration in the CSF provided by the novel drug delivery is approximately 6 times more than that provided by the conventional drug. Furthermore, there is a

constant bioavailability for the period of 24 hours. This is a tremendous advantage over the conventional drug.

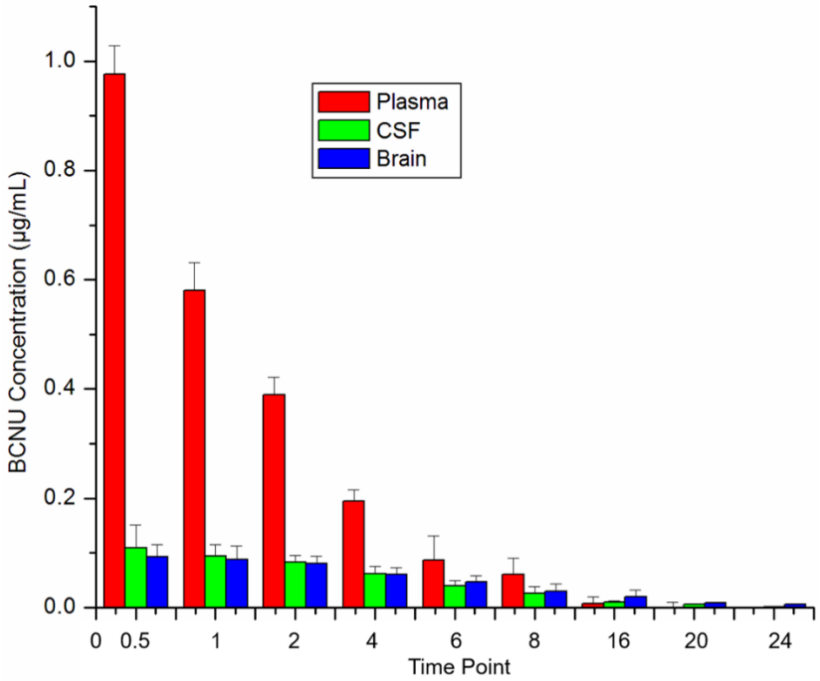

Figure 6.13: BCNU concentration in the Plasma, CSF and Brain tissue after IV injection of conventional BCNU.

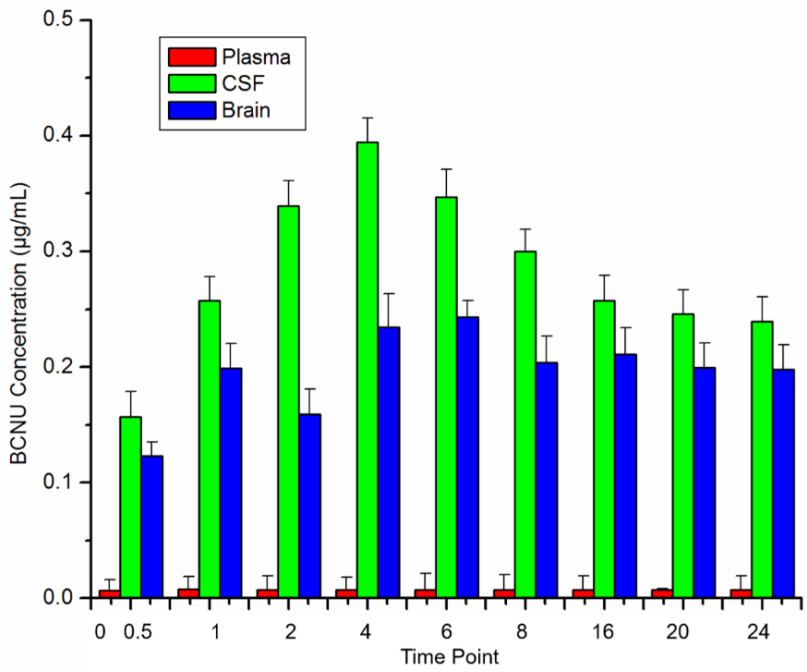

Figure 6.14: BCNU concentration in the Plasma, CSF and Brain tissue after IN administration of Nanogel Composite with application of ES and MF.

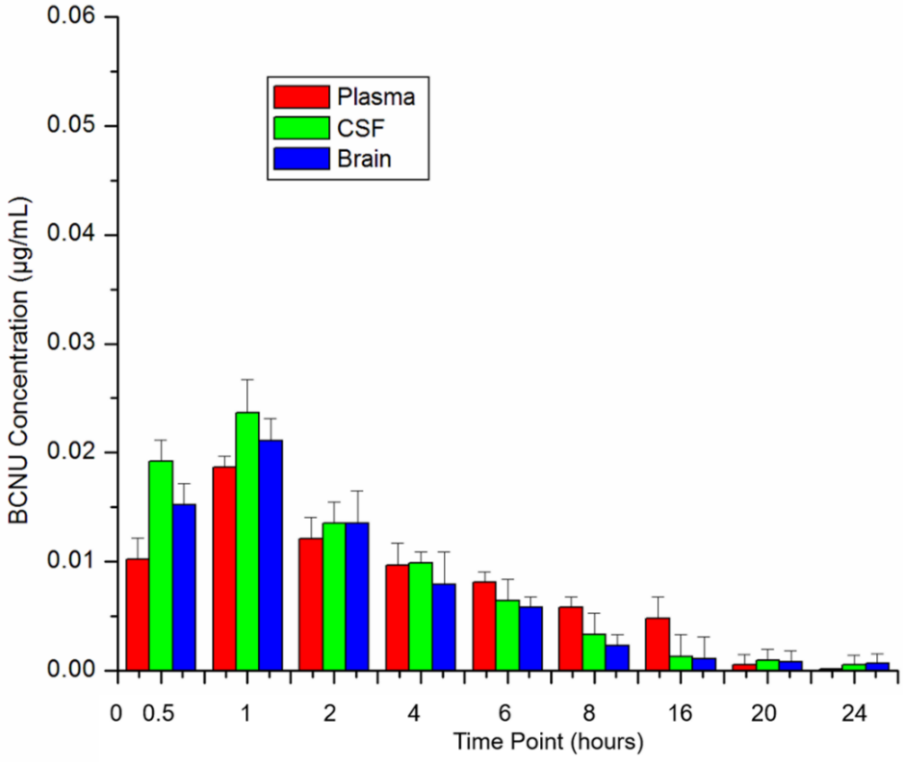

Figure 6.15: BCNU concentration in the plasma, CSF and brain tissue after IN administration of Nanogel Composite without application of ES and MF.

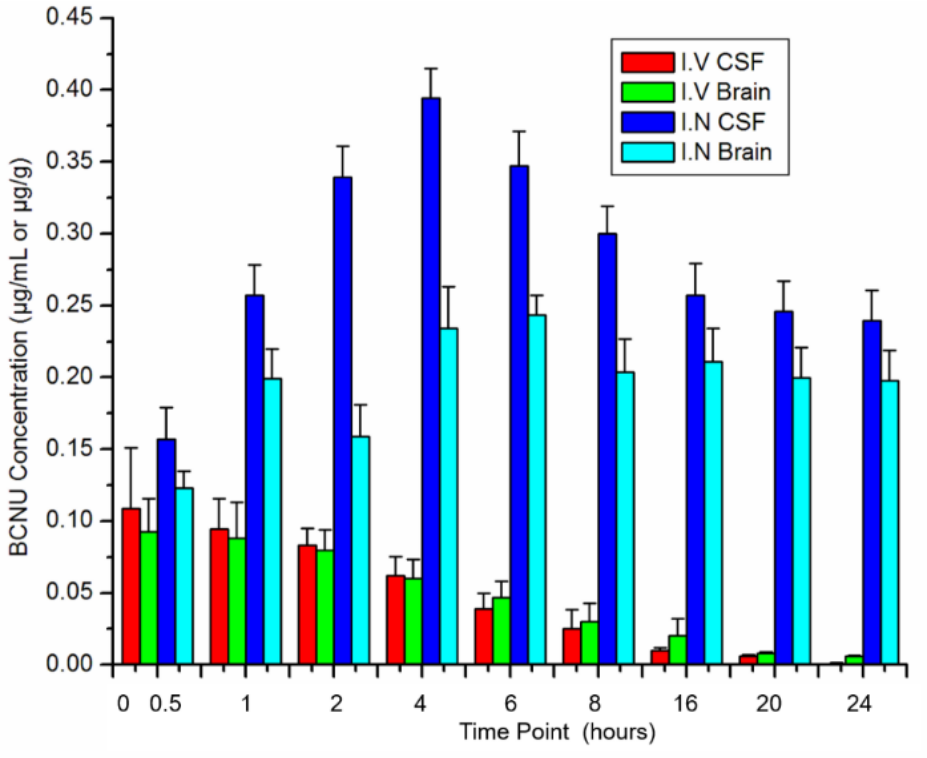

Figure 6.16: Comparison of the concentration of BCNU in CSF and brain following IV of conventional BCNU and IN administration of Nanogel Composite with application of ES and MF.

6.3.4. Assessment of BCNU-NCP in the Brain Tissue Employing Field Emission Electron Probe Micro Analyzer (FE EPMA)

The determination of the presence of BCNU-NCP in the brain tissue after IN administration of Nanogel Composite and application of ES and MF was performed by qualitative analysis of iron content in the brain tissue. Figure 6.17 shows the spectrum obtained from the FE EPMA, the spectra display peaks that belong to Fe at 0.6 and 6.4keV. This result is a confirmation of that Fe which is the core component of BCNU-NCP is present in the brain of the rabbit following IN administration Nanogel Composite. It can therefore be inferred that BCNU-NCP was delivered to the brain via the olfactory pathway. The Fe peaks are highlighted in the spectra.

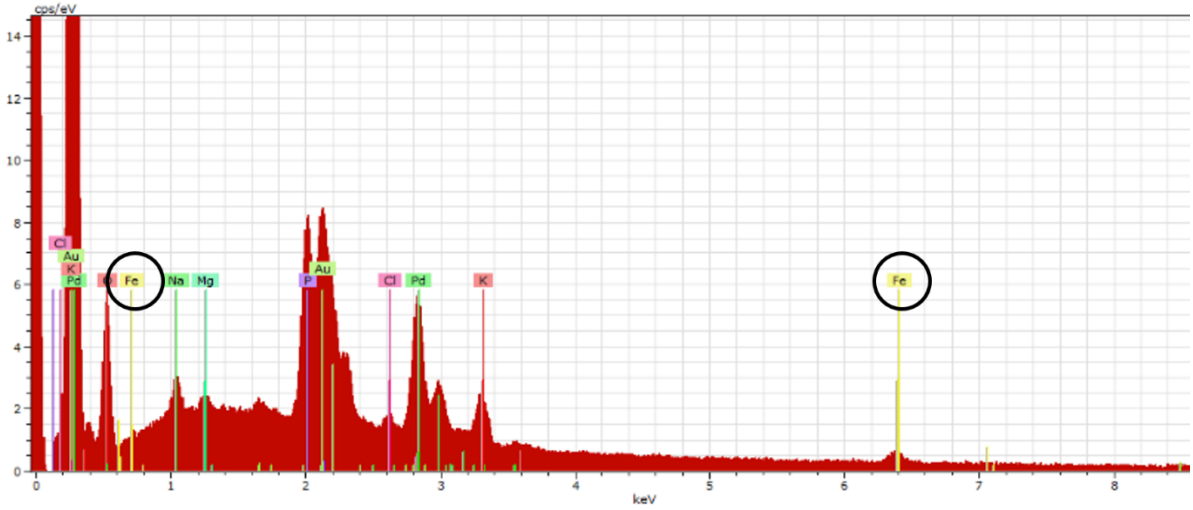

Figure 6.17: FE EPMA spectra of brain tissue of rabbit after IN administration of Nanogel Composite for Fe detection.

6.3.5. Histopathological Evaluation of the Nasal Epithelia of the Rabbit

Histopathological findings for the placebo, control and experimental group were carried out and the findings were compared to samples taken from normal healthy rabbit that was not dosed and was not exposed to ES and MF, to investigate the effect of Nanogel Composite on the nasal epithelial tissues and to evaluate the effect of application of ES and MF on the rabbit model. The microscopic digital image of the normal nasal epithelial tissue is shown in Figure 6.18a. The microscopic analysis of the placebo nasal tissue shows that the nasal turbinate and mucosal linings appear within normal limits. No sign of deformation, inflammation or necrosis was observed as shown in Figure 6.18b. For the control group, the microscopic analysis of the nasal tissue indicated that the nasal cavity contained multifocal, intraluminal amorphous, highly eosinophilic material surrounded by moderate degenerate heterophils and hemorrhage. The surrounding nasal epithelium was necrotic and replaced by macrophages and heterophilic infiltration. Moderate edema and hemorrhage was noted in the submucosa. Mild secondary lymphoid follicle development was also noted multifocally in the nasal submucosa as shown in Figure 6.18c.

The microscopic digital image of the experimental group demonstrated multifocal areas of moderate mucosal inflammation which was characterized by loss of the nasal epithelium and replacement by inflammation which consisted of

macrophages and heterophils. The adjacent lumen contained a few red blood cells and amorphous eosinophilic material. Other portions showed moderate submucosal heterophilic infiltration along with moderate edema and hyperemia with the development of a few secondary lymphoid follicles. An eosinophilic, roughly oblong object was also noted in the nasal cavity surrounded by degenerate heterophils as displayed in Figure 6.18d.

Examination of the nasal tissue showed an eosinophilic intraluminal material, which was found in both the control and the experimental groups. This observation may, however, represent the Nanogel Composite. Necropurulent rhinitis was also observed with moderate lesions noted in the control and experimental groups. This observation may be as a result of irritation of the rabbit to the test substance. No lesions were observed in the placebo group which is an indication that the application of ES does not have any effect on the histopathology of the rabbit's nasal epithelial tissue. Mild and minimal lesions were present in rabbits belonging to the experimental group. It can therefore be concluded that, Nanogel Composite administered intranasally with the application of both ES and MF, has no serious detrimental effect on the nasal epithelial tissues of the rabbits.

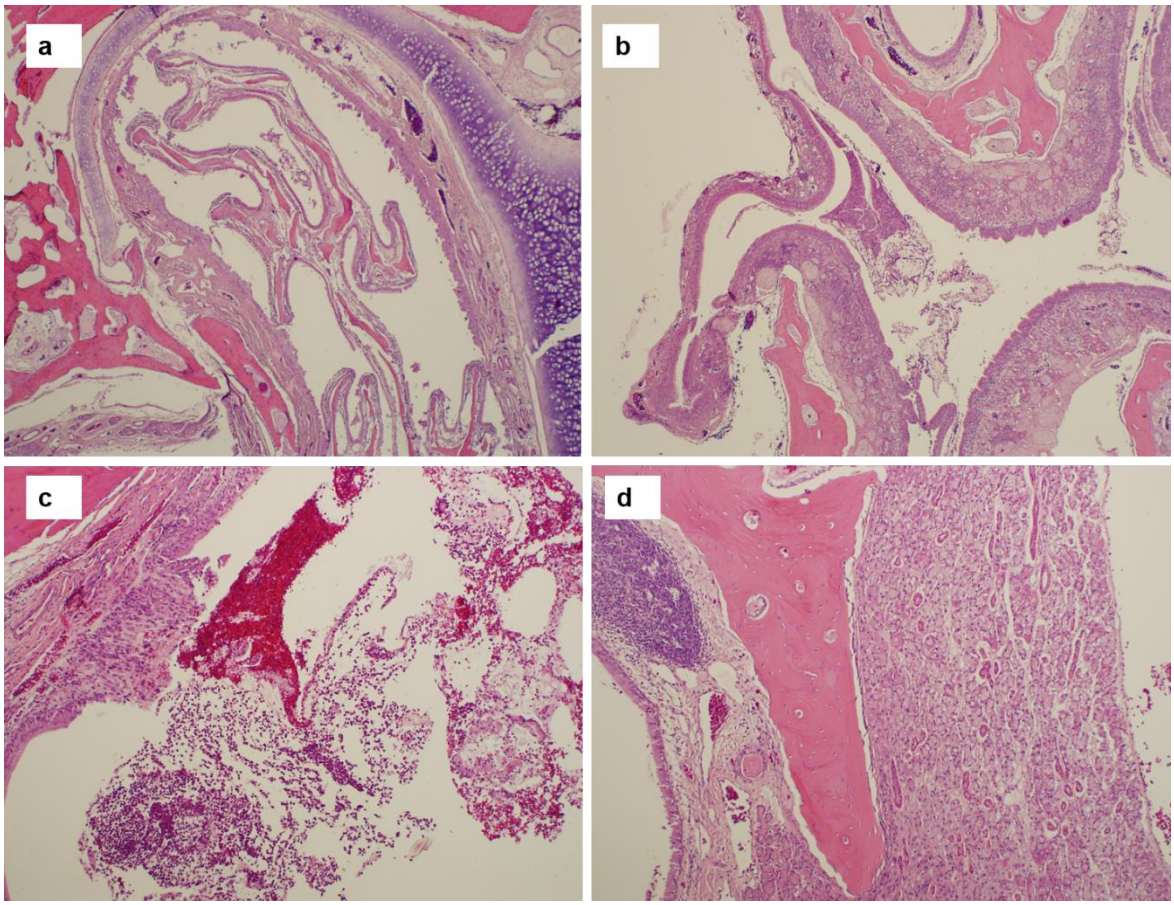

Figure 6.18: Histological evaluation of nasal epithelia tissue samples from rabbits showing light digital microscopic images of the H&E stained slides of a) normal nasal epithelia tissue, b) placebo sample, c) control group sample and d) experimental group sample. Magnification is x10.

6.4. CONCLUDING REMARKS

The novel drug delivery system formulated has been proven to be more superior than the conventional drug which was administered intravenously. The *in vivo* studies demonstrated greater concentration of BCNU in CSF and the brain of the rabbit delivered via the olfactory route for the novel drug delivery system compared to the conventional drug. The novel drug delivery system was found to be 6 times more efficient in delivering therapeutics to the brain and CSF, thereby circumventing the BBB and permitting high bioavailability of drug to the brain. The ES was found to control the release of drug in a pulsatile “on-off” manner and the MF in the form of a magnetic headband on the rabbit head was able to attract the nanoparticles to the brain by quickly transporting them across the olfactory region

to the brain and CSF following the release brought about by the ES. The delivery system was found to be easily administered, the application of 5V ES, and the application of 0.4 Tesla were found to be safe to the animal. The applications of electrodes on the nose of rabbit as well as the magnetic headband on the rabbits were successful without posing any discomfort to the rabbits. The microscopic examination of the nasal epithelial tissue following euthanization of the rabbits revealed that there were minimal and mild lesions on the nasal epithelial tissue. These findings indicated that the Nanogel Composite is biocompatible and suitable as a nasal formulation. It can therefore be concluded that the novel drug delivery system is non-toxic to the rabbits.

REFERENCES

Bojsen-Moller, F., Fahrenkrug, J., 1971. Nasal swell-bodies and cyclic changes in the air passage of the rat and rabbit nose. J. Anat. 110, 25–37.

Boon, V., Glass, B., Nimmo, A., 2006. High-Performance Liquid Chromatographic Assay of Indomethacin in Porcine Plasma with Applicability to Human Levels. J. Chromatogr. Sci. 44, 41–44.

Ho, W.-C., 2015. Self-Administered Electrical Therapy for Treatment of Nasal Polyps and Allergic Rhinitis. Am. J. Biomed. Eng. 5, 31–33.

Joshi, S., Wang, M., Etu, J.J., Suckow, R.F., Cooper, T.B., Feinmark, S.J., Bruce, J.N., Fine, R.L., 2007. Transient cerebral hypoperfusion enhances intraarterial carmustine deposition into brain tissue. J. Neurooncol. 86, 123–132.

Lerner, E.N., van Zanten, E.H., Stewart, G.R., 2004. Enhanced delivery of octreotide to the brain via transnasal iontophoretic administration. J. Drug Target. 12, 273–280.

Liu, L.H., Refojo, M.F., Ni, C., Ueno, N., Albert, D.M., 1983. Sustained release of carmustine (BCNU) for treatment of experimental intraocular malignancy. Br. J. Ophthalmol. 67, 479–484.

Traystman, R.J., 2003. Animal Models of Focal and Global Cerebral Ischemia. ILAR J. 44, 85–95.

Vaiman, M., Shlamkovich, N., Eviatar, E., Segal, S., 2004. Treatment of nasal valve collapse with transcutaneous and intranasal electric stimulation. Ear. Nose. Throat J. 83, 757–62, 764.

Ved, P.M., Kim, K., 2011. Poly(ethylene oxide/propylene oxide) copolymer thermo-reversible gelling system for the enhancement of intranasal zidovudine delivery to the brain. Int. J. Pharm. 411, 1–9.

CHAPTER 7

RECOMMENDATIONS AND FUTURE OUTLOOK

7.1. RECOMMENDATIONS

Brain diseases are highly difficult to treat due to the Blood-Brain Barrier (BBB). The current therapeutic interventions employed in managing these ailments are challenged with low bioavailability in the brain. Brain tumors for example, are currently treated with an invasive method which involves surgery and implants, in addition to IV injection. A novel Nano-co-Plex was synthesized, loaded with carmustine (BCNU); an effective brain tumor therapeutic, characterized employing techniques such as FTIR, XRD, NMR, TGA, SQUID, TEM and Zetasizer analysis. The Nano-co-Plex was found to be paramagnetic and responded adequately to MF. These nanoparticles have high drug loading capacity and the *in vitro* drug release profile was found to be appropriate.

The BCNU-loaded Nano-co-Plex synthesized was incorporated into a novel thermosensitive electro-responsive mucogel for potential stimuli controlled nose-to-brain drug delivery. This formulation (Nanogel Composite) was optimized employing a Box-Behnken Experimental Design and characterized for its rheological properties, its *in situ* gelling behavior, electroactiveness, mucoadhesiveness, porosity, surface morphology and *in vitro* release of the Nano-co-Plex upon application of electric stimulation in a controllable “on-off” pulsatile release. The BCNU-Nano-co-Plex was found to be highly toxic to tumor cells compared to the conventional drug, as demonstrated by the outcome of the cell work carried out using human glioblastoma A170 cell lines, and was non-toxic to normal brain cells demonstrated by evaluating PC 12 neuronal cell lines. Internalization of the BCNU-Nano-co-Plex was found to be enhanced by the application of MF.

The *ex vivo* test revealed an enhanced permeation of Nano-co-Plex through the nasal epithelial tissue of New Zealand white rabbit model when there was

application of a magnetic stimulus. Similarly, the *in vivo* studies were performed by employing New Zealand white rabbits as an appropriate model for evaluating the Nanogel formulation. The *in vivo* studies delineated that intranasal administration of Nanogel Composite with the application of electric stimulus brought about by using electrodes on the rabbit's nose released BCNU-loaded Nano-co-Plex in a pulsatile release fashion followed by quick transport of the BCNU-loaded Nano-co-Plex released in the nasal mucosa directly to the brain of the rabbit with the aid of a magnetic headband placed on the rabbit. This action resulted in high concentration of BCNU in the brain and CSF of the rabbit thereby improving bioavailability of drug in the brain with notably lower concentrations in the plasma. *In vivo* comparison of this system with the IV administration of the conventional BCNU indicated a very low concentration BCNU in the brain and CSF and a high concentration in the plasma. These results clearly demonstrated that this novel delivery system is superior to the conventional drug administered via IV. Furthermore, this delivery system is non-invasive and may therefore be a promising replacement of the highly invasive implant currently employed in the treatment of brain tumors.

This research involves the synthesis of drug-loaded nanoparticles with the nanoparticles incorporated into a novel *in situ* thermosensitive elecro-responsive mucoadhesive gel. Both the drug-loaded nanoparticles and the gel were extensively characterized followed by *in vitro*, *ex vivo* and *in vivo* studies. The Nano-co-Plex synthesized has the capability and capacity to load other drugs which may be used for the management of other brain diseases. For example, Galantamine can be loaded into the Nano-co-Plex. The Nano-co-Plex is a positively charged entity; the positively charged amine group can form ionic interaction with the OH and the CH_3-O- of the galantamine. There is also the possibility of H-bonding of Gal with the Nano-co-Plex as shown in the Figure 7.1 which may form stable interactions for loading of Gal into the Nano-co-Plex.

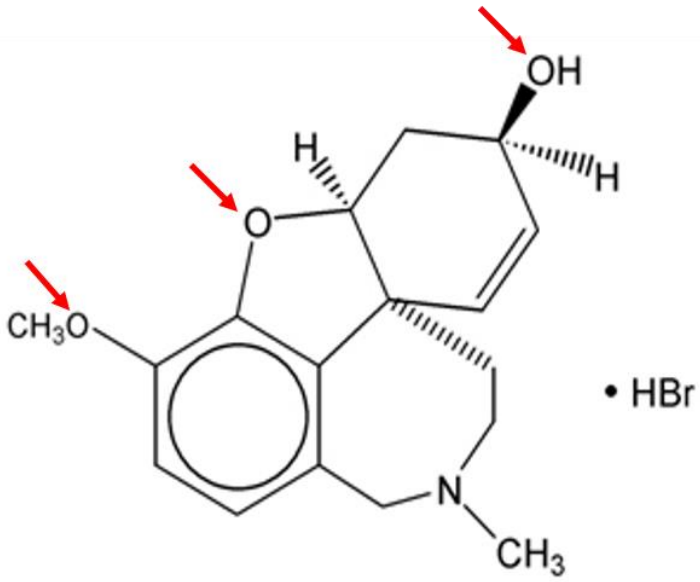

Figure 7.1: Molecular structure of Galantamine

Furthermore, the *in vivo* study was carried out as a proof of concept, to observe the effect of electric and magnetic stimuli on the release and transportation of the nanoparticles into the brain via a direct nose-to-brain pathway. This study can be advanced by inducing tumor growth in the animal model and the novel delivery system applied in order to further explicate the efficacy of the delivery system.

7.2. FUTURE OUTLOOK

The *in vivo* studies proved the workability of the Nanogel Composite starting from its intranasal administration to its *in situ* gelling capability in the nasal mucosa, the release of the drug loaded magnetic nanoparticles by electric stimulation and the quick transportation of the drug-loaded nanoparticles across the nasal epithelial tissue with the aid of a magnetic stimulus for direct nose-to-brain drug delivery. This *in vivo* study was carried out by employing the application of electrodes to discharge 5V of ES on the nose of the rabbit and a magnetic headband to deliver 0.4 Tesla of magnetic stimulus to attract the drug-loaded nanoparticles to the brain. In future the electrodes and the magnetic headband may be replaced by an eye glasses where the nose pads of the glasses may represent the electrodes and the top bar of the glasses may represent the magnet which may be fabricated to have a microchip that can be modulated from a cellular device, to actuate the

release of drug in a controllable manner while the magnet will target and transport the released drug to the brain. This may be a future technological advancement of this novel drug delivery system.

7.2.1. Hypothesis: Lactoferrin-Galantamine Proteo-Alkaloid Conjugate for The Management of Alzheimer's Disease

As part of the future outlook of this project, a Lactoferrin-Galantamine Proteo-Alkaloid Conjugate for the management of Alzheimer's Disease was hypothesized.

7.2.1.1. Introduction

Alzheimer's disease (AD) is the most common cause of dementia which affect mostly elderly people, and it is connected to the loss of cholinergic neurons in parts of the brain (Arendt et al., 2015). AD is one of the most severe neurodegenerative disorders. Approximately 13% of people who are 65 years and above are affected by this disorder in the United States alone (Tsai and Madabhushi, 2014) and is the sixth leading cause of death for people with ages 65 years and above (Alzheimer's Association, 2012). It is projected that by 2050, there will be almost one million new cases per year. Furthermore, it is expected that there will be remarkable increase in the number of people with AD who are 85 years and above across all racial and ethnic groups. AD is characterized by loss of memory in the patient wherein the patient finds it difficult to remember things that are learnt recently coupled with failure of acquiring new information (Arnáiz and Almkvist, 2003; Bäckman et al., 2004). The symptoms noticeable at the early stage include difficulties in reasoning, effective planning, attentiveness, as well as conceptual thinking. Episodic, semantic and implicit memories are less affected than new facts and memories (Carlesimo and Oscar-Berman, 1992). Progressively, the patient is unable to perform most common activities of daily living such as speech, reading and writing.

The cause of AD is associated with genetic heritability (Wilson et al., 2011) as well as cholinergic (Babic, 1999), amyloid and tau hypotheses. However, it is widely believed that advanced age is the major risk factor of AD. The genetic factor is brought about by gene mutations on chromosome 21 in the β-amyloid precursor

protein (APP) which are responsible for early-onset of AD in family that has history of the disease (Hardy and Allsop, 1991; Munoz and Feldman, 2000). The Cholinergic hypothesis proposed that AD is caused as a result of reduction in the synthesis of neurotransmitter acetylcholine (Contestabile, 2011). Protein misfolding disease is a characteristic of AD caused by the accumulation of deformed beta amyloid (Aβ) which results in senile plaques and also the accumulation of hyper phosphorylated tau proteins in the brain resulting into formation of neurofibrillary tangles. The aggregation and accumulation of these plaques and tangles in the brain have become the most prominent culprits of AD (Ittner et al., 2010; O'Brien and Wong, 2011; DeSai et al., 2014).

Iron is extremely reactive and in high concentration can lead to neuronal death (Raven et al., 2013). Iron is known to be so important in the mammalian cells for metabolism and oxygen transport (Oshiro et al., 2011), in excess may cause tremendous damage to the cells by generating free radicals and thereby causing oxidative stress which in turn triggers destructive effects that result in AD and other neurodegenerative disorders in general (Huang et al., 2014). *Ex vivo* and *in vivo* studies have shown and established an increase in brain iron in AD patients (Lovell et al., 1998; Castellani et al., 1999; Duce et al., 2010; Raven et al., 2013; Huang et al., 2014). The presence of elevated oxidative stress due to oxidation of iron has been confirmed in the brain of AD patients (Smith et al., 1997). More recently, Raven *et al*. (Raven et al., 2013) established that increased iron resulted in tissue breakdown associated with AD. They used an MRI technique to measure the amount of brain iron in 31 AD patients and 68 healthy subjects as control. They compared the results from the hippocampus and thalamus parts of the brain; their findings suggested strongly that iron accumulation is a possible cause of AD. From the evidences of various researches, it is therefore pertinent to infer that deposition and accumulation of iron in the brain is a center point of all the neuro-pathological operations which is not limited to amyloid plaques, tau phosphorylation as well as oxidative stress in AD. There is adequate evidence to pin down interaction of Aβ and transition metal especially neocortical iron as the culprit in initiating and causing the toxicity observed in AD (Ghribi et al., 2006; Bonda et al., 2012; Mufamadi et al., 2012; Ayton et al., 2013; Chitra et al., 2013).

7.2.1.2. The hypothesis

Several therapeutics have been researched, proposed and prepared for the treatment of AD, many of which have reached clinical trials and found to be ineffective due to some of the reasons enumerated above and are possibly discontinued because of their failure. Galantamine (Gal) is one of the therapeutic that has a success story and approval to be used for the treatment of AD. Even then it has not been found to be effective in treating the disease, which may be due to other factors such as accumulation of iron in the brain and free radical generation that accompanies the ailment. Combination of Gal and an iron chelator may be a promising strategy for dealing with this situation in order to obtain a more potent approach to the treatment of AD. In this study we propose the combination of free radical generation and the metal chelator approach to synthesize a single dosage form to manage effectively AD through “Proteo-Alkaloid” conjugate of Lactoferrin (Lf) and Gal. This is proposed to serve as “Neuroprotective-Neurotherapeutic” agent. We therefore propose Gal and Lf conjugate as a novel treatment for AD. This approach will act as both a neuroprotective as well as neurotherapeutic intervention.

7.2.1.3. Evaluation of the hypothesis

The successful management and treatment of AD has remained elusive despite much research that have been carried out and those that are still ongoing. Researchers are constantly looking for effective therapy to deal with and manage this neurodegenerative disorder. Quite a number of drugs with different mechanisms of action and targets are available and many are still under development for the management of AD. The strategies involved in making these drugs are based on firstly the amyloid hypothesis which delved into the reduction of Aβ production, its clearance and aggregate blocking (Kumar et al., 2011). Due to the connection of Aβ to AD, extensive clinical trials have been carried out with drugs designed to target this peptide in a way to absolutely prevent the production of Aβ plaques. These drugs are still inefficient in preventing the cognitive decline in AD patients (Ayton et al., 2013). Nonsteroidal anti-inflammatory drugs (NSAIDs) such as diclofenac (Scharf et al., 1999), rofecoxib (Aisen et al., 2003) and indomethacin (Bernardi et al., 2012) have been suggested to reduce the risk of

developing AD; however the efficacy of these drugs have not been proven and in fact all of the therapeutics developed based on amyloid-β approaches that reached Phase III clinical trials were unsuccessful (Karran et al., 2011).

The second strategy is based on the cholinergic hypothesis which involves the use of choline esterase inhibitors capable of reducing the hydrolysis of acetylcholine. Therapeutic agents such as, Gal, rivastigmine and donepezil are examples of drugs developed based on the cholinergic approach (approved for the management of mild to moderate AD). The clinical profiles of these therapeutic compounds are somewhat successful. The use of these drugs for treating AD patients improves their cognitive functions and generally gives symptomatic relief to the patients, however the efficacy of these compounds is still very low because only about 35% of the patients respond positively to the treatments with these drugs (Giacobini, 2000). These compounds are also associated with serious side effects such as diarrhea, vomiting and nausea (Maelicke et al., 2010) which places them in an inconvenient state.

Our strategy focuses on lowering brain metal ions and targeting their interaction with Aβ peptide. Metal ions mediate generation of free radicals and thereby result in oxidative damage of the brain. Employing the administration of metallo-complex therapy is a new and promising therapy for AD. Fang Du *et al*. (2014) showed in their study that hepcidin considerably minimized brain iron in rats overloaded with iron. Desferioxamine is a chelator approved by the FDA for iron overload; this chelator has been known to offer some benefits in the treatment of AD. Deferiprone is another chelator that binds iron and aluminum ions, this was approved only in Europe. The use of chelators is however limited due to their inability to effectively cross the BBB and their being neurotoxic due to lack of elimination process of the metal-chelator complex from the brain (Liu et al., 2005).

7.2.1.4. Galantamine and Alzheimer's intervention

Galantamine hydrobromide is an alkaloid obtained from various plants such as *Galanthus caucasicus*, *Galanthus woronowii*, *Narcissus*, and *Lycoris* species. It is a neuroactive therapeutic agent approved by both the European Medicines

Agency (EMA) and USA Food and Drug Administration (FDA). Its primary function is to inhibit the activities of the enzyme, acetylcholinesterase; this enzyme hydrolyses the neurotransmitter acetylcholine followed by the cessation of synaptic transmission. The use of Gal prevents this reaction and thereby allows the survival of acetylcholine for normal neurotransmission function in AD patients. Recently, Traykova *et al*. in their *in vitro* experiment found that Gal compound is a scavenger of reactive oxygen species (ROS) (Traykova et al., 2014). Additionally, Gal may also form a complex with nicotinic acetylcholine receptors by binding onto it, and thereby improving phagocytosis of microglial amyloid-beta peptides (Fong Yen et al., 2015). However, its clinical function is limited by its low bioavailability in the brain due to the BBB. Furthermore, it is associated with numerous side effects when administered systemically (Mufamadi et al., 2013). Owning to its ability of scavenging free radicals, Gal may help to treat oxidative stress due to free radicals generated within the brain of AD patients and hence may act as a neurotherapeutic agent.

7.2.1.5. Lactoferrin and metal chelation

Lactoferrin is a glycoprotein that has a strong binding affinity for iron. This cationic iron-binding globular glycoprotein is a member of the transferrin family. It has a molecular mass of approximately 80 kDa and consists of 892 amino acids (van der Strate et al., 2001; Baker and Baker, 2005). It was first discovered in human milk (Montreuil et al., 1960) and it is also known to exist in body fluids such as saliva, tears, vaginal fluids, semen, bile, gastrointestinal fluids, urine, nasal and bronchial secretions (García-Montoya et al., 2012). Lf is made up of two homologous domains which are called N- and C-lobes; the two globular lobes are folded and connected by a short α-helix. N-lobe is made up of N1 and N2 sub-domain, likewise C-lobe is made up of C1 and C2 sub-domain with one iron site and one glycosylation site at each lobe (Baker and Baker, 2012). The N-lobe consists of amino acid residues 1–333 while the C-lobe consists of amino acid residues 345–692 (Carmona et al., 2014). The main function of Lf is transportation of iron to the cells as well as regulation of free iron in the blood and external secretions. Lf also serves as a vital component of the biological functions including an immunoregulatory role (Latorre et al., 2012), anti-inflammatory role (Yeom et

al., 2011) and most importantly the exertion of its antimicrobial functions against viral, fungal and bacterial pathogens (Sinha et al., 2013). Lf is also known to have an anticarcinogenic function (Ma et al., 2013) and it is a targeting molecule for improving brain delivery of therapeutic agents (Huang et al., 2008). The iron binding capability is what we are focusing on in this hypothesis as this can be exploited in the clearance of excess iron in the brain of AD patients.

7.2.1.6. Lactoferrin-Galantamine Proteo-Alkaloid conjugate

The current treatments for AD aside from not being very effective and their association with various side effects, is that they only give symptomatic relief of the disease and not total cure of the dementia. Therefore, a combination of two of these strategies in the form of a single dosage form may however be a promising and more effective way of treating AD. Lf has been conjugated with various compounds in other to increase its functionality. Nojima *et al*. conjugated Lf with branched polyethylene glycol (PEG) using N-hydroxysuccinimide coupling method in order to improve its half-life (Nojima et al., 2009). Additionally, Lf has been conjugated to pegylated nanoparticles to form Lf nanoparticles employing thiolation reaction (Hu et al., 2011, 2009). Furthermore, superparamagnetic iron oxide nanoparticles (SPION) have been conjugated to Lf by using NHS/EDC coupling chemistry to form Lf-SPION nanoparticles (Xie et al., 2011).

In this study, we propose to conjugate Lf to Gal by “Proteo-Alkaloid” conjugation method through the self-assembly functionality of Lf. It is proposed that Lf may encapsulate the Gal molecules within its physical structure holding the Gal molecules inside its cavity while the Lf molecules self-assemble to form a protective shell around the Gal molecule. Hydrogen bonding as well as van der Waals forces are predicted to contribute to the stability of the complex formation. The demonstration of this concept is illustrated in Figure 1. This technique may be applied in developing a dosage form. Lf in itself is known to be a ligand for brain targeting; this attribute will therefore aid the penetration of the therapeutic agent into the brain. When the conjugate is delivered into the AD patient’s brain, the release of the Gal will only happen when there is interaction of the conjugate with Fe^{3+} wherein the conjugate will open up and release the Gal molecules

encapsulated within the Lf molecule and at the same time Fe^{3+} is attracted to the Lf and be absorbed into it.

The mechanism of conjugation and release is shown in Figure 7.2, where the conjugate was prepared by self-assembly of Lf and upon sensing accumulation of Fe^{3+} liberates the encapsulated Gal. The release can be explained by the fact that Lf changes conformational structure whenever it interacts with Fe^{3+}. Lf deprived of Fe^{3+} is known as apo-lactoferrin while those that are saturated with iron are known as holo-lactoferrin. The transition from apo-lactoferrin to holo-lactoferrin which happens when Lf is in contact with Fe^{3+} results into conformational change accompanied with protease resistance (Takayama, 2011; Jameson et al., 1998). Therefore, when the conjugate is in a Fe^{3+} environment, the conjugate will change its structural conformation and thereby cause the encapsulation to open up. It is envisaged that this process will allow Gal to be released while Fe^{3+} are been absorbed into the Lf as it has a very strong affinity for Fe^{3+}. The implication of this process will result in Gal being released to stop the activities of the free radicals produced through iron-initiated oxidative stress and the Lf mops up the excess iron in the brain of the AD patient. This is a dual action intervention that offers both neurotherapeutic and neuroprotective advantage. Lf, due to its ability to capture excess iron in the brain, may help in mediating the production of free radical that might result into the generation of oxidative stress which may eventually lead into the death of neuronal cells. Furthermore, any free radical generated will be scavenged by the action of the Gal. The process of the generation of free radical by iron in the brain, the outcome of oxidative stress and the point at which Lf-Gal can mediate the process is shown in the schematic diagram in Figure 7.3. This hypothesized technique may be a promising future strategy for managing AD.

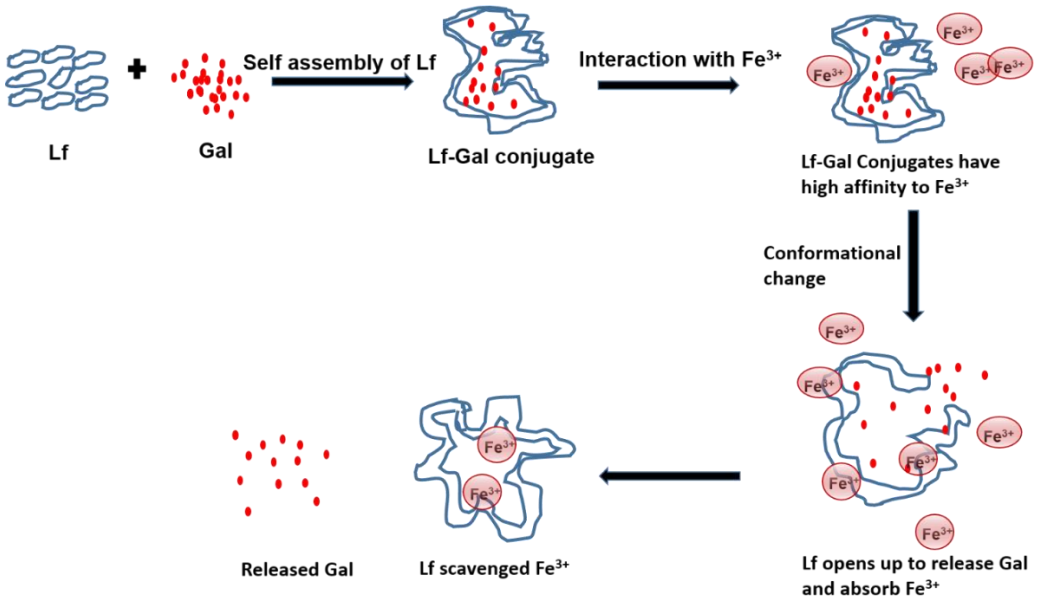

Figure 7.2: Schematic diagram of the mechanism of release of Galantamine and absorption of iron by Lf-Gal conjugate.

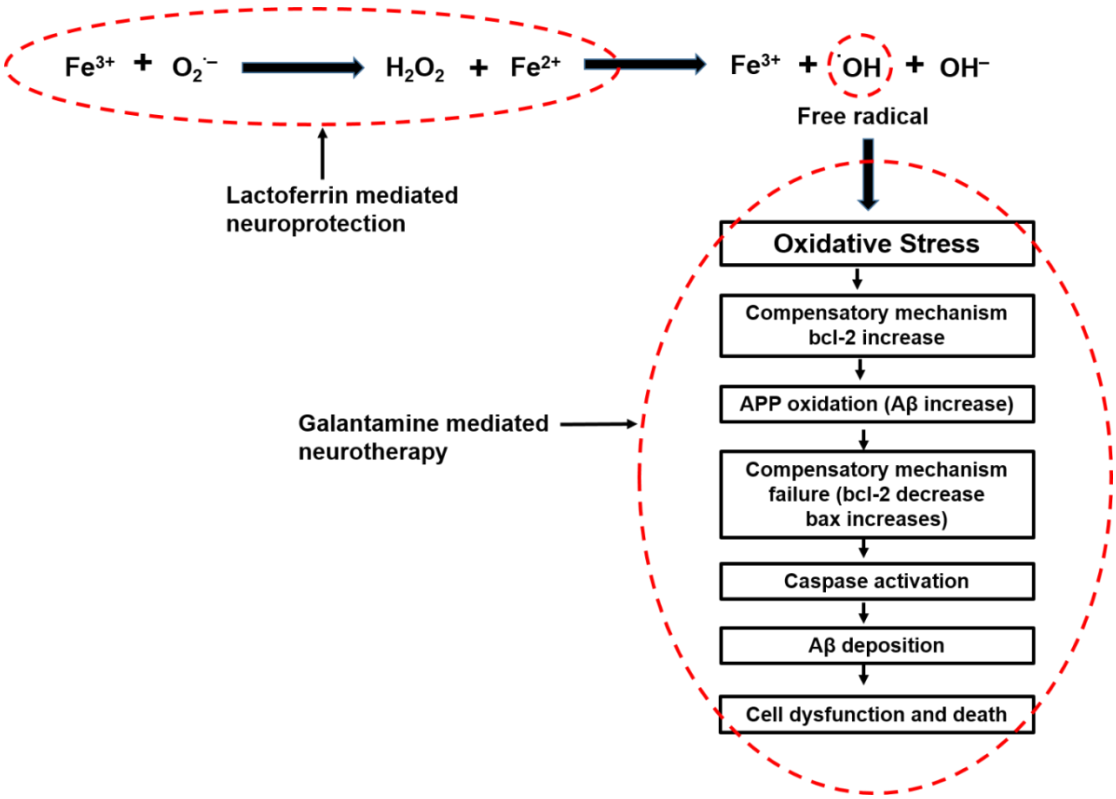

Figure 7.3: Schematic diagram demonstrating the potential neuroprotective-neurotherapeutic interventional mechanism of the lactoferrin-galantamine conjugate.

7.2.2. Concluding Remarks

This hypothesis demonstrated the theoretical analysis of the conjugation of Galantamine, an effective anti-cholinergic agent, and Lactoferrin, a protein with strong binding affinity for iron. The combination of these two compounds as one dosage form, with their iron and free radical scavenging ability, wherein, Lf has the ability to mop up excess iron in the brain and Gal acts as an antioxidant may be an advancement in the management of AD. This hypothesis may come to life by going further in carrying out the experiment in the laboratory to determine the potential of the conjugation as well as the *in vitro*, *ex vivo* and *in vivo* stability testing of the proteo-alkaloid so developed. It may, however, be suggested that the conjugate be embedded in a polymer matrix or be attached to nanoparticles that possess the ability to serve as a vehicle to propagate and consequently deliver the conjugate into the brain via a direct nose-to-brain pathway. This approach may present a formidable dual neuroprotection and neurotherapeutic interventional approach and may lead to be a novel advancement in the treatment of AD.

7.3. REFERENCES

Aisen PS, Schafer KA, Grundman M, et al, 2003. Effects of rofecoxib or naproxen vs placebo on alzheimer disease progression: A randomized controlled trial. JAMA 289, 2819–2826.

Alzheimer's Association, 2012. 2012 Alzheimer's disease facts and figures. Alzheimers Dement. J. Alzheimers Assoc. 8, 131–168.

Arendt, T., Brückner, M.K., Morawski, M., Jäger, C., Gertz, H.-J., 2015. Early neurone loss in Alzheimer's disease: cortical or subcortical? Acta Neuropathol. Commun. 3, 10.

Arnáiz, E., Almkvist, O., 2003. Neuropsychological features of mild cognitive impairment and preclinical Alzheimer's disease. Acta Neurol. Scand. 107, 34–41.

Ayton, S., Lei, P., Bush, A.I., 2013. Metallostasis in Alzheimer's disease. Free Radic. Biol. Med., Neurodegeneration 62, 76–89.

Babic, T., 1999. The cholinergic hypothesis of Alzheimer's disease: a review of progress. J. Neurol. Neurosurg. Psychiatry 67, 558–558.

Bäckman, L., Jones, S., Berger, A.-K., Laukka, E.J., Small, B.J., 2004. Multiple cognitive deficits during the transition to Alzheimer's disease. J. Intern. Med. 256, 195–204.

Baker, E.N., Baker, H.M., 2005. Lactoferrin. Cell. Mol. Life Sci. 62, 2531–2539.

Baker, H.M., Baker, E.N., 2012. A structural perspective on lactoferrin function. Biochem. Cell Biol. 90, 320–328.

Bernardi, A., Frozza, R.L., Meneghetti, A., Hoppe, J.B., Battastini, A.M.O., Pohlmann, A.R., Guterres, S.S., Salbego, C.G., 2012. Indomethacin-loaded lipid-core nanocapsules reduce the damage triggered by Aβ1-42 in Alzheimer's disease models. Int. J. Nanomedicine 7, 4927–4942.

Bonda, DJ., Liu, G., Men, P., Perry, G., A. Smith, M., Zhu, X., 2012. Nanoparticle Delivery of Transition-Metal Chelators to the Brain: Oxidative Stress will Never See it Coming! CNS Neurol. Disord. - Drug Targets Former. Curr. Drug Targets 11, 81–85.

Carlesimo, G.A., Oscar-Berman, M., 1992. Memory deficits in Alzheimer's patients: A comprehensive review. Neuropsychol. Rev. 3, 119–169.

Carmona, F., Muñoz-Robles, V., Cuesta, R., Gálvez, N., Capdevila, M., Maréchal, J.-D., Dominguez-Vera, J.M., 2014. Monitoring lactoferrin iron levels by fluorescence resonance energy transfer: a combined chemical and computational study. JBIC J. Biol. Inorg. Chem. 19, 439–447.

Castellani, R.J., Smith, M.A., Nunomura, A., Harris, P.L.R., Perry, G., 1999. Is increased redox-active iron in Alzheimer disease a failure of the copper-binding protein ceruloplasmin? Free Radic. Biol. Med. 26, 1508–1512.

Chitra, L., Kumar, C.R., Basha, H.M., Ponne, S., Boopathy, R., 2013. Interaction of metal chelators with different molecular forms of acetylcholinesterase and its significance in Alzheimer's disease treatment. Proteins Struct. Funct. Bioinforma. 81, 1179–1191.

Contestabile, A., 2011. The history of the cholinergic hypothesis. Behav. Brain Res., The cholinergic system and brain function 221, 334–340.

DeSai, C., Stovall, G.M., Ellington, A.D., Pierce-Shimomura, J., 2014. Inhibiting amyloid precursor protein to prevent neurodegeneration in Down syndrome and Alzheimer's disease.

Duce, J.A., Tsatsanis, A., Cater, M.A., James, S.A., Robb, E., Wikhe, K., Leong, S.L., Perez, K., Johanssen, T., Greenough, M.A., Cho, H.-H., Galatis, D., Moir, R.D., Masters, C.L., McLean, C., Tanzi, R.E., Cappai, R., Barnham, K.J., Ciccotosto, G.D., Rogers, J.T., Bush, A.I., 2010. Iron-Export Ferroxidase Activity of β-Amyloid Precursor Protein Is Inhibited by Zinc in Alzheimer's Disease. Cell 142, 857–867.

Du, F., Qian, Z.-M., Luo, Q., Yung, W.-H., Ke, Y., 2014. Hepcidin Suppresses Brain Iron Accumulation by Downregulating Iron Transport Proteins in Iron-Overloaded Rats. Mol. Neurobiol. 1–14.

Fong Yen, W., Basri, M., Ahmad, M., Ismail, M., Fong Yen, W., Basri, M., Ahmad, M., Ismail, M., 2015. Formulation and Evaluation of Galantamine Gel as Drug Reservoir in Transdermal Patch Delivery System, Formulation and Evaluation of Galantamine Gel as Drug Reservoir in Transdermal Patch Delivery System. Sci. World J. Sci. World J. 2015, 2015, e495271.

García-Montoya, I.A., Cendón, T.S., Arévalo-Gallegos, S., Rascón-Cruz, Q., 2012. Lactoferrin a multiple bioactive protein: An overview. Biochim. Biophys. Acta BBA - Gen. Subj., Transferrins: Molecular mechanisms of iron transport and disorders 1820, 226–236.

Ghribi, O., Golovko, M.Y., Larsen, B., Schrag, M., Murphy, E.J., 2006. Deposition of iron and β-amyloid plaques is associated with cortical cellular damage in rabbits fed with long-term cholesterol-enriched diets. J. Neurochem. 99, 438–449.

Giacobini, E., 2000. Cholinesterase Inhibitors Stabilize Alzheimer's Disease. Ann. N. Y. Acad. Sci. 920, 321–327.

Hardy, J., Allsop, D., 1991. Amyloid deposition as the central event in the aetiology of Alzheimer's disease. Trends Pharmacol. Sci. 12, 383–388.

Huang, R., Ke, W., Liu, Y., Jiang, C., Pei, Y., 2008. The use of lactoferrin as a ligand for targeting the polyamidoamine-based gene delivery system to the brain. Biomaterials 29, 238–246.

Huang, X.-T., Qian, Z.-M., He, X., Gong, Q., Wu, K.-C., Jiang, L.-R., Lu, L.-N., Zhu, Z., Zhang, H.-Y., Yung, W.-H., Ke, Y., 2014. Reducing iron in the brain: a novel pharmacologic mechanism of huperzine A in the treatment of Alzheimer's disease. Neurobiol. Aging 35, 1045–1054.

Hu, K., Li, J., Shen, Y., Lu, W., Gao, X., Zhang, Q., Jiang, X., 2009. Lactoferrin-conjugated PEG–PLA nanoparticles with improved brain delivery*, In vitro* and *in vivo* evaluations. J. Controlled Release 134, 55–61.

Hu, K., Shi, Y., Jiang, W., Han, J., Huang, S., Jiang, X., 2011. Lactoferrin conjugated PEG-PLGA nanoparticles for brain delivery: Preparation, characterization and efficacy in Parkinson's disease. Int. J. Pharm. 415, 273–283.

Ittner, L.M., Ke, Y.D., Delerue, F., Bi, M., Gladbach, A., van Eersel, J., Wölfing, H., Chieng, B.C., Christie, M.J., Napier, I.A., Eckert, A., Staufenbiel, M., Hardeman, E., Götz, J., 2010. Dendritic Function of Tau Mediates Amyloid-β Toxicity in Alzheimer's Disease Mouse Models. Cell 142, 387–397.

Jameson, G.B., Anderson, B.F., Norris, G.E., Thomas, D.H., Baker, E.N., 1998. Structure of Human Apolactoferrin at 2.0 Å Resolution. Refinement and Analysis of Ligand-Induced Conformational Change. Acta Crystallogr. D Biol. Crystallogr. 54, 1319–1335.

Karran, E., Mercken, M., Strooper, B.D., 2011. The amyloid cascade hypothesis for Alzheimer's disease: an appraisal for the development of therapeutics. Nat. Rev. Drug Discov. 10, 698–712.

Kumar, P., Pillay, V., Choonara, Y.E., Modi, G., Naidoo, D., Du Toit, L.C., 2011. In Silico Theoretical Molecular Modeling for Alzheimer's Disease: The Nicotine-Curcumin Paradigm in Neuroprotection and Neurotherapy. Int. J. Mol. Sci. 12, 694–724.

Latorre, D., Berlutti, F., Valenti, P., Gessani, S., Puddu, P., 2012. LF immunomodulatory strategies: mastering bacterial endotoxin1This article is part of a Special Issue entitled Lactoferrin and has undergone the Journal's usual peer review process. Biochem. Cell Biol. 90, 269–278.

Liu, G., Garrett, M.R., Men, P., Zhu, X., Perry, G., Smith, M.A., 2005. Nanoparticle and other metal chelation therapeutics in Alzheimer disease. Biochim. Biophys. Acta BBA - Mol. Basis Dis. 1741, 246–252.

Lovell, M.A., Robertson, J.D., Teesdale, W.J., Campbell, J.L., Markesbery, W.R., 1998. Copper, iron and zinc in Alzheimer's disease senile plaques. J. Neurol. Sci. 158, 47–52.

Maelicke, A., Hoeffle-Maas, A., Ludwig, J., Maus, A., Samochocki, M., Jordis, U., Koepke, A.K.E., 2010. Memogain is a Galantamine Pro-drug having Dramatically Reduced Adverse Effects and Enhanced Efficacy. J. Mol. Neurosci. 40, 135–137.

Ma, J., Guan, R., Shen, H., Lu, F., Xiao, C., Liu, M., Kang, T., 2013. Comparison of anticancer activity between lactoferrin nanoliposome and lactoferrin in Caco-2 cells *in vitro*. Food Chem. Toxicol. 59, 72–77.

Montreuil, J., Tonnelat, J., Mullet, S., 1960. Préparation et propriétés de la lactosidérophiline (lactotransferrine) du lait de femme. Biochim. Biophys. Acta 45, 413–421.

Mufamadi, M.S., Choonara, Y.E., Kumar, P., Modi, G., Naidoo, D., Ndesendo, V.M.K., Toit, L.C. du, Iyuke, S.E., Pillay, V., 2012. Surface-Engineered Nanoliposomes by Chelating Ligands for Modulating the Neurotoxicity Associated with β-Amyloid Aggregates of Alzheimer's disease. Pharm. Res. 29, 3075–3089.

Mufamadi, M.S., Choonara, Y.E., Kumar, P., Modi, G., Naidoo, D., van Vuuren, S., Ndesendo, V.M.K., Toit, L.C. du, Iyuke, S.E., Pillay, V., 2013. Ligand-functionalized nanoliposomes for targeted delivery of galantamine. Int. J. Pharm. 448, 267–281.

Munoz, D.G., Feldman, H., 2000. Causes of Alzheimer's disease. Can. Med. Assoc. J. 162, 65–72.

Nojima, Y., Suzuki, Y., Yoshida, K., Abe, F., Shiga, T., Takeuchi, T., Sugiyama, A., Shimizu, H., Sato, A., 2009. Lactoferrin Conjugated with 40-kDa Branched Poly(ethylene Glycol) Has an Improved Circulating Half-Life. Pharm. Res. 26, 2125–2132.

O'Brien, R.J., Wong, P.C., 2011. Amyloid Precursor Protein Processing and Alzheimer's Disease. Annu. Rev. Neurosci. 34, 185–204.

Oshiro, S., Morioka, M.S., Kikuchi, M., Oshiro, S., Morioka, M.S., Kikuchi, M., 2011. Dysregulation of Iron Metabolism in Alzheimer's Disease, Parkinson's Disease, and Amyotrophic Lateral Sclerosis, Dysregulation of Iron Metabolism in Alzheimer's Disease, Parkinson's Disease, and Amyotrophic Lateral Sclerosis. Adv. Pharmacol. Sci. Adv. Pharmacol. Sci. 2011, e378278.

Raven, E.P., Lu, P.H., Tishler, T.A., Heydari, P., Bartzokis, G., 2013. Increased Iron Levels and Decreased Tissue Integrity in Hippocampus of Alzheimer's Disease Detected *in vivo* with Magnetic Resonance Imaging. J. Alzheimers Dis. 37, 127–136.

Scharf, S., Mander, A., Ugoni, A., Vajda, F., Christophidis, N., 1999. A double-blind, placebo-controlled trial of diclofenac/misoprostol in Alzheimer's disease. Neurology 53, 197–197.

Sinha, M., Kaushik, S., Kaur, P., Sharma, S., Singh, T.P., 2013. Antimicrobial Lactoferrin Peptides: The Hidden Players in the Protective Function of a Multifunctional Protein. Int. J. Pept. 2013, e390230.

Smith, M.A., Harris, P.L.R., Sayre, L.M., Perry, G., 1997. Iron accumulation in Alzheimer disease is a source of redox-generated free radicals. Proc. Natl. Acad. Sci. 94, 9866–9868.

Takayama, Y., 2011. Lactoferrin and its Role in Wound Healing. Springer Science & Business Media.

Traykova, M., Traykov, T., Hadjimitova, V., Bojadgieva, N., 2014. Antioxidant Properties of Galantamine Hydrobromide. Z. Für Naturforschung C 58, 361–365.

Tsai, L.-H., Madabhushi, R., 2014. Alzheimer's disease: A protective factor for the ageing brain. Nature 507, 439–440.

van der Strate, B.W.A., Beljaars, L., Molema, G., Harmsen, M.C., Meijer, D.K.F., 2001. Antiviral activities of lactoferrin. Antiviral Res. 52, 225–239.

Wilson, R.S., Barral, S., Lee, J.H., Leurgans, S.E., Foroud, T.M., Sweet, R.A., Graff-Radford, N., Bird, T.D., Mayeux, R., Bennett, D.A., 2011. Heritability of Different Forms of Memory in the Late Onset Alzheimer's Disease Family Study. J. Alzheimers Dis. 23, 249–255.

Xie, H., Zhu, Y., Jiang, W., Zhou, Q., Yang, H., Gu, N., Zhang, Y., Xu, H., Xu, H., Yang, X., 2011. Lactoferrin-conjugated superparamagnetic iron oxide nanoparticles as a specific MRI contrast agent for detection of brain glioma *in vivo*. Biomaterials 32, 495–502.

Yeom, M., Park, J., Lee, B., Choi, S.-Y., Kim, K.S., Lee, H., Hahm, D.-H., 2011. Lactoferrin inhibits the inflammatory and angiogenic activation of bovine aortic endothelial cells. Inflamm. Res. 60, 475–482.

8.1. APPENDIX A

8.1.1. Research Publications

8.1.1.1. Book chapter

ISBN: 978-1-63278-036-2
DOI: http://dx.doi.org/10.4172/978-1-63278-036-2-037-006

Chapter-6

Nose-to-Brain Neurotherapeutic Interventions

Olufemi D Akilo, Yahya E Choonara, Pradeep Kumar, Lisa C du Toit and Viness Pillay*

Wits Advanced Drug Delivery Platform Research Unit, Department of Pharmacy and Pharmacology, School of Therapeutic Sciences, Faculty of Health Sciences, University of the Witwatersrand, Johannesburg, 7 York Road, Parktown, 2193, South Africa

***Corresponding author:** Viness Pillay, Wits Advanced Drug Delivery Platform Research Unit, Department of Pharmacy and Pharmacology, School of Therapeutic Sciences, Faculty of Health Sciences, University of the Witwatersrand, Johannesburg, 7 York Road, Parktown, 2193, South Africa, Tel: +27-11-717-2274; Fax: +27-11-642-4355, +27-86-553-4733; E-mail: viness.pillay@wits.ac.za

Abstract

The delivery of drugs to the brain has been fraught with low bioavailability of drugs in the brain. This is caused by the Blood Brain Barrier (BBB) and the Blood Cerebrospinal Fluid Barrier (BCSFB) which block therapeutics from gaining access to the Central Nervous System (CNS). Drugs that are administered via oral and intravenous are faced with this challenge of BBB thereby making the treatment of neurodegenerative diseases difficult to manage. Delivery of drugs via the nasal route directly to the brain utilizing the olfactory pathway is purportedly known to be more efficient and deliver neurotherapeutics to the brain by circumventing the BBB and thereby increasing bioavailability of drugs in the brain. This chapter explores the nose-to-brain neurotherapeutic interventions by focusing on recent development in nasal drug delivery systems, evidence of direct drug delivery from nose-to-brain, challenges facing intranasal drug delivery, various specialized nasal drug delivery devices and various intranasal delivery approaches that have been employed in circumventing the BBB in order to effectively deliver neurotherapeutic agents to the brain with increase bioavailability. The olfactory pathway as an opportunity for CNS drug delivery and mechanism of direct delivery of therapeutic agents to CNS was discussed. Future advancement was also enumerated in this chapter.

Keywords: Bioavailability; Blood Brain Barrier; Central Nervous System; Intranasal

8.1.1.2. Research paper

Contents lists available at ScienceDirect

International Journal of Pharmaceutics

journal homepage: www.elsevier.com/locate/ijpharm

AN *in vitro* evaluation of a carmustine-loaded Nano-co-Plex for potential magnetic-targeted intranasal delivery to the brain

Olufemi D. Akilo[a], Yahya E. Choonara[a], André M. Strydom[b], Lisa C. du Toit[a], Pradeep Kumar[a], Girish Modi[c], Viness Pillay[a,*]

[a] Wits Advanced Drug Delivery Platform Research Unit, Department of Pharmacy and Pharmacology, School of Therapeutic Sciences, Faculty of Health Sciences, University of the Witwatersrand, Johannesburg, 7 York Road, Parktown, 2193, South Africa
[b] Highly Correlated Matter Research Group, Department of Physics, University of Johannesburg, Kingsway Road, Auckland Park, 2006, Johannesburg, South Africa
[c] Division of Neurosciences, Department of Neurology, Faculty of Health Sciences, University of the Witwatersrand, Johannesburg, 7 York Road, Parktown, 2193, South Africa

ARTICLE INFO

Article history:
Received 17 August 2015
Received in revised form 14 January 2016
Accepted 16 January 2016
Available online 19 January 2016

Keywords:
Carmustine
Iron oxide nanoparticles
Magnetite
Superparamagnetic
Core-shell
Chemotherapeutics
Blood brain barrier
Brain tumor
Polyplex
Nano-co-Plex

ABSTRACT

Targeted delivery of carmustine (BCNU), an efficient brain tumor therapeutic, has been challenged with bioavailability issues due to the Blood Brain Barrier (BBB). The currently effective delivery approach is by implants at the site of the tumor, but this is highly invasive. The intranasal route, which is non-invasive and bypasses the BBB, may be alternative route for delivering BCNU to the brain. In this work, polyvinyl alcohol/polyethyleneimine/fluorecein isothiocyanate complex (Polyplex) coated iron-oxide nanoparticles (Magnetite) were synthesized employing co-precipitation, epoxidation and EDC/NHS coupling reactions. The Polyplex coated magnetite (Nano-co-Plex) was loaded with BCNU for potential magnetically targeted delivery to the brain following intranasal administration. The Nano-co-Plex was characterized employing Thermogravimetric analysis (TGA), Superconducting Quantum Interference Device (SQUID) magnetometry, Fourier Transform Infrared Spectroscopy (FTIR), Nuclear Magnetic Resonance (NMR), X-ray Diffractometry (XRD), Transmission Electron Microscopy (TEM) and Zetasize analysis. Results revealed superparamagnetic hexagonally shaped "core-shell" nanoparticles with cell labeling attributes, of size ranging between 30–50 nm, and a zeta potential value of +32 ± 2 mV. The Nano-co-Plex synthesized was found to possess high degree of crystallinity with 32% Polyplex coating. The loading and release studies indicated a time-dependent loading with maximum loading capacity of 176.82 μg BCNU/mg of the carrier and maximum release of 75.8% of the loaded BCNU. Cytotoxicity of the BCNU-loaded Nano-co-Plex displayed superiority over the conventional BCNU towards human glioblastoma (HG) cells. Cell studies revealed enhanced uptake and internalization of BCNU-loaded Nano-co-plex in HG cells in the presence of an external magnetic field. These Nano-co-Plexes may be ideal as an intranasal magnetic drug targeting device for BCNU delivery.

© 2016 Elsevier B.V. All rights reserved.

8.2. APPENDIX B

8.2.1. Abstracts of Research Outputs at Conference Proceedings

8.2.1.1. School of Therapeutic Sciences Research Day, University of the Witwatersrand, Johannesburg, South Africa, September 10, 2013, Poster presentation).

Preparation and Characterization of a Dual Responsive Polymeric gel for Intranasal Drug Delivery.

Olufemi David Akilo[1], Yahya EssopChoonara[1], Girish Modi[2], Viness Pillay[1].

[1]Wits Advanced Drug Delivery Platform Research Unit, Department of Pharmacy and Pharmacology, School of Therapeutic Sciences, Faculty of Health Sciences, University of the Witwatersrand, Johannesburg, 7 York Road, Parktown, 2193, South Africa. [2]Division of Neurosciences, Department of Neurology, University of the Witwatersrand, Johannesburg, 7 York Road, Parktown, 2193, South Africa.

A biodegradable and biocompatible electro-magneto responsive polymeric gel composite was prepared and characterized. The gel was synthesized by blending a Chitosan based polymer, with Polyaniline (PANI) a conductive polymer with high dielectric properties in the presence of metal oxide nanoparticles thus formed a crosslinked Interpenetrating Polymer Networks (IPN). This composite which is referred to as a 'Metalogel' with the ability to respond to an external electric stimulus was characterized for both its magnetic properties as well as its electrical conductivity. The magnetic property of the gel was based on the super paramagnetic nature of the said nanoparticles embedded in the matrix of the composite which provided the ability to respond to an externally applied magnetic field. The electric property of the gel was attributed to the electroactive capability of polymer combination which showed a response aptitude to an externally applied electric field. This composite was characterized using Scanning Electron Microscopy to examine the morphology of the gel composite, a homogenous blended composite with well dispersed nanoparticles embedded in the matrix was observed. The magnetic property was characterized by Vibrating Sample Magnetometer, which demonstrated a hysteresis loop of the composite. An increase in the concentration of nanoparticles showed a corresponding increase in the magnetization of the gel. Measurement of the electrical conductivity of the Metalogel showed an increase in conductivity with increase in the concentration of polymer combination in the composite. This dual responsive polymeric gel may be a good candidate for biomedical applications in the area of intranasal drug delivery.

Key words: Metalogel, biodegradable, biocompatible, nanoparticle

8.2.1.2. 6th Cross-Faculty Graduate Symposium, University of the Witwatersrand, Johannesburg, South Africa, September 17, 2014, (Poster presentation).

Synthesis of carmustine loaded ferrous-based nanoconstructs for targeted intranasal delivery to the brain

Olufemi David Akilo[1], Yahya Essop Choonara[1], Girish Modi[2], Viness Pillay[1].

[1]Wits Advanced Drug Delivery Platform Research Unit, Department of Pharmacy and Pharmacology, School of Therapeutic Sciences, Faculty of Health Sciences, University of the Witwatersrand, Johannesburg, 7 York Road, Parktown, 2193, South Africa. [2]Division of Neurosciences, Department of Neurology, University of the Witwatersrand, Johannesburg, 7 York Road, Parktown, 2193, South Africa.

Targeted delivery of carmustine (an efficient brain tumor therapeutic) has been challenged with bioavailability issues, thus the most known effective delivery approach is by localized delivery with implants at the site of the tumor which is a highly invasive method of drug delivery. Nasal drug delivery has been considered as an alternative route of administering drug to the brain as it is non-invasive, bypasses the BBB and improves convenience and compliance. Magnetic drug targeting via the nasal route may be a promising method of delivering carmustine to the brain. In this work magnetic ferrous-based nanoconstructs with superparamagnetic capability was synthesized successfully and loaded with carmustine for magnetically targeted delivery of carmustine to the brain following intranasal administration. This was achieved by first synthesizing the ferrous-based nanoconstructs using co-precipitation, after which the nanoconstructs were coated with a carmustine-loaded polymeric derivative complex. Thermogravimetric analysis was used to estimate the quantity of polymeric complex coat bound to the nanoconstructs. The magnetic behavior was confirmed by Vibrating Sample Magnetometery. The structure of the carmustine loaded ferrous based nanoconstructs was confirmed by Fourier Transform Infrared Spectroscopy and X-ray Diffractometery. The morphology and size of the nanoconstructs were determined by the Transmission Electron Microscopy and the Zetasize analysis. Results revealed spherically shaped “core-shell” nanoparticles coated with polymeric complex of size ranging between 30-70nm with a zeta potential value of +27mV. These ferrous-based nanoconstructs may be ideal as a magnetic drug targeting device for other chemotherapeutic agents that require delivery to the brain via the nasal mucosa.

Key words: carmustine, ferrous-based, nanoconstructs, polymeric, core-shell, chemotherapeutic, BBB

8.2.1.3. International Society of Biomedical Polymers and Polymeric Biomaterials, Orlando, Florida USA, 8th-10th July, 2015, (Poster presentation).

Synthesis of a carmustine-loaded Polyplex coated iron oxide nanoparticles for targeted intranasal delivery to the brain

Olufemi David Akilo[1], Yahya Essop Choonara[1], Lisa du Toit[1], Pradeep Kumar[1], Girish Modi[2], Viness Pillay[1].

University of the Witwatersrand
[1]Wits Advanced Drug Delivery Platform Research Unit, Department of Pharmacy and Pharmacology, School of Therapeutic Sciences, Faculty of Health Sciences, 7 York Road, Parktown, Johannesburg, 2193, South Africa. [2]Division of Neurosciences, Department of Neurology, University of the Witwatersrand, 7 York Road, Parktown, 2193, Johannesburg, South Africa.

olufemi.akilo@students.wits.ac.za

SUMMARY

The aim of this work was to synthesize polyvinyl alcohol/polyethyleneimine/fluorecein isothiocyanate (Polyplex) complex coated iron oxide nanoparticles (ION) with superparamagnetic capability and cell labeling attributes loaded with the anticancer agent carmustine (BCNU) for magnetically targeted delivery of BCNU to the brain following intranasal administration for the treatment of brain tumor.

INTRODUCTION

Brain cancer is a life threatening disease. Delivery of carmustine (BCNU), an efficient brain tumor therapeutic has been challenged with bioavailability issues due to the blood brain barrier (BBB) and it is also faced with numerous side effects such as hepatic toxicity and pulmonary fibrosis [1]. Thus the most known effective delivery approach is by localized delivery with implants at the site of the tumor which is highly invasive. Nasal drug delivery has been considered as an alternative route of administering drug to the brain as it is non-invasive, bypasses the BBB and improves convenience and compliance. Magnetic drug targeting via the nasal route directly to the brain may be a promising method of delivering BCNU to the brain.

EXPERIMENTAL METHODS

Polyplex coated ION was prepared by co-precipitation reaction of Fe^{2+} and Fe^{3+} at high pH under N_2, epoxidation of PVA and EDC/NHS coupling reaction of FITC with PEI. Drug loading [2] was carried out in the dark. The polymeric complex coated ION was dispersed in solution of ethanol containing BCNU. At fixed time intervals, ION was removed from the mixture and the residual BCNU in the supernatant was determined using HPLC. The release study was carried out by dispersing the dried BCNU-loaded ION in PBS pH 7.4 at 37 °C. At fixed time, the BCNU-loaded ION was separated using a magnet. Xu's method [3] was employed in determining the quantity of drug released using HPLC. The formulation was characterized employing Fourier Transform Infrared Spectroscopy (FTIR), Thermogravimetric Analysis (TGA), Transmission Electron Microscope (TEM), Zetasizer, Vibrating Sample Magnetometer (VSM) and X-ray Diffraction (XRD) techniques.

RESULTS AND DISCUSSION

FTIR spectra confirmed the synthesis of BCNU-loaded Polyplex coated ION based on the characteristics peaks of the bonds (N-H, C-N, C-H and O-H) that were formed and those that were unique to the native components (PVA, PEI, FITC and ION) of the formulation. The morphology, size and stability of the formulation showed spherically shaped particles with average size of 45nm with zeta potential of +21mV and polydispersity index (PDI) of 0.22. XRD results further confirmed the crystalline nature of the formulation. The thermal analysis indicated that 1/3 of the total weight of the formulation constituted the drug-loaded polymeric coating. The Magnetization curve showed a superparamagnetic attribute of the formulation with high magnetization value. The loading capacity of the synthesized Polyplex coated ION was found to be efficient for BCNU. The release profiles indicated a sustainable release of BCNU, with up to 75% of drug released after 72 hours.

CONCLUSION

BCNU-loaded Polyplex coated iron oxide nanoparticles were synthesized successfully. The formulation possesses fluorescent ability for cell labeling and was confirmed to be superparamagnetic with high magnetization value. Loading and release profiles were efficient. It may therefore be a suitable magnetic targeted intranasal drug delivery system for delivering anticancer therapeutics directly to the brain.

REFRENCES

1. Qian, L., et al. (2013). Biomaterials **34**, 8968–8978.
2. Kayal, S. and Ramanujan, R. V. (2010). Mater. Sci. Eng. C **30**, 484–490.
3. Xu, X., et al. (2006). J. Contr. Rel. **114**, 307–316.

8.2.1.4. International Society of Biomedical Polymers and Polymeric Biomaterials, Orlando, Florida USA, 8th-10th July, 2015, (Podium presentatation).

Synthesis of a carmustine-loaded Polyplex coated iron oxide nanoparticles for targeted intranasal delivery to the brain

Olufemi David Akilo[1], Yahya Essop Choonara[1], Lisa du Toit[1], Pradeep Kumar[1], Girish Modi[2], Viness Pillay[1].

University of the Witwatersrand
[1]Wits Advanced Drug Delivery Platform Research Unit, Department of Pharmacy and Pharmacology, School of Therapeutic Sciences, Faculty of Health Sciences, 7 York Road, Parktown, Johannesburg, 2193, South Africa. [2]Division of Neurosciences, Department of Neurology, University of the Witwatersrand, 7 York Road, Parktown, 2193, Johannesburg, South Africa.

olufemi.akilo@students.wits.ac.za

SUMMARY

The aim of this work was to synthesize polyvinyl alcohol/polyethyleneimine/fluorecein isothiocyanate (Polyplex) complex coated iron oxide nanoparticles (ION) with superparamagnetic capability and cell labeling attributes loaded with the anticancer agent carmustine (BCNU) for magnetically targeted delivery of BCNU to the brain following intranasal administration for the treatment of brain tumor.

INTRODUCTION

Brain cancer is a life threatening disease. Delivery of carmustine (BCNU), an efficient brain tumor therapeutic has been challenged with bioavailability issues due to the blood brain barrier (BBB) and it is also faced with numerous side effects such as hepatic toxicity and pulmonary fibrosis [1]. Thus the most known effective delivery approach is by localized delivery with implants at the site of the tumor which is highly invasive. Nasal drug delivery has been considered as an alternative route of administering drug to the brain as it is non-invasive, bypasses the BBB and improves convenience and compliance. Magnetic drug targeting via the nasal route directly to the brain may be a promising method of delivering BCNU to the brain.

EXPERIMENTAL METHODS

Polyplex coated ION was prepared by co-precipitation reaction of Fe^{2+} and Fe^{3+} at high pH under N_2, epoxidation of PVA and EDC/NHS coupling reaction of FITC with PEI. Drug loading [2] was carried out in the dark. The polymeric complex coated ION was dispersed in solution of ethanol containing BCNU. At fixed time intervals, ION was removed from the mixture and the residual BCNU in the supernatant was determined using HPLC. The release study was carried out by dispersing the dried BCNU-loaded ION in PBS pH 7.4 at 37 °C. At fixed time, the BCNU-loaded ION was separated using a magnet. Xu's method [3] was employed in determining the quantity of drug released using HPLC. The formulation was characterized employing Fourier Transform Infrared Spectroscopy (FTIR), Thermogravimetric Analysis (TGA), Transmission Electron Microscope (TEM), Zetasizer, Vibrating Sample Magnetometer (VSM) and X-ray Diffraction (XRD) techniques.

RESULTS AND DISCUSSION

FTIR spectra confirmed the synthesis of BCNU-loaded Polyplex coated ION based on the characteristics peaks of the bonds (N-H, C-N, C-H and O-H) that were formed and those that were unique to the native components (PVA, PEI, FITC and ION) of the formulation. The morphology, size and stability of the formulation showed spherically shaped particles with average size of 45nm with zeta potential of +21mV and polydispersity index (PDI) of 0.22. XRD results further confirmed the crystalline nature of the formulation. The thermal analysis indicated that 1/3 of the total weight of the formulation constituted the drug-loaded polymeric coating. The Magnetization curve showed a superparamagnetic attribute of the formulation with high magnetization value. The loading capacity of the synthesized Polyplex coated ION was found to be efficient for BCNU. The release profiles indicated a sustainable release of BCNU, with up to 75% of drug released after 72 hours.

CONCLUSION

BCNU-loaded Polyplex coated iron oxide nanoparticles were synthesized successfully. The formulation possesses fluorescent ability for cell labeling and was confirmed to be superparamagnetic with high magnetization value. Loading and release profiles were efficient. It may therefore be a suitable magnetic targeted intranasal drug delivery system for delivering anticancer therapeutics directly to the brain.

REFRENCES

1. Qian, L., et al. (2013). Biomaterials **34**, 8968–8978.
2. Kayal, S. and Ramanujan, R. V. (2010). Mater. Sci. Eng. C **30**, 484–490.
3. Xu, X., et al. (2006). J. Contr. Rel. **114**, 307–316.

8.2.1.5. Faculty of Health Sciences Research Day, University of the Witwatersrand, Johannesburg, South Africa, September 8-9, 2015. (Podium Presentation).

Preparation of a Gadolinium based Nanoparticles Coated with Polyethylene imine-Galantamine-Lactoferrin Complex for Intranasal Drug Delivery in Treating Alzheimer's Disease

Olufemi David Akilo[1], Yahya Essop Choonara[1], Lisa Du Toit[1], Pradeep Kumar[1], Girish Modi[2], Viness Pillay[1].

[1]Wits Advanced Drug Delivery Platform Research Unit, Department of Pharmacy and Pharmacology, School of Therapeutic Sciences, Faculty of Health Sciences, University of the Witwatersrand, Johannesburg, 7 York Road, Parktown, 2193, South Africa. [2]Division of Neurosciences, Department of Neurology, University of the Witwatersrand, Johannesburg, 7 York Road, Parktown, 2193, South Africa.

Alzheimer's disease (AD) is the most common cause of dementia which affects mostly elderly people. The cause of AD is known to be due to the accumulation of deformed beta amyloid and hyperphosphorylated tau proteins in the brain which resulted into formation of senile plagues and neurofibrillary tangles. Furthermore, iron has been identified as the main cause of neuronal death in AD by generating free radicals and thereby causing oxidative stress which in turn triggers destructive effects that result into AD. Galantamine is one of the therapeutic agents that have been successfully used in treatment of AD. However, it is saddled with numerous side effects and is unable to address accumulation of iron in the brain. Combination of galantamine and iron chelator may be a promising strategy for dealing with these challenges. In this study, Galantamine was conjugated to lactoferin a natural iron chelator to form a dual intranasal drug delivery system. This process was achieved by synthesizing gadolinium oxide nanoparticles and then coated them with polyethyleneimine (PEI). Galantamine-lactoferin conjugate was then incorporated into the PEI coated gadolinium nanoparticles for magnetically targeted intranasal delivery of galantamine and lactoferin into the brain. FTIR, TGA, XRD, SQUID and TEM were employed to characterize the formulation. FTIR and XRD results confirmed the conjugate of galantamine to lactoferin and their incorporation into the PEI coated nanoparticles. SQUID results indicated superparamagnetic properties of the nanoparticles, TEM result showed spherically shaped nanoparticles with average size of 20nm. A dual therapeutic intervention in a single vehicle that can address the symptomatic issue via the cholinergic approach as well as clearance of iron in the brain of AD patients was prepared. This may be advancement in magnetically targeted intranasal drug delivery in managing AD.

Keywords: Alzheimer's disease, galantamine, lactoferin, gadolinium nanoparticles, polyethyleneimine, intranasal drug delivery.

8.2.1.6. Academy of Pharmaceutical Sciences of South Africa, Johannesburg, South Africa, September 17-19, 2015, (Podium Presentation).

An *in vitro* evaluation of Carmustine-loaded Nano-co-Plex for potential magnetically targeted intranasal delivery to the brain

Olufemi D Akilo[1], Yahya E Choonara[1], Lisa C du Toit[1], Pradeep Kumar[1], Girish Modi[2] and Viness Pillay[1]

[1]Wits Advanced Drug Delivery Platform Research Unit, Department of Pharmacy and Pharmacology, School of Therapeutic Sciences, Faculty of Health Sciences, University of the Witwatersrand, Johannesburg, 7 York Road, Parktown, 2193, South Africa.

[2]Division of Neurosciences, Department of Neurology, Faculty of Health Sciences, University of the Witwatersrand, Johannesburg, 7 York Road, Parktown, 2193, South Africa.

Purpose: The aim of this work was to synthesize polyvinyl alcohol/polyethyleneimine/fluorecein isothiocyanate (Polyplex) complex coated Magnetite (Nano-co-Plex) with superparamagnetic capability and cell labeling attributes loaded with carmustine (BCNU) for potential magnetically targeted delivery of BCNU to the brain following intranasal administration for brain tumor management.

Method: This was achieved by co-precipitation reaction of Fe^{2+} and Fe^{3+} at high pH under N_2, epoxidation of PVA and EDC/NHS coupling reaction of FITC with PEI. Drug loading was carried out in the dark. The release study was carried out by dispersing the dried BCNU-Nano-co-Plex in PBS pH 7.4 at 37°C. The formulation was characterized employing Fourier Transform Infrared Spectroscopy (FTIR), Thermogravimetric Analysis (TGA), Transmission Electron Microscope (TEM), Zetasizer, Superconducting quantum interference device (SQUID) and X-ray Diffraction (XRD) techniques.

Results: FTIR spectra confirmed the synthesis of BCNU-loaded Polyplex coated Magnetite. The morphology, size and stability of the formulation showed hexagonally shaped particles with average size of 45nm with zeta potential of +21mV and poly dispersity index (PDI) of 0.22. XRD results further confirmed the crystalline nature of the formulation. The thermal analysis indicated that 1/3 of the total weight of the formulation constituted the drug-loaded polymeric coating. The magnetic studies showed superparamagnetic attribute of the formulation with high magnetization value. The loading capacity of the synthesized Nano-co-Plex was efficient for BCNU. The release profiles indicated a sustainable release of BCNU, with up to 75% of drug released after 72 hours.

Conclusions: BCNU**-**loaded Nano-co-Plex was synthesized successfully.

8.2.1.7. 7th Cross-Faculty Graduate Symposium, University of the Witwatersrand, Johannesburg, South Africa, March 2-3, 2016, (Podium presentation).

Synthesis of gadolinium oxide coated with Galantamine-loaded PEG for the management of Alzheimer's disease

Olufemi D Akilo[1], Yahya E Choonara[1], Lisa C du Toit[1], Pradeep Kumar[1], Girish Modi[2] and Viness Pillay[1]

[1]Wits Advanced Drug Delivery Platform Research Unit, Department of Pharmacy and Pharmacology, School of Therapeutic Sciences, Faculty of Health Sciences, University of the Witwatersrand, Johannesburg, 7 York Road, Parktown, 2193, South Africa.

[2]Division of Neurosciences, Department of Neurology, Faculty of Health Sciences, University of the Witwatersrand, Johannesburg, 7 York Road, Parktown, 2193, South Africa.

Alzheimer's disease (AD) is the most common cause of dementia which affects mostly elderly people. The cause of AD is known to be due to the accumulation of deformed beta amyloid and hyperphosphorylated tau proteins in the brain which resulted into formation of senile plagues and neurofibrillary tangles. Galantamine is one of the therapeutic agents that have been successfully used in treatment of AD. However, it is saddled with numerous side effects and it is challenged by the blood-brain barrier (BBB). In this study Gadolinium oxide nanoparticles were synthesized and then coated with galantamine loaded Polyethylene glycol (PEG) intended for intranasal administration for direct nose-to-brain delivery for the management of AD. The synthesized coated nanoparticles were characterized using Fourier Transform Infrared Spectroscopy (FTIR), Thermogravimetric Analysis (TGA), Transmission Electron Microscope (TEM), Zetasizer, Quantum Design Superconducting Quantum Interference Device (SQUID) magnetometery, and X-ray Diffraction (XRD) techniques. FTIR results confirmed the synthesis of the Gadolinium oxide coated with the galantamine-loaded PEG. The XRD result revealed the crystallinity of the particles. TGA results confirmed the coating and also indicated the amount of PEG coating on the gadolinium oxide. The TEM micrographs showed a spherically shaped morphology of both the coated and the uncoated gadolinium oxide with average size of 15 to 25nm. The galantamine-loaded nanocarriers are superparamagnetic as indicated by the SQUID results. Gadolinium oxide coated with galantamine-loaded PEG was successfully synthesized. This formulation has potential in delivering galantamine directly into the brain following intranasal administration.

Keywords: Galantamine, Gadolinium oxide, Alzheimer's disease, intranasal

11.3. APPENDIX C

11.3.1. Certificate of research presentation



International Society for Biomedical Polymers and Polymeric Biomaterials

Certificate of Presentation

Olufemi David Akilo

Synthesis of a Carmustine-Loaded Polyplex Coatedlron Oxide Nanoparticles for Targeted Intranasal Delivery to the Brain

Second Annual Conference
July 8-10, 2015
Wyndham Orlando Resort International Drive

Mila Galijasevic, Executive Director

July, 10 2015

11.3.2. Certificate of research presentation



11.3.3. Certificate of research presentation

11.4. APPENDIX D

11.4.1. Animal ethics approval

STRICTLY CONFIDENTIAL

ANIMAL ETHICS SCREENING COMMITTEE (AESC)

CLEARANCE CERTIFICATE NO. 2015/05/C

APPLICANT: Mr OD Akilo

SCHOOL: Therapeutic Sciences
DEPARTMENT: Pharmacy
LOCATION: Medical School

PROJECT TITLE: In vivo animal studies to assess the performance of an intranasal drug delivery system in a rabbit model

Number and Species

105 rabbits

Approval was given for to the use of animals for the project described above at an AESC meeting held on 2015/02/24. This approval remains valid until 2017/02/23.

The use of these animals is subject to AESC guidelines for the use and care of animals, is limited to the procedures described in the application form and is subject to any additional conditions listed below:

A pilot study, using 3 rabbits should first be carried out and the results reported to the AESC

Signed: _____ (Chairperson, AESC) Date: 1/4/2015

I am satisfied that the persons listed in this application are competent to perform the procedures therein, in terms of Section 23 (1) (c) of the Veterinary and Para-Veterinary Professions Act (19 of 1982)

Signed: _____ (Registered Veterinarian) Date: 1st April 2015

cc: Supervisor: Professor V Pillay
Director: CAS

Works 2000/lain2015/AESCCert.wps